Doctoral Dissertation
Doctoral Program in Materials Science and Technology
(36th Cycle)

Innovative smart composite coatings endowing antimicrobial properties to several materials

Angelica Luceri

Supervisors
Prof. Cristina Balagna, Supervisor
Prof. Monica Ferraris, Co-supervisor

Politecnico di Torino
September, 2024

Acknowledgments

I would like to thank my supervisors, Cristina Balagna and Monica Ferraris, for guiding me through this journey.

A sincere thank you to everyone I have worked and collaborated with over the years for their valuable help and suggestions that have allowed me to grow and learn.

A heartfelt thank you to all my lab colleagues and friends, for helping me and making this period enjoyable.

Thank you to those who have always been there, to those who have shared travels and experiences with me, and to those I have recently met, for all the wonderful moments we've had together.

Thank you to my family for the support and help you have given me over the years.

Finally, thank you to my mom, dad, and Fede for your unconditional support, for backing my every decision, and for believing in me, always being there for me even when miles apart.

A tutti voi, grazie di cuore!

Abstract

The issue of bacterial colonization and proliferation has consistently attracted research attention, especially with the ongoing development and spread of bacteria and microorganisms resistant to traditional therapies or antibiotics. This concern impacts various aspects of human life, as well as environmental safety.

The aim of this thesis is to develop a ceramic/glass matrix composite coatings containing silver nanoparticles (AgNps), that exhibit antibacterial properties suitable for diverse applications in numerous fields. The radio-frequency (RF) magnetron sputtering technique was utilized for depositing these coatings, offering the advantage of applying thin layers on a wide range of substrates, from metallic to polymeric materials, without causing damage. Furthermore, the process parameters can be easily optimized to obtain coatings with varied compositions and properties tailored to specific application requirements.

This research focused on developing antibacterial composite coatings intended for three primary applications: air filtration systems, water filtration systems, and textiles in the automotive sector.

The employment of antibacterial composite coating in air filtration systems aims to reduce or prevent the growth of microorganisms and bacteria on filter surfaces, which could be promoted under specific temperature and humidity conditions. The developed coatings, constituted by silica or zirconia matrix embedding silver nanoclusters, as antibacterial agents, were applied onto metallic, glass fibre-based, and polymeric air filters. They were comprehensively characterized in terms of composition, morphology, and structure.

Antibacterial analyses, performed against *S. epidermidis* and *E. coli*, Gram-positive and Gram-negative bacterial strains, and against *C. albicans,* a fungal species, revealed strong bactericidal and fungicidal properties of the coatings. Moreover, the coatings retained their bactericidal effectiveness even after thermal regeneration treatments, allowing for potential reuse following sterilization processes.

In collaboration with Università di Torino, antiviral tests were carried out, revealing that the coatings effectively inactivate strains of Human Coronavirus (HCoV-OC43), Human Rotavirus (HRoV), Influenza A virus (Flu A H1N1), Human rhinovirus (HRhV A1), and Respiratory Syncytial Virus (RSV A2).

In addition, composite coatings with a silica matrix containing copper or zinc nanoparticles as antibacterial agents were studied, which did not demonstrate antibacterial efficacy.

Bactericidal composite coatings could be also involved in water filtration systems, aiming to reduce the use of chemical products and minimize waste. To achieve this goal, ZrO2-based coatings with embedded silver nanoparticles were developed for deposition on highly thermosensitive polymeric filter membranes. The process parameters and deposition time were optimized specifically for this application to prevent substrate damage and ensure robust antibacterial properties.

The coatings successfully inhibited the proliferation of *S. epidermidis* bacteria. However, their hydrophobic nature was found to slow down the filtration processes.

In collaboration with the CRF-FCA company, an attempt was made to develop antibacterial transparent composite coatings for use in automotive textile applications. The objective was to create coatings that maintain the original color of the substrate while providing antibacterial activity. Process parameters were optimized, and deposition times were minimized.

The resulting coatings, despite containing low silver content, successfully inhibited the proliferation of *S. epidermidis* bacteria. However, they did not meet the project's requirement for complete transparency.

This thesis aims to explore alternative technologies to magnetron sputtering for developing antibacterial composite coatings consisting of a silica matrix embedded with silver nanoparticles. To achieve this, a study involving a silica coating derived from the transformation of a pre-ceramic polymer, perhydropolysilazane (PHPS), is proposed. The kinetics and mechanisms of polymer transformation were investigated using FT-IR analysis under various conditions.

Silver nanoparticles were synthesized in situ by reducing silver nitrate through UV light irradiation. Morphological analyses indicated that the resulting coating exhibited a dense and compact structure. However, this structure hindered the release of silver ions, which consequently rendered the coating ineffective in inhibiting bacterial proliferation.

Table of Contents

List of tables

List of Figures

1. Silver nanoparticles: antibacterial and antiviral effect

1.1. Antibacterial mechanisms and effect of silver nanoparticles

Silver, a chemical element belonging to the transition metals and classified as one of the precious metals, has long been recognized for its strong antimicrobial and antiviral properties. Dating back to ancient times, silver was used in the fabrication of coins, liquid containers, foils, and other applications. Throughout history, silver has played a pivotal role across several fields, including textiles, cosmetics, water and air purification systems, the food industry, transportation field, and it finds extensive use in healthcare for the manufacturing of medical equipment and devices [1][2][3][4]. Additionally, silver is widely employed therapeutically for drug delivery and for the treatment of wounds and burns, to name just a few applications [5][6][7]. Despite its interesting properties, its use has often been limited due to its instability with oxygen, leading it to easy oxidization [8].

In recent years, nanotechnologies and their application in nanoscience have seen an increase involving silver as well. It is widely used to produce materials at the nanoscale, exhibiting peculiar physical, chemical, and biological properties that bulk material does not possess [9][10].

Nanomaterials have size in a range between 1-100 nm and they could be classified according to dimension, shape, size, and biological behavior. In particular, silver nanoparticles (AgNPs) exhibit unique physicochemical properties, due to the large surface area to volume ratio [11], which allows them to interfere with viral and bacterial replication, based on different mechanisms. For this reason, AgNPs are widely involved in preventing infectious diseases since they are considered excellent alternatives to traditional therapies against antibiotic-resistant microorganisms [12][13]. Silver nanoparticles could be employed in different ways, including the development of antimicrobial and antiviral coatings to be applied in several fields.

The antimicrobial effect of silver nanoparticles has attracted the interest of several researchers who have evaluated the efficacy of AgNPs against a broad spectrum of microorganisms, including both Gram-positive and Gram-negative bacteria, viruses, and fungi. Although many studies have been conducted, the precise mechanism of action of nanoparticles remains not fully understood [14]. Nevertheless, it is still possible to outline certain aspects that elucidate the interaction between cells and nanoparticles and identify the same mechanisms explaining the strong effect of the NPs. The phases, illustrated in Figure 1, can be divided as follows: (i) adhesion of nanoparticles to the membrane and the cell wall of the microorganisms; (ii) penetration inside the cell and subsequent damage to intracellular structures, such as mitochondria, ribosomes, or biomolecules, such as DNA

or proteins; (iii) generation of reactive oxygen species (ROS) and induction of oxidative stress; (iv) modulation of signal transduction [9][15].

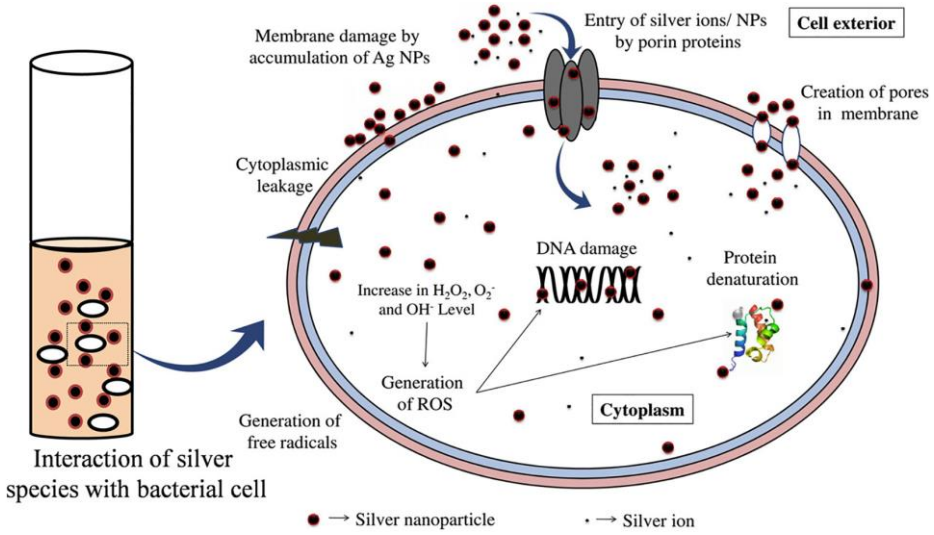

Figure 1: Antibacterial mechanisms of silver nanoparticles AgNPs: adhesion on the bacterial cell wall, penetration inside the cell, generation of ROS, and induction of oxidative stress [16]

During the adhesion phase, electrostatic interactions between positively-charged silver particles and the negatively-charged membrane of microorganisms play a crucial role [17]. In particular, the bonding between AgNPs and sulfur groups on the cell wall induces irreversible changes in cell shape, resulting in observable morphological alterations and eventual cell rupture due to their accumulation. These interactions affect membrane permeability, disrupt transport activities, cause the leakage of cellular contents, and induce condensation of genetic material, with inhibition of vital functions, ultimately leading to cell necrosis [18].

It has been observed that the effect of silver nanoparticles on bacteria is strongly dependent on the composition and thickness of the bacteria cell wall. In general, Gram-negative bacteria are more susceptible to the antimicrobial effects of AgNPs compared to Gram-positive bacteria. This phenomenon is attributed to their different cellular structures [19], as shown in Figure 2. The cell wall of Gram-positive bacteria is approximately 30 nm thick, with a high abundance of peptidoglycan molecules, which carry a negative charge, acting as a barrier for silver nanoparticles, and impeding their action. The cell wall of Gram-negative bacteria is thinner (only a few nanometers) and it is composed of layers of lipopolysaccharides, which are crucial for maintaining membrane structure integrity and defending against potential chemical attacks. However, the negative charge of

lipopolysaccharides facilitates the adhesion of silver nanoparticles, rendering Gram-negative bacteria highly susceptible to their effects [20]. Furthermore, Gram-negative bacteria possess water-filled channels called porins on their outer membrane wall, which allow the passage of hydrophilic molecules through the membrane [9].

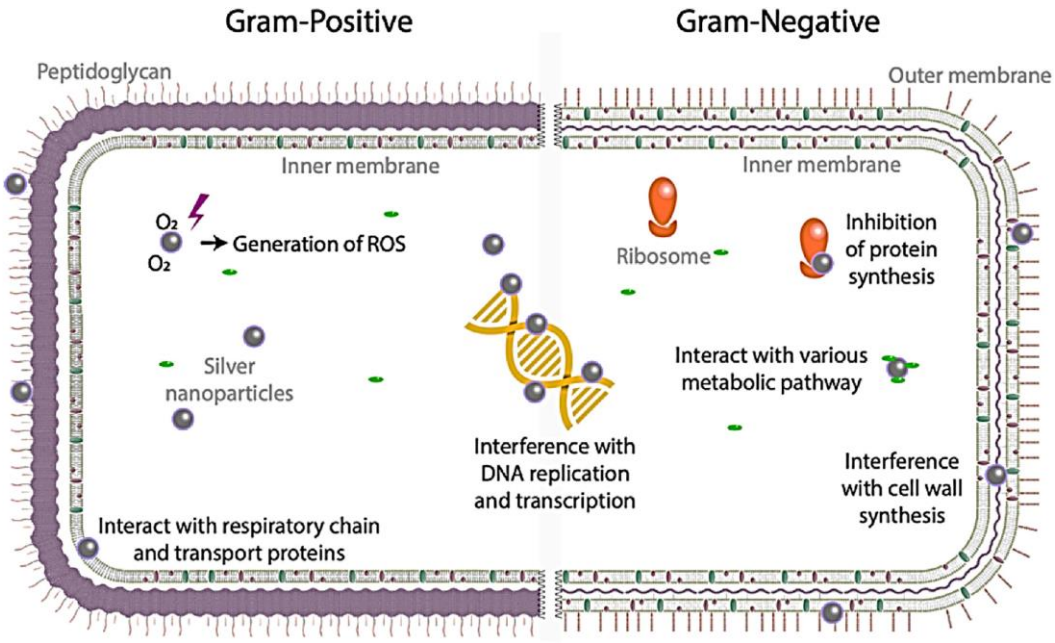

Figure 2: Comparative analysis of cellular structure and potential mechanisms of action of silver nanoparticles against Gram-positive and Gram-negative bacteria [19]

Another aspect to be considered is that silver nanoparticles release Ag^+ ions, considered the cause of bacterial cell wall disruption, together with the nanoparticles themselves. However, researchers' opinions regarding the action of AgNPs and Ag^+ ions are divided. Some studies demonstrated that the antibacterial effect is due to the ions released by the nanoparticles, while others attribute the toxicity effect to the nanoparticles themselves. In general, a synergistic effect of AgNPs and ions is widely recognized and AgNPs with smaller sizes have a higher rate of ion release due to their higher surface area-to-volume ratio. This consequently leads to greater antibacterial activity, reducing the values of the minimum inhibitory concentration (MIC) and minimum bactericidal concentration (MBC) [21] [22].

Once silver nanoparticles interact with the cell membrane, they alter its structure, modifying its permeability, and disrupting vital cellular functions. As mentioned earlier, porins can play a fundamental role by allowing the antimicrobial agent to enter the cell and interact with biomolecules, proteins, and DNA, with harmful effects on the microorganism. This can lead to the inhibition of translation and protein synthesis, or deactivation of certain functional groups of proteins.

Additionally, the action of silver nanoparticles can lead to a blockage of sugar metabolism or cause DNA breakage, denaturation, and mutations [9].

The antibacterial actions of silver involve also the mitochondrial Electron Transport Chain (ETC). The ETC is crucial for redox reactions and electron transfer from donors to receptors, a process that generates adenosine triphosphate (ATP), essential for cellular respiration. AgNPs and the released ions disrupt this process due to the accumulation of silver in the mitochondria, which causes the depolarization of the mitochondrial membrane, thereby stopping the ETC and increasing oxidative stress [23]. The key phase in this mechanism regards the generation of Reactive Oxygen Species (ROS). In general, controlled production of ROS is fundamental in regulatory processes within the cell, for maintaining proper redox processes, for implementing defense mechanisms, and for energy generation [24]. An excessive production of ROS can disable polyunsaturated fatty acids or inhibit enzymes, causing structural damage [25].

Heavy metal ions such as silver can generate reactive oxygen species and free radicals, such as hydrogen peroxide (H_2O_2) and hydroxyl radical, creating oxidative stress, although the mechanism is still not fully understood. ROS production is closely linked to nanoparticle toxicity, with dramatic consequences for microorganisms. They compromise fundamental activities such as immune protection, transmission of nerve impulses, regulation of cell growth, and crucial functions, while also inhibiting enzymes [26][27].

In these conditions, the effects on bacteria are irreversible and the cells are not able to repair damage caused by excessive ROS production. ROS species attack the sugar-phosphate backbone or DNA bases, resulting in the formation of oxidized DNA bases, single or double-strand breaks, or lesions in the DNA, leading to chromosomal aberrations such as anomalies in the number or structure of chromosomes, which are important and responsible for genetic disorders [28].

Based on the described studies, silver nanoparticles or nanoclusters have more and more attracted researcher's attention, enlarging widely the use as antibacterial agents. Dominguez *et al.* [29] studied the antibacterial effect of colloidal silver against a wide spectrum of multidrug-resistant (MDR) Gram-negative and Gram-positive bacteria. In particular, 270 strains were used, including *A. baumannii*, *P. aeruginosa*, *E. coli, K. pneumoniae*, *S. aureus*, *S. epidermidis*, and *Enterococcus* species. It has been observed that colloidal silver produces a lot of ROS in Gram-negative bacteria while producing fewer in Gram-positive bacteria, thus explaining why the bactericidal action of silver is stronger in Gram-negative bacteria. This difference in response to the silver effect depends on the cellular structure of the two types of bacteria as explained earlier [29].

Several factors could impact the antibacterial effect, such as size, shape, and concentrations. Literature is rich in scientific papers and reviews that expose or summarize these features and their consequences [30][31][32].

Li et al. [33] highlighted the different antibacterial contributions and role of silver ions and nanoparticles in the bacteria inhibition process. The authors considered the action of AgNPs with two different sizes (5 and 20 nm) and various concentrations and the Ag^+ released from them against *E. coli, P. aeruginosa, S. aureus,* and *S. epidermidis*. It was found that the minimum inhibitory concentration (MIC) for silver ions was 0.5 μg/mL for *E. coli* and 1 μg/mL for the other types of bacteria. Nevertheless, nanoparticles with smaller sizes were more effective in inhibiting bacterial growth than larger ones regardless of the bacterial strain. In fact, for smaller silver nanoparticles, the MIC was 1 μg/mL for *E. coli* and 2 μg/mL for the other strains, while using larger nanoparticles, it was 2 μg/mL for *E. coli* and *S. epidermidis*, 4 μg/mL for *S. aureus*, and 8 μg/mL for *P. aeruginosa*. Therefore, the activity of silver ions seems to be more effective than that of silver nanoparticles [33].

Figure 3 depicts the modification of the structure of bacteria exposed to silver ions and nanoparticles. In the first line, the morphology of bacteria in normal conditions is shown. In particular, *E. coli* and *P. aeruginosa* (Figure 3 A1 and B1, respectively) appeared rod-shaped, while *S. aureus* and *S. epidermidis* (Figure 3 C1 and D1, respectively) appeared coccus-shaped [33]. After exposure to Ag ions, bacteria in A2-D2 images are characterized by destroyed membranes, with holes and gaps on their surfaces. Contact with silver nanoparticles led to a modification of typical shapes, cells were severely deformed and irreversibly destroyed. No discernible differences in the alterations caused by ions or different size nanoparticles are evident, suggesting in all the cases a similar mechanism of action.

Nanoparticle sizes can be modulated according to synthesis methods. So, obtaining smaller nanoparticles can lead to benefits in terms of antibacterial effect, because they easily penetrate inside the cell wall, with the consequence of an increment of reactive oxygen species (ROS) production and a more severe effect on mitochondrial electron transport [34]. Relating to the case in which nanoparticles are in contact with a liquid medium, the size affects the contact area of interaction between NPs and the medium. It was observed that the dissolution rate of smaller AgNPs in the medium increases, and consequently the release of ions, which highly contribute to the antibacterial activity [30].

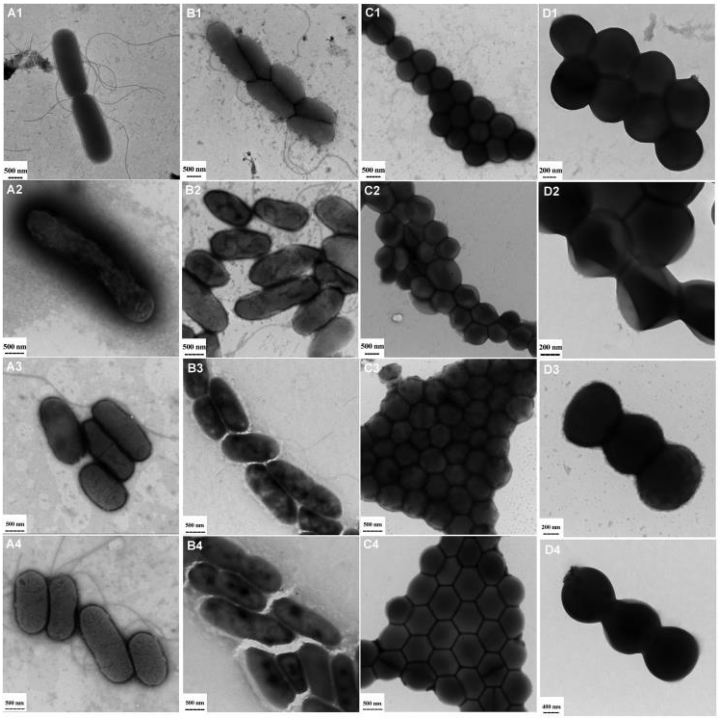

Figure 3: Cellular structure modifications of bacteria after exposure to Ag^+, Ag NPs (5 nm), and Ag NPs (20 nm) for 5h. Normal structure of (A1) E. coli, (B1) P. aeruginosa, (C1) S. aureus, (D1) S. epidermidis; structural interaction after exposure to Ag^+ of (A2) E. coli, (B2) P. aeruginosa, (C2) S. aureus, (D2) S. epidermidis; structural interaction after exposure to Ag NPs (5 nm) of (A3) E. coli, (B3) P. aeruginosa, (C3) S. aureus, (D3) S. epidermidis; structural interaction after exposure to Ag NPs (20 nm) of (A4) E. coli, (B4) P. aeruginosa, (C4) S. aureus, (D4) S. epidermidis [33]

Referring to the shape of nanoparticles, it is necessary to consider various factors that affect their biocidal properties, including geometry, surface area, crystal facets, and sharpness of edges. AgNPs in spherical and rod-shaped forms were synthesized by the chemical reduction method by *Acharya et al.*[35], and the bactericidal activity was tested against both Gram-positive and Gram-negative bacteria. Both shaped nanoparticles, tested in several concentrations, showed an antibacterial effect, dependent on the Nps amount, and attributable to the plane (111), characterized by the higher atomic density, but the death rate of microorganisms was found to be higher if exposed to spherical shaped-AgNPs. This is because the antibacterial effect is determined by the direct contact between nanoparticles and bacterial cells; higher nanoparticle concentrations led, consequently, to a higher probability of interaction between bacteria and NPs, so the effect is enhanced. *Hong et al.* [36], compared the effect of Ag nanospheres, nanowires, and nanocubes revealing that nanospheres and nanocubes were more effective in *E. coli* inhibition than nanowires, due to the higher specific surface area. As shown in Figure 4, because of their structure and shape, nanocubes and nanospheres ((b), (c), (d), and (f)), establish closer contact with the bacteria, leading to alterations and destruction of the membrane, unlike nanowires, which due to their one-dimensional structure and low specific surface area (Figure 4 (e)), interact less with the bacterium.

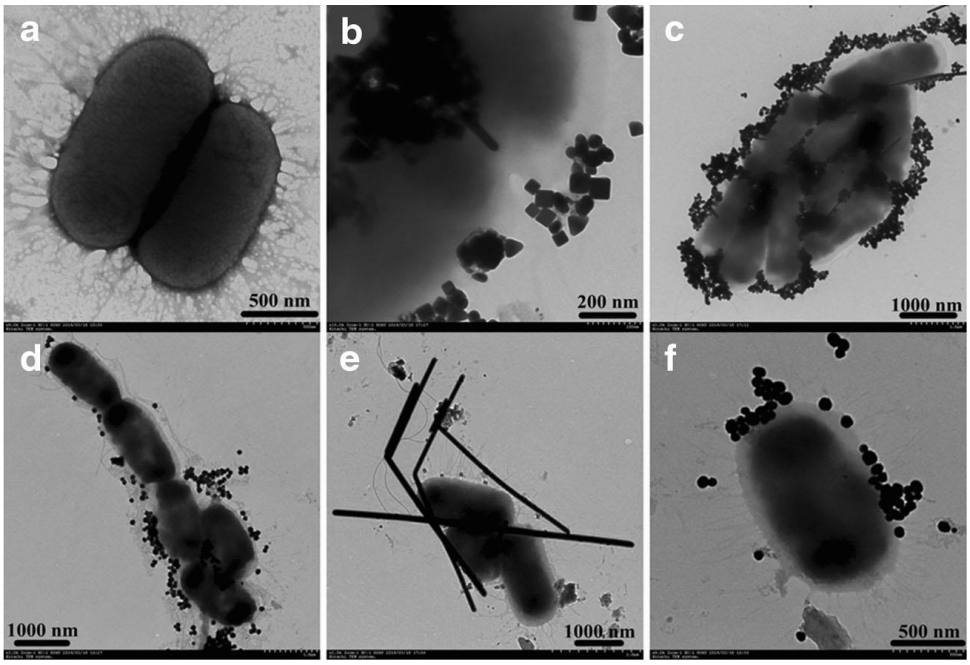

Figure 4: (a) untreated E. coli; (b) and (c) E. coli treated with silver nanocubes; (d) and (f) E. Coli treated with silver nanospheres; (e) E. coli treated with silver nanowires [36]

For certain applications of silver nanoparticles as antimicrobial agents, it is important to ensure their stability and controlled release. If silver nanoparticles demonstrate low stability during the synthesis as an example, they will surely tend to aggregate resulting in bigger nanoparticles or clusters, impacting negatively on the antibacterial effect. To overcome this inconvenience, two different features must be taken into account. First of all, the charge of nanoparticles affects their stability. It was established that AgNPs are considered stable if the charge is more than +30 mV or less than -30 mV, as the repulsive interactions are formed, preventing agglomeration [37].

Secondly, the surface of the nanoparticle could be chemically modified or coated. For this purpose, it is possible to add different agents during the nanoparticle synthesis process or to later be coated with a layer of another material, or to embed them in a matrix obtaining a composite material. The presence of a coating constitutes the first line of interaction between particles and bacteria, microorganisms, or other nanoparticles, influencing the properties. For this reason, it is possible to exploit the synergistic effect of silver nanoparticles, and of coatings or matrix material used for functionalization or composite systems.

In a recent and interesting study, green AgNPs were synthesized starting from chitosan and brown marine algae extract, obtaining stable nanoparticles of 12nm with good antibacterial effect towards *Salmonella enterica* and *Bacillus cereus*. The results revealed that the bacterial effect of nanoparticles obtained with the combination of chitosan and algae was stronger than that exhibited by silver or extract alone [38]. Using green methods, AgNPs obtained in conjunction with *Pyrenacantha*

grandiflora tubers acetone extracts and antibiotics, showed a very low value of MIC (0.0064 mg/mL) against *K. pneumoniae*, compared with that of antibiotic alone (0.8 mg/mL) [39].

Based on this point of view, different composite materials based on silver nanoparticles embedded in matrices were developed. For example, polydopamine shells have been used to embed Ag NPs in a sandwich structure with sulfated polystyrene (SPS), in order to achieve quick release of Ag nanoparticles and prolonged antibacterial activity [40]. Polyethylene glycol (PEG) with different molecular weights was used in the microemulsion-assisted co-precipitation method to obtain size-controlled silver nanoparticles. Antibacterial assays, conducted against *S. aureus*, revealed that the strongest effect was exhibited by smaller-size AgNPs, which can easily interrupt the respiratory functions of the bacteria, and the effect was improved by PEG with the higher molecular weight, due to the high hydrophilic properties [41].

Ag nanoparticles were anchored to graphene oxide sheets (GO) forming a nanocomposite (GO-Ag) to evaluate the efficacy against *E. coli*. The antibacterial effect was strong, enhanced by the synergistic activity of silver and graphene oxide [42]. For the same reason and with the same results, carbon nanotubes efficiently increase the bactericidal effect of silver nanoparticles [43].

1.2 Antiviral mechanisms and effect of silver nanoparticles

Silver nanoparticles have attracted the attention of researchers also due to their wide-spectrum antiviral activity, and, consequently, their potential applications in numerous fields. In addition to the described antibacterial effect, metal nanoparticles could be also used for their virucidal effect. Although vaccines remain the most efficient method to prevent or control the diffusion of viral disease, there are still some viruses for which no therapies have been found. Moreover, numerous viruses have developed resistance to current strategies [44]. To overcome this serious problem, AgNPs are adopted as antiviral agents. Several studies demonstrated that AgNPs could be involved in virucidal therapy, with a possible antiviral mechanism involving:

- the phase of virus attachment to the cell membrane: Ag NPs could physically interact with the structural proteins constituting the surface of extracellular viruses, morphologically altering and damaging its structure to prevent attachment or entry to the host cell, or creating a physical obstacle to prevent contact between cells and the virus [45] [46]. There is evidence that silver nanoparticles play a crucial role also in the inhibition of the first steps of viral replication, in particular during the binding to the host cells and during the penetration process [46][47].
- the early steps of viral replication: when the virus binds and enters the host cell [9][48]. In this case, the action of silver consists of interacting with and destroying of the viral genomic

material, inhibiting nucleocapsids of the virus, impeding the replication of the viral entity in the host cell, or interrupting the protein synthesis which is fundamental for cellular life [46].

- the late phases of viral replication, but this mechanism is rarely observed and less understood [47].

Figure 5 compares virus activity in the presence or absence of silver nanoparticles. On the left, the virus infection mechanism is illustrated, showing attachment to the cell membrane, subsequent penetration into the host cell, replication of the virus's genetic material, and budding. On the other hand, the presence of metallic nanoparticles physically hinders virus attachment to the cell membrane, thereby preventing its penetration. The production of ROS, ions, and radicals alters the structure and functions of viral nucleic acids and proteins, inhibiting their vital functions. Additionally, they stimulate the cell nucleus for a higher immune response capable of preventing virus budding, replication, and diffusion [49].

The efficacy of silver nanoparticles was tested against numerous viruses, both enveloped and non-enveloped. Hydrogels decorated with Tannic Acid-silver nanoparticles, (TA-AgNPs) were developed to create a system effective against Herpes Simplex Virus, HSV, infections. The studies confirmed the strong effect of AgNPs against both HSV-1 and HSV-2. In particular, HSV-1 was blocked in its attachment to the cells, and HSV-2 was inhibited in its entry into the host cells [50]. Functionalization of silver nanoparticles could enhance the antiviral effect: AgNPs capped with mercaptoethane sulfonate (MES) inhibited the early steps of viral replication [51]. Cellular heparan sulfates (HS) are the key receptors of the HSV-1 virus for interacting with host cells; AgNPs with MES compete in the binding to the host cell with the virus, leading to an inhibition of its. The dependence of a lot of viruses on HS for binding to host cells is very exploited for antiviral therapies.

An interesting study compared the antiviral activity of bare silver nanoparticles and those with five different capping agents (branched polyethyleneimine, BPEI, polyvinylpyrrolidone, PVP, polyethylene glycol, PEG, mercaptoacetic acid, MAA, and citrate) against MS2 bacteriophages. It was demonstrated that AgNPs without functionalization reduced viral units at a low level. The antiviral effect increased using strongly negative agents (Ag/MAA and Ag/citrate), while the introduction of weakly negative nanoparticles (Ag/PVP and Ag/PEG) results in a good virucidal action. Since the size and concentration of NPs play a crucial role, the best results were found considering 10 nm, cationically stabilized Ag/BPEI nanoparticle, in a concentration of 0.02 mg/ml. In this case, there is a synergetic effect between the polymer and the particle: the cationic polymer interacts with the negatively charged virus and allows the AgNPs direct contact with the virus [52].

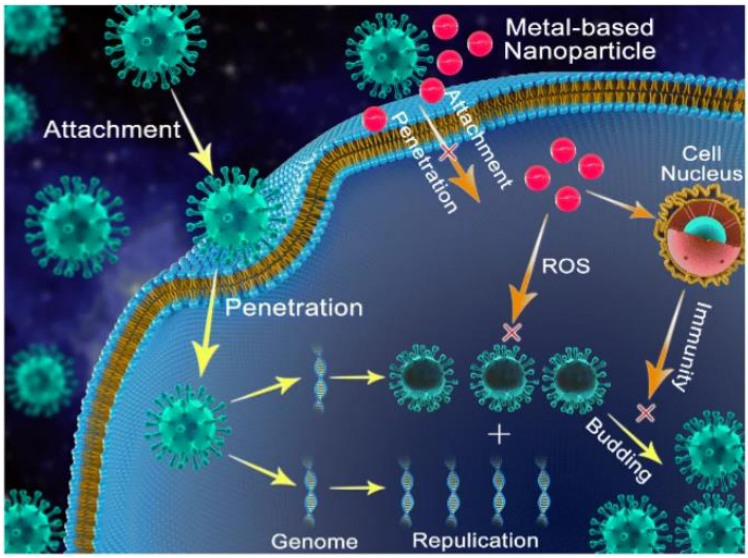

Figure 5: Mechanism of viral infection and antiviral effect of metallic nanoparticles [49]

In literature, recent papers reported the strong antiviral activity of silver nanoparticles against SARS-CoV-2 and indicated their employment in strategy to prevent and control potential further pandemic period. Ten types of silver nanoparticles with different sizes and surface functionalizations were studied in their antiviral activity and safety in cells exposed to SARS-CoV-2 [52]. They demonstrated that the viability of infected cells is strongly dependent on surface modification and NPs sizes, but all studied AgNPs increased the viability of infected cells, proving safe for use. In addition, it was shown that smaller AgNPs were the most effective. Confirming the effect of the surface modification, nanoparticles modified with BPEI also showed the most important effect in the inhibition of the virus [53].

Silver nanoparticles are often used in combination with other materials, creating composite coatings with specific properties required by the final applications. Films created by polyurethane/silver nanoparticles, PU/AgNPs, were produced and showed good mechanical properties, such as tensile modulus or ultimate tensile strength, but also excellent biological effect, since they were able to reduce the amount of virus of 67% [54]. In an interesting study, silver nanoparticles were incorporated in mouthwash and nasal solutions and used by health personnel working in hospitals, in contact with patients affected by CoronaVIrus Disease 19 (COVID-19). The group involved men and women, involving doctors, nurses, and administrative, and lasted 9 weeks during the COVID-19 pandemic period (April-June 2020). Test revealed that they were not infected, probably due to the treatment with AgNPs, and the in vitro assay showed that the use of this solution could prevent the spread of viral infection, benefiting healthcare personnel as well as the general population [55]. Figure 6 shows SARS-CoV-2 plaque formation at different diluitions

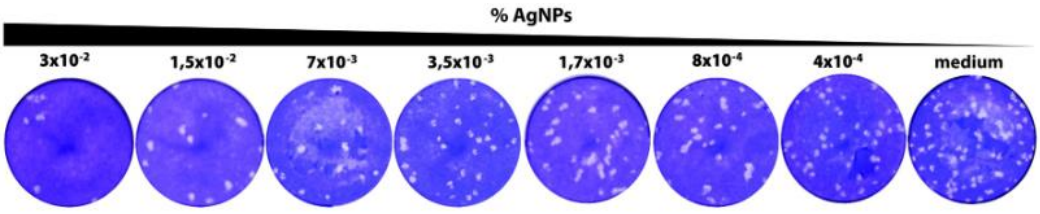

Figure 6: Virus plaque formation at different dilutions of silver nanoparticle solutions [55]

According to World Health Organization (WHO) report, the Influenza A virus is the cause of approximately 3-5 million diseases and about 500000 deaths every year. Among the different strategies that could be adopted to minimize its effect, the use of silver nanoparticles could represent a solution. Considering concentrations from 0.4 to 2000 μg/ml, the evaluation of the cytotoxic effect showed that cell viability increased as nanoparticle concentration decreased, while the highest concentration led to a significant cytotoxic effect. The antiviral activity was observed at higher concentrations, from 4 to 100 μg/ml during pre-exposure treatment, achieving inhibition percentage in a range between 82% and 100%. Post-exposure treatment with silver nanoparticles at lower concentrations did not significantly affect the virus, while complete inhibition was observed with higher concentrations [56].

In another study, to prevent the effect of the Influenza A virus, a composite material of silica decorated with silver nanoparticles (dimension 30 nm) was used, analyzing the effect after different exposure times at two different temperatures (5 and 20° C). The highest concentrations showed the best antiviral results at both temperatures, and the effect increased with increasing the exposure time [57].

Green silver nanoparticles, with size in the range between 10 nm and 50 nm, were tested against Bovine Alpha Herpesvirus-1, BoHV-1, which dramatically affects bovine rhinotracheitis. The nanoparticles were found to exhibit low toxicity to MDBK cell cultures when concentrations between 25 and 50 μg/ml were used. Additionally, they effectively inactivated BoHV-1, thereby protecting rabbits from infections [58].

A crucial aspect that must be taken into account with the use of silver nanoparticles is their potential toxicity for humans and the environment. In general, the toxicity of human cells could cause immunotoxicity and an increase in inflammatory responses [59]. Silver in ionic form is more toxic than silver in nanoparticle shape, but it depends on different biokinetics. In addition, it is well known that the effect depends on several factors, such as shape, exposure time, and dose. It is important to note that the effect depends on the amount of released silver [53][60]. To safeguard the environment and human health, researchers have made an effort to synthesize nanoparticles with green methods

instead of chemical ones, in order to avoid the use of chemicals and to reduce waste, for example using plant extract or environmentally friendly synthesis methods [61].

Another method to preserve the environment and ensure a slow release of nanoparticles or ions is to use composite materials composed of matrices, which allow for gradual and controlled release over time without negatively impacting environmental safety [62]. The materials used for nanocomposites are several. Graphene oxide sheets were used to graft AgNPs, and their peculiar features such as high carrier mobility, biocompatibility, and large surface area were exploited. The system obtained guarantees no agglomeration of AgNPs, limiting the risk of toxicity, and was successfully tested against Infectious Bursal Disease virus, IBDV, and Feline Coronavirus, FCoV [63]. Chitosan, collagen, or gelatin could be an organic matrix encapsulating silver nanoparticles [64]. With the same aim, silver nanoclusters were embedded in a porous silica matrix to obtain an antiviral coating deposited on facial masks. The composite coating, tested against SARS-CoV-2, exhibited strong virucidal efficacy, being safe for humans and the environment [65].

2. Sputtering technique

2.1. Description of sputtering deposition methods

The sputtering technique is a physical vapor deposition (PVD) method, widely used for the deposition of thin films, reported for the first time in literature in 1853 by Sir W.R. Grove. Over time, this process has been progressively implemented and refined to achieve high-quality depositions, including single crystals, complex alloys, and materials with varying compositions tailored to specific requirements. It is classified as a vacuum coating method, based on the bombardment of a target by ions generated by a plasma. This causes the "sputtering", i.e. the removal of atoms from the target. These atoms then condense on a substrate creating a thin film [66][67].

The process occurs in a chamber, where a high vacuum pump guarantees a pressure lower than 10^{-3} or 10^{-4} Pa, to ensure high purity of the coatings. To induce ion bombardment, a continuous flow of high-purity gas, typically Argon (Ar) due to its atomic mass, inertness, and low price, is introduced into the evacuated chamber, normally achieving a pressure of 0.1-1 Pa. Ar is ionized, becoming positively charged; due to the presence of an electric magnetic field, the ions are attracted by the negative charge of the cathode target. Atoms are ejected from the target and sputtered onto the substrate, and the deposition process continues [67].

This process has been used for many years, to successfully deposit various materials on different substrates. However, it is characterized by limitations such as a low deposition rate, low ionization efficiency, and low film density. To overcome these issues, magnetron sputtering was developed. Magnets are arranged to create a magnetic field with a pole at the center of the target and another pole as a ring on the edge of the target. This configuration traps electrons and enhances the probability of collisions between electrons and atoms. This leads to an increase of the ions bombardment, so the efficiency and the rate deposition of the process are enhanced, and the process could occur at lower pressure and lower voltage than the traditional sputtering process [66][68]. Generally, planar diodes are used for thin coatings and small-scale productions (in research and laboratory settings). On the contrary, for thicker coatings, or substrates with particularly complex shapes and greater thermal sensitivity, the use of triode systems and magnetron-type sources is the most appropriate choice [69]. Depending on the conductivity of the target, power could be applied in radio frequency (RF), direct current (DC), microwave, or pulse (P) mode [70].

A representation of the sputtering deposition process is shown in Figure 7.

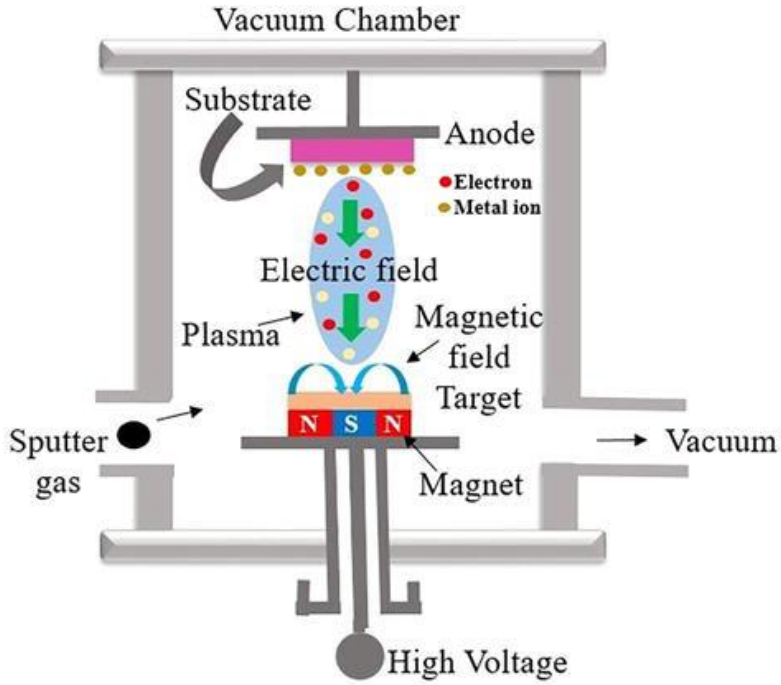

Figure 7: Scheme of magnetron sputtering deposition equipment [71]

Magnetron sputtering technology has the advantage of depositing very thin, high-purity coatings, at high speed but low temperature. The process is straightforward and environmentally friendly [72] and is suitable for several types of substrates such as metal, textile, cotton, wool, and polymer [73].
Coating composition could be optimized, using targets of various materials, or multiple targets simultaneously to obtain alloys, or sequentially to create composite coating or more than one layer. Additionally, a reactive sputtering process can be achieved by introducing gases such as O_2, N_2, or H_2 into the chamber [74].

One of the major advantages of employing this technique is its universality and adaptability. Process parameters, such as the number of pumps, type, and number of targets, pressure, substrate type and geometry, gas type and flow, and current density, could be modified and adjusted in order to obtain coatings customized for several purposes. They could impact the microstructure, chemical composition, grain size, deposition rate and coating thickness, adhesion, and mechanical properties, and impart or enhance properties and behavior [75][76]. In Figure 8, some of the most notable characteristics of coatings that can be altered by adjusting the process parameters of deposition are listed. Many other properties can be modified by varying and combining different factors to optimize the process.

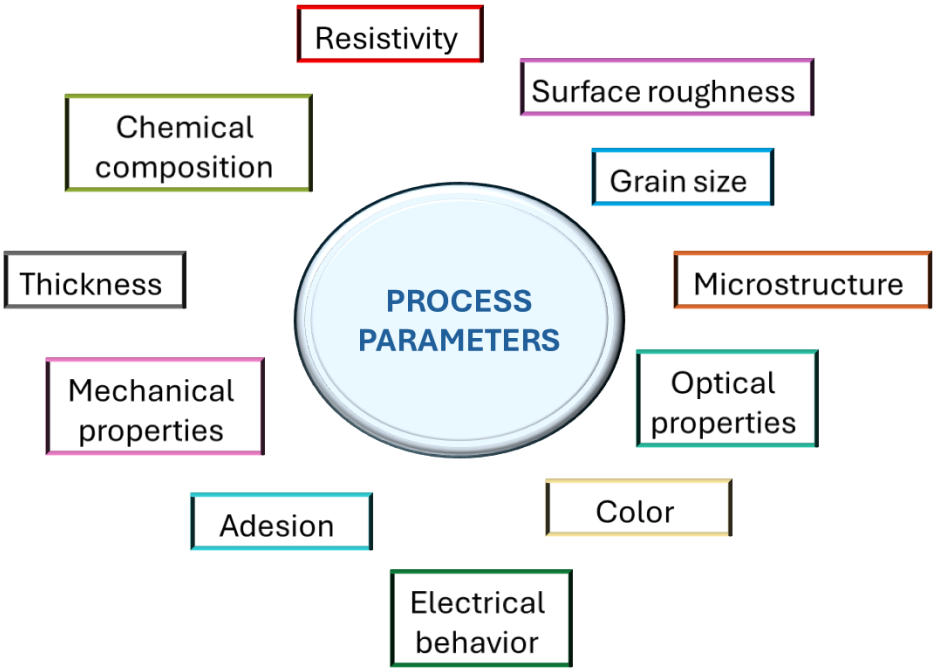

Figure 8: Coating characteristics and properties affected by selected parameters during the deposition process

Wang et al. [77] demonstrated that power and bias voltage are the two parameters that most influence the microstructure of TiO_2 coating on aluminum alloy, as summarized in Figure 9. Specifically, the increase of these parameters leads to an increase in particle size and coating roughness; hardness and elastic modulus increase with increasing bias voltage, resulting in an improve of mechanical properties and of corrosion resistance and antifouling effect.

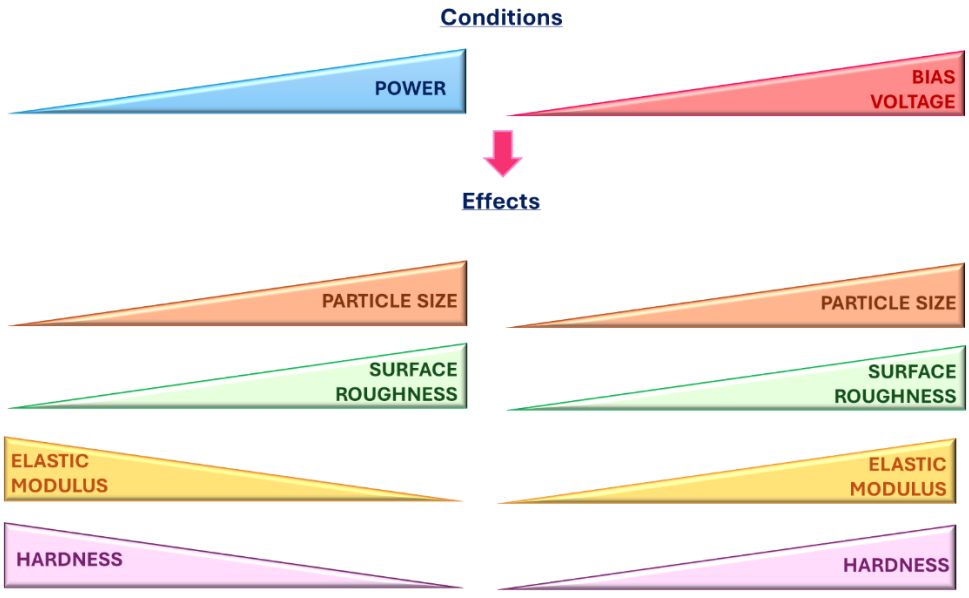

Figure 9: Effects of changes in power and bias voltage on TiO_2 coating on aluminum alloy

Changes in coating microstructure could be determined by variations in the composition of the film. In a ZnO-B_2O_3 ceramic coating, the addition of a small amount of B_2O_3 to ZnO regularizes the crystals size as the undoped-ZnO film was characterized by irregular polyhedrons. The presence of B_2O_3 reduces the polyhedrons' size and the deposition rate, due to the low density of the target, and alters the morphology from bacilliform to ball-shaped and then flake-like particles. Consequently, this modification in the morphology affected grain size and surface roughness [78]. In Figure 10, the microstructure of coatings with a progressive increase of B_2O_3 are shown.

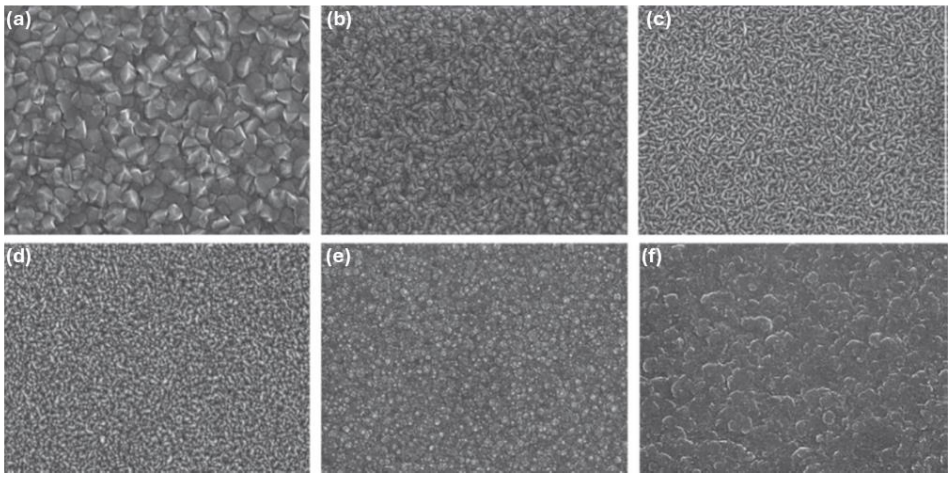

Figure 10: Morphology of ZnO-B_2O_3 coatings with different compositions: (a) ZnO, (b) 99% ZnO, 1% B_2O_3, (c) 97% ZnO, 3% B_2O_3, (d) 95% ZnO, 5% B_2O_3, (e) 93% ZnO, 7% B_2O_3, (f) 90% ZnO, 10% B_2O_3 [78]

The flow rate also plays a crucial role in the definition of coating morphology. Studying the film obtained by sputtering ZrO_2 on 316 stainless steel at different argon flow rates, it was observed a gradual increase in the surface roughness from 5 sccm to 10 sccm, which became sharp after 10 sccm, showed in Figure 11.

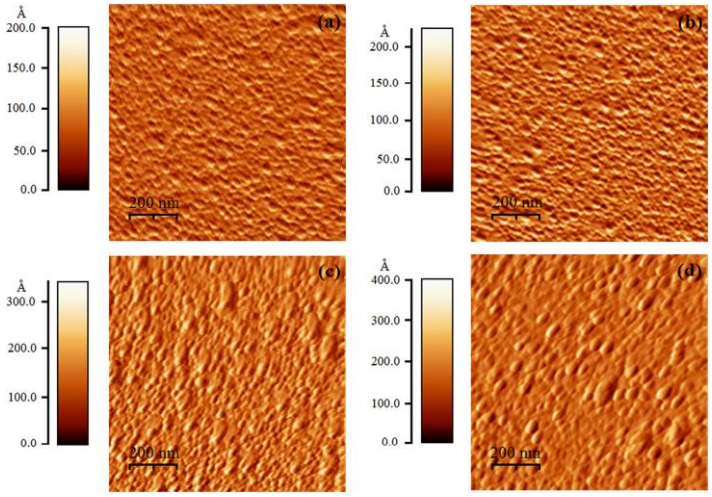

Figure 11: ZrO_2 coatings deposited on 316 stainless steel at Ar flow rates of (a) 5 sccm, (b) 10 sccm, (c) 15 sccm, (d) 20 sccm [79]

The structure was granular, and the size of the grains was uniformly distributed. This growth mechanism is related to the energy of the atoms. When atoms reach the substrate, their momentum transforms into heat, which increases the diffusion phenomenon and therefore the mobility of the atoms. Increased deposition rate leads to greater diffusion mobility, grain growth, and granular structure [79].

Optical and electrical changes were studied for Al-doped zinc oxide (AZO) layers deposited on flexible ultra-thin glass [79]. The resistivity of AZO thin film decreases when power is increased from 50 to 100W, but for high power, it slightly increases. The decrease in the value of the working pressure causes an increase in the mean free path and in the ability of atoms to diffuse, resulting in a higher deposition rate. In the case of optical properties, transmittance decreases increasing the power, but it is also affected by the temperature of the substrate and working pressure [80].

2.2. Antibacterial and antiviral coatings via sputtering technique

Since this technique is useful for depositing several coatings for a wide range of applications, sputtered nanocoatings with bactericidal and virucidal effects have recently spread significantly. These coatings can be designed to inactivate and destroy microorganisms, preventing the spread of infectious diseases, without decreasing mechanical, thermal, or optical properties.

The production of bactericidal and virucidal devices with the use of coatings has been developed on a large scale, finding applications in hospital sectors and health care, in medical devices and equipment to reduce the risk of nosocomial infections. The same types of film could be used in the food industry, to improve food safety and preservation, or in public transport where they play a crucial role [68] [71] [76].

In this scenario, the sputtering technique proves to be versatile, for the wide spectrum of substrates and the various compositions and features obtainable. To produce antibacterial and virucidal materials, various strategies could be applied.

The use of silver in the shape of nanoparticles or as a nanolayer is the most commonly pursued route, thanks to its well-known good properties. Morphological analysis of *E. coli* in contact with $TiO_2/SiO_2/Ag$ coatings obtained through RF magnetron co-sputtering method on glass showed severe damage to bacteria colonies, shown in Figure 12(a), which lost their original shape, appeared with pits and depressions and a ruffle surface; on the contrary, cells on TiO_2/SiO_2 coating without silver were less significant damaged (Figure 12 (b)) [81].

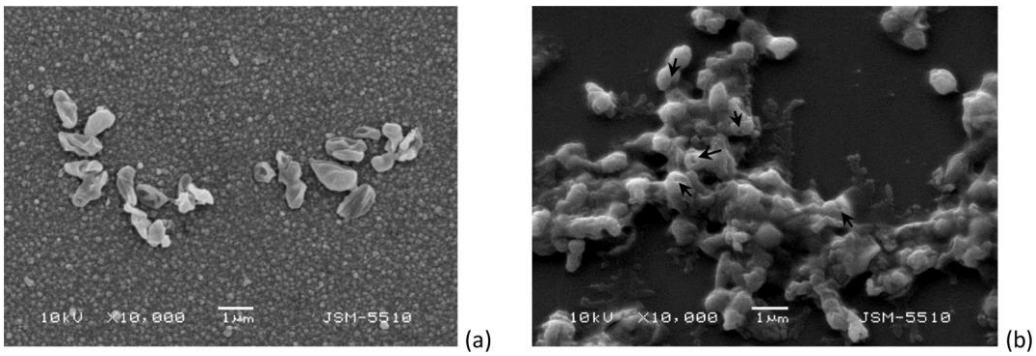

Figure 12: Morphological analysis of E. coli on (a) $TiO_2/SiO_2/Ag$ sputtered coating and on TiO_2/SiO_2 sputtered coating [81]

When silver nanoparticles are embedded in a composite coating, the choice of the matrix is crucial for achieving the desired performance. Sputtered coatings of SiO_2 or TiO_2, containing silver nanoparticles were much more effective in inhibiting *E. coli* compared to non-doped TiO_2 material. However, considering that it is an excellent photocatalyst, the antibacterial activity is improved after UV activation [82].

In addition to nanoparticles, silver can be deposited in the form of a thin film to impart bactericidal properties to materials. Polyetheretherketone, PEEK, for example, exhibits excellent mechanical properties, corrosion resistance, and biocompatibility, making it widely used in the medical field for oral implants, orthopedic trauma care, or wound healing. However, its lack of antibacterial properties requires surface modification, such as coatings, surface treatments, or chemical etching, to enhance its performance. *Liu et al.* [83] attempted to confer antibacterial properties by depositing a homogeneous layer of nano-silver using magnetron sputtering. They obtained and studied coatings of different thicknesses (ranging from 3 to 12 nm), which showed an increase in the amount of Ag, as well as variations in the material's surface characteristics, such as roughness or contact angle, with increasing thickness. All the coatings exhibited strong inhibitory effects against *S. mutans* and *S. aureus*, which were not observed with uncoated PEEK, and they were biologically safe according to cytotoxicity tests. Bacterial adhesion was reduced. As the thickness increased, the number of viable bacterial colonies, adherent to the material, drastically decreased compared to those adherent to the uncoated material. However, it is well-known that an increase in roughness is correlated with better bacterial adhesion, but in this case, the roughness remains below 0.2 μm, which is the reference value for surface roughness in medical implants. Furthermore, an increase in contact angle generates hydrophobic surfaces that worsen bacterial surface adhesion [83].

Since deposition could occur in a reactive atmosphere, it is interesting to evaluate how different flow conditions impact on coating characteristics and behaviors. In the studies conducted by *Rebelo et al*. [84], Ag layers were compared to AgO_x coatings, deposited using pulsed DC magnetron sputtering in

a reactive atmosphere, with variations in oxygen flow from 0 to 15 sccm, and consequently in the oxygen fraction in the coating. The obtained Ag layer was compact and dense, with limited ion release, resulting in noneffective against *S. epidermidis*. Introducing O_2 flow, AgO, and Ag_2O were deposited as demonstrated by XRD and XPS analyses, and the antibacterial effect was strong due to the increase of ROS formation [84].

Thanks to the combination of different techniques, an antibacterial coating was sputtered on bioactive glass (BG) deposited on PEEK substrates through the electron phoretic deposition (EPD) technique [84]. The idea was to enhance the biostability and bioactivity of the system and to confer antimicrobial properties at the same time. In particular, the composite coatings were made up of silica and silver nanoparticles, deposited in different thicknesses. The thickness of the first layer was too thin and the morphology of PEEK/BG remained unchanged because the roughness of the substrate was higher than the sputtered coating thickness. However, its presence was confirmed by EDS and XPS analysis. The thicker coatings appeared with a globular structure, typical of sputtered silica. Both of them exhibited antibacterial effects against *E. coli* and *S. carnosus*, and the silver amount in the thinner coatings was sufficient to kill bacteria, without compromising the surface morphology of the substrate [85].

It is possible to include other antibacterial agents in the sputtering deposition process or to combine some of them. As an example, a titanium oxide coating doped with silver and copper, whose morphology is shown in Figure 13, demonstrated a strong antibacterial effect on *E. coli, S. epidermidis, P. aeruginosa and S. holeresius*.

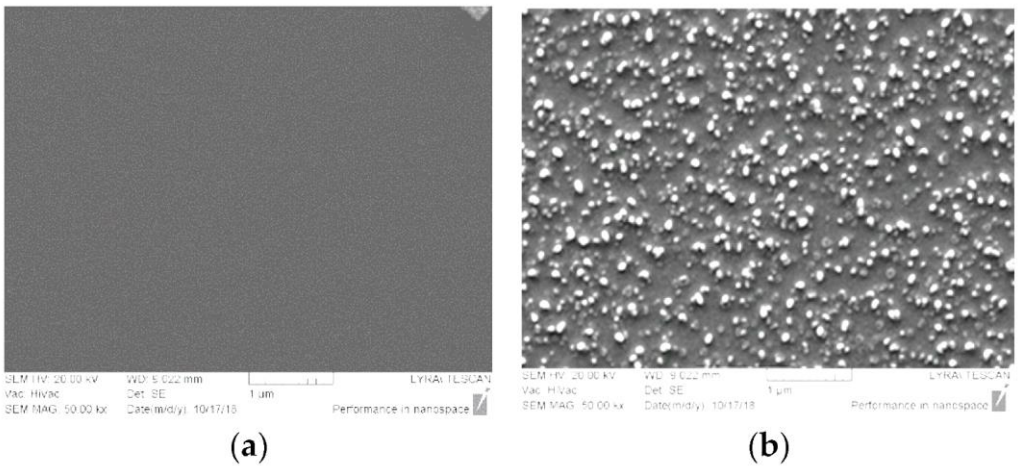

Figure 13: Morphological analysis of (a) TiO2 coating by magnetron sputtering on glass substrate, (b) TiO2/Ag/Cu coating by magnetron sputtering on glass substrate [86]

In Figure 14 the *S. epidermidis* and *E. coli* growth on coated samples is shown. It is well evident that an increase in Ag amount (curves 4 and 5) leads to a stronger bactericidal effect, while with the

constant silver amount and an increase in the copper content (curves 1,2 and 3), the antibacterial activity improves only slightly [86].

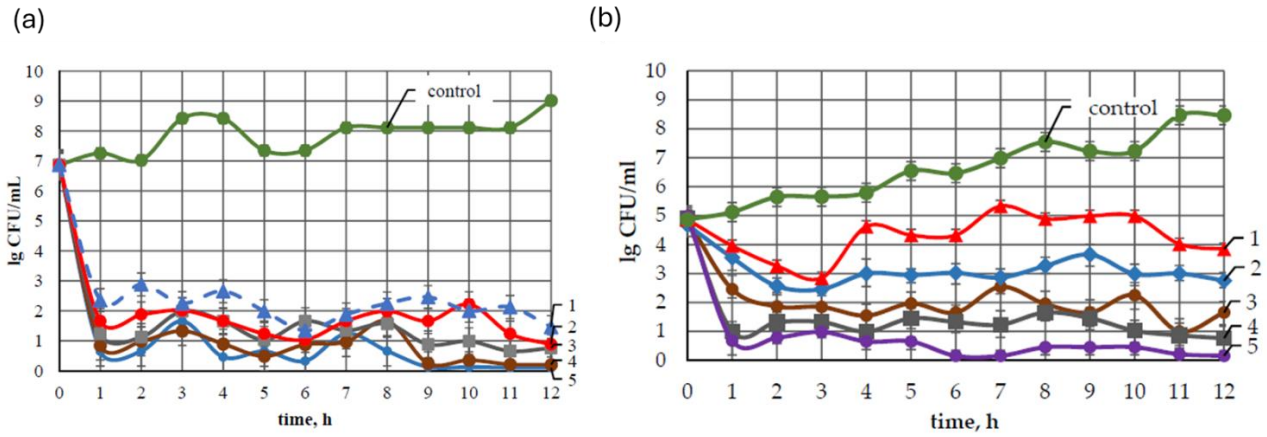

Figure 14: (a) S. epidermidis and (b) E. coli grown on TiO2/Ag/Cu coating with progressive increment in Cu copper (curves 1, 2, and 3) and progressive increment of Ag (curves 4 and 5) [86]

Considering the co-sputtered antiviral agents, *Meister et al.* [87] highlighted the changes in microstructure and antiviral/antibacterial efficiency depending on the used methods. They compared thin and dense films of Ag and Cu, with nanostructured coatings obtained or by the co-deposition of Ag and Pt, and Cu and Ag or by sequential deposition of Ag on Pt, and Cu on Ag. Film made up of pure Ag showed higher roughness than that of pure Cu. Furthermore, they noticed that, in the case of sequential deposition, the single elements tended to remain separately, while the co-deposition method resulted in a mix of the elements. In Figure 15 the fluorescence images of adhered bacteria colonies for each coting system and related blood agar plates are shown. In the case of Pt, Ag and Cu patches, no antibacterial effect against *S. aureus* was exhibited, due to an insufficient release of ions, while the higher effect was obtained with Ag/Cu systems, both co-deposited and sequentially deposited. From an antiviral point of view, the sputtered Cu film reduced the viral titer of SARS-CoV-2, otherwise, no effect was shown by Ag film. Regarding the systems containing the two elements, silver enhanced the antiviral effect of copper, probably because the presence of silver promotes the reduction process of copper and its release.

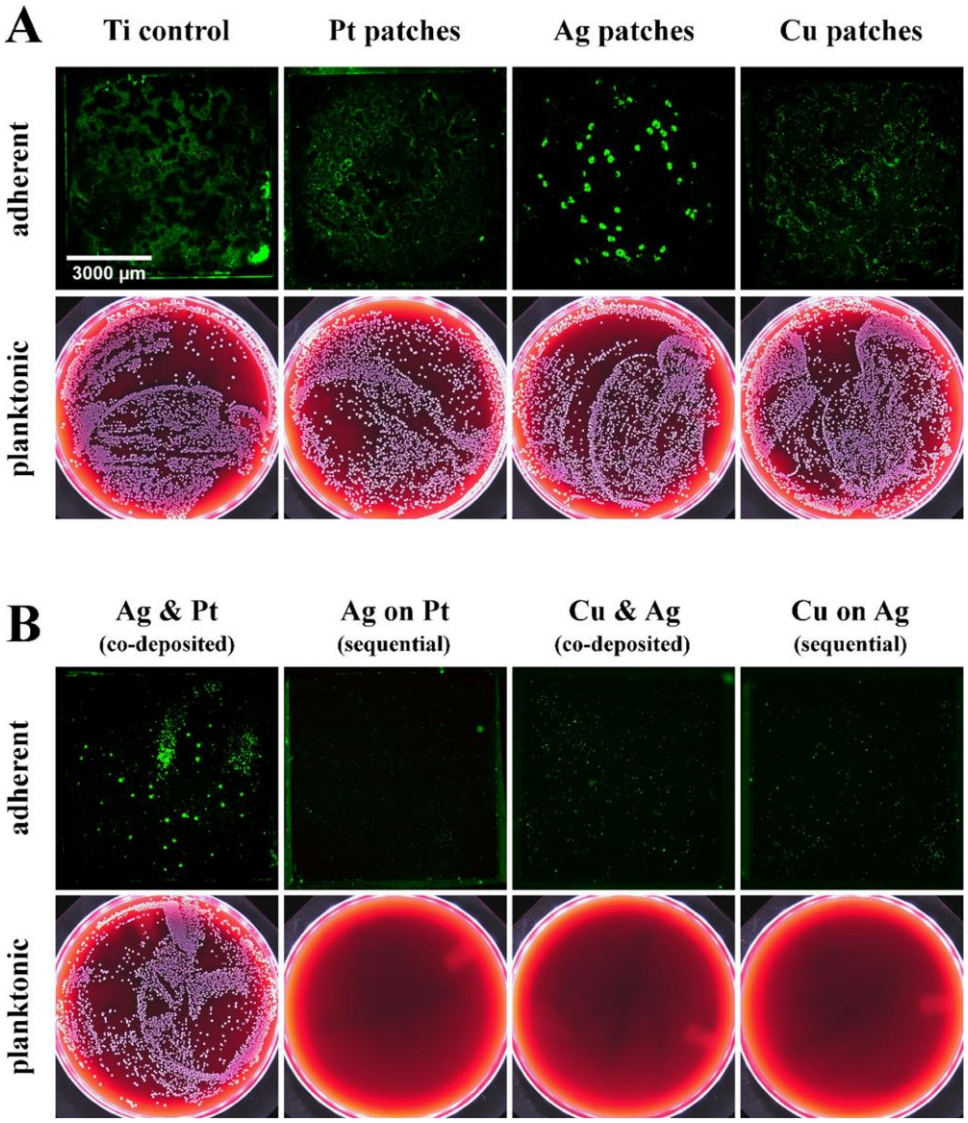

Figure 15: Fluorescence images and related blood agar plates of S. aureus growth on Ti as control, Pt, Ag, and Cu patches and on Ag/Cu coatings (A) co-deposited and (B) sequentially deposited [87]

The possibility to co-deposit different materials at the same time was exploited to develop ternary systems, combining their characteristics and features. For example, trimetallic oxide nanocomposite coatings made up of zirconium oxide, zinc oxide, and titanium oxide were deposited on stainless steel via magnetron sputtering to merge their good antibacterial, mechanical, and photocatalytic properties in a single layer. The sputtering process successfully occurred, generating a homogenous compact coating, with no cracks, and a good performance to corrosion. Under UV-A irradiation, they exhibited a strong efficiency by killing about 80% of the amount of *E. coli* and about 70% of the amount of *S. aureus*, enhancing the effect of the coatings without irradiation [88].

The use of a multi-target reactor allowed the deposition of a ternary Zr-Cu-Ag film metallic glass. The coating obtained showed a uniform thickness and homogenous distribution of the single element, as well as a very homogenous surface and nanometer roughness, typical of the magnetron sputtering

process. From a biological point of view, this system had an antibacterial rate against S. *aureus* of 99.99% [89].

Recently, with the spread of SARS-CoV-2, great attention has been focused on the antiviral effect of devices. Exploiting the properties of silver nanoclusters, composite silica coating containing silver nanoparticles was deposited on facial masks and tested against SARS virus. The result was promising, showing a complete reduction of virus titer [65].

With the same aim, *Jung et al.* [90] deposited a copper film on a polypropylene, PP, filter facial mask, in order to not compromise the filtration efficiency of the facial masks but to inactivate viruses that remained on the mask surface. To enhance the adhesion between film/surface, a surface treatment using an oxygen ion beam was performed. The filter exhibited a virucidal effect against the SARS-CoV-2 virus. Since it is well known that copper oxide is effective against Influenza A virus, the possible oxidation of the superficial layer, due to moisture or oxygen, probably did not compromise the antiviral effect.

3. Field of applications of antibacterial and antiviral coatings

3.1. Application of antibacterial/antiviral coatings in air filtration systems

Among environmental issues that could impact human health, the reduction of air quality plays a pivotal role in everyday life. The causes are numerous, including industrial activities, fuel consumption, transportation, and the combustion of biomass and coal [91]. Generally, the air stream contains pollutants, airborne particles, and bioaerosols, constituted by bacteria, fungi, viruses and fungal spores. Several strategies as the use of ultraviolet irradiation, air ion emission, or heating, have been adopted to remove bioaerosols and decrease risks to human and environmental health [92].

Air filters serve the primary function of purifying air and can be optimized based on porosity, size, and material to meet diverse needs across different application fields. According to their effectiveness against particulate matter, air filters are categorized into prefilters, medium-efficiency filters, high-efficiency particulate air (HEPA) filters, and ultra-low particulate air (ULPA) filters. HEPA and ULPA filters are the most commonly used because they can capture particles, bacteria, and microorganisms of 0.3 μm and 0.12-0.17 μm, respectively, with an efficiency approaching 99.97%. [93]. For treating Volatile Organic Compounds (VOCs) absorption-based granular activated carbon filters (GAC) are commonly involved [94]. Other air purification technologies involve plasma treatment, which can be thermal, suitable primarily for eliminating high concentrations of toxic compounds, especially in industrial settings; or low-temperature, capable of removing fungi, bacteria, and spores present in the air even after short exposures, with the production, however, of ozone and nitrogen oxides [93]. Another method concerns catalytic purification, which exploits photogenerated electrons in materials such as TiO_2, often used for heating, ventilation, and air-conditioning (HVAC) systems [94]. These systems could improve air quality in buildings, vehicles, and clean rooms. Figure 16 clarifies how the use of HVAC systems in indoor environments could prevent the diffusion of airborne diseases. In buildings, they are useful to prevent the diffusion of several diseases and the attention increased with the diffusion of COVID-19 disease.

To improve air quality in buildings or vehicles, HVAC systems are the main used. However, these devices are affected by a critical aspect. Although they can trap microorganisms, they usually have no intrinsic antimicrobial effect. So bioaerosols remain on the surface of the filter and can therefore grow, promoted by certain conditions of humidity and temperature. In this way they could be reintroduced into the air stream, becoming a secondary source of pollution [95].

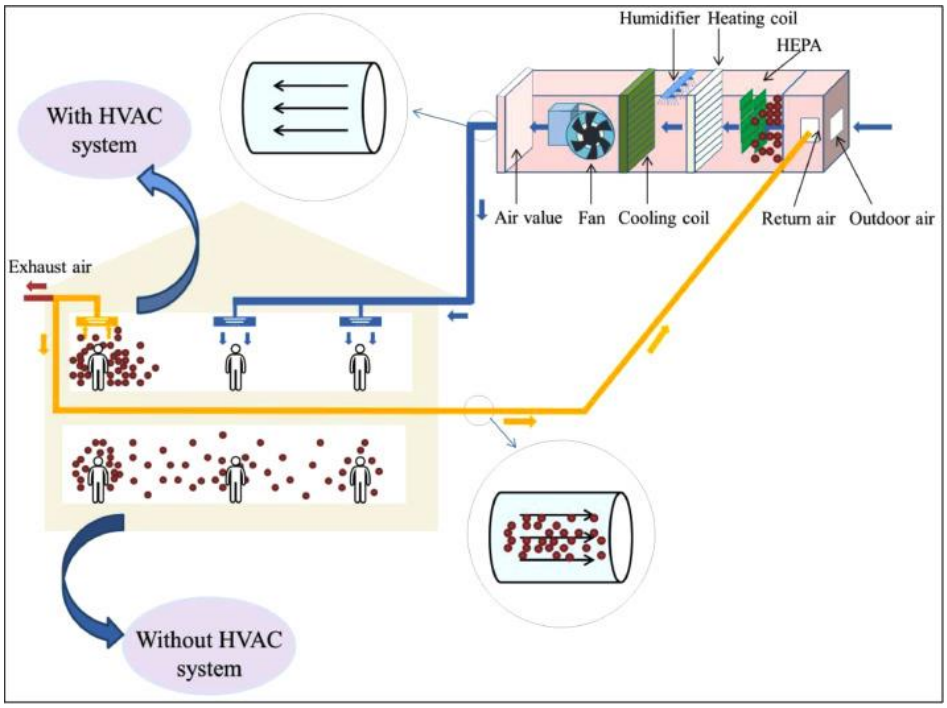

Figure 16: HVAC effect in controlling and preventing virus diffusion [96]

As an example microorganisms, trapped in high-efficiency particulate air (HEPA) filters, can survive for long periods [97].

For this reason, several approaches conferring antibacterial and antiviral properties to air filters have been developed, adding or doping materials with, antimicrobial agents.

Antimicrobial surfaces could be anti-biofouling, creating unfavorable conditions for bacteria to adhere and to grow on the surface, or could be bactericidal, and inhibit bacterial metabolism through chemical modifications or with the introduction of specific agents [98].

Recently, attention has shifted to conferring antimicrobial properties to air filters using green and eco-friendly methods. An example is represented by natural sea salt particles used to coat air purification systems. The antimicrobial activity against *S. epidermidis* and *E. coli* strains was evaluated and confirmed, but the amount of nanoparticles must be optimized to find a good balance between bactericidal effect and filtration performances [99]. Green particles with antibacterial effects were also obtained from plant extracts, from garlic, tea-tree oil, and rosemary [100]. These natural extracts behaved differently in contact with bacteria. Tea tree oil extract showed an inactivation and prolonged effect on both *E. coli* and *M. luteu*s, while garlic and rosemary extracts promoted cell growth, after an initial inactivation. Only the tea-tree oil inactivated *M. luteus*, when it coats air filters. Probably, microorganisms adapted to the antimicrobial mechanism of garlic and rosemary and so no effect is

exhibited, but all coated air filetrs inactivated S. aureus and K. pneumonia, as it is visible in Figure 17.

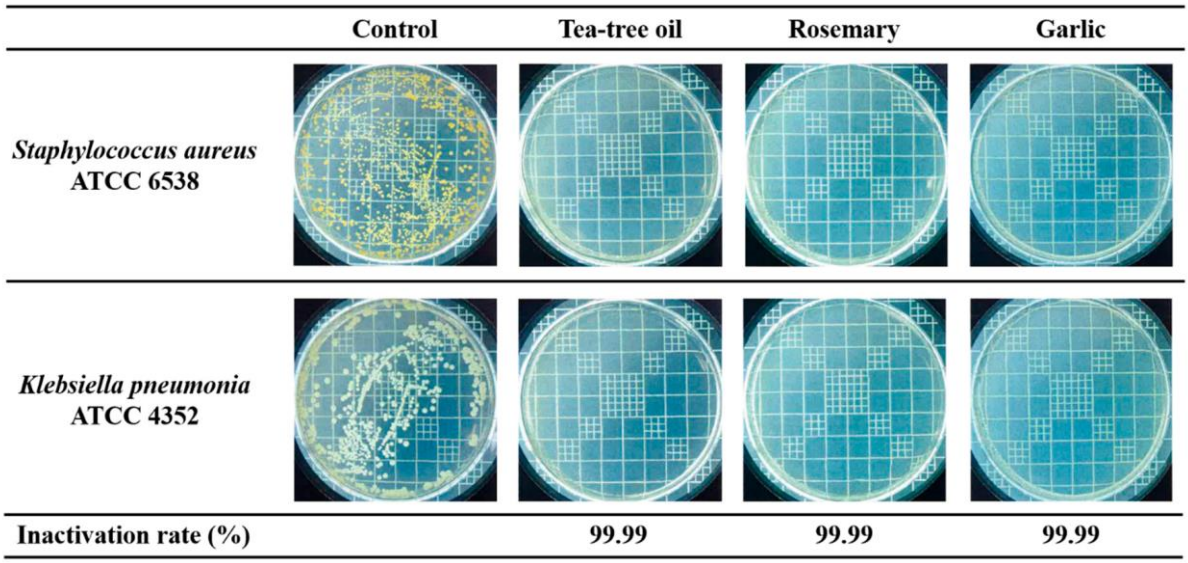

Figure 17: Inhibition of uncoated and plant-extract coated air filters against S. aureus and K. pneumonia [100]

As an alternative to natural agents, an environmentally friendly approach is represented by the synthesis of water-soluble copolymer with biocidal properties. The whole process was conducted in water and the polymer obtained in an aqueous solution was used to coat HEPA filters [95]. The antibacterial assays showed a strong effect, inhibiting Gram-positive and Gram-negative strains after a few minutes and the cytotoxic and permeability of air tests demonstrated that the so obtained filters have no risks for human health [101].

The use of silver nanoparticles and the exploitation of their strong bactericidal and virucidal effect relative to air filters is largely explored in literature. *Cruz-Pacheco et al*. [102] coated polyetheretherketone (PEEK) with one or two layers of AgNPs via a chemical reduction technique. Antibacterial tests towards *E. coli*, *S. marcescens, and B. licheniformis* confirmed the bactericidal effect dependent on the silver amount. Evaluating the diameter of inhibition zones, depicted in Table 1, it was observed that a low concentrated-Ag single layer did not show an inhibitory effect, but by increasing the silver amount and the number of films deposited, the effect became stronger [102].

Combining different techniques, nano-fibrous polyamide 6 was electrospun on polypropylene non-woven and impregnated with Ag nanoparticles. The so obtained system was composed of several layers, with nano-rough surface and high surface area, which improved the capacity to capture and inactivate viruses and bacteria. The filtration efficiency remained very high and excellent antibacterial and antiviral activity was exhibited against *E. coli, S. aureus,* and Porcine Delta-coronavirus PDCoV [103].

Table 1: Diameter of inhibition zones of silver nanoparticles films deposited on PEEK [102]

Sample	Diameter of Inhibition Zone (mm) ± SD		
	E. coli	*S. marcescens*	*B. licheniformis*
PEEK	0	0	0
PEEK/Ag0.04 – 1 Layer	0	0	0
PEEK/Ag0.08 – 1 Layer	1.1 ± 0.2	0	0
PEEK/Ag0.12 – 1 Layer	1.2 ± 0.2	0.6 ± 0.2	0.5 ± 0.1
PEEK/Ag0.04 – 2 Layer	1.2 ± 0.2	0.8 ± 0.2	0.5 ± 0.1
PEEK/Ag0.08 – 2 Layer	1.4 ± 0.1	0.9 ± 0.2	0.7 ± 0.1
PEEK/Ag0.12 – 2 Layer	2.7 ± 0.3	1.2 ± 0.3	1.0 ± 0.2

SD: standard deviation.

Another important aspect to be taken into account is related to the possibility to re-use the filter. Since the deposition of nanoparticles could hider the airflow through HEPA and make the systems less easily regenerable, AgNPs were immobilized on white-silica-gel beads (SiG) with one or more layers of chitosan as a stabilizer (AgNPs-[chi-SiG]) and used as a coating on acrylic glass for purification system. Results revealed that chitosan deposited on the substrate, chi-SiG, without silver nanoparticles, exhibited bacterial inhibition activity higher than that observed with AgNPs-[chi-SiG], against *S. aureus* and *E. coli*. This difference is likely attributed to the hydrophilicity of chitosan; when chitosan swells in water, the exploitation of its antibacterial effect is facilitated. Conversely, in the case of AgNPs, the hydrophobic nature of the system may reduce its effectiveness. The interaction between chitosan's amino groups and bacterial cell walls led to the rupture of the cell membrane and increased permeability, resulting in the leakage of intracellular components. Then SiG, chi-SiG granules, and AgNPs-[chi-SiG] were integrated into a real filtration system where airflow was simulated. Bacterial colonies of *B. subtilis* completely disappeared upon contact with AgNPs-immobilized filters, making the air clean, while some of them survived in contact with SiG and chi-SiG [104]. In addition, silver nanoparticles and chitosan have strong antiviral effects. *Mori et al.* [105], for example, demonstrated that the virucidal activity of Ag/chitosan composites against the H1N1 Influenza A virus was exclusively attributed to the presence of silver nanoclusters, while the chitosan matrix had the aim of preventing the dispersion of nanoparticles in the environment

Among the several materials that could be chosen to embed and incorporate silver nanoparticles, silica has attracted great attention. Recently, *Acharya et al.* [106] compared the effects of AgNPs and Ag-doped SiO_2 nanoparticles against various bacteria. The enhanced antibacterial effect of silver was due to the presence of a silica shell, for all the tested concentrations. As confirmed by the MIC test, the lowest concentration of core-shell nanoparticles was enough to obtain the same effect achieved with a higher amount of AgNPs. Considering the mechanism, no differences were evident between

the two types of nanoparticles, independent of the bacteria strain. Probably the main role was attributed to released ions as Ag doped-SiO_2 nanoparticles guaranteed a prolonged release of Ag^+ through the porous shell, but also the AgNPs themselves contributed to the antibacterial effect [106]. A strong antibacterial effect was also observed when SiO_2 nanoparticles were used as a shell for AgCl nanoparticles, as demonstrated by *Tan et al*. [107]. Due to silver and silica properties, systems composed of silver/silica nanoparticles were employed in the HVAC system to mitigate bacterial proliferation and inactivate viruses. The filtration quality was subjected to a decrement with increasing dust load, but the amount of Ag nanoparticles did not significantly affect filter performance, and the virucidal effect exhibited a similar trend.

Another study reports the effect of aerosolized SiO_2-Ag nanoparticles on air filters and subsequently dries them using a sheath air flow. With this approach, antiviral properties were imparted to the filters, demonstrating an efficiency of approximately 92%, and no significant variation in filtration performance was observed [108].

As an alternative to coatings, electrospun Polyvinylidene Fluoride/Silica, PVDF/SiO_2, solutions with silver nitrate as the precursor for AgNPs were used to produce PVDF/SiO_2/Ag composite nanofiber membranes. After bacteria exposure, *E. coli* colonies extensively contaminated bare PVDF nanofibers but the introduction of SiO_2 limited the bacteria growth around PVDF/SiO_2 composite nanofibers, but not in contact with them. The addition of silver significantly improved the antibacterial effect because of the complete absence of bacterial colonies. Conversely, *S. aureus* proliferation was inhibited only by the PVDF/SiO_2/Ag system. Analysis of filtration performance demonstrated that the developed system is capable of capturing fine particles in dust airflow without compromising permeability, maintaining excellent filtration performance in humid environments. Additionally, the system displayed superhydrophobicity and self-cleaning capacity, making it suitable for HEPA applications [109].

The co-sputtering technique was used to develop composite coatings for glass-fiber air filters. The thin films were made up of a silica matrix that embedded silver nanoclusters, guaranteeing ion released in a controlled and gradual manner. The antiviral tests were conducted against RSV, HRV, and FluVA, and revealed a strong virucidal effect against RSV and FluVa, with a reduction of two and three orders of magnitude if the titer, but no action against HRV was reported [62].

The same coating was deposited on facial masks (Figure 18) during the COVID pandemic period, and tested against the SARS-CoV-2 virus, showing excellent inhibitory effect on the viral replication phases. Silver nanoparticles incorporated in facial masks in different concentrations resulted efficient

in the inhibition of *E. coli* and *S. aureus*, and could prevent infections in places where high pathogenic microorganisms are highly present, such as hospitals [110].

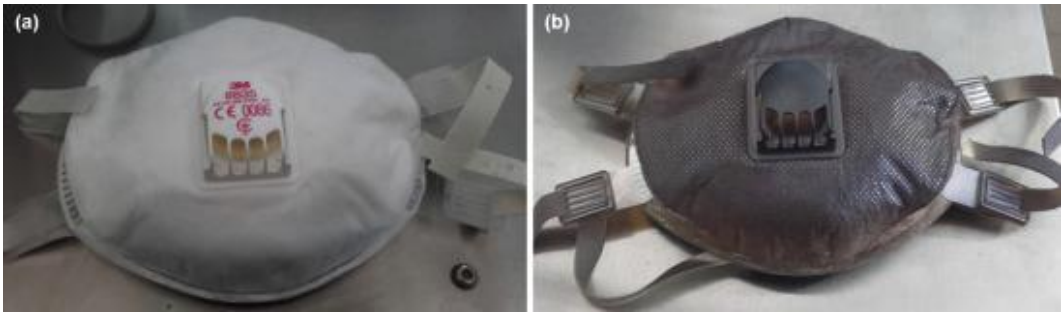

Figure 18: (a) uncoated and (b) silica/silver composite coated facial masks [65]

3.2. Application of antibacterial/antiviral coatings in water filtration systems

The presence of pollutants in surface water and wastewater represents a serious problem due to the toxicological effects they can have on human health and the environment. Unfortunately, the number of people without access to clean drinking water remains unacceptably high (approximately over 2 billion people) especially in developing countries according to UNICEF and WHO documents [111]. Global industrialization, urbanization, climate changes, and population growth have severe consequences on the availability of clean and safe water in some areas of Asia and Africa. It is estimated that many current diseases are transmitted through improperly purified and thus contaminated water [112][113]. The microorganisms can easily proliferate and spread, leading to a deterioration in water quality, corrosion phenomena, decreased energy efficiency, and above all, the growth and spread of pathogenic microorganisms that are dangerous for humans, animals, and the environment [114].

Recently, it has been demonstrated that drinking water from water pumps or cartridge filters used in household refrigerators is contaminated with various bacteria, such as *S. faecalis* or *E. coli* [115] [116]. Additionally, water also becomes contaminated with the passage through pipes, fittings, and faucets, further exacerbating the situation [115][117]. Groundwater can become contaminated due to pollutants present in the soil, which enter underground water bodies. Groundwaters mostly contain viruses, bacteria, and protozoa that can cause various diseases in humans or harm the environment [118]. In addition, the use of fertilizers, pesticides, and herbicides, which reach water bodies through rain or flooding, contributes to contamination. For example, some nitrogen-rich fertilizers cause a drastic decrease in oxygen in rivers, lakes, and coastal areas, leading to severe problems for fauna [119] [120].

Air pollutants also easily contaminate aquifers, as they are readily transported by rain. Most water treatment systems often have limitations. Generally, the most commonly used ones involve the use of chemical disinfectants such as chlorine and ozone, recognized as potentially carcinogenic, and produce waste by-products during water treatment [121]. Moreover, these substances are difficult to recycle and reuse. The UV-based methods for water disinfection have high costs and require energy, in addition to dangerous byproducts formed [122].

This led to the need for new strategies for the development of safe systems, capable of filtering and purifying water from bacteria, fungi, and viruses, without introducing risks to humans and the environment.

Metals, in the form of coating or nanoparticles, are widely involved also in these applications. Thin layers of different metals, including silver, copper, and aluminum, deposited on water filter paper through the DC magnetron sputtering method, showed good coverage and excellent adhesion with no delamination effect and without affecting filter flexibility. The efficiency of these metallic coatings was tested in the inactivation of *E. coli* and total coliforms. The titanium-coated filter did not exhibit an antibacterial effect, similar to the uncoated filter. Zirconium and aluminum layers demonstrated a low bactericidal effect, whereas copper and silver coatings showed the best performances. Coatings with thicknesses of 30 nm and 300 nm had the same efficacy in killing bacteria, confirming that a thin film is sufficient for a strong antibacterial effect. Combinations of Cu and Ag metals also demonstrated a high bactericidal effect, comparable with that of copper, which remained unaltered after consecutive exposures to bacteria [123].

As already said for the air filters, nanomaterials offer a promising approach for the production of next-generation water filters. In a study, cutting liquid was filtered using AgNPs-coated and uncoated polypropylene membranes. The filtered liquids were collected in agar plates. The colonies grew more numerous on the agar-containing liquids filtered by a bare membrane, compared with the liquid after the passage through an AgNPs-coated filter [124].

Poly(ether sulfone), PES, is another material used for water filtration, coated with AgNPs using an in situ photoreduction method [118]. This study aimed to reduce the formation of biofouling and the risk of spreading infectious diseases, particularly after activities such as washing, bathing, or food preparation. Analysis of the released silver ions indicated that the maximum concentration reached after 720 hours was below the levels reported for water treated with silver, which is 50 µg/L [125]. The AgNPs-coated PES filter demonstrated a strong antibacterial effect against *E. coli* following exposure to UV for 20 minutes. The same samples were incubated in water for one month to assess the long-lasting antibacterial effect, and tested at different times. Figure 19 revealed that coatings still

exhibited bactericidal effects after 4, 8, 12, 24, 48, 72, 504, and 720 hours, demonstrated by the halos around all the samples, which had different diameters [126].

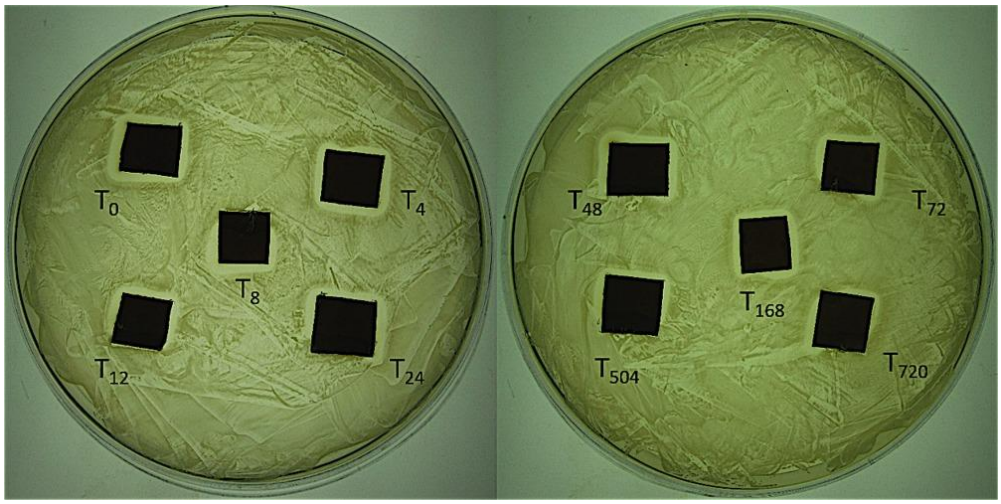

Figure 19: Inhibition halo test against E. coli on silver-coated filters after incubation in water at different times [126]

In recent work, biosynthesized AgNPs were impregnated into ceramic water filters using 3-aminopropyltriethoxysilane, APTES, as a coupling agent. The correlation between efficacy and silver nanoparticle concentrations was noticed towards both Gram-positive and Gram-negative bacterial strains, with greater effectiveness observed against Gram-positive strains. A flow test demonstrated that the untreated filter removed 99% of bacterial contamination, due to pore size, with only a small minority of bacteria able to pass through. The presence of even a small amount of bacteria that could potentially form a biofilm on the filter surfaces underscores the importance of ensuring the complete removal of bacteria from the water filtration system. This highlights the essential role of silver nanoparticles in achieving a 100% removal of bacteria and effectively disinfecting the filter, thereby enhancing its performance and preventing any potential secondary contamination of the water supply. To determine the stability of AgNPS, filters were washed under ultrasonic irradiation for 30 min, and Inductively Coupled Plasma Mass Spectrometer, ICP-MS spectra showed that a very small amount of silver passes in water, guaranteeing unaltered bactericidal efficacy. An ultrafiltration pretreatment was performed for 3 months, and the amount of silver lost was below the acceptable threshold [127]. A commercial water filter, called Nexar^{TM}, demonstrated to be antifouling and antibacterial through negative surface charge, acidity, and hydrophobicity. Nexar^{TM} is a pentablock-sulfonated copolymer, s-PBC, deposited on polypropylene, PP, which does not exhibit any antibacterial effect towards *P. aeruginosa*, in dry conditions. However, the addition and the diffusion of only 0.2 mL of water into the material increases the inhibitory effect of the coated samples (Figure 20). With an increment in the amount of water, the bactericidal efficacy increased as well. Since s-PBC is hydrophobic and highly acidic, contact with water reduces the pH, reaching values crucial for bacteria survival [128].

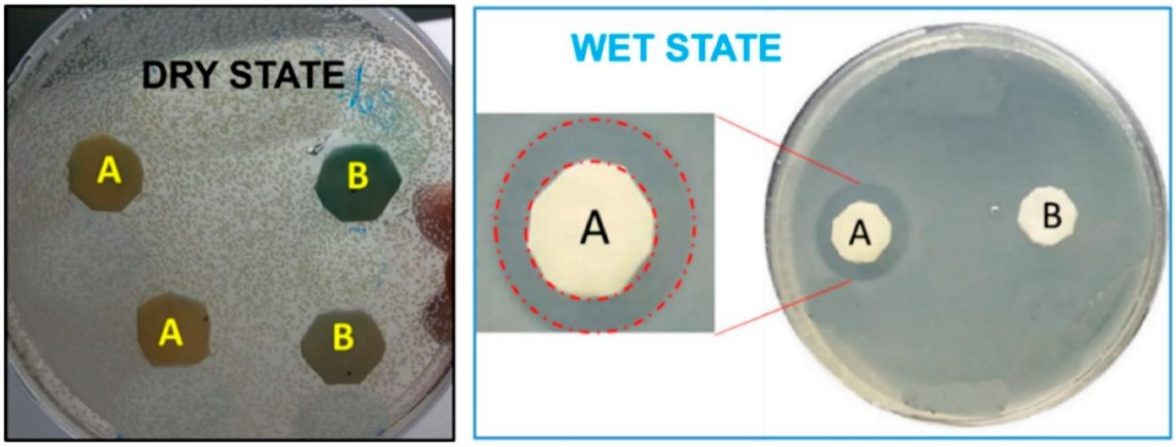

Figure 20: Inhibition halo test on (A) PBC deposited on PP, and (B) uncoated PP in dry conditions (left) and adding 0.2 mL of water (right) [128]

A reusable system for water purification was developed using TiO_2 particles, treated with 3-Aminopropyltriethoxysilane, APTES, or Hexadecyltrimethoxysilane, HDTMS. Using this system, the number of *E. coli* was drastically reduced after 2 h of exposure and this filter could be used more than 150 times thanks to photocatalytic effect [129].

Another effective method for water decontamination is represented by the use of hollow microspheres. Poly(methylmethacrylate) microspheres, PMMA, and Ag-coated PMMA microspheres were obtained and tested against Gram-positive *Bacillus subtilis* and Gram-negative *E. coli* strains [122]. Coated PMMA microspheres were efficient also in a low concentration, 2mg, with a reduction of approximately 94% for both studied bacterial strains, reaching a complete reduction at a concentration of 8 mg. In this case, the material was more efficient against *E. coli*. To simulate real environment conditions, water with a high concentration of bacteria was forced to pass through a pen shell filter column, obtaining completely bacteria-free water in the case of Ag-coated PMMA. It has also been demonstrated that this system can be used for five consecutive experiments without losing effectiveness. After this, at the sixth test, a slight decrease in performance due to system saturation was noticed, the the initial conditions were obtained again after a counter-wash [130].

3.3. Application of antibacterial/antiviral coatings on fabrics

An important field in which antimicrobial and antiviral coating find large applications is the textile industry. Textile materials could be involved in the medical field, or everyday life, in technical clothing or shoes, where microbial colonization could be promoted by particular conditions such as humidity, and cause transmission of infectious diseases, in addition to changes in color and odor [131] [132][133].

Cotton is well known as a natural, low-cost cellulose fiber with excellent mechanical properties such as high strength, a soft feel, good biocompatibility, and biodegradability. These qualities make it suitable for numerous applications, and in biomedical fields, it is used in particular as medical dressings or gauze for wound healing [134][135][136]. However, because of its porous structure, the presence of a hydrophilic group, and its moisture affinity, cotton represents an optimal environment for bacteria and microorganisms to grow and survive for a long time. Bacterial proliferation could be promoted and accelerated by specific conditions of temperature, pH, and moisture, and the consequences could be the breakdown of the fibers and the hydrolysis of the cellulose, resulting in a deterioration of the fabric [136][137][138].

Different strategies were adopted to prevent bacterial replication on cotton surfaces and to exploit its features. For its use for wound healing, in a recent study, cotton was coated with AgNPS functionalized with antibiotic and anti-inflammatory drugs by a one-step method. Thanks to the enzymatic cleavage of the amide bonds, drugs were released *in situ*, and the bactericidal and anti-inflammatory activity was not affected. This system was developed for medical gauzes, to avoid infectious and promote wound healing [135].

Another technique involved functionalized silica nanoparticles incorporating quaternary ammonium salt (QAS) for obtaining a superhydrophobic and antibacterial coating on cotton fabric. The antibacterial efficacy was assessed both before and after multiple washing cycles. Polydopamine, PDA, was used to improve the adhesive bond between the nanoparticles and the cotton surface. Untreated samples and cotton coated solely with PDA demonstrated negligible antibacterial activity. However, cotton samples functionalized with silica exhibited strong bactericidal effects, resulting in a remarkable reduction of approximately 99.8% in the growth of both *E. coli* and *S. aureus*. This antibacterial effect remained strong even after 30 washing cycles, with a slight reduction to 96.2% attributed to the minimal loss of silica NPs during the washing process. Furthermore, the presence of functionalized silica nanoparticles notably enhanced the hydrophobicity of the cotton fabric. While the application of PDA increased the contact angle compared to uncoated cotton, it did not achieve the threshold for superhydrophobicity observed with the addition of functionalized silica nanoparticles [139].

An alternative environmentally friendly approach for incorporating antibacterial agents into cotton entails the application of chitosan nanofibers loaded with silver phosphate nanoparticles as a coating. Among the various properties enhanced by these coatings, water absorption stands out. While uncoated cotton fabric exhibits hydrophilic behavior, the presence of chitosan nanofibers, especially when loaded with silver nanoparticles, increases water absorption due to the abundance of hydroxyl

and amine groups in the chitosan structure and the hydroxyl groups of Ag_3PO_4. The antibacterial efficacy was tested against *S. aureus* and *E. coli*, demonstrating antibacterial activity with both the as-synthesized Ag_3PO_4 nanoparticles and the chitosan nanofiber coating. However, it was observed that the antibacterial effect was enhanced if using the hybrid system (Figure 21). Even after 5 and 10 successive washing cycles, the bactericidal properties remained robust, attributed to the strong adherence of nanoparticles to the chitosan coating, thus ensuring durability [140].

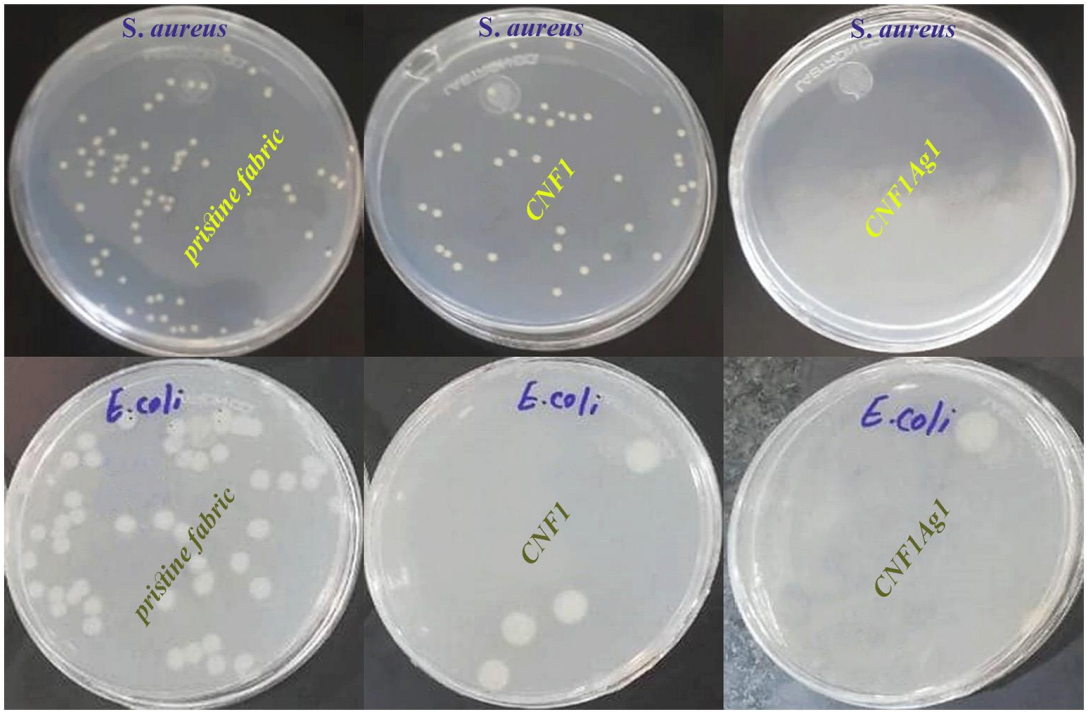

Figure 21: Bacterial growth of S. aureus and E. coli in the presence of pristine fabric, fabric coated with chitosan nanofibers, and fabric coated hybrid system with silver and chitosan nanofiber

In a recent study, researchers aimed to address the issue of cotton's high inflammability while enhancing both thermal stability and microbicidal activity. To achieve this goal, coatings were developed with combined antibacterial effects and flame retardancy, using nano chitosan and polyvinyl alcohol, PVA, supplemented with melamine phosphate. This coating prevented flame propagation in both horizontal and vertical directions, and enhanced bactericidal activity against both Gram-positive and Gram-negative bacteria, resulting in a significant zone of inhibition. Moreover, the presence of the coating improved other important properties such as wettability, tensile strength, and air permeability [141].

A nanocomposite comprising graphene oxide (GO) with silver nanoparticles deposited on cotton textiles for medical applications was used to investigate the antibacterial mechanism. When evaluating the effect on *P. aeruginosa* growth, it became evident that the combination of silver and

graphene oxide enhanced the effect, resulting in a larger inhibition zone, compared with that of bare AgNPs. Further analysis of the interaction between bacteria and nanomaterials using TEM (Figure 22) revealed that silver nanoparticles, indicated by the white arrows, were in direct contact with bacterial cells, while graphene oxide, formed a substantial platform, blending in the point indicated by the black arrows, on which bacterial colonies were placed. The synergistic effect of the combined GO-AgNPs system is attributed to graphene oxide's ability to envelop bacterial colonies, ensuring direct contact between silver nanoparticles and bacteria [142].

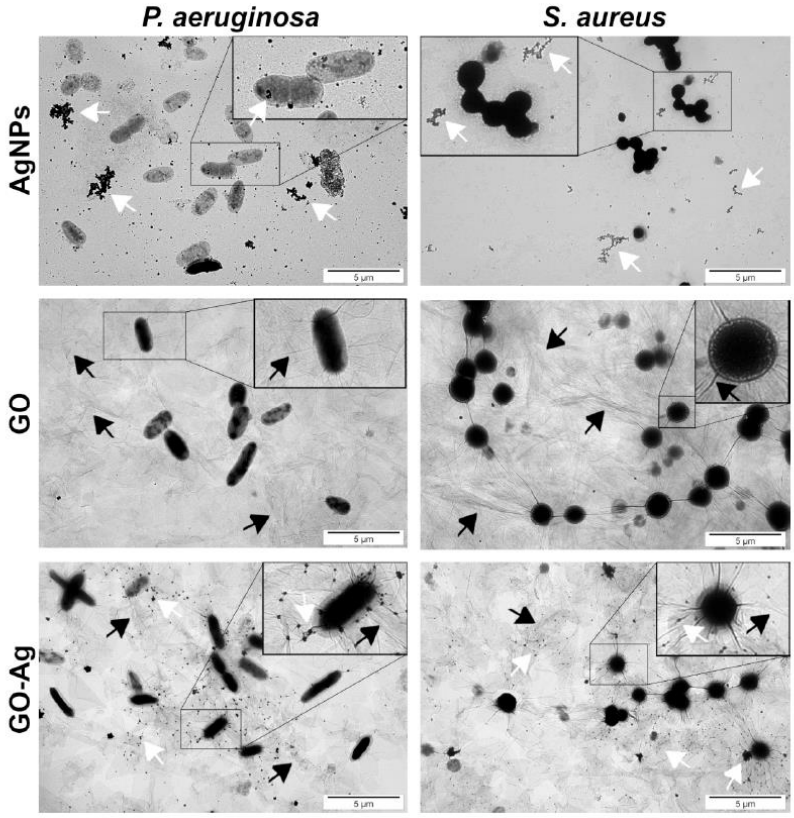

Figure 22: TEM analysis of bacteria interacting with silver nanoparticles (AgNPs), graphene oxide (GO), and graphene oxide with silver (GO-Ag) [142]

Another material commonly encountered in everyday life and often in contact with the skin is leather, which is utilized in the production of clothing, shoes, and various accessories. Its widespread use in the fashion industry is attributed to its softness, breathability, and high moisture-absorbing capacity. However, this moisture-absorbent property also serves as a nutrient source for the growth of bacteria and fungi on leather goods [143] [144]. A method to confer biocidal activity is the modification of leather with bio-synthetized AgNPs through immersion technique. The results highlighted a color change, becoming darker with an increase in silver nanoparticles, but also more strong against bacteria, *S. aureus* and *E. coli*, and fungi *C. albicans*. Physical-chemical properties were not affected by the antibacterial treatment [145]. Thin layers of silver and silver oxide were deposited on leather

using DC magnetron sputtering technology with the aim of creating antibacterial interiors and insoles for footwear to reduce infections and diabetic foot pathologies [138]. These coatings, of about 1-1.3 μm in thickness, did not block fabric pores, and increased surface roughness, thereby modifying the morphological appearance of the leather. As a result, the coefficient of friction was higher compared to that of untreated leather, with the best results achieved with the oxide layer, limiting micro-movements and preventing wound formations. Evaluation of the antibacterial behavior showed that the modified leathers were effective in inhibiting *S. aureus* and *C. parapsilosis*, in addition to a strong antifungal effect. AgO_x coatings exhibited a higher oxidation rate compared to Ag coatings, allowing them to easily release ions and confer an antibacterial effect [146].

In addition to the bactericidal properties, the action against SARS-COV-2 was evaluated on SiO2-Ag coating deposited on white bovine leather. The coating modified surface fabric, increased roughness, improved water repellency, and was effective in eliminating pathogens. Data showed that SiO_2-Ag coatings reduced *S. aureus* at 99,99% after 24h, and the same rate was observed after 10 washing cycles. SARS-CoV-2 was impressed inactivated, with a reduction of 56.38% and 99.93% after 15 and 30 min of contact [147]. *S. aureus* was also inhibited by coatings based on silica obtained by volcanic ash and silver nanoparticles as bactericidal agents [148].

An alternative approach involves the synthesis of hybrid nanocomposite xerogels, obtained through silica gelation and dispersion of silver nanoparticles. The properties conferred include antibacterial protection, tested against Gram-positive and Gram-negative bacterial strains such as *S. aureus*, *E. coli*, and *P. aeruginosa*, antiviral protection against the SARS-CoV-2 virus, and anti-biofilm activity [149].

4. Antibacterial effect of copper and zinc oxide nanoparticles

Among the other nanomaterials used as antibacterial and antiviral agents, copper and zinc oxide nanoparticles could be mentioned for their good antimicrobial efficacy. It was demonstrated that copper nanoparticles can inhibit a huge spectrum of bacteria when interacting with cell walls. The proposed mechanism is related to ions released by nanoparticles, that cause bacterial protein damage and generate reactive hydroxyl radical, with consequences on DNA, proteins, and enzymes and the consequent destruction of bacterial membrane [150][151].

In addition, also zinc oxide nanoparticles are used in numerous areas due to their ability to control and reduce microbial growth. ZnO has the advantage of being more biocompatible than other nanomaterials, and it is resistant to heat. The mechanism by which zinc nanoparticles exhibit their antimicrobial power is similar to previous cases, involving the generation of ROS, the release of ions, and the destruction of cell membranes, compromising the vital function of microorganisms [152].

Cu NPs synthesized in the presence of *Allium Eriophyllum* leaf extract exhibited efficacy against Gram-positive and Gram-negative bacteria, in particular, *S. aureus*, *B. subtilis*, *E. coli*, and *P. aeruginosa*, in addition to fungi Candida species, such as *C. guilliermondii*, *C. krusei*, *C. glabrata*, and *C. albicans*. Interestingly, their bactericidal and antifungal activity was better than that exhibited by the antibiotic tested [153]. Copper nanoparticles obtained by extract of *Calotropis gigantea* confirmed the efficacy in inhibiting *E.coli*, *S. aureus*, *K. pneumoniae*, and methicillin-resistant *S. aureus*, MRSA bacterial strains [154].

The unique physical and chemical characteristics of CuNPs are often exploited in antibacterial and virucidal coatings, which find applications in several fields. Recently, PET filters used for facial masks were coated with copper after an ion beam treatment to enhance the adhesion between the coating and the surface and to prevent humans from inhaling it. The coated filters showed strong inhibition activity against *S. aureus, K. pneumoniae, E. coli,* and *P. aeruginosa*, and also inactivated SARS-CoV-2 by approximately 98%, as shown in Figure 23 [155].

For the same purpose, CuNPs were immobilized in a poly(acrylic acid) (PAA) layer, used for functionalization on polypropylene nonwoven fabrics for surgical masks. With the impregnation of CuNPs, the hydrophobicity of the mask increased, making it a physical barrier against viral infections, which is crucial since respiratory diseases spread through droplets or aerosols. The level of protection against viruses of coated masks is higher compared to uncoated ones, even though the presence of a layer with metal NPs decreased the mask porosity, resulting in a slight reduction in breathability. In any case, the masks remained comfortable. Antibacterial tests revealed that coated filters can inhibit

the growth of Gram-positive and Gram-negative bacteria, in contrast with the lack of bactericidal activity of uncoated samples. The antibacterial effect did not change if the samples underwent sterilization processes through UV or autoclaving, or if they were washed. A strong antiviral effect is shown against SARS-COV-2 within 3 hours, even after washing and rinsing cycles [156].

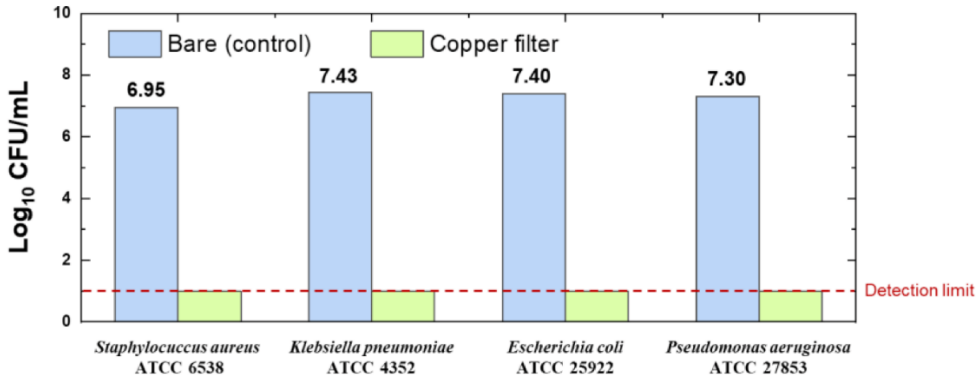

Figure 23: Uncoated (control) and copper-coated filters activity against S. aureus, K. pneumoniae, E. coli, and P. aeruginosa [155]

Strong copper antiviral properties are well-known, and it is often used in oxide forms and particle shapes. Air filters for cars were sonochemically coated with CuO NPs, exploiting a method that is cheap, green, and could be employed on an industrial scale. They showed strong antibacterial activity inactivating *E. coli* and *S. aureus* after 2 h of exposure, and a reduction of about 99% of SARS-CoV-2 and about 96% of H1N1 influenza and mutant coronavirus. The impregnation of CuO particles did not affect the dust-holding capacity of the filters and no difference in pressure loss was found [157].

An alternative, fast, and effective method to incorporate Cu into coatings, enhancing their antimicrobial activity, is to combine the sputtering technique with heat treatments. For example, it is possible to obtain a TiO_2/CuO coating on titanium by starting with a sputtering process of a metallic titanium target containing pure copper wires. The thin film obtained in TiCu underwent an annealing process to obtain TiO_2 and CuO. The resulting film demonstrated bactericidal activity of 99%, unlike pure Ti and TiO_2, which exhibit poor antibacterial activity. The presence of CuO in the coating improved the biocompatibility, corrosion resistance, and bactericidal activity of pure Ti and TiO_2 [158]. With the same aim, *Sunghoon Jung et al.* [90] deposited on a PP filter a thin copper film, in order to not compromise the filtration efficiency of the facial masks but to inactivate viruses that remained on the fiber surface. To enhance the adhesion between the film/surface, an oxygen ion beam surface treatment was performed. The filter exhibited a virucidal effect against the SARS-CoV-2

virus. Since it is well known that copper oxide is effective against influenza A, the possible oxidation of the superficial layer, due to moisture or oxygen, probably didn't compromise the antiviral effect.

Due to their ability to promote the proliferation of osteoblasts, zinc oxide nanoparticles are frequently used for medical applications, such as antibacterial agents in hydroxyapatite coatings, obtained through precipitation, and deposited on Ti substrates. Their ability to kill bacteria has been demonstrated against *S. epidermidis* and *E. coli*, compared to hydroxyapatite without zinc. After 4 hours of incubation, the number of bacterial colonies had significantly decreased compared to that observed for non-ZnO-doped coatings. The antibacterial effect likely depends on both ion release and direct contact with the nanoparticles [159]. ZnO nanoparticles were also deposited on hydroxyapatite tablets using the sputtering technology, obtaining a uniform distribution of crystalline nanoparticles, in a size between 1 and 3 μm. The bactericidal effect against *E. coli*, was confirmed, suggesting that the mechanism included the interaction of ZnO NPs to cell membrane and the production of ROS. In addition, the increased roughness prevented the formation of biofilm [160].

T. S.Roy et al. [161], developed Zn oxide nanoparticles cotton coated, to be used for bactericidal and antifungal activity. Modifying nanoparticle concentration, they found that aggregates formed for low concentrations with no homogenous distribution, while increasing the concentration better results were found in terms of nanoparticle adhesion on cotton and distribution. The antifungal activity was tested against *A. niger*, while the antibacterial effect against *S. aureus* and *E. coli*. The presence of the coating conferred a microbiocidal effect in all the cases, as a function of concentration.

In another interesting work, superhydrophobic ZnO coatings were used to exploit its behavior against water, which is enhanced by the micro and nanostructure obtained after coating deposition. Both the hydrophobic surface and bactericidal effect of ZnO drastically reduced *S. aureus* colonies [162].

Recently copper/zinc oxide nanocomposite was sputtered on bacterial cellulose, a material that in recent years has been used as substrate for porous aerogel nanocomposites thanks to its high porosity, crystallinity, and excellent mechanical and physical features, but that does not exhibit antibacterial activity. On the contrary, *E. coli* and *S. aureus* proliferation was reduced by about 96-98%, in the presence of coating, while pure bacterial cellulose did not exhibit this property [163].

Copper oxide and zinc oxide nanoparticles synthesized in water or ethanol were deposited on cotton for the bandage, showed in Figure 24, and the antibacterial effect and the influence of the solvent on coating behavior were assessed. Bandages coated with CuO particles obtained in both water and ethanol completely eradicated *S. aureus* and *E. coli* after 30 minutes, while those coated with zinc oxide particles reduced bacterial viability by 5 logarithms. Studies on the nanotoxicity of the two

coatings reveal that nanoparticles synthesized in water are safer and have less impact on embryo development compared to those obtained in ethanol [164].

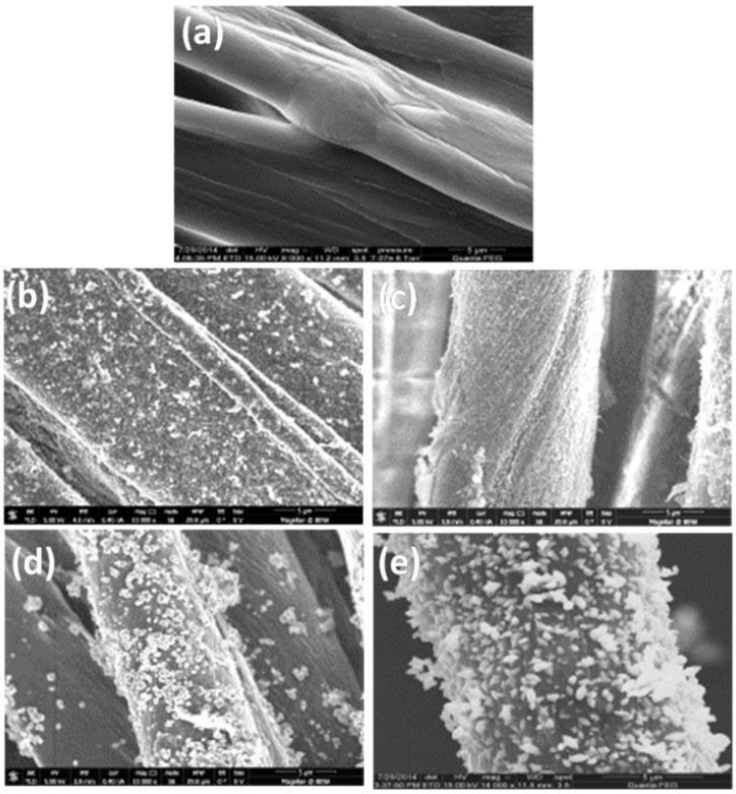

Figure 24: FESEM image of (a) uncoated cotton, cotton coated with (b) CuO and (c) ZnO NPs in ethanol, cotton coated with (d) CuO and (e) ZnO NPs in water [164]

With the aim of surface-modifying porous filter materials like face masks, nanoparticle coatings of silver, copper oxide, and zinc oxide were achieved by aerosol self-assembly and evaluated for their efficacy against SARS-CoV-2. Silver coating emerged as the most effective, reducing viral load by 98% within minutes. Moderate activity was demonstrated by copper oxide nanoparticles, with around a 75% reduction, while zinc oxide showed no apparent effects in its interaction with the virus [165].

5. Composite coatings derived from pre-ceramic polymers

In literature, several works about the development of antibacterial and antiviral SiO_2-Ag systems were published, which involved different techniques and materials, such as rice husk silica sols and silver nitrate as silica and silvers precursors respectively [166], or involving sol-gel methods [167], just to mention some example.

An alternative method for developing ceramic coatings involves using inorganic precursors and pre-ceramic polymers, commonly employed to synthesize thin silica films through hydrolysis or oxidation [168]. Among pre-ceramic polymers, Perhydropolysilazane, PHPS, has attracted research interest for the synthesis of compounds such as silicon-nitride or silicon-carbide. PHPS is a polymer in which [-SiH2-NH-SiH2-] units repeat. The reaction (Figure 25) with atmospheric moisture causes the hydrolyzation of the Si-H and Si-NH bonds, and the silanol group is formed as an intermediate, then condensation and cross-linking lead to Si-O bonds, creating the typical structure of silica [169].

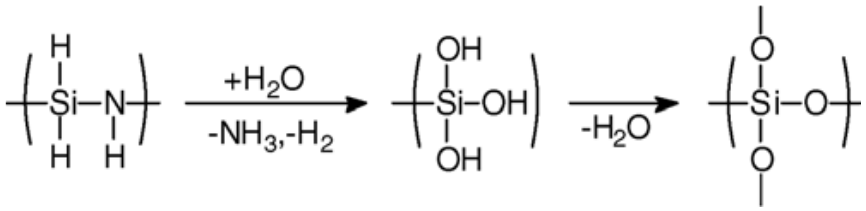

Figure 25: Reaction of PHPS to water and its transformation into silica [170]

In some studies, thin silica films have been obtained after thermal treatment at 450°C [171], but this high temperature limits their potential applications. Recently, *Wen-Yue Wanga* et al. [172] attempted to synthesize silica coating at low temperatures for application on thermal-sensitive substrates. They used (3-aminopropyl)triethoxysilane, APTES, as a catalyst, converting the polymer into silica within 10 min at 80°C and with 90% humidity. The transition to silica structure was confirmed by the FTIR spectrum (Figure 26), which showed a decrease in intensity of Si—H, and Si—N absorption bands, and the appearance of a pick attributed to Si-OH appears at 950 cm^{-1}. The effect of temperature and humidity was evaluated, demonstrating that higher values of both parameters resulted in a higher conversion rate. The increased diffusion coefficient and humidity facilitated more water molecules to penetrate the coating, leading to increased hydrolysis of Si-H and Si-N bonds, promoting condensation reactions and Si-O bond formation. The use of APTES also improved mechanical properties, such as elastic modulus and hardness [172].

However, it has been observed that exposure to excimer light or ultraviolet ray irradiation enables the formation of compact layers and can be influenced by temperature. Specifically, irradiation at 100°C, a much lower temperature than that of the typical thermal treatment, allows for the formation of a

dense layer, smoothing out surface irregularities during the transformation [173]. Other techniques were investigated, for example, vacuum ultraviolet VUV irradiation [174], but an inhomogeneous layer was obtained, in a strict control on oxygen and temperature; or the exposure to aqueous ammonia vapor [175], which requires long processing time and led to film chemically unstable. Good results were found using intense pulsed UV light. The properties of the obtained films vary with the intensity of the irradiation energy. It was possible to achieve a silica layer thickness of 160 nm with a 100% conversion, similar to that treated thermally at 600°C. Properties such as refractive index and hydrophilicity comparable to amorphous silica were obtained, along with excellent values of hardness, abrasion resistance, and elastic modulus. The advantages of this technique are not requiring high temperatures for thermal treatment, no need for gas control equipment, and obtaining thin, flexible films in a short time [176].

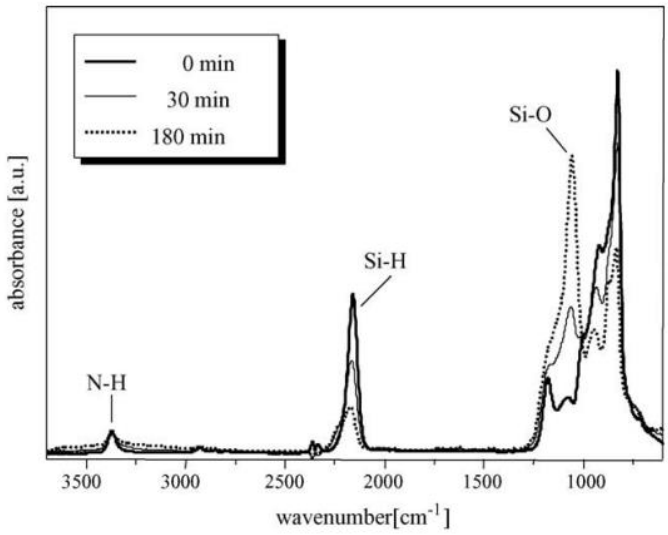

Figure 26: FT-IR spectra of PHPS to silica transition at 50°C, 90% humidity [170]

The evaluation of silica structure layers derived from the deposition of PHPS on different substrates, Si, Al_2O_3, PVA, and MgO was studied. FT-IR spectroscopic analysis indicated that in all cases, the molecular structure obtained was SiO_2. All synthesized layers exhibited uniform density, lower than that of natural silica. This suggests that during condensation, nano-air holes form both on the surface and within. Interestingly, the density of the synthesized material was found to depend on the substrate, particularly its acidity. Since PHPS reacts with -OH groups, an increase in density has been noted with a decreasing acid dissociation constant [168].

Among the various advantages of using PHPS coatings, are homogeneity, low tendency for crack formation, and shrinkage during polymerization. This is due to the increase in molecular weight

during the transformation into silica through reaction with air and moisture, resulting in good ceramic yield [177].

The potential applications are several. In a study, for instance, the transition from PHPS to silica was leveraged to create a barrier film and encapsulate organic electronic devices that can degrade upon contact with oxygen or water vapor. The transition into silica layers was achieved through UV irradiation, and to ensure flexibility, the PHPS layers were alternated with organic polymers [177].

Over the years, various efforts have been undertaken to develop nanocomposites derived from polymeric precursors with metal nanoparticles. Early studies involved the direct mixing of preceramic polymer with metal oxides or its powder, followed by controlled thermolysis under controlled atmospheres, However, this approach often resulted in non-uniform distribution and agglomeration of nanoparticles.

To address these issues, attempts have been made to achieve *in situ* formation of NPs using metallopolymers, which pyrolyze at low temperatures. However, many of these are toxic and require very harsh reaction conditions. Nanocomposites of SiOCN containing Ni nanoparticles were synthesized *in situ* by reacting Ni(Ac)2·4H2O with PHPS and poly(vinyl)silazane (Durazane 1800). The obtained nanoparticles remained stable after treatment at 700°C, but at higher temperatures, they reacted with the SiOCN matrix. The materials obtained by pyrolysis of PHPS exhibit a dense, non-porous structure, with nanoparticles of an average size of 2.5 nm [178].

Hydrophobized indium tin oxide (ITO) nanoparticles, measuring 10 nm in size, were synthesized through a liquid-phase process and dispersed in PHPS, used as a precursor for obtaining silica. The transformation of the ceramic polymer precursor into silica occurred completely through exposure to vapors from an aqueous ammonia solution. The hardness of the obtained coating is comparable to that of pure silica films, allowing for automotive glass applications [179].

6. Materials and Methods

6.1. Deposition of coatings via the co-sputtering technique

This research aims to develop and investigate the antimicrobial properties of composite coatings composed of ceramic/glass matrix, containing silver nanoparticles/nanoclusters distributed in it. These coatings are intended for applications in several fields and the final products can be employed in a wide range of sectors. However, the appropriate deposition technology must be selected according to the requirements and needs.
In this work, the radio frequency (RF) co-sputtering technique was used, since it has numerous advantages, making it suitable for the applications and purposes of this study.
Several coating compositions have been explored, selecting the material which constitutes the matrix between silica and zirconia, and adjusting process parameters according to the requirements of the final application. Mainly, silver has been used as an antimicrobial agent, but a preliminary study on the use of copper and zinc nanoparticles will be presented here. Investigations in terms of chemical, physical, and morphological features, as well as antibacterial properties were performed.

6.1.1. Coatings containing silver nanoclusters

The studied composite coatings, composed of silica or zirconia as a matrix, and silver nanoclusters as the antimicrobial agent, were deposited through the co-sputtering technique. The equipment used was the Microcoat™ MS450 system.

The coatings were deposited by applying constant powers to the matrix targets, in particular, 200 W in RF mode for the silica target (Franco Corradi S.r.l. 99.9% purity, 3 inches in diameter) and 250W in RF mode for the zirconia one (Nanovision™, 99.98% purity, 3 inches in diameter). However, powers between 3 and 5 W in DC mode on the silver target (Sigma–Aldrich 99.99% purity, 3 inches in diameter) were applied, to obtain nanoclusters in the required sizes and quantities, according to the final purpose or application field. The variation of power within this range results in slight changes in the quantity of Ag nanoclusters in the coating, which affects its color and properties. For all the coatings studied in this work, deposition occurred in a pure argon (Ar) atmosphere at a pressure of 5.5 dPa. Deposition time was modulated from a few minutes to one hour, according to the intended final applications.
The obtained coatings were very thin, less than 200 nm, depending on time deposition, in addition, they were flexible and well adherent to substrates.

Table 2 and Table 3 summarize the parameters set during the process, in particular, the power to Ag target and the deposition time, for SiO_2-based coatings and ZrO_2-based coatings respectively, and the related acronym used in the discussion of the results. The coating name is made up of matrix_power applied to silver target_deposition time. In cases where the time is not specified, a one-hour deposition process was performed for coating.

Table 2: Process parameters set and acronyms of silica/silver composite coatings

SiO2_Ag coatings				
Power to Ag target	**5 min**	**10 min**	**30 min**	**60 min**
1W	*/*	*/*	*SiO2_Ag1_30*	*SiO2_Ag1_60*
2W	*/*	*/*	*SiO2_Ag2_30*	*SiO2_Ag2_60*
3W	*/*	*/*	*/*	*SiO2_Ag3*
4W	*SiO2_Ag4_5*	*SiO2_Ag4_10*	*SiO2_Ag4_30*	*SiO2_Ag4*
5W	*/*	*/*	*SiO2_Ag5_30*	*SiO2_Ag5*

Table 3: Process parameters set and acronyms of zirconia/silver composite coatings

ZrO2_Ag coatings				
Power to Ag target	**10 min**	**20 min**	**30 min**	**60 min**
1W	*/*	*/*	*ZrO2_Ag1_30*	*ZrO2_Ag1_60*
2W	*/*	*/*	*ZrO2_Ag2_30*	*ZrO2_Ag2_60*
4W	*ZrO2_Ag4_10*	*ZrO2_Ag4_20*	*ZrO2_Ag4_30*	*ZrO2_Ag4*
5W	*/*	*/*	*/*	*ZrO2_Ag5*

6.1.2. Coatings containing copper or zinc nanoclusters

Composite coatings containing copper or zinc nanoparticles embedded in silica matrix were studied, to evaluate alternatives to silver nanoclusters as antibacterial agents. In this case, only SiO_2 was used as a matrix, and the power applied to the SiO_2 target was 200 W, while powers in the range of 5W and 30W were applied to the copper target (Nanovision, 99.99% purity, 3 inches in diameter) and from 60W to 180W to the zinc target (Nanovision, 99.99% purity, 3 inches in diameter), to find

best coating compositions. The deposition process lasted for 1 hour and occurred under the same conditions as previously, in a pure Ar atmosphere, at a pressure of 5.5 dPa.
After some preliminary compositional analysis, coatings obtained by applying powers of 20 W and 30 W on the Cu target, and powers of 140, 160, and 180 W to the Zn target were excluded, and no further investigations were conducted.
On the selected coatings, indicated in Table 4, deeper analyses were performed.

Table 4: Process parameters set and acronyms of silica/copper and silica/zinc composite coatings

SiO2_Cu coating		***SiO2_Zn coating***	
Power to Cu target	***Acronym***	***Power to Zn target***	***Acronym***
5 W	*SiO2_Cu5*	***60 W***	*SiO2_Zn60*
10 W	*SiO2_Cu10*	***120 W***	*SiO2_Zn120*

6.2. Substrates

During this research work, several substrates for different applications have been used for the coating deposition, depending on the final purpose. The process parameters were selected according to the substrate and the requirement of the final application. In particular, in this work, the antibacterial coatings were intended to be involved in air filtration systems, water filtration systems, and automotive textiles.

Some materials as soda-lime glass and cotton were used as model substrates for some general characterization analysis. Soda-lime glass, owing to its properties, serves as an excellent substrate for structural investigation techniques such as UV–Visible spectroscopy (UV–Vis) and X-ray diffraction (XRD) analysis, which will be described later.

A cotton sample, provided by Tessitura Ballesio, (Figure 27) was used to investigate zirconia and silica-based coatings' resistance to water and several washing cycles.

Figure 27: Uncoated cotton

6.2.1. Air filters

Antibacterial coatings were deposited on systems for air filtration, in the context of "*Bio-Killer, antiBIOpollutant coatIng for reusabLe filter*" project, funded by Piedmont Region within the Transnational MANUNET III call 2018. The project, in particular, aimed to improve air quality, by preventing the proliferation and subsequent spreading of microorganisms, bacteria, and viruses in enclosed environments.

The aforementioned coatings were deposited onto air filters of various types of materials. The substrates were provided by GV Filtri company, a project partner. Three filtration media were used, shown in Figure 28, a metallic one, made of AISI 316L steel, with a thickness of 0.14 mm, which will be called "Met" in the text; a glass-fiber-based filter with acrylic and vinyl-acrylic binders, with a thickness of 0.48 mm, called "Glass" in the discussion, and a polymeric membrane made of polypropylene (PP), with a thickness of 0.35 mm, named "Memb" in the text.

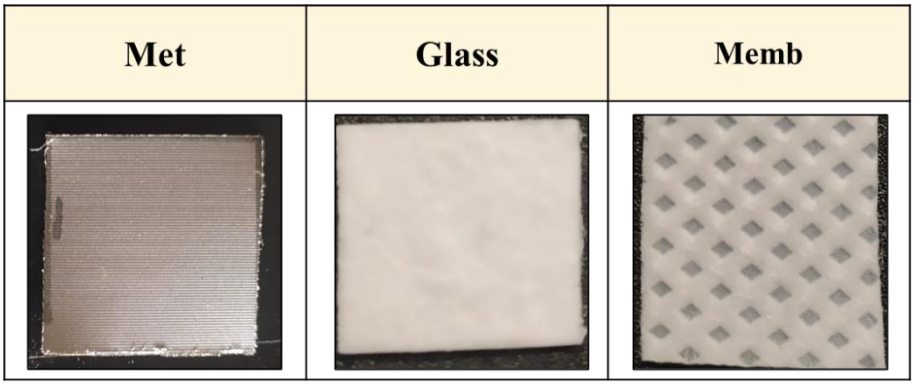

Figure 28: As-received metallic filter, glass fiber-based filter, and polymeric membrane for air filtration used in the BIOKILLER project

For this application, silica- and zirconia-based coatings containing silver nanoclusters were developed and deposited on the filters; in addition, silica-based composite coatings with copper and zinc as bactericidal agents, were studied.

All the composite coatings deposited on Met, Glass, and Memb, and deeply studied, are listed in Table 5, and the related acronyms, used in the text, are indicated.

Table 5: Silica/silver, zirconia/silver, silica/copper, and silica/zinc composite coatings deposited on filters for air filtration systems

Substrate	***SiO2_Ag coatings***	***ZrO2_Ag coatings***	***SiO2_Cu coatings***	***SiO2_Zn coatings***
Met	*Met_SiO2_Ag5*	*Met_ZrO2_Ag4* *Met_ZrO2_Ag5*	*Met_SiO2_Cu5* *Met_SiO2_Cu10*	*Met_SiO2_Zn60* *Met_SiO2_Zn120*
Glass	*Glass_SiO2_Ag3* *Glass_SiO2_Ag5*	*Glass_ZrO2_Ag4* *Glass_ZrO2_Ag5*	*Glass_SiO2_Cu5* *Glass_SiO2_Cu10*	*Glass_SiO2_Zn60* *Glass_SiO2_Zn120*
Memb	*Memb_SiO2_Ag3*	*Memb_ZrO2_Ag4* *Memb_ZrO2_Ag5*	*Memb_SiO2_Cu5* *Memb_SiO2_Cu10*	*Memb_SiO2_Zn60* *Memb_SiO2_Zn120*

6.2.2. Water filters

Another field of application for antibacterial coatings involves water purification systems. For this purpose, polymeric membranes obtained through an electrospinning process were chosen. In particular, composite coatings were deposited on two membranes: one entirely composed of polycaprolactone, PCL, 12%wt, under conditions of relative humidity between 27-28%, and the other one composed of 70% polyacrylonitrile, PAN, and 30% polyacrylate, PCL, realized in conditions of relative humidity of 35%, named in the text PAN-PCL. These electrospun membranes were produced by Nanofaber company, which evaluated their thickness in a range between 40 and 140 μm. Images of bare membranes are reported in Figure 29.

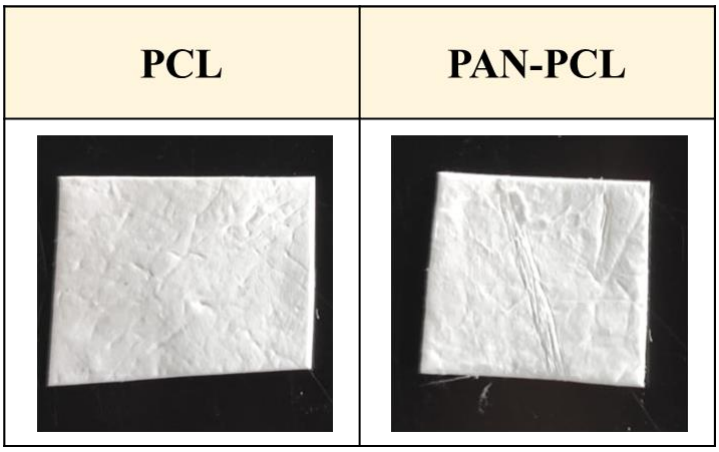

Figure 29: As-received PCL, and PAN-PCL membranes for water filtration systems

Considering that the final product will be in prolonged contact with water and based on the results of previous studies [180], coatings made up of zirconia matrix and silver nanoclusters were selected, as they seem to be less soluble in water compared to the coating of silica matrix, and more suitable for this purpose.

According to the specific features of the substrates, process parameters were optimized. In particular, deposition times were drastically reduced to 10 and 20 minutes since the membranes were very thin and particularly sensitive to heat, and could be damaged if subjected to long processes. Composite coatings developed and evaluated for this purpose are summarized in Table 6.

Table 6: Zirconia/silver composite coatings deposited on PCL and PCL-PAN for water filtration systems

Substrate	***ZrO2_Ag4 coatings***
PCL	*PCL_ ZrO2_Ag4_5* *PCL_ ZrO2_Ag4_10*
PAN-PCL	*PAN-PCL_ ZrO2_Ag4_5* *PAN-PCL_ ZrO2_Ag4_10*

6.2.3 Textiles for the automotive field

In the context of antibacterial coatings for textiles, the project "*Antimicrobial/virucidal PVD coatings for automotive*", funded within a framework collaboration agreement between Politecnico di Torino and FCA-CRF company, aimed to impart antimicrobial properties to automotive textiles

through the deposition of coatings via co-sputtering technique. The challenge was to obtain coatings that were effective against bacteria strains, but without altering the original color of the fabrics.

Several textiles, in different colors, were involved in the study, shown in Figure 30. They were:

- two black fabrics, consisting of layering of a thin layer of polyamide, an intermediate layer made of polyurethane foam, and a surface layer of polyester fibers, differing in thickness (3.3 mm and 2 mm) (*Fabric_1* and *Fabric_2*);
- a leather-like fabric, made of PVC with a polyurethane finish in white or black (*Leather*);
- two genuine leather fabrics, colored in blue or brown after processing (*Leather _blue* and *Leather _brown*).

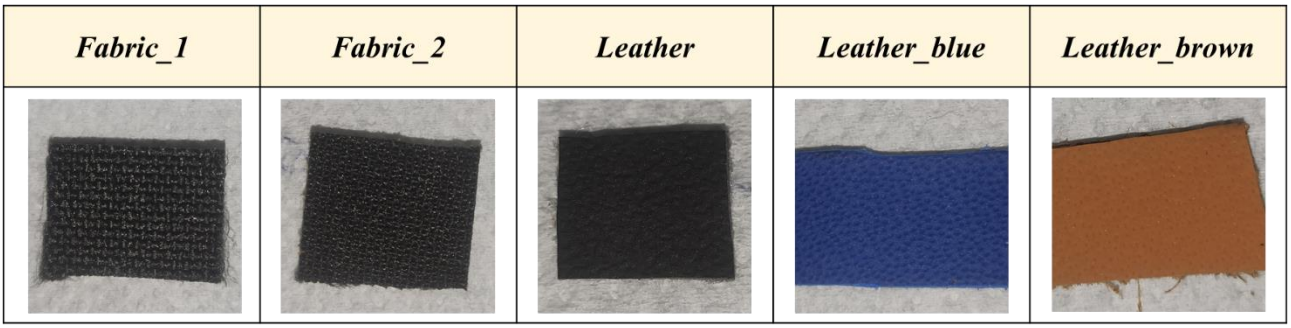

Figure 30: As-received Fabric_1, Fabric_2, Leather, Leather_blue and Leather_brown for application in automotive textiles

Due to the stringent conditions regarding color, process parameters were optimized to obtain transparent coatings. Composite coatings containing silver nanoclusters are generally yellow or brown colored, due to the plasmonic resonance phenomenon of silver nanoclusters, in dependence on their amount and size [181].

To obtain coatings with antibacterial properties, but without affecting the color of the fabrics, it was decided to reduce the amount of silver in the deposited coatings. Two approaches were followed: reduction of power values set on the Ag target and reduction of deposition time.

In particular, it was decided to reduce power to 1 and 2 W and to perform coating deposition for 30 and 60 minutes. Both coatings with silica and zirconia matrices were analyzed. Since the results were not satisfactory in terms of color, blue and brown leather were excluded from further investigations, and additional changes in process parameters for the deposition of SiO_2-based coatings on black fabrics and leather were employed.

In particular, the new coatings were developed, setting a power of 4 W to the Ag target, but reducing processing times to 5 and 10 minutes.

In Table 7, SiO_2 and ZrO_2 composite coatings deposited on each substrate are indicated, with the related acronyms.

Table 7: Silica/silver and zirconia/silver composite coatings deposited on fabrics and leathers for automotive textiles

Substrate	***SiO2_Ag coatings***	***ZrO2_Ag coatings***
Fabric_1	*Fabric_1_SiO2_Ag1_30* *Fabric_1_SiO2_Ag1_60* *Fabric_1_SiO2_Ag2_30* *Fabric_1_SiO2_Ag2_60* *Fabric_1_SiO2_Ag4_5* *Fabric_1_SiO2_Ag4_10*	*Fabric_1_ZrO2_Ag1_30* *Fabric_1_ZrO2_Ag1_60* *Fabric_1_ZrO2_Ag2_30* *Fabric_1_ZrO2_Ag2_60*
Fabric_2	*Fabric_2_SiO2_Ag1_30* *Fabric_2_SiO2_Ag1_60* *Fabric_2_SiO2_Ag2_30* *Fabric_2_SiO2_Ag2_60* *Fabric_2_SiO2_Ag4_5* *Fabric_2_SiO2_Ag4_10*	*Fabric_2_ZrO2_Ag1_30* *Fabric_2_ZrO2_Ag1_60* *Fabric_2_ZrO2_Ag2_30* *Fabric_2_ZrO2_Ag2_60*
Leather	*Leather_SiO2_Ag1_30* *Leather_SiO2_Ag1_60* *Leather_SiO2_Ag2_30* *Leather_SiO2_Ag2_60* *Leather_SiO2_Ag4_5* *Leather_SiO2_Ag4_10*	*Leather_ZrO2_Ag1_30* *Leather_ZrO2_Ag1_60* *Leather_ZrO2_Ag2_30* *Leather_ZrO2_Ag2_60*
Leather_blue	*Leather_blue_SiO2_Ag1_30* *Leather_blue_SiO2_Ag1_60* *Leather_blue_SiO2_Ag2_30* *Leather_blue_SiO2_Ag2_60*	*Leather_blue _ZrO2_Ag1_30* *Leather_blue _ZrO2_Ag1_60* *Leather_blue _ZrO2_Ag2_30* *Leather_blue _ZrO2_Ag2_60*

Leather_brown	*Leather_brown_Ag1_30* *Leather_brown_Ag1_60* *Leather_brown_Ag2_30* *Leather_brown_Ag2_60*	*Leather_brown_ZrO2_Ag1_30* *Leather_brown_ZrO2_Ag1_60* *Leather_brown_ZrO2_Ag2_30* *Leather_brown_ZrO2_Ag2_60*

6.3.Silica/silver composite coatings derived from Pre-Ceramic Polymer

Given the promising antimicrobial results of the silica and zirconia coatings with silver nanoclusters, it was decided to explore alternative techniques to sputtering, to achieve coatings with the same bactericidal properties. For this reason, in this research, preliminary studies were conducted on the transformation of pre-ceramic polymers into silica, to synthesize the matrix of the coating, and on methods to incorporate silver nanoparticles. The studied pre-ceramic polymer was perhydropolysilazane, PHPS, an inorganic polymer consisting mainly of Si-N bonds and Si-H terminal groups, in a solution with dibutyl ether (20% (w/w)) (NN120-20, DurXtreme).

To promote the transformation of the polymer into silica, the solution was exposed to basic vapors, obtained by heating a 1M aqueous ammonia solution to 80°C for 4 and 8 hours, and results were compared with the structure obtained with the same solution exposed to air at room temperature for 24 hours.

For the synthesis of silver nanoparticles, it was decided to proceed with an *in situ* photochemical reduction of silver nitrate, $AgNO_3$, as a precursor for AgNPs, promoted by UV light irradiation. Since silver nitrate could not be solubilized in the polymeric solution, it was dissolved in acetone, a solvent that is miscible with dibutyl ether present in the PHPS solution. Solutions containing acetone, silver nitrate, and Darocur 1173 (Ciba Specialty Chemicals Inc.), a photoinitiator, were prepared. The concentration of AgNO3 was 0.44%.

These solutions were then mixed with PHPS in different ratios, PHPS: AgNO3 1:0, 1:0.5, 1:0.75 and1:1. The maximum ratio between silver nitrate solution and PHPS was 1:1, since increasing the ratio leads to salt precipitation.

In order to increase the viscosity of the solution, and to facilitate the deposition, a rotary evaporator (Bibby Scientific RE300 Rotary Evaporator) was used, which allows the separation of the solvent from the solution. Once a more viscous solution was obtained, it was deposited on a soda-lime glass substrate using a bar to achieve a homogeneous coating with a thickness of 50 μm. Other coatings

were obtained by depositing a droplet, achieving higher but uncontrollable thicknesses. Deposited solutions were UV irradiated to promote the silver nanoparticles reduction, and UV chamber (DYMAX) with a power of 195.507 mW/cm2 was used, with exposure times of 30 and 45 minutes. N_2 was constantly purged during the irradiation process. These preliminary studies on the coating obtained from polymer precursors were conducted using AISI 304 steel and soda-lime glass substrates.

Coatings obtained using PHPS as silica matrix precursors, in solution with $AgNO_3$ could be summarized as follows in Table 8. The related acronyms for the films obtained are indicated, specifying the ratio of PHPS and $AgNO_3$ in the solution; in the case of the deposition of a droplet, "_droplet" is added to the name.

Table 8: Silica/silver composite coatings obtained by PHPS pre-ceramic polymer and $AgNO_3$ solutions in different ratio

PHPS:AgNO₃	***PHPS_AgNO3 coatings***
1:0	*PHPS*
1:0.5	*PHPS_AgNO3_0.5* *PHPS_AgNO3_0.5_droplet*
1:0.75	*PHPS_AgNO3_0.75* *PHPS_AgNO3_0.75_droplet*
1:1	*PHPS_AgNO3_1* *PHPS_AgNO3_1_droplet*

6.4. Compositional, morphological and structural analysis (SEM-EDS, FESEM, TEM, XRD, UV-Vis)

Compositional, morphological, and structural properties of as-received substrates and developed coatings were studied employing different techniques, such as scanning electron microscopy and energy dispersion spectrometry (SEM-EDS), Field-Emission Scanning electron microscopy (FESEM), Transmission electron microscopy (TEM), UV-Visible (UV-Vis), X-ray diffraction (XRD).

The composition of the uncoated samples and the coatings was analyzed using scanning electron microscopy and energy dispersion spectrometry (SEM-EDS, Philips 525M) at a voltage of 15 kV, at a magnification of 150X. Three distinct areas were examined to obtain a statistical quantification of the elements.

UV-Vis analyses evaluated the light absorbed or transmitted by the sample. In this case, the UV–Vis lamp, Shimadzu, UV 2600, was used in absorbance mode. The analysis was conducted in a range between 300 and 800 nm, to investigate the presence of silver nanoclusters in composite coatings, comparing to data obtained analyzing coatings made up of pure silica or zirconia.

FESEM analysis (QUANTA INSPECT 200, Zeiss SUPRA 40) was used to observe the morphology of substrates and deposited coatings. By this technique, the size and the dispersion of silver nanoclusters, the eventual modification in the structure of the coatings, and the homogeneity of the coatings were estimated, giving important information for a deeper understanding of the effects of process parameters on coating features.

For a more detailed investigation of silica/silver and zirconia/silver coatings, analyses through Transmission Electron Microscope, TEM, and related EDS maps, were conducted at AGH University of Science and Technology, in Krakow, Poland. The instrumentation used was Titan Cubed G2 60–300 (FEI), equipped with a field emission electron gun (X-FEG) Schottky high brightness source with a monochromator. Images were obtained in the bright field mode. The compositional analysis was performed through the Energy Dispersive X-ray spectroscopy (EDX) with a ChemiSTEM EDX system. In order to perform the TEM analyses, the samples were reduced into very thin slices, of the order of 50-100 nm, and positioned on the TEM grids. A Pt layer of a few nanometers was deposited on the sample with a protective function.

The presence of a matrix in the crystalline or amorphous phase and the presence of silver nanoclusters were evaluated through XRD (X' Pert Philips diffractometer) using an incident angle fixed at 1° and the Cu K_ incident radiation, in order to study mainly the structure of the coating without interference from the substrate on which it is deposited. This is due to the small thickness of the coating less than 200 nm.

During the study of coatings obtained from the transformation of the polymeric solution, Fourier-Transform Infrared Spectroscopy, (Perkin Elmer Spectrum 2000 FTIR) equipment was used. Spectra were collected in a range between 4000 and 500 cm^{-1}, and 32 scans. The successful transformation of the PHPS coating in silica was evaluated by observing the formation of a Si-O bond, around 1050 cm^{-1}.

6.5. Ions release test

Since the antibacterial mechanism of silver nanoparticles involved both silver nanoparticles and silver ions, the amount of Ag ions released by coatings was evaluated to determine their quantity as a function of the time and verify the potential toxic level. The coated samples, 1 x1 cm^2, were immersed in 30 ml of Milli-Q water and left in immersion at room temperature. After different immersion periods, 3 hours, 1, 3, 7, and 14 days, samples were retrieved, and the concentration of silver ions released in water was determined using a Hanna Instruments™ spectrophotometer. For each time and each coating, the test was repeated three times.

6.6. Resistance to washing cycles

The resistance to water and several washing cycles of composite coatings was evaluated in a preliminary study [180], on SiO2_Ag3 and ZrO2_Ag3 deposited on cotton as substrate. A solution of 100 ml of MilliQ water mixed with 0.2 g of detergent, (1993 WOB Standard detergent Testfabrics, Inc.) was prepared and three samples of coated cotton, 2 x 2 cm^2, were immersed in it. To simulate the washing machine process, the test was conducted in a thermostatic bath, set at 50°C, with an oscillation rate of 130 rpm, for 30 minutes. After each cycle, the samples were rinsed in distilled water to remove any detergent residual. Compositional analyses were performed before and after 1, 5, and 10 washing cycles, to evaluate the change in silver and silica or zirconia amount. In addition, the bactericidal efficacy of coatings after 1, 5, and 10 washing cycles was assessed against *S. epidermidis* through an inhibition halo test.

6.7. Antibacterial tests

To assess the antibacterial action of the coatings studied in this work, qualitative and quantitative antibacterial tests were conducted. Specifically, the inhibition zone test gave a qualitative evaluation of the coating's efficacy against bacteria, while for more precise results and data, the colony-forming unit (CFU) count test could be employed. A third test evaluated the antibacterial effect of coatings after contamination through a bioaerosol generator and thermal regeneration process. In this case, the evaluation was both qualitative and quantitative.

6.7.1. Inhibition halo test

The inhibition halo test [182] is a rapid method for qualitatively determining the effectiveness of the coating against bacteria and fungi.

First of all, bacterial colonies, obtained from a previous bacterial culture on nutrient plates, were inoculated into a nutrient broth, to obtain a standard bacterial solution. The number of colonies must reach a fixed value of the McFarland index, a parameter related to the turbidity of the solution, evaluated by an optical photometer (Phoenix Spec BD McFarland). According to the NCCLS M2-A9 standard, the starting bacterial concentration in the broth is $1*10^8$ CFU/ml which corresponds to 0.5 of the McFarland index. Increasing the number of bacterial colonies, the greater the turbidity of the solution will be and the greater the index will be.

The obtained bacterial solution was spread on the surface of a nutrient agar plate and both uncoated and coated samples, 1x1 cm^2, were placed in contact with the agar, with the coated side to be tested in contact with the bacteria solution.

After 24 hours of incubation at 35°C, the effectiveness of the coatings was examined. The bacterial colonies tend to grow across the entire plate, but the presence of a halo around the sample indicates a bacteria-free zone, where bacterial proliferation does not occur, as well as visible in Figure 31.

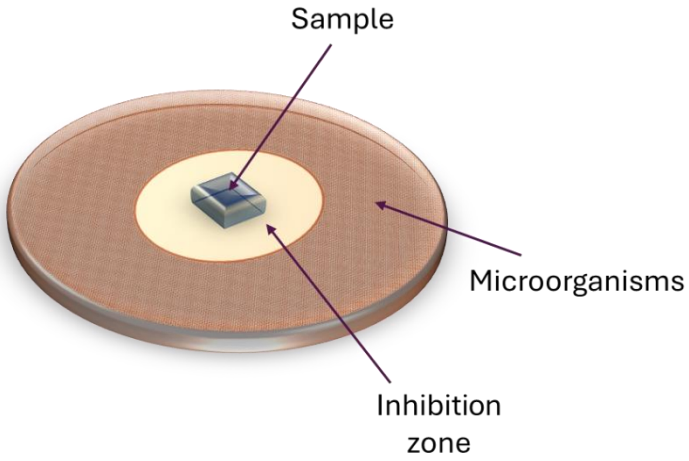

Figure 31: Scheme of the inhibition halo test

It was assessed the effect against both Gram-positive bacteria and Gram-negative bacteria strains. In this work, non-pathogen microorganisms were used as *S. epidermidis* (ATCC14990) and *E. coli* (ATCC8739), and *C. albicans* (ATCC10231) for the antifungal analysis.

6.7.2. CFU count through dilution test

The colony-forming unit (CFU) count test, based on a series of dilutions of bacterial solutions, was performed to quantitatively determine the reduction in bacterial proliferation. Specifically, this test was conducted according to the NCCLS M7-A6 standard [183], which specifies a starting standard concentration of bacterial colonies of $5*10^5$ CFU/ml.

A bacterial solution without samples as control, two solutions containing uncoated samples of dimensions 2 x 0.5 cm² each, and three solutions containing samples coated on one side, also of dimensions 2 x 0.5 cm² each, were prepared and incubated at 35°C for 24 hours. After the incubation period, the samples were removed from the broth, and the McFarland index of each solution was evaluated. Each solution was then serially diluted adding a physiological solution and spread onto nutrient agar plates, as shown in Figure 32. 24 hours of incubation at 35 °C followed. At this point, the number of colonies proliferated in each broth was counted.

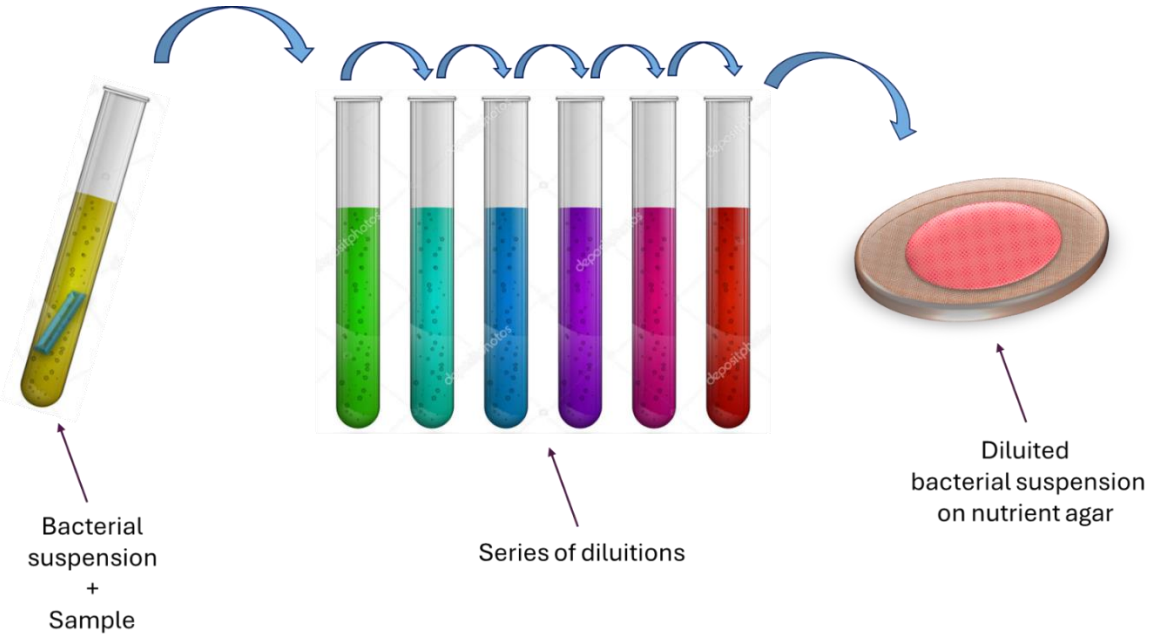

Figure 32: Scheme of the CFU count test

To evaluate the colonies that adhered to the surface of the samples, filters removed from the bacterial solutions were immersed in 3 ml of physiological solution and vortexed at room temperature for 5 minutes, causing the detachment of colonies from the samples. After sample removal, rinsing bacterial solutions were diluted, incubated, and analyzed as previously described. In the section "*Results*", the discussion of the results related to filters that were vortexed was indicated by adding the suffix "_VORTEX" to the name of the sample.

Contrary to the previous case, in this test, the efficacy was evaluated against *S. epidermidis*. Only in the case of SiO2_Cu and SiO2_Zn coatings, the test was performed against the *E. coli* bacteria strain.

6.7.3. Contamination and Thermal Regeneration test

An important phase of the study of antibacterial coatings for air filters was dedicated to the evaluation of possible reuse of the filters after sterilization treatment, so the antibacterial effect was

tested after a thermal regeneration process. The test consisted of two phases. The first step involved bacterial contamination of the samples using a bioaerosol generator (TOPAS ATM 220). An experimental setup was developed, described in [184] and shown in Figure 33.

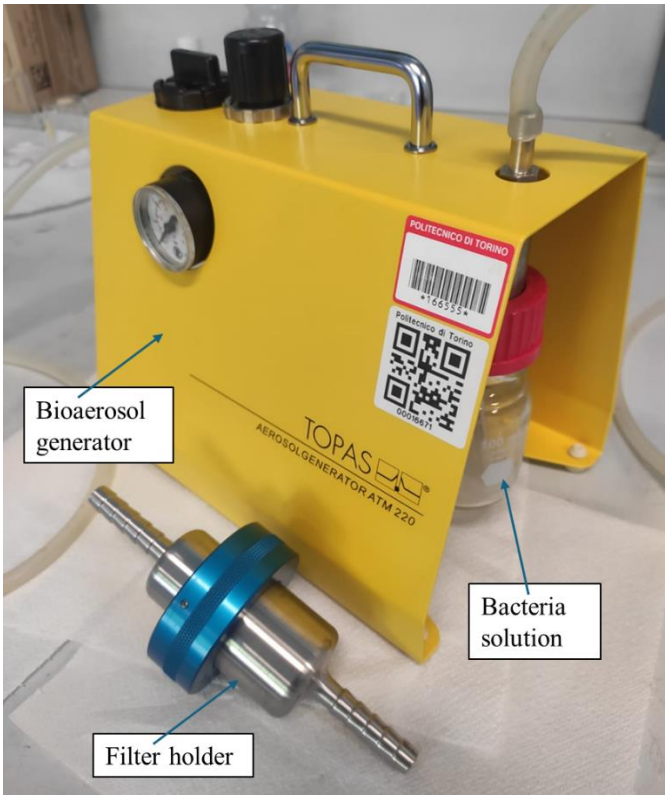

Figure 33: Setup of the bioaerosol generator and filter holder used for the contamination test

A bacterial suspension, containing a high number of colonies, with a McFarland index of about 5.0, was prepared. This solution was used to generate a bioaerosol, obtained by an airflow passing through the aerosol generator with a pressure of 0.5 bar. Entering in a filtration column, the bacterial suspension is nebulized in samples placed in the filter holder.

To determine the contamination times, the bacterial solution was previously nebulized onto nutrient agar plates for various times: 5, 10, 15, and 30 minutes. After incubation at 35°C for 24 hours, bacterial growth on each plate was assessed, and it was decided to proceed with the contamination process for 30 minutes, which represents the most severe condition.

The contamination test was conducted on metallic, glass-fiber and polymeric filters, for both the uncoated and silica/silver and zirconia/silver coated samples. The coated side was exposed to the bioaerosol flow, and the contaminated surface was placed in contact with a nutrient agar plate. After incubation at 35°C for 24 hours, the proliferation of bacterial colonies on filters was evaluated.

The second step involved the thermal regeneration process. The contaminated samples were removed from the agar surface and placed in glass petri plates. Here, they underwent three cycles of thermal treatment, constituted by heating to 200°C, isotherm for 10 minutes, and slow cooling in air to room temperature. The polymeric membrane was not subjected to thermal regeneration since high temperatures could damage the thermosensitive substrate. For a easier understanding of the results obtained, coatings that were thermally regenerated will be indicated by adding "_TR" to the name of the sample, in the "*Results*" section.

After completing the third cycle, the samples were put into the sample holder and a second contamination occurred, under the same conditions as previous. An incubation period of 24 hours followed. In the end, the growth or the absence of bacterial colonies was qualitatively evaluated to determine if the antibacterial effectiveness of the coatings remained unchanged even after thermal treatment. The phases of the entire process are outlined in Figure 34.

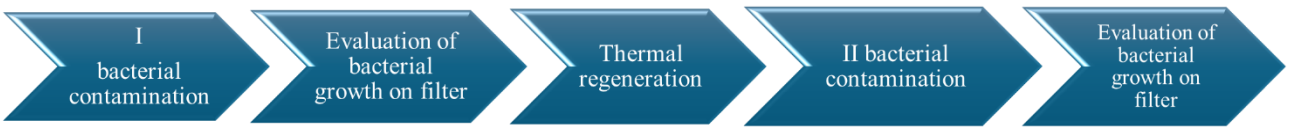

Figure 34: Phases of the contamination and thermal regeneration test

For a quantitative evaluation, the CFU count test was performed after contamination and thermal regeneration.

In this experiment, both the uncoated and coated filters, contaminated with bacteria using a bioaerosol generator, were immersed in nutrient broth and then incubated for 24 hours. After incubation, bacterial solutions were obtained and serially diluted with a physiological solution. These diluted solutions were spread onto nutrient agar plates, which were then incubated for another 24 hours to allow bacterial colony growth. The colonies were evaluated as previously described.

Thermal regeneration and second contamination experiments were conducted on metallic and glass-fiber filters, and the bacterial load was evaluated using the same procedure.

The evaluation of colonies adhered to the surfaces was possible due to the vortex step, which allowed detaching the bacteria from the surface and counting their number.

7. Results

In this section, the results obtained during this research work will be reported and discussed. The chapter will be divided into two main parts:

1. The first one is focused on the study of antibacterial silica or zirconia composite coatings, deposited on various substrates through the co-sputtering technique. It will be divided based on the applications for which the coatings were developed and studied into different sections:
    - Antibacterial coatings for air filtration systems, focused on the study of silica- and zirconia-based coatings, with silver nanoparticles as antibacterial agent (SiO_2/Ag and ZrO_2/Ag), and silica-based coatings with copper and zinc as antibacterial agents (SiO_2/Zn and SiO_2/Cu), deposited on air filters;
    - Antibacterial coatings for water filtration systems focused on the characterization of optimized ZrO_2/Ag coatings, deposited on polymeric membranes used for the filtration of aqueous solutions;
    - Antibacterial coatings for automotive textiles focused on the development and study of transparent and antibacterial composite coatings deposited on textiles and both natural and synthetic leathers, commonly used in the automotive industry.
2. The second part will focus on a preliminary study for the development of composite coatings with a silica matrix, derived from the transformation of pre-ceramic polymer, embedding silver nanoclusters.

The results of the compositional, structural, and morphological analysis will be shown, in addition to the evaluation of the antibacterial efficacy of the coatings.

7.1. Antibacterial composite coatings via the co-sputtering technique for several applications

In this part, results obtained from the study and the analysis of antibacterial composite coatings deposited by means of the co-sputtering technique and intended for applications in air and water filtration, and in the automotive textiles field will be shown and discussed.

7.1.1. Antibacterial composite coatings for air filters

Antimicrobial and antiviral coatings could play a crucial role in enhancing air quality, particularly in indoor environments. Given that microorganisms captured by air filtration systems can persist on

filter surfaces for extended periods, and that conditions such as humidity and dirt can foster their growth, filters capable of inhibiting their spread indoors and limiting their proliferation could offer a viable solution to improve human health and everyday life [97].
In the context of the "BIOkILLER- antiBIOpollutant coatIng for reusabLe fiLtER" project, coatings composed of silver nanoclusters embedded in silica or zirconia matrices were deposited through the co-sputtering technique and characterized on three different types of filters, metallic stainless steel (Met) and glass-fiber (Glass) based filters, and polymeric membrane (Memb). Some of the results discussed in this section were published in [180] [185].

Silica and zirconia composite coatings containing Ag nanoclusters for air filters

The use of silica as a matrix offers several advantages, including preventing the agglomeration of nanoparticles and enhancing antimicrobial activity [186] [187]. On the other hand, zirconia, often used for its biocompatibility and resistance to corrosion, exhibited an improvement in antibacterial effect, if used in composite materials with silver nanoparticles [188].

Silica/silver coating has already been extensively deposited and studied in previous works [62][65][184]. According to the final application, it was decided to apply the following parameters for the deposition of silica-based coatings:

- SiO_2 200W – Ag 5 W for metallic filter (**Met_SiO2_Ag5**)
- SiO_2 200W – Ag 3-5 W for glass-fiber filter (**Glass_SiO2_Ag3**, **Glass_SiO2_Ag5**)
- SiO_2 200W – Ag 3W for polymeric membrane (**Memb_SiO2_Ag3**)

Regarding coatings of zirconia matrix and silver nanoclusters, a wide range of process parameters and compositions were evaluated to study which ones are most suitable, depending on the substrate and applications. In particular, the power applied to the zirconia target was selected at 250W after several considerations in terms of stability and reproducibility of the process. Based on the compositional analysis of coatings obtained by applying several powers to the Ag target, it was decided to deeply investigate the following coatings, which exhibited the best balance in the amount of Zr and Ag:

- ZrO_2 250W – Ag 4-5 W for metallic filter (**Met_ZrO2_Ag4, Met_ZrO2_Ag5**)
- ZrO_2 250W – Ag 4-5 W for glass-fiber filter (**Glass_ZrO2_Ag4, Glass_ZrO2_Ag5**)
- ZrO_2 250W – Ag 4-5 W for polymeric membrane (**Memb_ZrO2_Ag4, Memb_ZrO2_Ag4**)

Each deposition lasted one hour.

Figure 35 shows the photos of the uncoated filters and those with the chosen deposited coatings. As can be observed, the coating deposition significantly altered the appearance of the filters, which is attributed to the plasmonic resonance of the silver nanoclusters. Differences attributed to the matrix are noticeable. In the case of a fiber-glass filter, the difference in silver amount affected coating color in a very visible way.

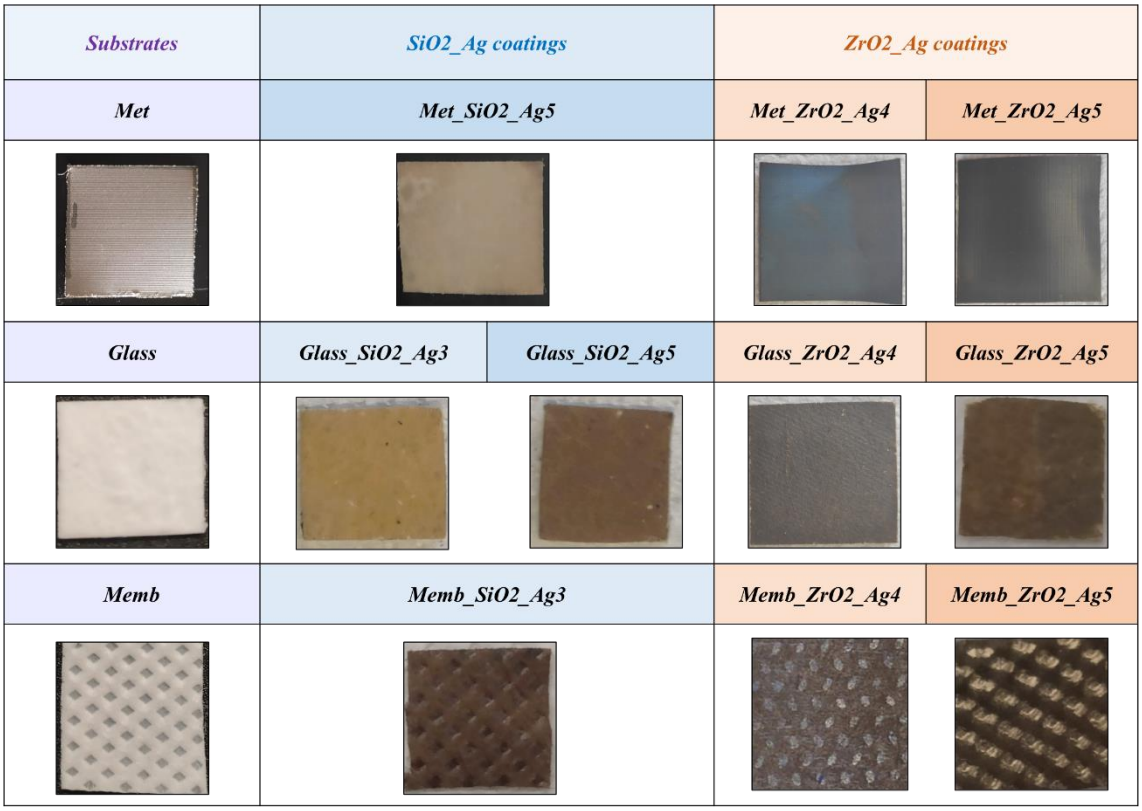

Figure 35: Macroscopic aspect of uncoated and of SiO2_Ag3, SiO2_Ag5, ZrO2_Ag4, and ZrO2_Ag5 coated Met, Glass, and Memb filters.

Compositional, structural, and morphological analysis

To verify the success of the deposition coatings process, compositional analysis was performed on all the uncoated and coated filters, to quantify the atomic percentage of Si, or Zr, and Ag, in the coatings.

Uncoated metallic filters were made of stainless steel, composed mainly of iron, with a high chrome content, which confers high corrosion resistance. A small amount of Si was detected. Regarding glass fiber-based filters, the EDS revealed a high content of oxygen and silicon, as expected, with very low percentages of other elements, such as sodium and magnesium. The main elements which constituted the polymeric membrane were carbon and oxygen.

Table 9 summarizes the obtained EDS data regarding SiO2_Ag and ZrO2_Ag coatings, and the value of power applied to the silver target was specified.

Table 9: EDS analysis on silica/silver and zirconia/silver composite coatings deposited on air filters

Substrate	*SiO2_Ag coating*			*ZrO2_Ag coating*		
	Power to Ag target	***Si (at. %)***	***Ag (at. %)***	***Power to Ag target***	***Zr (at. %)***	***Ag (at. %)***
Met	***5 W***	4.31 ± 0.09	2.72 ± 0.11	***4 W***	1.52 ± 1.51	1.02 ± 0.10
				5W	2.73 ± 0.48	4.17± 0.48
Glass	***3 W***	12.14 ± 0.65	0.94 ± 0.01	***4 W***	0.98 ± 0.03	0.59 ± 0.04
	5 W	12.04 ± 0.72	1.62 ± 0.03	***5W***	0.85 ± 0.07	1.22 ± 0.06
Memb	***3 W***	0.98 ± 0.03	0.78 ± 0.03	***4 W***	0.97 ± 0.04	0.33 ± 0.02
				5W	0.77 ± 0.01	1.21 ± 0.22

Analyzing the results of silica-based coating deposited on Met, it is possible to predict a homogenous deposition of the coating, due to the low value of standard deviation. The amount of Si in the coating is about 4.31 at. %, but it must be considered that a low amount of Si is present in the composition of the uncoated substrate. The amount of silver, obtained by applying a power to the Ag target of 5 W, was high, about 2.7 at. %, if compared to coatings on other filters.

The two coatings studied for glass-fiber filters showed an amount of silicon about 12.20 at. %, higher compared to the other cases. This is because silicon is one of the main elements constituting fiber-glass filters and is inevitably detected during the analysis. Increasing the power applied to Ag target from 3W to 5 W, the silver amount increased, from a value of about 0.95 at. % for SiO2_Ag3 to about 1.60 at. % for SiO2_Ag5.

The coating deposited on the Memb filter showed the lowest amount of silicon, revealing that during the deposition process, the different interactions between the substrate and the matrix occurred, depending on the material substrate. The silver content, approximately 0.80 at. %, is consistent with that obtained by depositing the same coating (SiO2_Ag3) on Glass, for which a value of 0.94 at. % was registered.

Regarding ZrO_2-based coatings, the increase in power applied to the silver target, from 4 to 5 W, led to an increment of silver content in all the coatings. In the case of Met and Memb as substrates, the

rising is very high, and the value corresponding to a power of 5 W is quadrupled compared to the ZrO_2_Ag4 coating, reaching values of approximately 4.20 and 1.20 at. %, respectively. In Glass filters, the content of silver is 0.60 at. % and 1.20 at. % in ZrO_2_Ag4 and ZrO_2_Ag5, respectively, so the amount is doubling. The amount of Zr in the coatings was very similar for Glass and Memb filters, in a range between 0.8 and 1.00 at. %, but it was higher for Met, reaching a value of 2.73 at. %.

Morphological evaluation of uncoated substrates at low magnification, 500 X, was performed through FESEM analysis and the results are shown in Figure 36. The stainless steel metallic filter, (Figure 36 (a)) was composed of metal fibers, approximately 30 µm in diameter, neatly intertwined; in contrast, the structure of Glass and Memb (Figure 36 (b) and (c)), was made up of fibers arranged randomly. In the polymeric membrane, each fiber is approximately 20 µm in diameter.

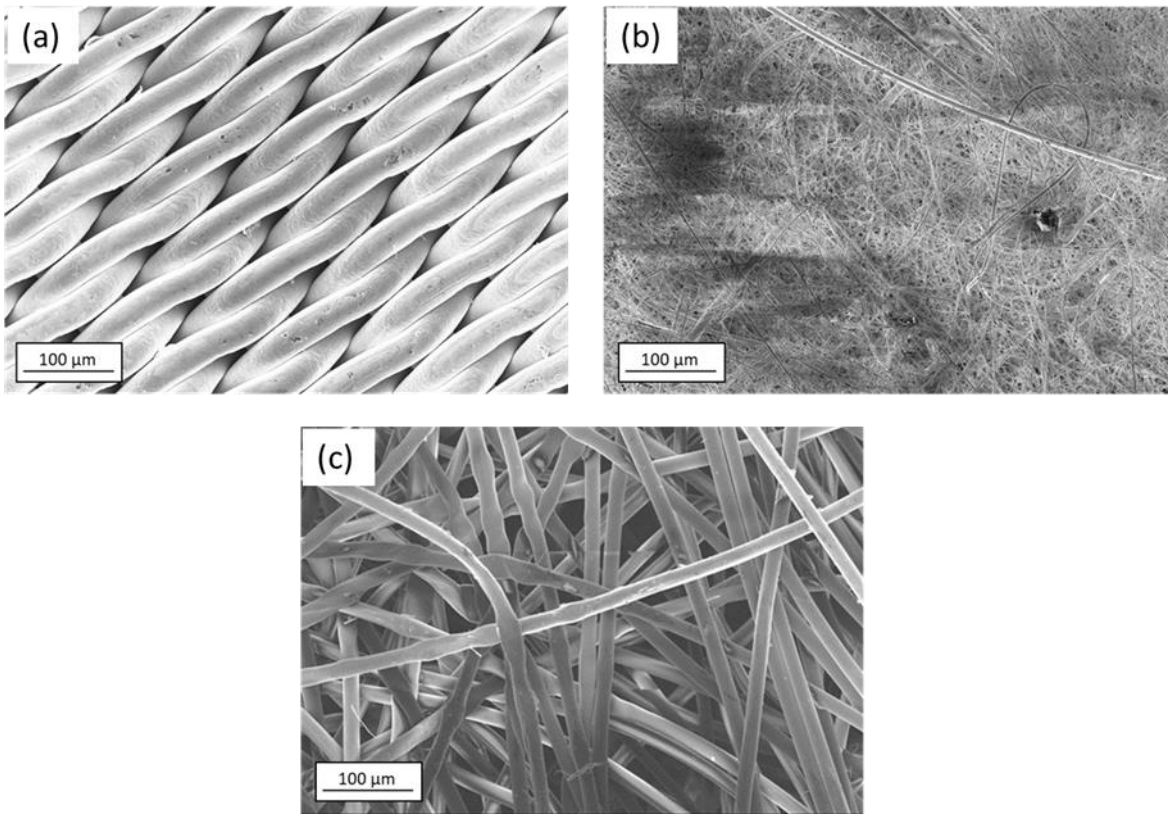

Figure 36: Morphological analysis at low magnification of uncoated (a) Met, (b) Glass, and (c) Memb filters

A comparison of the morphological aspect of coated samples and bare filters at high magnifications was performed. Regarding the metallic filter (Figure 37), a substantial morphological variation occurred before and after coating deposition. The as-received filter (Figure 37 (a)) had an extremely smooth surface, which changed after the deposition process. The composite coating composed of silica as matrix and silver nanoclusters, SiO2_Ag5, Figure 37 (b), was uniformly deposited across the entire surface of the filter, as suggested by small standard deviations in EDS data (Table 9) previously described, and it appeared globular, due to the typical sputtered silica morphology.

Based on the obtained images, it is difficult to accurately identify the silver nanoparticles. Numerous large gray particles distributed throughout the coating are visible, but, considering their size and concentration, they are probably related to silica aggregates, and not silver nanoparticles, which should appear as small, very bright spots. Since EDS, and as will be described, XRD and UV-Vis analyses had confirmed the presence of Ag nanoparticles, they were likely embedded within the matrix, inside the silica aggregates, and some were distributed on the outer surface. Compared to SiO_Ag5, the morphology of zirconia coatings, (Figure 37(c) and (d), respectively) appeared to be finer and more compact. As previously, it is very difficult to distinguish silver nanoparticles, which are probably embedded in the zirconia matrix of the coating. Deeper investigations through TEM analysis on ZrO2_Ag5 will confirm the presence of silver nanoclusters inside the coating.

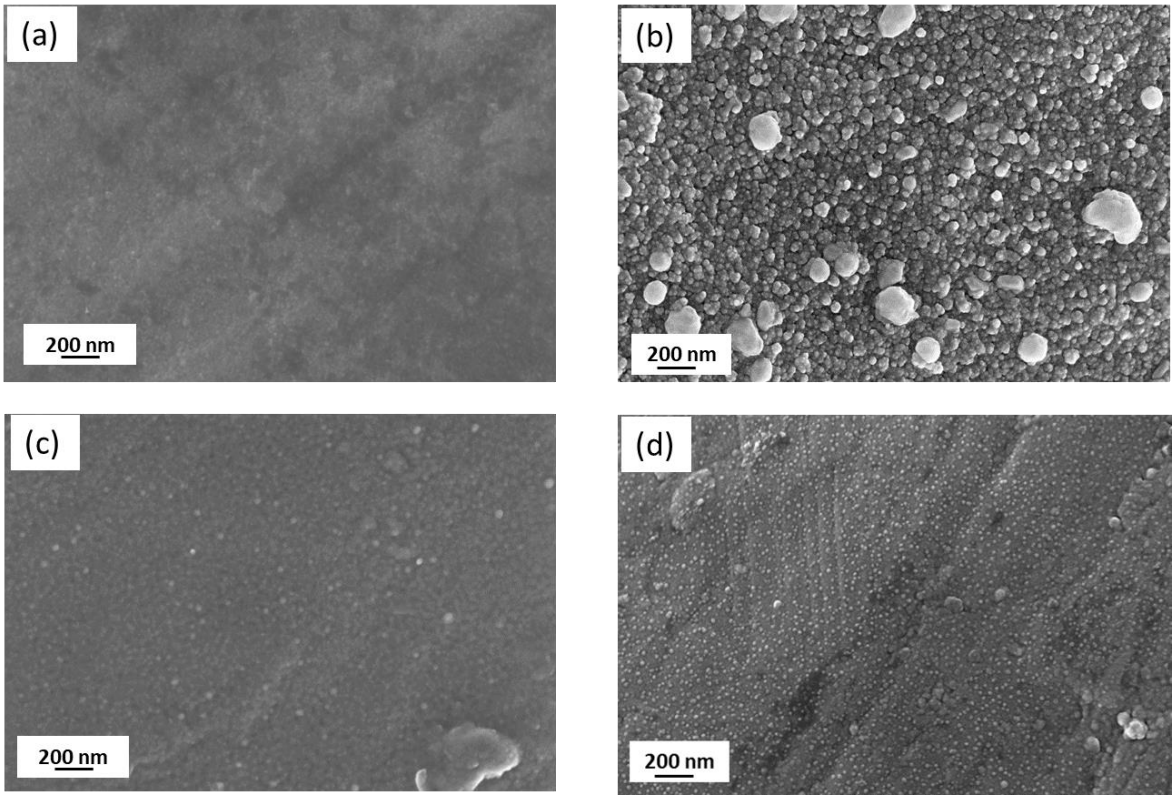

Figure 37: Morphological analysis of (a) uncoated Met (b) Met_SiO2_Ag5, (c) Met_ZrO2_Ag4 and (d) Met_ZrO2_Ag5

Morphological differences are visible in the case of the uncoated and coated glass fiber-based filter, as shown in Figure 38. The uncoated sample showed a smooth surface, which changed a lot after the deposition of the coating. Glass_SiO2_Ag3 appeared globular and covered the entire surface of the fiber, but some aggregates were formed, in spherical or wormlike shapes. The bright spots indicating the silver nanoclusters are not visible, but considering that their presence was confirmed by the compositional and will be demonstrated in structural analysis, it is probable that they were embedded in the silica matrix. In the case of Glass_SiO2_Ag5, small particles distributed across the entire surface are clearly visible, which can also be attributed to silica aggregates, probably

containing silver nanoparticles or nanoclusters. This morphology is finer than that obtained by applying the same process parameters for the deposition of the coating on the metallic filter, Met_SiO2_Ag5. This suggests that different interactions between the material substrate and matrix of the composite coating could occur during the deposition process.

The coatings composed of zirconia matrix (Figure 38(d) and (e)) appeared globular, fine and compact, similar to that obtained on metallic filters. Some particles, probably due to zirconia aggregate are visible, the results of compositional and structural analysis, which confirmed the presence of silver nanoclusters, suggested that they are embedded in the matrix of the coating.

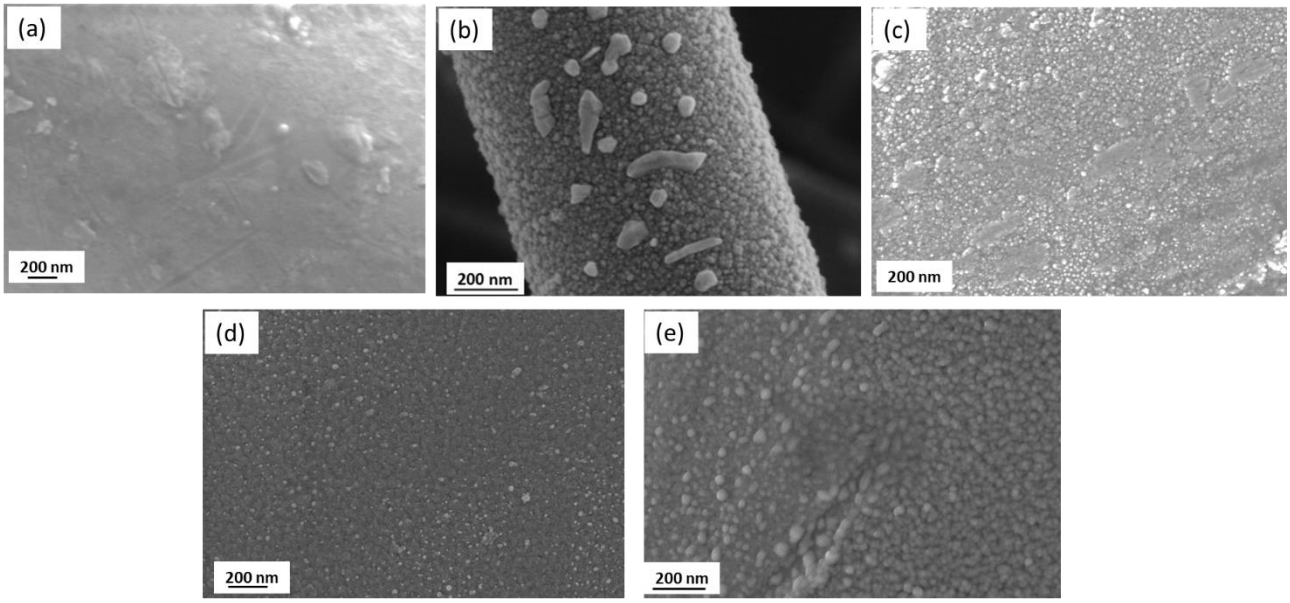

Figure 38: Morphological analysis of (a) uncoated Glass, (b) Glass_SiO2_Ag3, (c) Glass_SiO2_Ag5, (d) Glass_ZrO2_Ag4 and (e) Glass_ZrO2_Ag5

In the case of the polymeric membrane, the coating Memb_SiO2_Ag3 (Figure 39 (b)) appeared different from the previous cases. In particular, it seemed to be more compact and fine than the other cases, no large aggregates of silica are visible, as for coatings on metallic filters. It is probably due to the different interaction between material substrates and silica coatings, as also EDS data suggested. Coatings made up of zirconia matrix, (Figure 39 (c) and (d)), appeared compact, and some zirconia aggregates are visible, embedding, probably silver nanoclusters. In the case of ZrO2_Ag5 coatings, the clearly visible nanoparticles are most likely not attributable to silver nanoparticles but rather to the zirconia matrix, as their concentration is high and does not align with the compositional analysis data obtained.

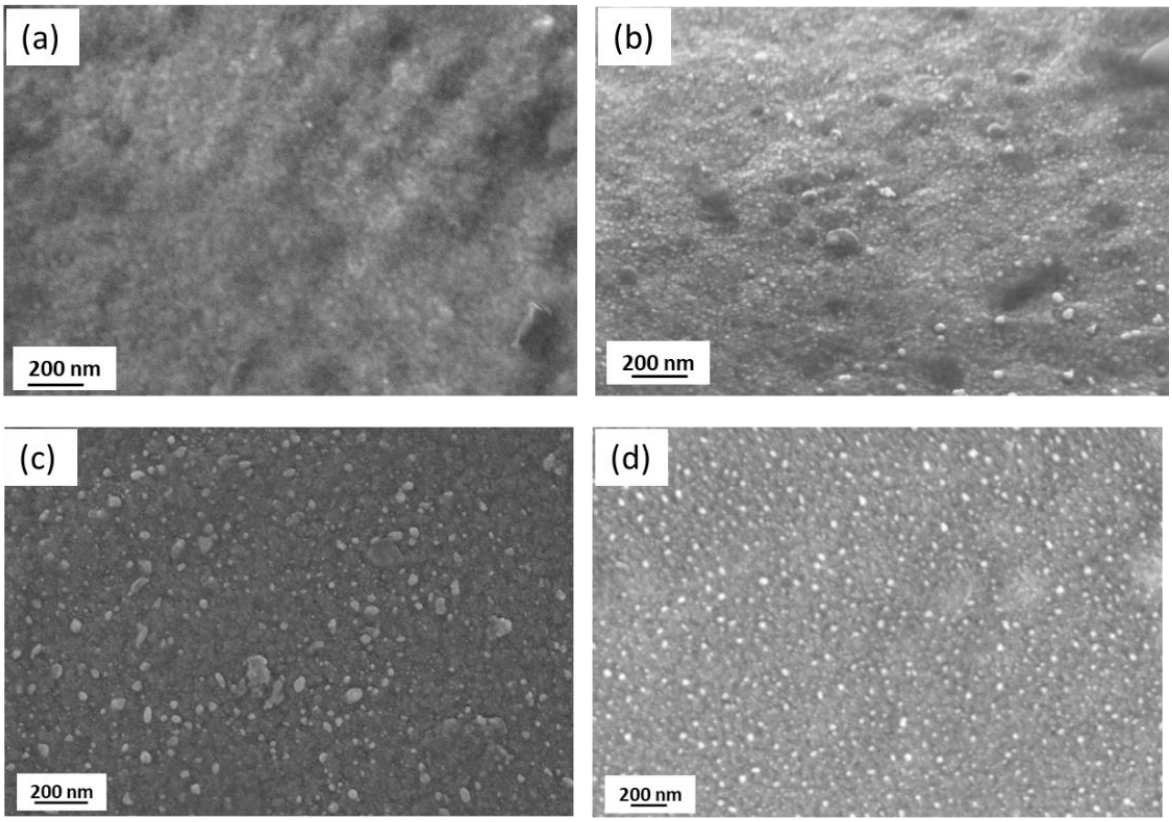

Figure 39: Morphological analysis of (a) uncoated Memb, (b) Memb_SiO2_Ag3, (c) Memb_ZrO2_Ag4 and (d) Memb_ZrO2_Ag5

The obtained silica coatings were amorphous, as will be revealed by XRD analyses, with a globular and porous morphology, typical of the deposition method. *Anton et al* [189] obtained the same globular morphology in their coatings, depositing silicon on Mo-based alloy through the magnetron sputtering technique.

For a more in-depth investigation into the size, shape, and distribution of silver nanoclusters in the coating, TEM analysis was conducted at AGH University of Science and Technology in Krakow, on SiO2_Ag5 and ZrO2_Ag5 coatings deposited on a Met filter as substrate.

In Figure 40, results of TEM analysis at different magnifications of Met_SiO2_Ag5 were reported. Figure 40 (a), shows the substrate and the coating at low magnification, with the protective Pt layer, deposited on the coating during sample preparation. Figure 40 (b), (c), and (d) are zoomed images focusing only on the coating. The structure of the composite coating appeared globular, with gray particles representing the SiO_2 matrix and the brighter areas indicating silver. The results showed that the deposited silver nanoclusters are small in size, only a few nanometers, and well distributed within the matrix. Data obtained by EDS maps, Figure 41, performed on the green area indicated in Figure 41 (a), showed a homogenous distribution of Si and O elements, which form the silica

matrix of the composite coating, while silver, represented in purple in Figure 41 (d), was detected in some spherical areas, corresponding to the nanoclusters embedded in the SiO_2 coating.

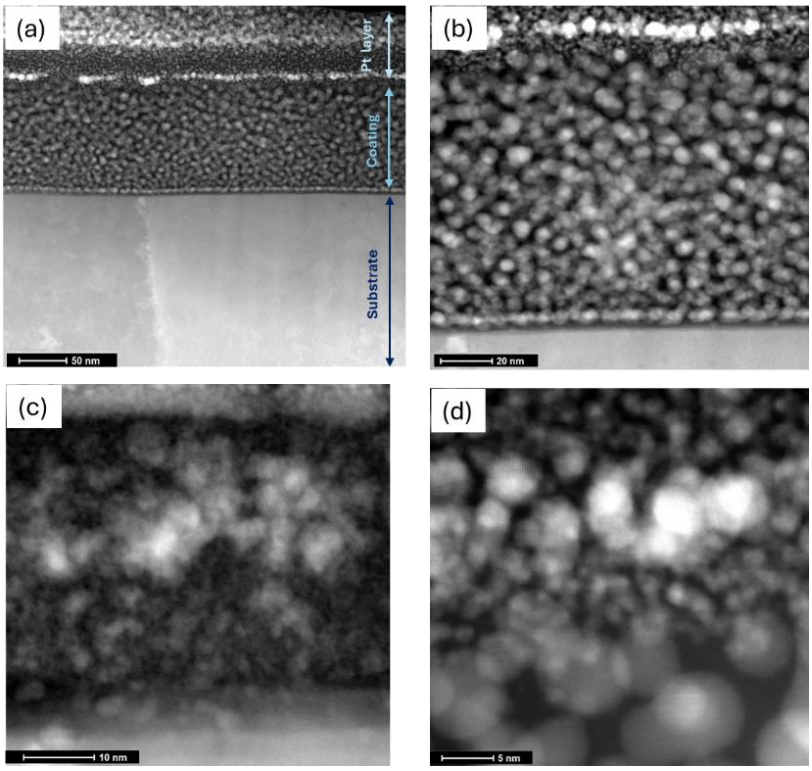

Figure 40: TEM analysis of Met_SiO2_Ag5 at different magnifications

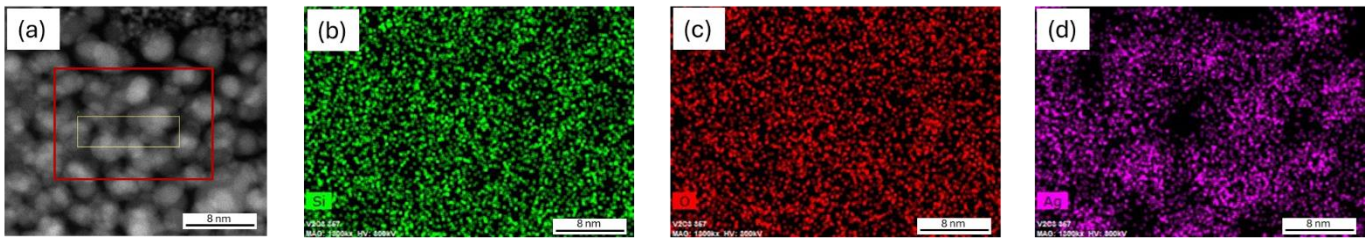

Figure 41: EDS map of Met_SiO2_Ag5: Si (green), O (red), Ag (purple)

Regarding, Met_ZrO2_Ag5, the presence of silver nanoclusters is confirmed by TEM analysis, as shown in Figure 42.

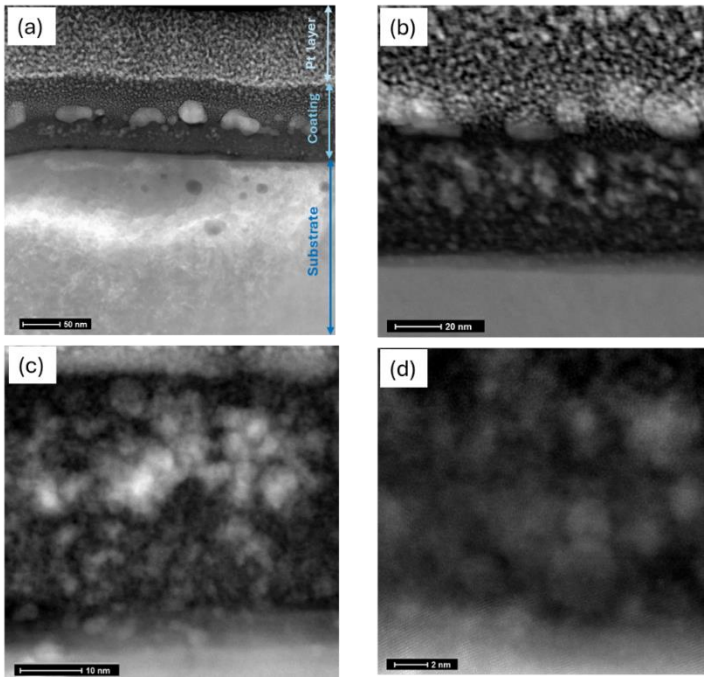

Figure 42: TEM analysis of Met_ZrO2_Ag5 at different magnifications

As previously, the substrate, the analyzed coating, and the Pt layer are indicated in the images at low magnification. In Figure 42 (a), brighter gray nanoparticles are well visible, and distributed in the middle of the coatings. As the following EDS maps will be revealed, they were probably nanoclusters of silver. Analyzing images at higher magnification, the ZrO2_Ag5 coating structure appeared globular. The bright areas indicate silver nanoclusters, small in size, about 20-30 nm, distributed in the entire zirconia matrix of the coating.

The EDS map (Figure 43) was performed on the area delimited by the red square in Figure 43 (a), and punctual EDS analysis was performed on the area delimited by green squares in Figure 43 (b). The images showed a silver nanocluster of about 20 nm, in yellow, in the coating made up of a zirconia matrix, represented by orange and green points, which indicate Zr and O, respectively.

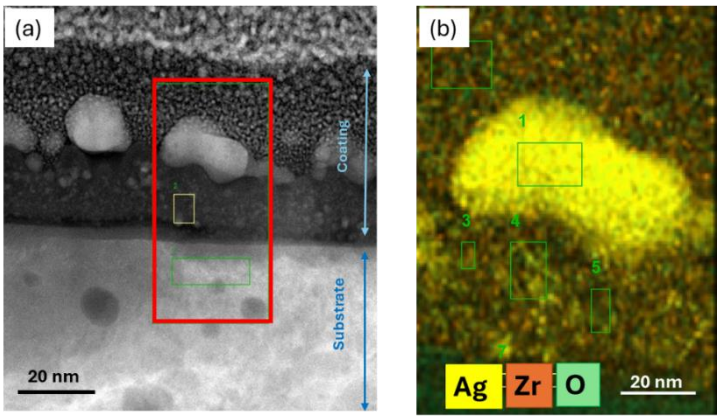

Figure 43: EDS map of Met ZrO2_Ag5 coating: Zr (orange), Ag (yellow), O (green)

For the structural evaluation of the studied coatings, silica- and zirconia-based coatings were deposited on soda-lime glass samples, to conduct XRD and UV-Vis analysis. For a simple explanation of the results obtained, they will be divided and shown according to the matrix taken into account. In Figure 44, a comparison of XRD spectra obtained by analyzing the coating made up of only silica, SiO_2, and composite coatings with a progressive increase in the amount of silver SiO2_Ag3 and SiO2_Ag5 is shown.

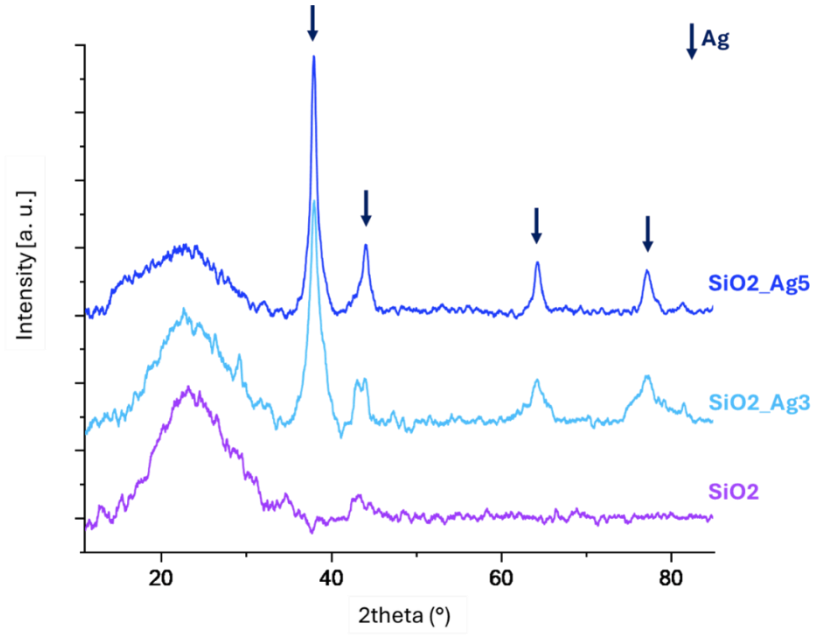

Figure 44: XRD analysis of SiO2, SiO2_Ag3 and SiO2_Ag5 coatings

Results revealed that the sputtered silica matrix had an amorphous structure, demonstrated by the presence of a halo at 2θ between 15 and 35°, and confirmed by recent studies through Raman spectroscopy analysis [190]. The silver nanoclusters were in a metallic state, indicated by peaks at 2θ = 38°, 44°, 64°, 77°, and 81°, corresponding to those of metallic Ag reference (ref code PCPDF 01-089-3722) [191]. The intensity of the peaks increases with the increase in the quantity of silver.

The UV-visible spectra of silica matrix and composite coatings are shown in Figure 45. For SiO_2 coating without silver, no absorption peak is detected; on the other hand, the curves referring to SiO2_Ag coatings show a clearly visible peak at a wavelength of about 414 nm, due to the plasmonic resonance of silver nanoclusters [192]. In the case of SiO2_Ag5, the peak is higher and shifted to a wavelength of 427 nm, probably because of a slight increment in the size of the nanoclusters or an increment of the Ag amount [193].

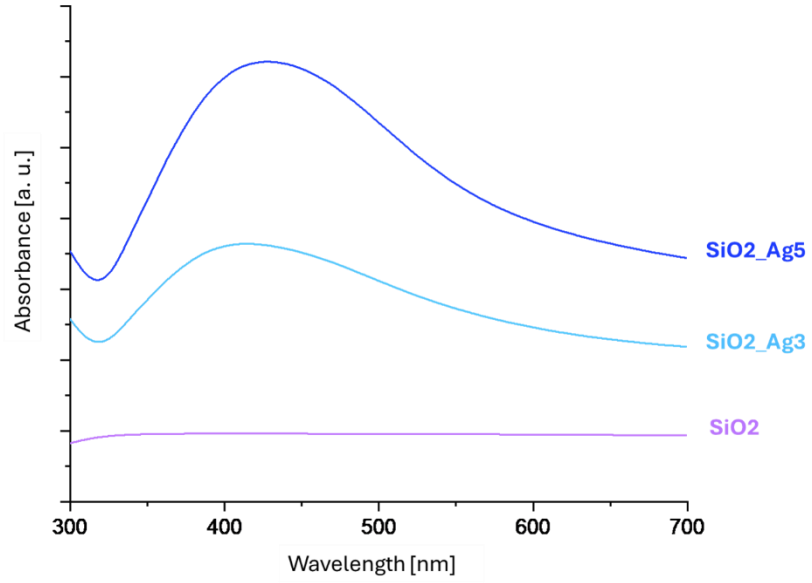

Figure 45: UV-Vis analysis of SiO2, SiO2_Ag3 and SiO2_Ag5 coatings

Considering zirconia-based coatings, the presence of the peaks at 2θ = 28°, 31°, and 34° in the XRD spectra in Figure 46 shows that zirconia matrix had a crystalline structure, in the monolithic form [194] even after the sputtering process. Conversely, when the composite coating was deposited, an amorphization process was induced and the matrix structure partially transformed into an amorphous phase, suggested by the broadening of the peaks that generates the halo-like structure, at 2θ between 20 and 30° [195]. The transition from the crystalline phase to an amorphous one was probably due to the deposition of a composite material. In previous studies, *Ben Amor et al.* [196] obtained crystalline zirconia through magnetron sputtering. However, it assumed an amorphous and globular structure when silica was introduced to obtain a composite coating SiO_2-ZrO_2. Peaks referred to the presence of silver nanoclusters are also detected, with a slight increase in the case of ZrO_Ag5.

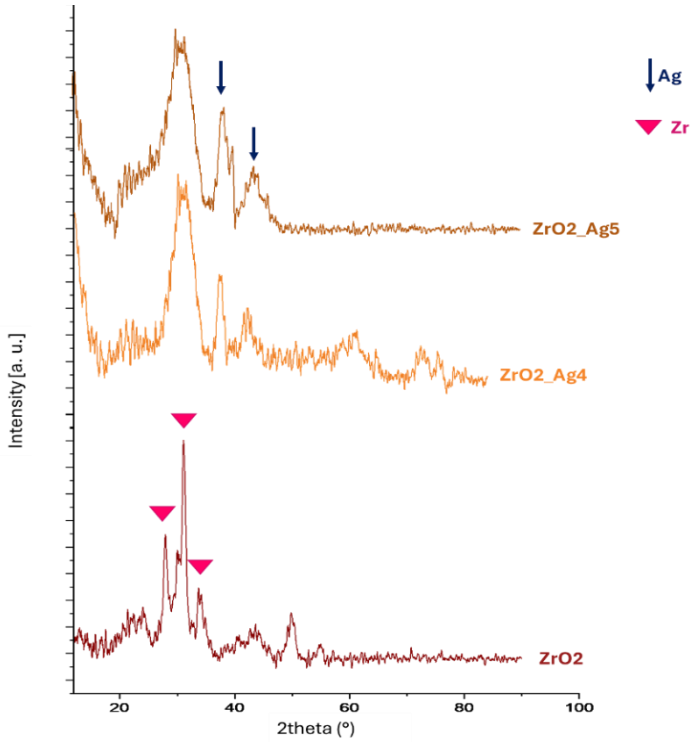

Figure 46: XRD analysis of ZrO2, ZrO2_Ag4 and ZrO2_Ag5 coatings

The UV-visible analysis is reported in Figure 47, comparing the two spectra of the coatings made up of zirconia matrix containing silver and without silver. In the curve related to ZrO_2 matrix, no peaks are shown, as aspectable due to the absence of silver nanoclusters. In the case of ZrO2_Ag4 and ZrO2_Ag5 curves peaks were detected in ranges of 448-466 nm and 376-385 nm, respectively. In addition, the ZrO2_Ag4 curve appears to be shifted to a higher value of wavelength, widened, and less intense, probably due to a smaller quantity of silver [193].

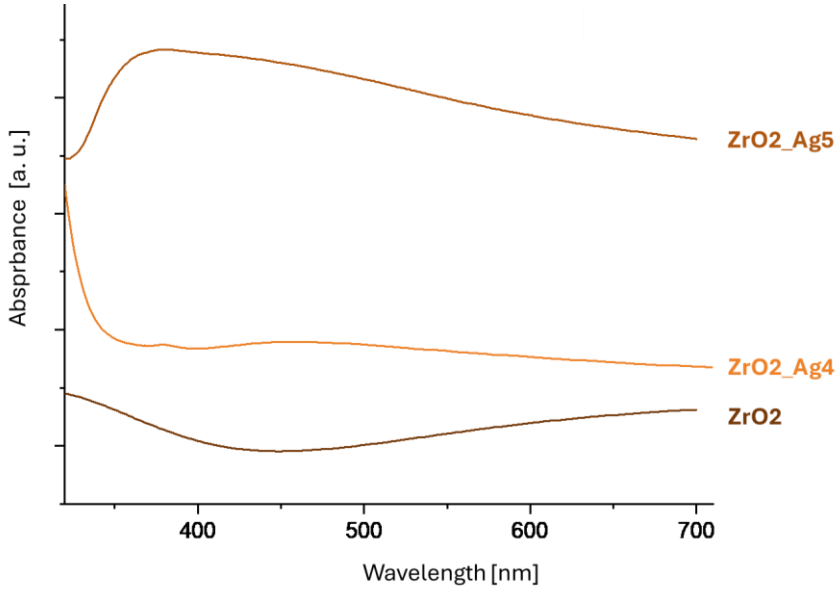

Figure 47: UV-Vis analysis on ZrO2, ZrO2_Ag3, and ZrO2_Ag5 coatings

Ions release test

An analysis of the amount of silver ions released from the silica or zirconia composite coatings was conducted in water at room temperature, for different times.

The release kinetics of Ag ions from silver nanoclusters/silica coatings was illustrated in Figure 48.

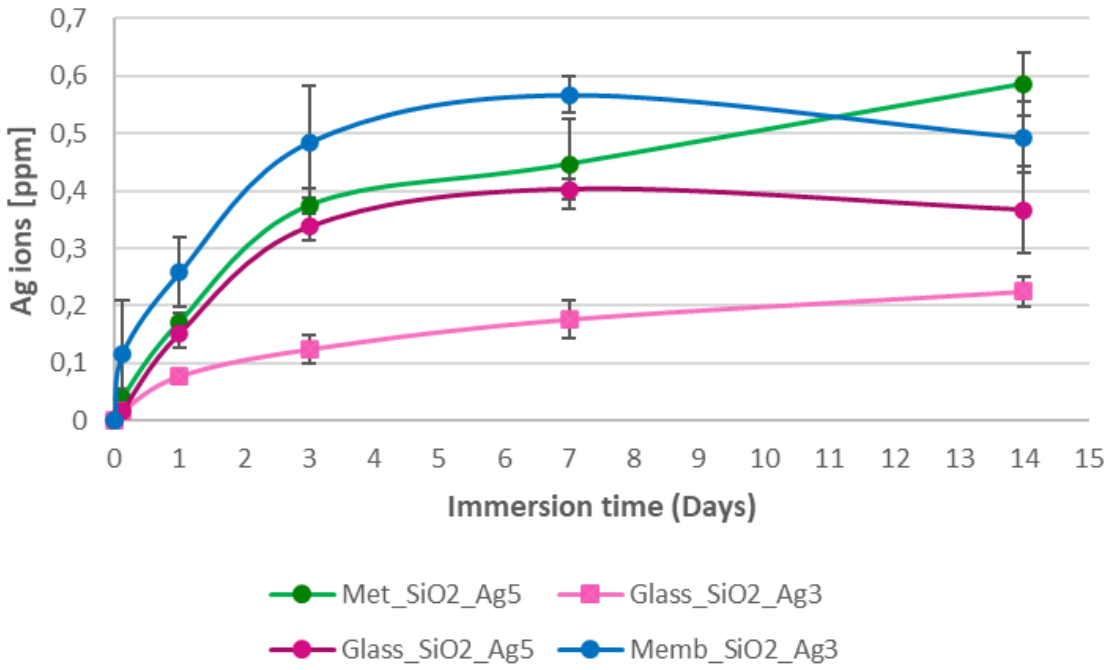

Figure 48: Amount of silver ions released from SiO2_Ag3 and SiO2_Ag5 coatings deposited on Met, Glass, and Memb filters, after two weeks in water at room temperature

As shown, the maximum value of released ions was 0.6 ppm, attributed to the coating on the metallic filter, Met_SiO2_Ag5. This datum is consistent with the results of EDS analyses, which demonstrated that the Met_SiO2_Ag5 coating exhibited the highest silver content when compared to the other cases. A particular trend is observable for the polymeric membrane, Memb_SiO2_Ag3, where a value of released ions around 0.6 ppm was detected already after 7 days of immersion, despite the reduced silver content (about 0.8% at.) detected in this coating by EDS analysis (Table 9) is probably due to the peculiar aptitude of the polymeric membrane to absorb water, facilitating the ion-release process.

Considering the coatings on the glass fiber filter, it is observed that the trend is the same for both coatings, but the amount of ions released by the Glass_SiO2_Ag5 coating is significantly higher than that from Glass_SiO2_Ag3, due to a greater amount of silver (0.94 at. % and 1.62 at. %, respectively).

Regarding the coatings with zirconia as a matrix (Figure 49:), in general, the amount of ions released by the coatings was gradual, and, the maximum value reached is 0.2 ppm, lower than that achieved with silica-based coatings.

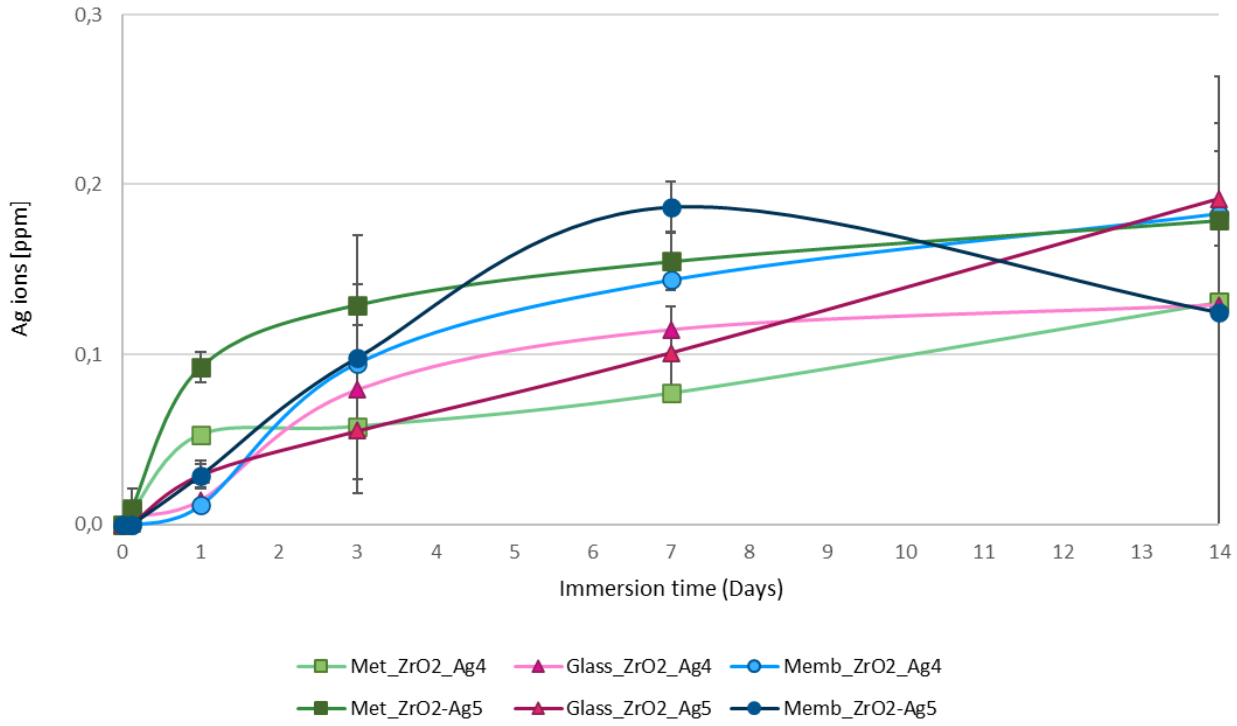

Figure 49: Amount of silver ions released from ZrO2_Ag4 and ZrO2_Ag5 coatings deposited on Met, Glass, and Memb filters after two weeks in water at room temperature

The explanation probably lies in the fact that, as already said, zirconia is less soluble in water compared to silica, which slows down the ions release. Furthermore, the amount of silver present in zirconia-based composite coatings, ranging from 0.33 to 1.20 % at., is generally lower than that detected in silica-based coatings, which ranges from 0.59 to 2.7 % at. However, the Met_ZrO2_Ag5 coating is an exception, exhibiting a significantly higher silver content compared to the other cases (4.17 at. %).

Regarding metallic filter as substrate, the amount of ions released by Met_ZrO2_Ag5 is higher than that in the case of Met_ZrO2_Ag4, as aspected. Similar to the coating composed of silica matrix, the amount of silver released by the polymeric membrane is similar to that of the metallic substrate after 7 days of immersion, reaching the highest value, confirming the behavior shown and described previously. The curve related to glass-fiber filters indicated a slower ions release, but the amount after two weeks is comparable to that of the other considered substrates.

In all cases, the value of released silver ions is higher than the minimum threshold to achieve antibacterial effects (0.1 ppm) [197], and the concentrations remain below the toxicity threshold for

human cells, which is defined as 10 ppm [198]. In addition, the presence of the matrix allowed controlled ions released, minimizing the cytotoxic effect [85].

Resistance to washing cycles

In a study conducted on silica and zirconia composite coatings containing silver nanoclusters deposited on cotton as a substrate, the behavior of SiO2_Ag3 and ZrO2_Ag3 coatings, in prolonged contact with water was evaluated. Specifically, their resistance to 1, 5, and 10 washing cycles was examined, and results were published in [180].

The macroscopic aspect of both silica and zirconia coatings as-deposited on cotton (0), and after 1, 5, and 10 washing cycles is shown in Figure 51.

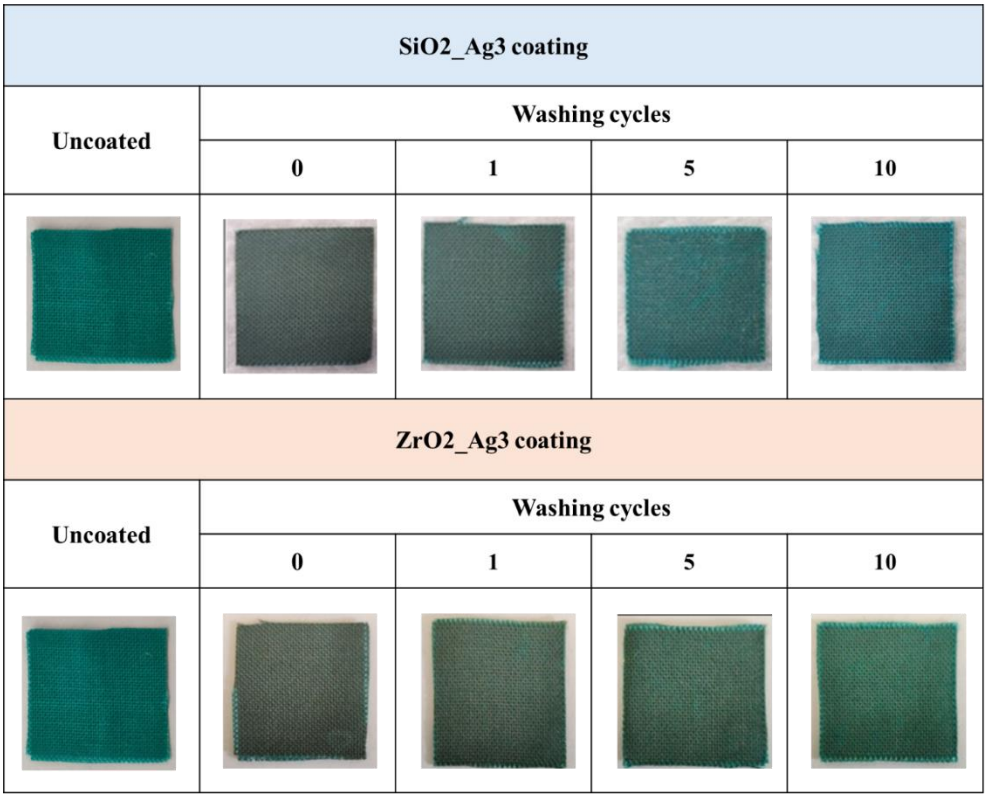

Figure 50: Macroscopic aspect of uncoated cotton, and of SiO2_Ag3 and ZrO2_Ag3 deposited on cotton, as-deposited (0) and after 1,5 and 10 washing cycles

In both cases, the cotton appeared darker after the deposition, as a consequence of the absorption effect of the silver nanoclusters, in addition, the dissolution of the coating in water led to a color change after the washing cycles. The color change is more evident in SiO_2-based coating, suggesting its solubility in water. The EDS analysis (Table 10), and the related histograms Figure 51(a) confirmed that the amount of Si was halved after the 1 wash, and drastically reduced, quite to zero, after 10 cycles demonstrating that the silica matrix of the coating dissolved in water faster than silver. Conversely, the reduction in the amount of Zr and Ag in zirconia-based coatings is only

30% as these composite coatings dissolved more slowly in water than silica and with a similar trend between Zr and Ag, exhibiting a better resistance when in prolonged contact with water. Probably, this is because zirconia is not completely amorphous, or it is due to the higher bond dissociation energy and stronger covalent bond of Zr-O-Zr compared to that of Si-O-Si, which makes the coating more stable in water, thus limiting hydrolysis. Furthermore, it has been demonstrated that certain functional groups can restrict the contact of aqueous solutions with the Zr-O-Si bond, thereby allowing the coating to remain anchored to the cotton [199].

Table 10: EDS analysis on silica/silver and zirconia/silver composited coatings deposited on cotton, as-deposited (0) and after 1, 5, and 10 washing cycles

Washing cycles	***SiO2_Ag coatings***		***ZrO2_Ag coatings***	
	Si (at. %)	***Ag (at. %)***	***Zr (at. %)***	***Ag (at. %)***
0	1.91 ± 0.07	0.97 ± 0.04	1.17 ± 0.03	1.14 ± 0.08
1	0.78 ± 0.06	0.66 ±0.03	0.72 ± 0.02	0.59 ± 0.01
5	0.54 ± 0.08	0.27 ± 0.02	0.50 ± 0.03	0.36 ± 0.01
10	0.07 ± 0.01	0.25 ± 0.01	0.37 ± 0.50	0.32 ± 0.02

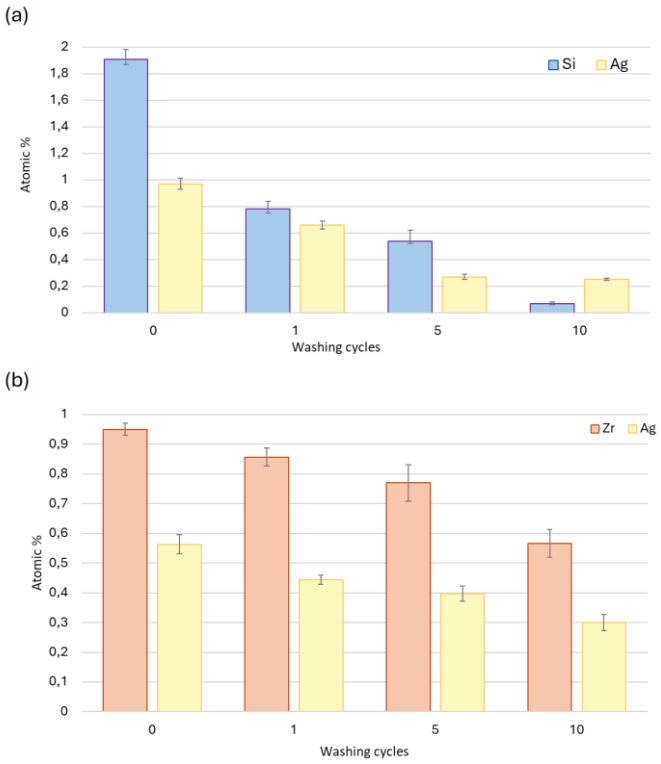

Figure 51: (a) Si and Ag amount in SiO2_Ag3 coatings and (b) Zr and Ag amount in ZrO2_Ag3 coatings deposited on cotton, as-deposited (0) and after 1, 5, and 10 washing cycles

To understand the effect of the washing cycles and of prolonged contact with water on the antibacterial efficacy of the coatings, an inhibition halo before and after washing test was performed on coated SiO2_Ag3 and ZrO2_Ag3 cotton against *S. epidermidis* (Figure 52). Both silica and zirconia-based coatings demonstrated antibacterial properties, shown by an area free of bacteria around the samples before the washing test, not visible around the uncoated cotton. In the case of SiO2_Ag3 coatings, the size of the halos decreased after washing cycles, due to the coating solubility in water, but an inhibition area around washed samples is visible. Regarding zirconia-based coating, the dimensions of the halos did not change so much after the washing process. These results revealed that the amount of silver detected by EDS analysis in composite coatings after 10 washing cycles was enough to ensure antibacterial activity.

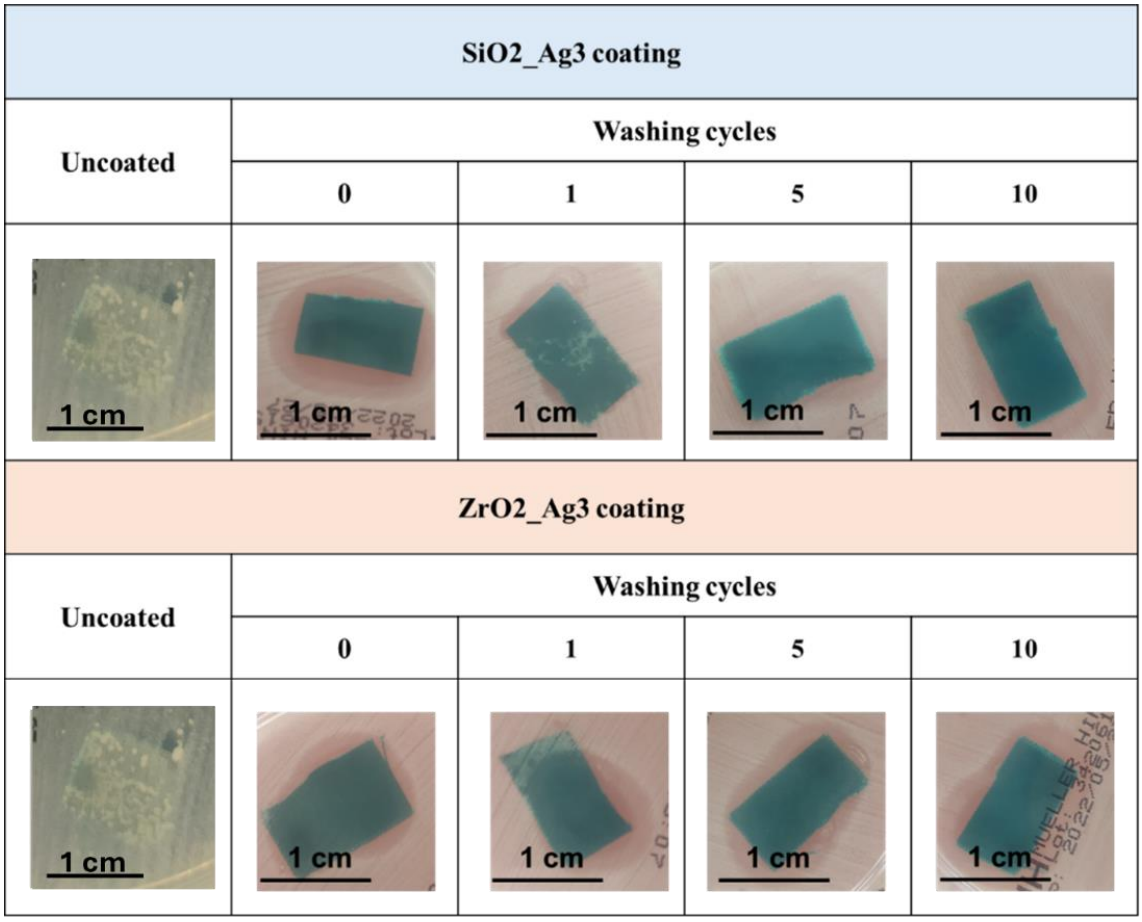

Figure 52: Inhibition halo test against S. epidermidis on uncoated cotton, and SiO2_Ag3 and ZrO2_Ag3 coated cotton, as-deposited (0) and after 1, 5, and 10 washing cycles

In general, several methods were evaluated to obtain cotton with an antibacterial effect even after washing cycles. For example, recently *Chen et al*. [200] introduced a method to synthesize silver nanoparticles in situ on cotton samples, using hyperbranched polymer (EPDA-HBP), obtaining an amino-grafted fabric. The fabrics exhibited great durability and excellent antibacterial properties

against *E. coli* and *S. aureus* and remained stable even after 30 washing cycles. In another study, the wash durability of cotton functionalized with in situ reduced silver nanoparticles was enhanced through mercerization pretreatment, a chemical process generally used to confer greater strength to cotton fibers, as well as shine and improved dye absorption, and under hydrothermal conditions. The resulting fabrics, resistant to numerous washing cycles, exhibited high antibacterial activity against *B. licheniformis*, and moderate activity against *K. pneumoniae*, and *E. coli* [201]. Conversely, pretreatments are not required in the case of the coating under investigation in this study. This is because the presence of the porous matrix, either silica or zirconia, allows the prolonged antibacterial action, attributed to the slow release of silver ions, and relative wash resistance, particularly in the case of the zirconia matrix.

Antibacterial test

The antibacterial and antifungal effects of silica- and zirconia-based coatings were qualitatively evaluated through the inhibition zone test against *S. epidermidis* and *E. coli*, as Gram-positive and Gram-negative bacteria strains respectively, and *C. Albicans*, as an example of a fungus.

The results of uncoated and coated filtering media obtained by the inhibition halo test for metallic filters are reported in Figure 53.

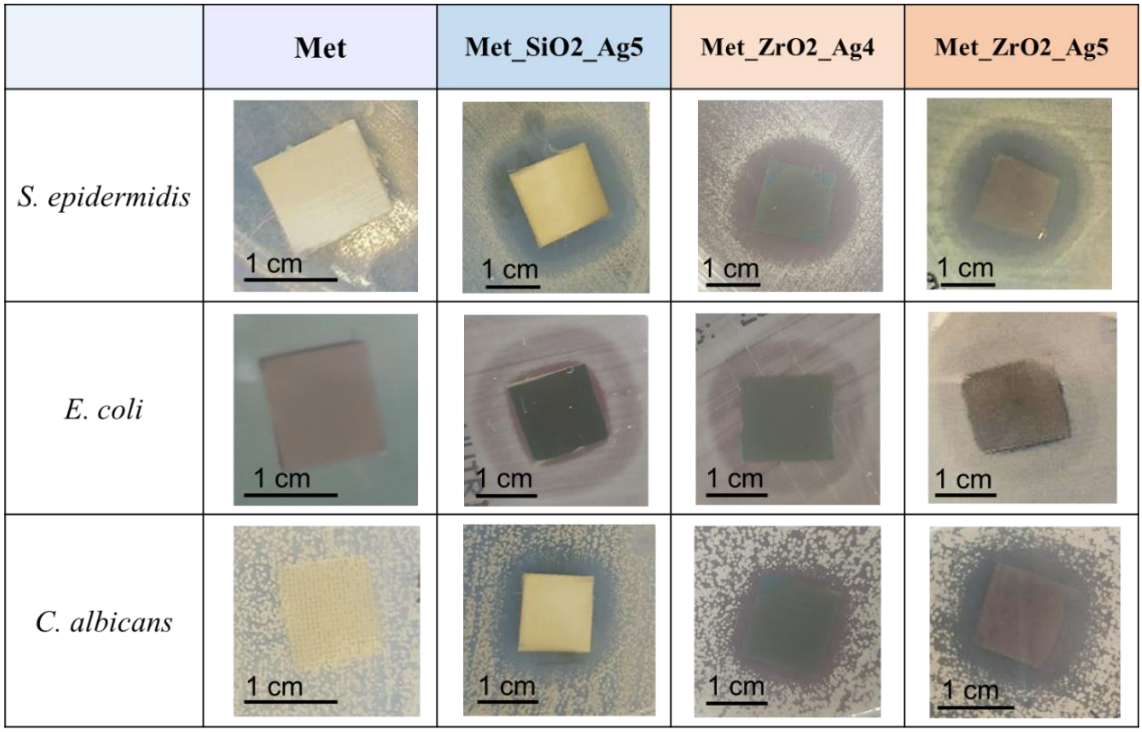

Figure 53: Inhibition halo test against S. epidermidis, E. coli, and C. albicans on Met, Met_SiO2_Ag5, Met_ZrO2_Ag4, Met_ZrO2_Ag5

Both silica- and zirconia-based coatings exhibited evident bactericidal and antifungal activity as the formation of an inhibition zone of approximately 3-5 mm around the coated samples is very clear. This zone indicates an area where bacterial colonies and fungi have not proliferated, likely due to the action of silver nanoclusters and released ions. The difference with uncoated samples is well evident. The uncoated Met sample did not exhibit an effect against bacteria and fungal growth, but colonies proliferated on the surface and around the filters. Data obtained testing coatings toward *E.coli* revealed a double inhibition zone, consisting of an area completely devoid of bacteria, which is closer to the sample, and an external and slightly darker zone where microbial growth has been slowed. This behavior was found and confirmed in other works [202] [203], but in any case, the combination of the two areas should be considered as the inhibition zone. No significant differences are evident when comparing the coating with higher and lower silver amounts in zirconia-based coatings, Met_ZrO2_Ag4 and Met_ZrO2_Ag5 coatings, but it is crucial to emphasize that this is a qualitative test, so further deeper investigations are needed.

A similar consideration could be done for glass-fibre-based filters (Figure 54).

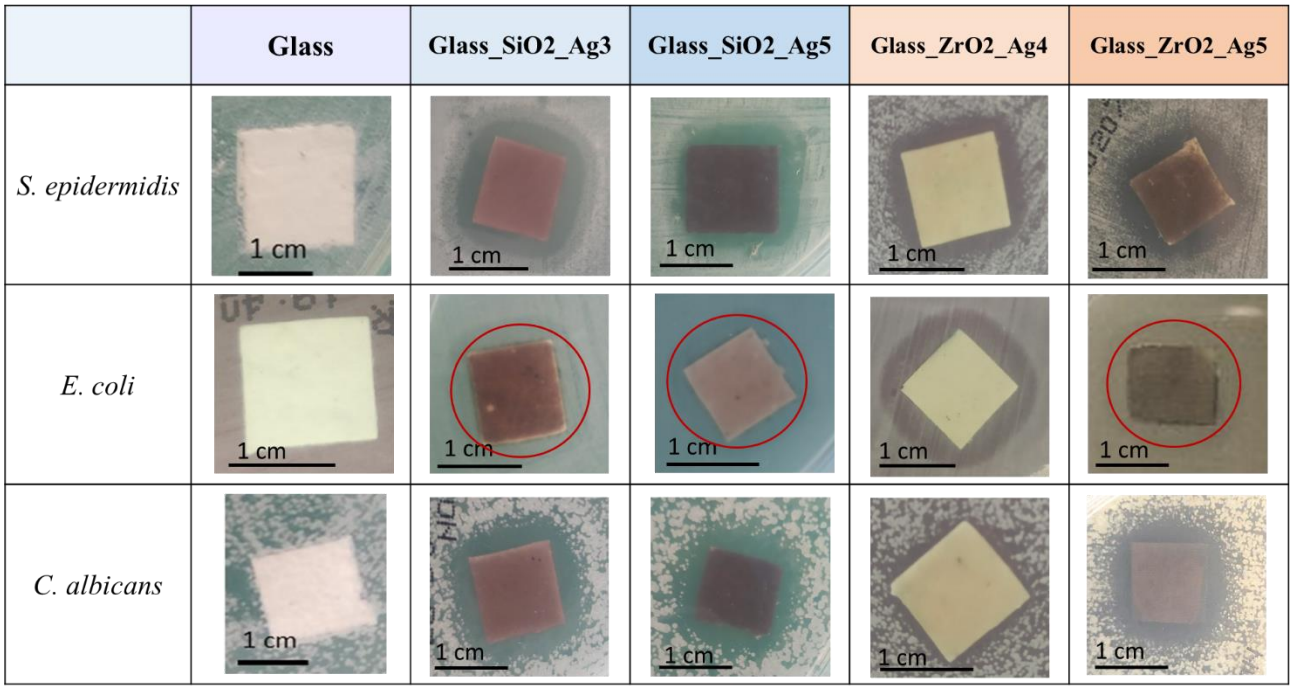

Figure 54: Inhibition halo test against S. epidermidis, E. coli, and C. albicans on Glass, Glass_SiO2_Ag3, Glass_SiO2_Ag5, Glass_ZrO2_Ag4, Glass_ZrO2_Ag5

In the case of filters without coating, bacteria growth was not inhibited, and colonies were visible on the surface of the sample and around it. The halos are well visible considering *S. epidermidis* and *C. albicans* strains, where the zone free from bacteria and fungi is well recognizable. On the contrary, the halos obtained when coatings were in contact with *E. coli* are less clear, but the bactericidal effect could be attested. Considering Glass_SiO2_Ag3 and Glass_SiO2_Ag5, the

difference in silver amount did not cause a significant difference in halo size, which appeared very similar. Deeper investigations through quantitative assays will be reported below. In the case of Glass_ZrO2_Ag4 and Glass_ZrO2_Ag5, some differences could be revealed, especially regarding the case of *C. albicans,* where the size of the inhibition areas is very different.

It is important to note that in the case of the polymeric membrane as a substrate, the effect varies depending on the matrix considered, as shown in Figure 55.

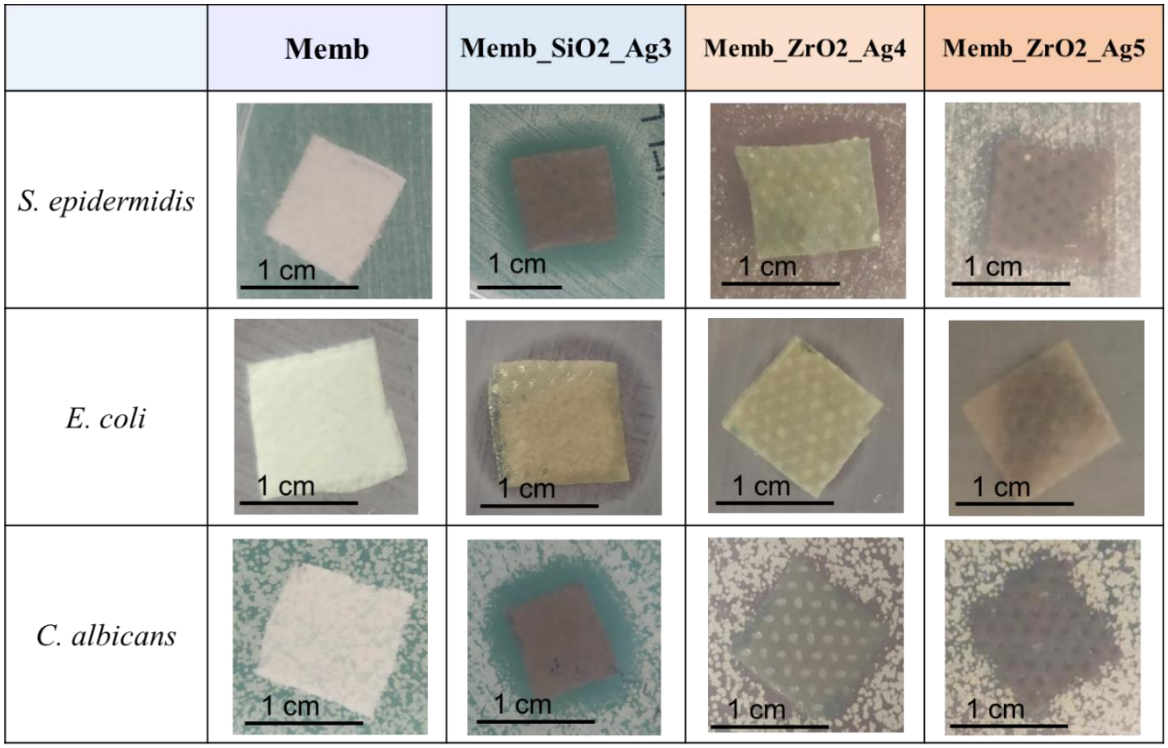

Figure 55: Inhibition halo test against S. epidermidis, E. coli, and C. albicans on Memb, Memb_SiO2_Ag3, Memb_ZrO2_Ag4, Memb_ZrO2_Ag5

In the case of coatings made up of silica matrix, the inhibition zone is clear and well-defined, while in the case of the zirconia matrix, it is not possible to identify a distinct inhibition zone. However, it should be noted that no visible bacterial colonies are present in contact with the coated surface of the samples, unlike for all uncoated substrates, where bacterial and fungal colonies grew both around the sample and in contact with it. It could be explained by referring to data obtained from the leaching test. In the case of silica matrix, the amount of silver ions released from the coating is high, comparable to that obtained from the coating on the metallic filter with a higher amount of silver, and showed an important bactericidal effect towards Gram-positive and Gram-negative bacteria and the fungus. Coating with zirconia matrix, on the other hand, is less soluble compared with silica, so the ions were released slowly, and after 24h the amount released was very low and not enough to obtain a well-evident halo.

The effect of silver nanoclusters against both Gram-positive and Gram-negative bacteria is well known and deeply evaluated in the literature, as a lot of reviews reported. Even though the mechanism is not fully understood, the action is due to the ability of silver nanoparticles and silver ions to interact with the bacteria cell wall and to destroy it, enter the cell, and product reactive oxygen species (ROS), which led to the apoptosis of the cell [9][27][204][205].

Recently, *Acharya et al.*[106], compared the bactericidal activity of silver nanoparticles and Ag-SiO_2 core-shell systems against *B. subtilis*, *S. aureus*, *S. marcescens*, and *K. pneumoniae*. They found that both NPs exhibited an antibacterial effect, but it was enhanced in Ag@SiO2, due to a prolonged release of ions through the porous silica shell, and to silver nanoparticles attached on the surface. Recently, *Young-Seon Ko et al.* [206] developed hybrid materials composed of silica nanospheres decorated with silver nanoparticles, AgNP@SiO2, which have been atomized onto air filters exposed to bacterial aerosols. This hybrid system demonstrated the ability to trap both *S. epidermidis* and *E.coli* bacteria, destroying their cell walls in an attempt to free themselves. Further analysis revealed that bare silver nanoparticles can create a groove on the membrane of Gram-negative bacteria, while the hybrid particles, AgNP@SiO2, act upon contact with the cell wall. This system proves to be particularly effective due to the synergistic effect of AgNP@SiO2 and exposed bare silver nanoparticles. It differs from the one developed in this thesis work, where silver nanoclusters are not only exposed on the surface but they are well distributed within a porous silica matrix. In this case, the antibacterial effect is likely due to the action of nanoclusters themselves and ions released from the coating in a controlled and gradual manner, allowing for prolonged bactericidal effects over time. Alternatively, to coatings, the antibacterial agent can be integrated into the filter, in order to obtain membranes of polyvinylidene fluoride, PVDF, nanofiber, by electrospinning, modified by impregnation in SiO_2 solution containing silver nitrate as Ag precursor. *E. Coli* was inhibited by PVDF/SiO2 membrane and the effect was enhanced by adding Ag, while *S. aureus* was sensitive only to PVDF/SiO2/Ag membranes [109]. Recently, *Balagna et al*. deposited silica/silver composite coating through a co-sputtering method on an air filter, which was put in a real conditioner in a laboratory for 30 days. The results showed that colonies of different bacterial and fungi strains (not identified) grow on the uncoated filters, while they did not grow in the presence of the composite coating [184]. The inhibition of Ag-SiO_2 nanoparticles of *C. albicans* was tested by *Natalia et al.* [207], who found that the minimum inhibition concentration in presence was 1000 μg/ml.

Zirconia is largely used for its biocompatibility, low affinity to the formation of biofilm, and low cytotoxicity in vitro [208][209]. The antibacterial effect of silver is exhibited also in the presence of

of zirconia as the matrix. ZrO_2 nanoparticles, functionalized with dihydroquercetin, DHQ, and decorated with Ag nanoparticles showed an antibacterial effect against *S. aurueus* and *E. coli* as a function of exposition time and concentration [210]. Core-shell silver-zirconia nanoparticles exhibited a strong bactericidal effect against *E. coli* and *S. aureus*, and antifungal activity against *C. albicans* [211].

For a deeper and better understanding of the antibacterial properties of the studied coatings, a quantitative test was conducted to quantify the number of bacterial colonies proliferating in a bacteria solution in the presence of coated and uncoated samples. In addition, it was possible to determine the number of colonies adhering to the surface. This test was performed considering only *S. epidermidis* as the bacterial strain.

First, the solutions' McFarland index was evaluated, and the values, and related images of the broths, are reported in Figure 56.

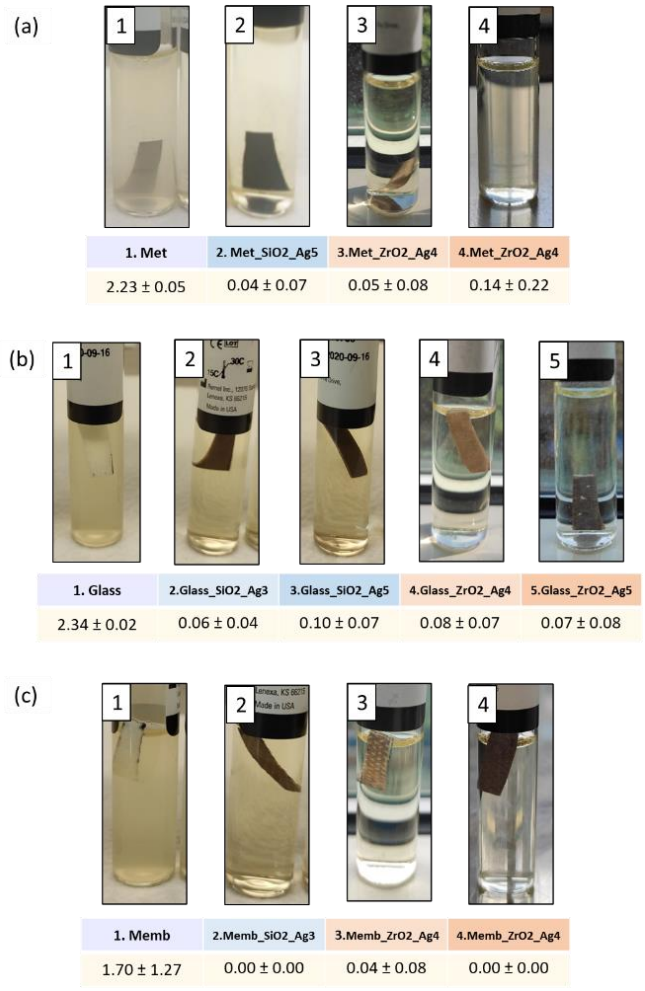

Figure 56: McFarland index of bacterial solutions with uncoated and SiO2_Ag3, SiO2_Ag5, ZrO2_Ag4, and ZrO2_Ag5 coated (a) Met, (b) Glass and (c) Memb filters

As can be clearly observed, in the case of uncoated substrates, the McFarland index values were very high, approximately 2.3 for Met and Glass, and around 1.7 for Memb, compared to the starting one that was less than 0.5, and they referred to solutions very turbid. In the presence of the coating, however, the values were drastically reduced, and qualitatively, it can be noted that the solutions are clear.

In the case of SiO2_Ag3 and SiO2_Ag5, there was a strong reduction of McFarland index, especially considering that the coatings were deposited on only one side for each sample. In the case of Memb_SiO2_Ag3 the value reached is around 0.0, and for metallic and glass-fiber filters is around 0.03-0.10. Considering zirconia-based coatings, the values are very low, in a range between 0.00 for Memb_ZrO2_Ag5 and 0.14, for Met_ZrO2_Ag5. All the solutions containing coated samples appeared very limpid, on the contrary, the turbidity of solutions with uncoated samples was visible.

Figure 57 represents the histograms obtained from the analysis of bacterial broths for the three tested substrates and related silica- and zirconia-based coatings. The red line indicates the initial concentration of bacterial colonies in each broth, equal to $5*10^5$ CFU/ml.

A strong bactericidal effect of the silica-based coating is immediately noticeable regarding the metallic filter Figure 57 (a). In the absence of any coating, bacterial colonies proliferate in the broth to reach an order of magnitude of 10^{12} CFU/ml. On the other hand, the Met_SiO2_Ag5 composite coating reduced the amount of CFU proliferated by 7 orders of magnitude, to approximately 10^5 CFU/ml, after 24 hours of incubation. For both Met_ZrO2_Ag4 and Met_ZrO2_Ag5, the number of proliferated colonies was about 10^8 CFU/ml, and was not affected by the different silver amounts. These results are very interesting, considering that, for all the samples studied, the coatings were deposited on only one side of the filters, which is the side in contact with the air flux when used in air filtration systems. The silica-based composite coating on the metallic filter showed a more effective bacteria-killing effect, if compared to the zirconia one, due to the already described higher solubility of silica in water, which allowed a higher and faster amount of released ions, resulting in a more intense inhibition effect.

Regarding the results of glass-fiber filters, the behavior of the four analyzed coatings is shown in Figure 57(b). Specifically, in the case of silica-based coatings, SiO2_Ag3 and SiO2_Ag5, the bactericidal activity was not affected by the different amounts of silver in the coating, with a reduction of colonies proliferated in both cases of 5 orders of magnitude, concerning the uncoated sample, for which a value of about $9.3 *10^{12}$ CFU/ml was achieved. Regarding coatings composed

of zirconia as a matrix, the increment of silver amounts led to a slight increment in the inhibitory effect.

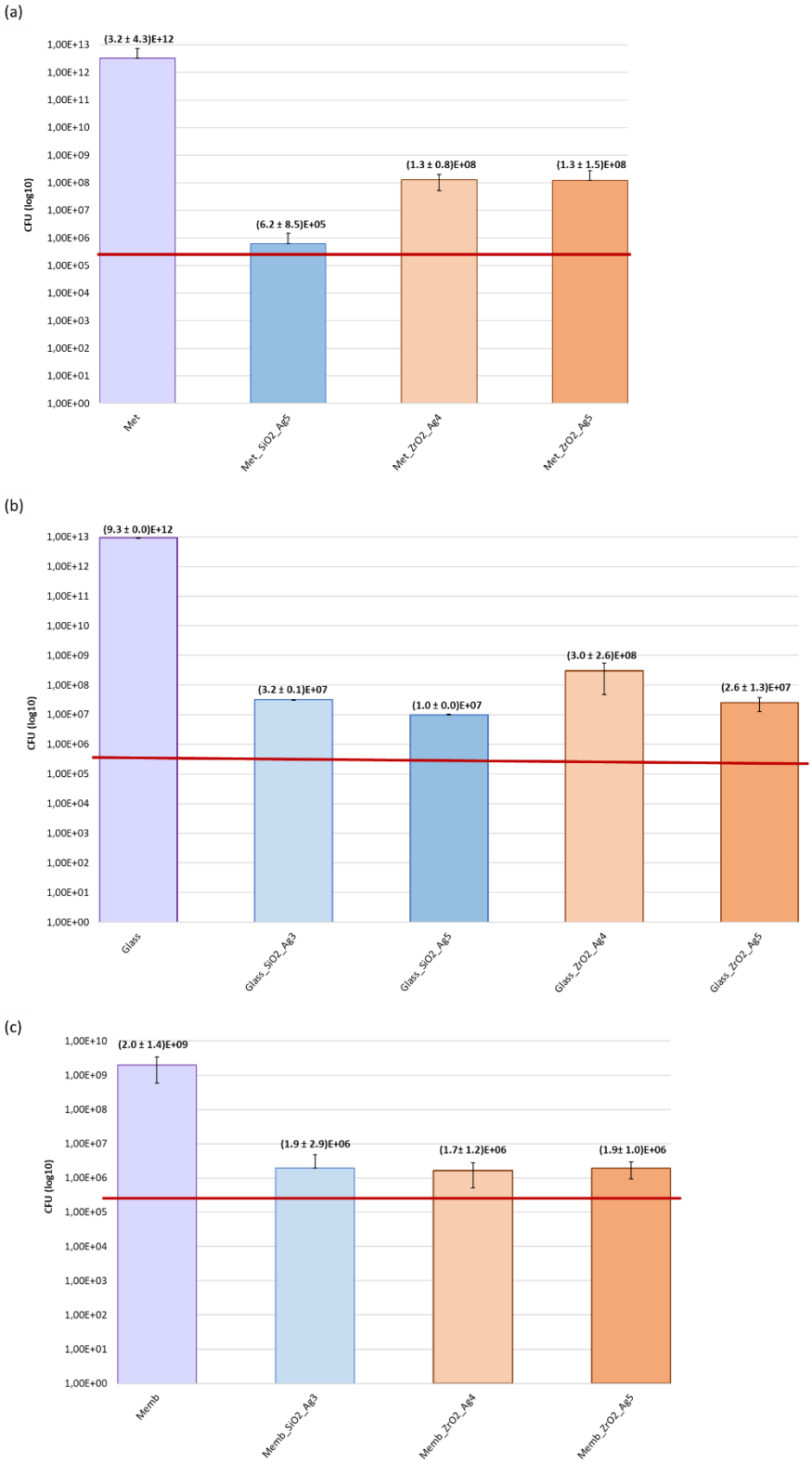

Figure 57: Count of S. epidermidis colonies proliferated in broth with uncoated and SiO2_Ag3, SiO2_Ag5, ZrO2_Ag4, and ZrO2-Ag5 coated (a) Met, (b) Glass and (c) Memb filters

The last case is represented by the polymeric membrane, whose results are depicted in Figure 57(c). In the case of the uncoated Memb, the proliferated colonies reached an amount of about 10^9 CFU/ml. In the cases of Memb_SiO2_Ag3, Memb_ZrO2_Ag4, and Memb_ZrO2_Ag5, the proliferated colonies were about 10^6 CFU/ml, without substantial differences for each coating.

After vortexing all the contaminated samples in a sterile physiological solution, it was possible to determine the amount of bacteria colonies that adhered to the surface of the samples during the incubation in 24 h. The data are summarized in Figure 58.

The concentration of colonies proliferated on uncoated substrates was about 10^7 CFU/ml for Glass, and 10^8 CFU/ml, for Met and Memb. Compared to the uncoated filter, Met_SiO2_Ag5_VORTEX and Met_ ZrO2_Ag4_VORTEX samples, (Figure 58 (a)) reduced the value to 10^4 CFU/ml, while Met_ZrO2_Ag5_VORTEX unexpectedly demonstrated a slightly higher value (10^6 CFU/ml), which nonetheless remains lower compared to the uncoated case.

The results obtained from comparing the coatings deposited on the glass fiber-based filter (Figure 58 (b)) are consistent with those obtained in the broths counting. The varying amount of silver in the coatings did not result in a significant difference in bactericidal action, regarding both cotings in silica and zirconia matrix. For all the studied cases, the number of colonies adhered on coated samples was about 10^5-10^6 CFU/ml, reduced compared to uncoated Glass (about 10^7 CFU/ml). Furthermore, there are no apparent differences in behavior between the two different matrices.

Considering the polymeric membrane (Figure 58 (c)), the presence of the composite silica/silver coating has reduced the bacterial colonies adhered on the filters of 3 orders of magnitude if compared with that on the uncoated samples (10^8 CFU/ml for Memb_VORTEX, 10^5 CFU/ml for Memb_SiO2_Ag3_VORTEX), whereas the deposition of the zirconia/silver coating resulted in a reduction of two orders of magnitude, with negligible differences between the two different quantities of silver.

So far, it has been demonstrated that the application of antibacterial coatings on the surface of air filters is useful in limiting the proliferation of bacteria or fungi, thus preventing their dispersion into the environment during the use of filtration systems. In addition, the coating also performs a

protective function for the filter, as it reduces the risk of deterioration and corrosion caused by the possible formation of a bacterial biofilm.

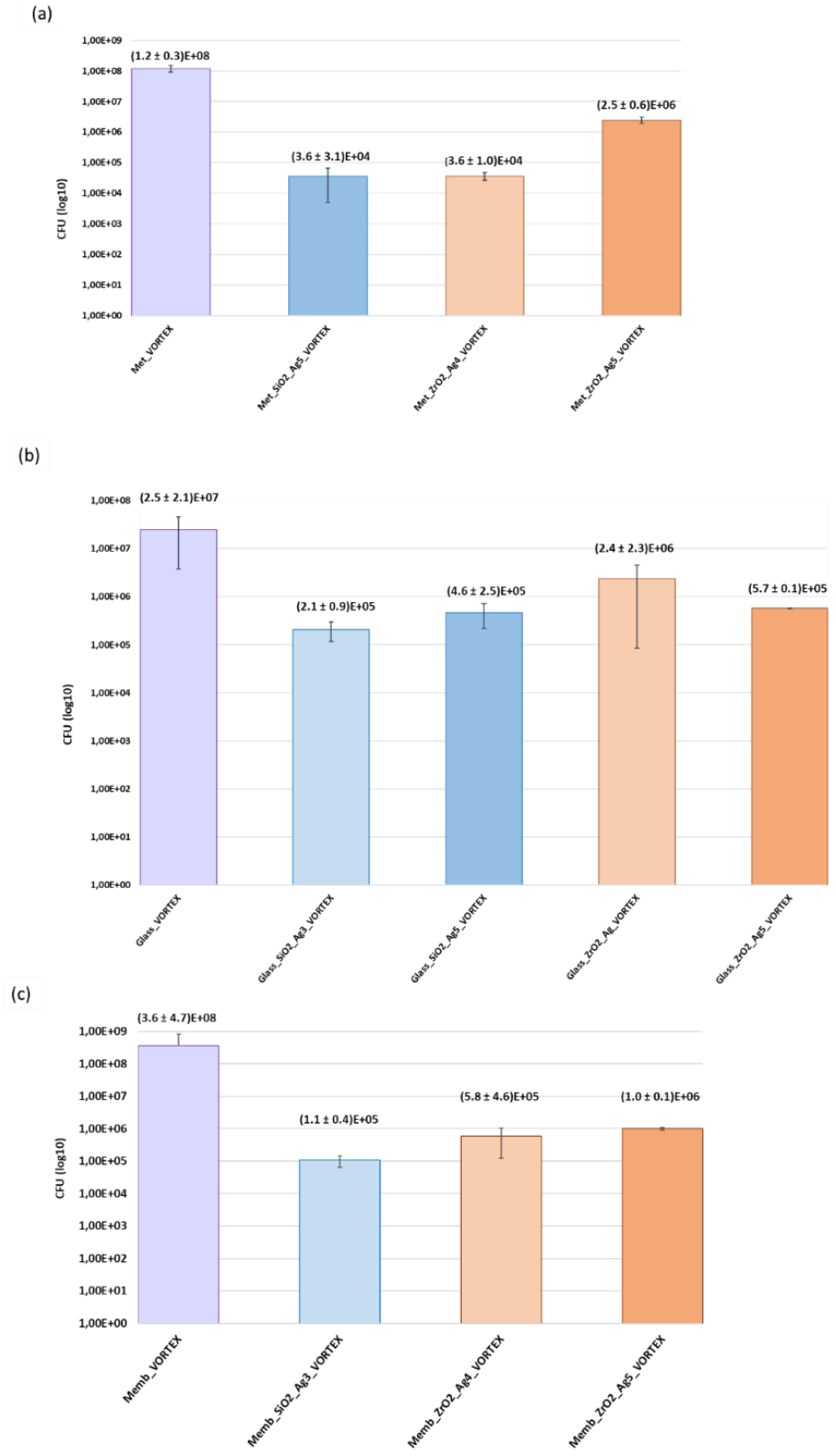

Figure 58: Count of S. epidermidis colonies adhered on the surface of uncoated and SiO2_Ag3, SiO2_Ag5, ZrO2_Ag4 and ZrO2_Ag5 coated (a) Met, (b) Glass and (c) Memb filters, after vortex process

Another important aspect to consider in the development of these materials is the possibility of reusing them, aiming to decrease waste production. Heat treatments are effective and rapid methods for sterilization. For this reason, contamination and thermal regeneration tests on the as-received and coated samples were performed, to evaluate if the coatings lost their antibacterial efficacy after the sterilization process. For this reason, a two-step, very rigorous test was conducted using a high-concentration bacterial solution of *S. epidermidis*, with a McFarland value equal to 5. The first step consisted of the contamination of the filter surface with the nebulization for 30 minutes of the bacterial broth using a bioaerosol generator. After placing the filters in contact with the agar nutrient plate and incubating for 24 hours, bacterial growth was evaluated, and the results are shown in Figure 59.

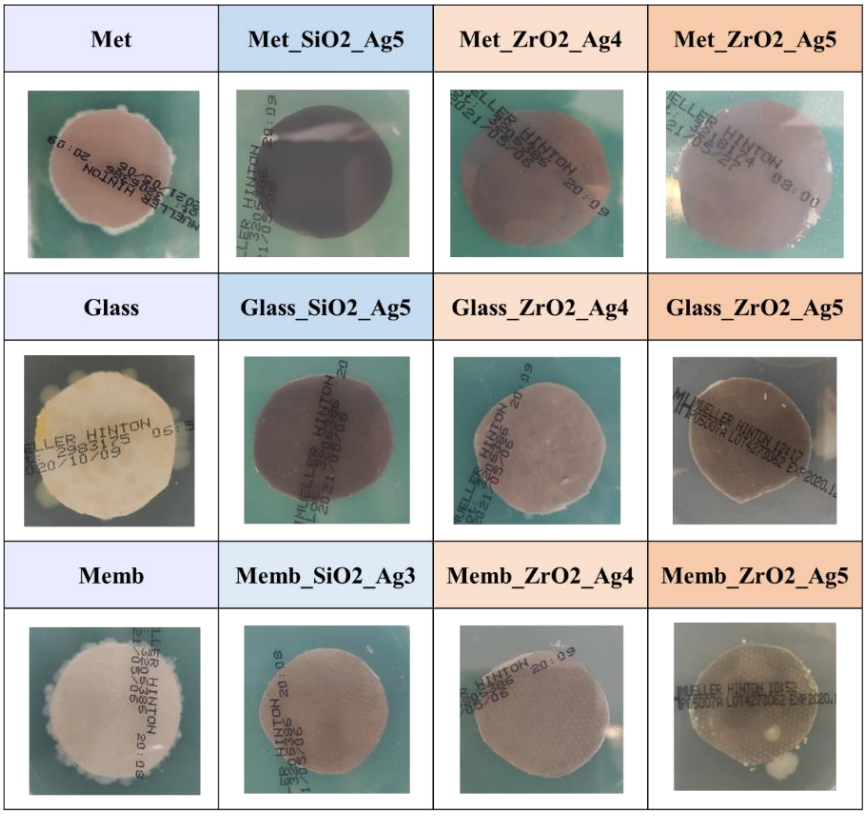

Figure 59: 30-minute contamination test against S. epidermidis on uncoated and SiO2_Ag3, SiO2_Ag5, ZrO2_Ag4, and ZrO2_Ag5 coated Met, Glass, and Memb filters

Both silica/silver and zirconia/silver composite coatings inhibited, or significantly reduced, *S. epidermidis* colonies on filtering media. In particular, in the case of Met and Glass filters, no colonies proliferated in contact with coated samples, and no differences were visible among SiO2_Ag5, ZrO2_Ag4, and ZrO2_Ag5 coatings. On the contrary, microorganisms grow around and in contact with the uncoated samples. Regarding Memb, the presence of SiO2_Ag3 and ZrO2_Ag4 coatings exhibited a strong antibacterial effect, and no colonies proliferated on them, in contrast

with what happened on uncoated Memb. Memb_ZrO2_Ag5 showed slight contamination, probably caused by the drop of the broth used during the test.

The subsequent thermal regeneration test was conducted only on metallic and glass-fiber-based filters. Since the heat treatment occurred at a high temperature (200° C) for three cycles, the test was not performed on the polymeric membrane, as the process would damage it. After the thermal treatment, a second contamination occurred following the same procedure previously described, and after incubation for 24 hours, the bacterial growth was evaluated. The results are shown in Figure 60.

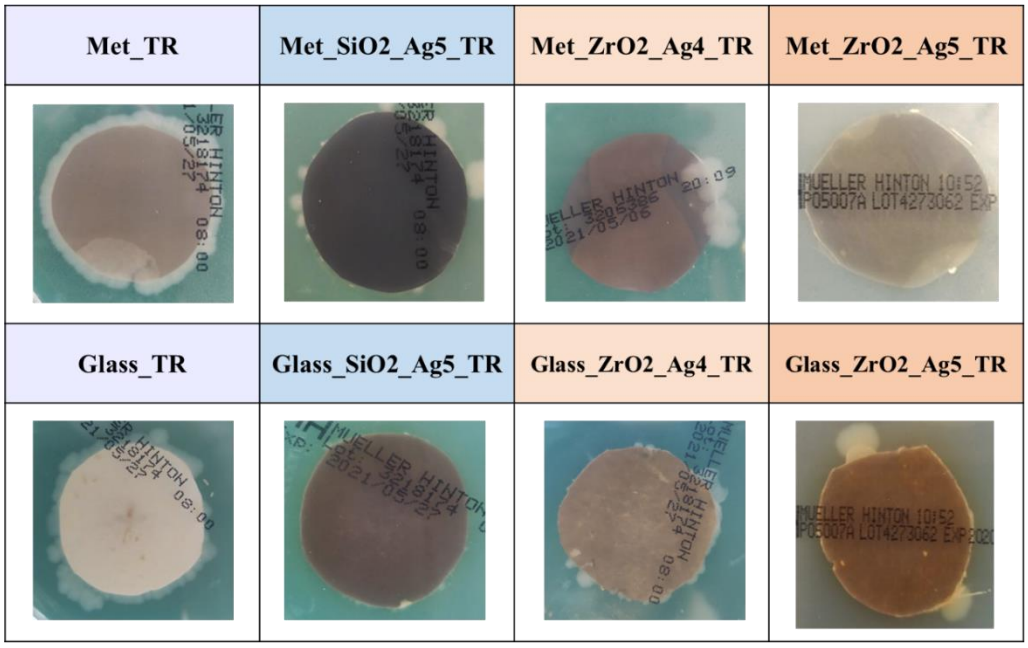

Figure 60: 30-minute contamination test against S. epidermidis on uncoated and SiO2_Ag5, ZrO2_Ag4, and ZrO2_Ag5 coated Met, Glass, and Memb filters after the thermal regeneration process

Regarding the metallic filter, both Met_SiO2_Ag5_TR and Met ZrO2_Ag4_TR showed a reduction in the number of proliferated colonies, while in the case of Met_ZrO2_Ag5_TR, no bacteria colonies grew, showing that the thermal treatment did not alter the antibacterial effect of the coating. In contrast, numerous bacterial colonies are visible in contact with Met_TR.

In the case of filters made of glass fiber, no bacteria were detected in contact with Glass_SiO2_Ag5_TR, but a few colonies are visible on both thermal regenerated zirconia-based coatings. In all the cases, the number of colonies proliferated on the uncoated filter was higher than that present on coated samples, demonstrating that the bactericidal efficacy of the coatings was not compromised by thermal treatment. No significant differences can be highlighted between the two matrices.

To have a deeper understanding of the effect of the thermal sterilization process on the bactericidal activity of coatings, the CFU counting test was also performed on SiO2_Ag5 and ZrO2_Ag5 coatings for Met and Glass, and on SiO2_Ag3 and ZrO2_Ag5 coating for Memb.

Figure 61 shows the results relative to the McFarland index of contaminated metallic, glass-fiber, and polymeric filters before and after the thermal regeneration process.

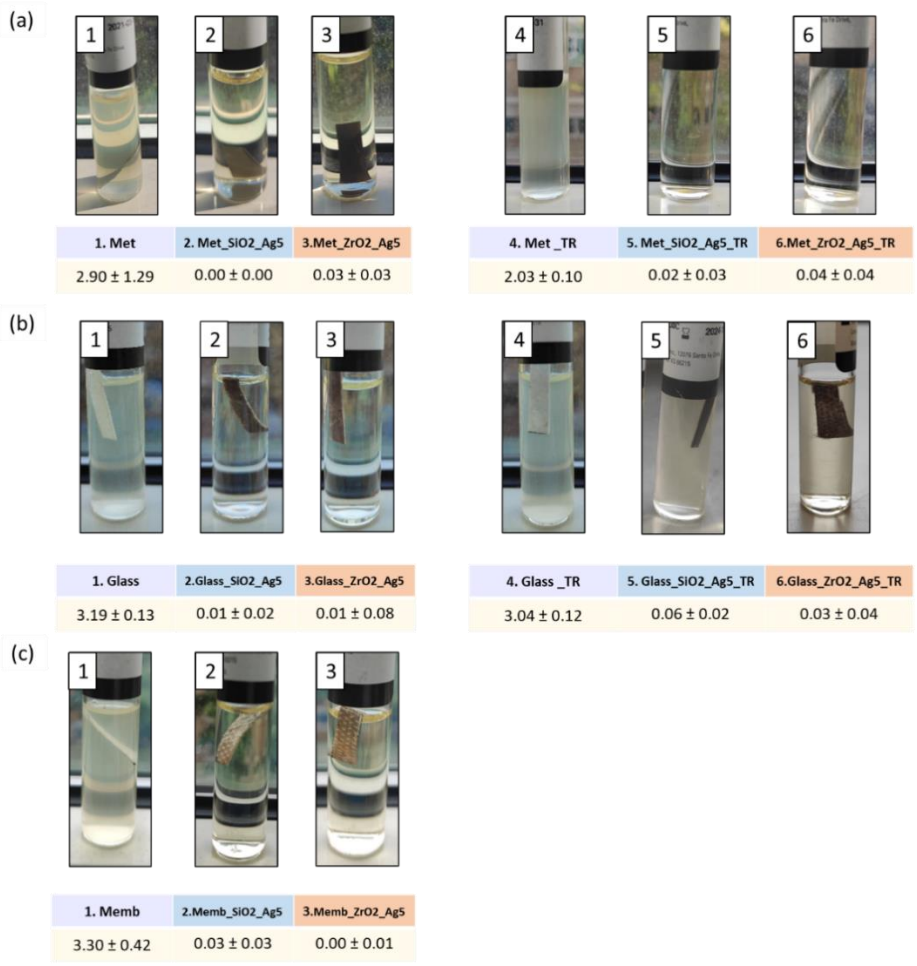

Figure 61: McFarland index of bacterial solutions with uncoated f and SiO2_Ag5 and ZrO2_Ag5 coated (a) Met, (b) Glass, and (c) Memb filters before and after the thermal regeneration process

For the metallic filter, Figure 61(a), the McFarland index of the broth with Met_SiO2_Ag5 and Met_ZrO2_Ag5 was about 0.00, drastically reduced compared with that of the solution containing uncoated Met, which was 2.90. After the thermal regeneration process and second contamination, the values of the McFarland index for coated samples remained very low, and also the turbidity of the solutions confirmed these considerations.

Solutions in contact with contaminated uncoated Glass reached high values of McFarland, more than 3.00, which remained quite equal to that of Glass_TR. In the presence of silica- and zirconia-based coatings, these values were drastically reduced, even after the sterilization treatment, where the highest value was about 0.06, as shown in Figure 61(b). As for the previous case, for the polymeric membrane (Figure 61(c)), only the first step of the test was performed, which concerned the

contamination of the uncoated and coated samples, while the thermal regeneration process was not conducted. The solution containing Memb is very turbid, and the relative Mc Farand value is very high, more than 3.00, while the presence of SiO2_Ag5 and ZrO2_Ag5 coatings drastically reduced the index.

Figure 62(a) summarizes the number of colonies that proliferated in broths containing contaminated Met, Met_SiO2_Ag5 and Met_ZrO2_Ag5, before and after thermal regeneration, while in Figure 62(b) the number of bacterial colonies adhered on the surfaces of the same samples is shown. In the case of uncoated Met, the amount of *S. epidermidis* colonies proliferated was the same before and after the thermal regeneration process, about 10^{11} CFU/ml. Met_SiO2_Ag5 is confirmed to have a strong antibacterial effect. The number of proliferated colonies was about 10^3 CFU/ml, and did not change if the samples underwent to thermal treatment, Met_SiO2_Ag5_TR. Regarding Met sample with the coating made up of zirconia and silver, no bacterial colonies were counted, probably because bacteria proliferated and adhered on the sample surface, as will be shown below, considering the vortex process, while after the sterilization process and second contamination, in Met_ZrO2_Ag5_TR broth, colonies proliferated were about 10^3 CFU/ml, like silica-based coating. After vortexing all the samples analyzed, the number of adhered bacteria was quite similar before and after the thermal process, both for uncoated and coated Met. Considering Met_SiO2_Ag5_VORTEX and Met_SiO2_Ag5_TR_VORTEX, the number of adhered colonies was quite the same, while in the case of ZrO2_Ag5 coating, adhered colonies were about 10^4 CFU/ml before thermal treatment and about 10^3 CFU/ml after thermal treatment. In this case, there was not necessarily a greater proliferation, but all the proliferated colonies adhered to the surface rather than passed in the broth. This could explain why bacterial colonies were not detected in the broth analyzed earlier, whereas in the vortex case, their number is slightly higher.

Regarding the case of glass fiber filters, Figure 63 (a) evaluates the numerical count of proliferated colonies. It is noticeable that for the uncoated filter, the colonies reach values of 10^{12} CFU/ml both before and after thermal regeneration. This data, higher compared to the metallic case, agrees with the McFarland values found. In the case of SiO2_Ag5 coating, after the thermal regeneration process, the colonies count is slightly higher compared to that found before treatment, but still considerably lower than the value obtained from an uncoated filter, both thermally treated and untreated. For the zirconia coating, the colonies count is higher (10^4 CFU/ml) than silica/silver coating, confirmed by a slightly higher McFarland index value, but still comparable to that obtained post-treatment (10^3 CFU/ml).

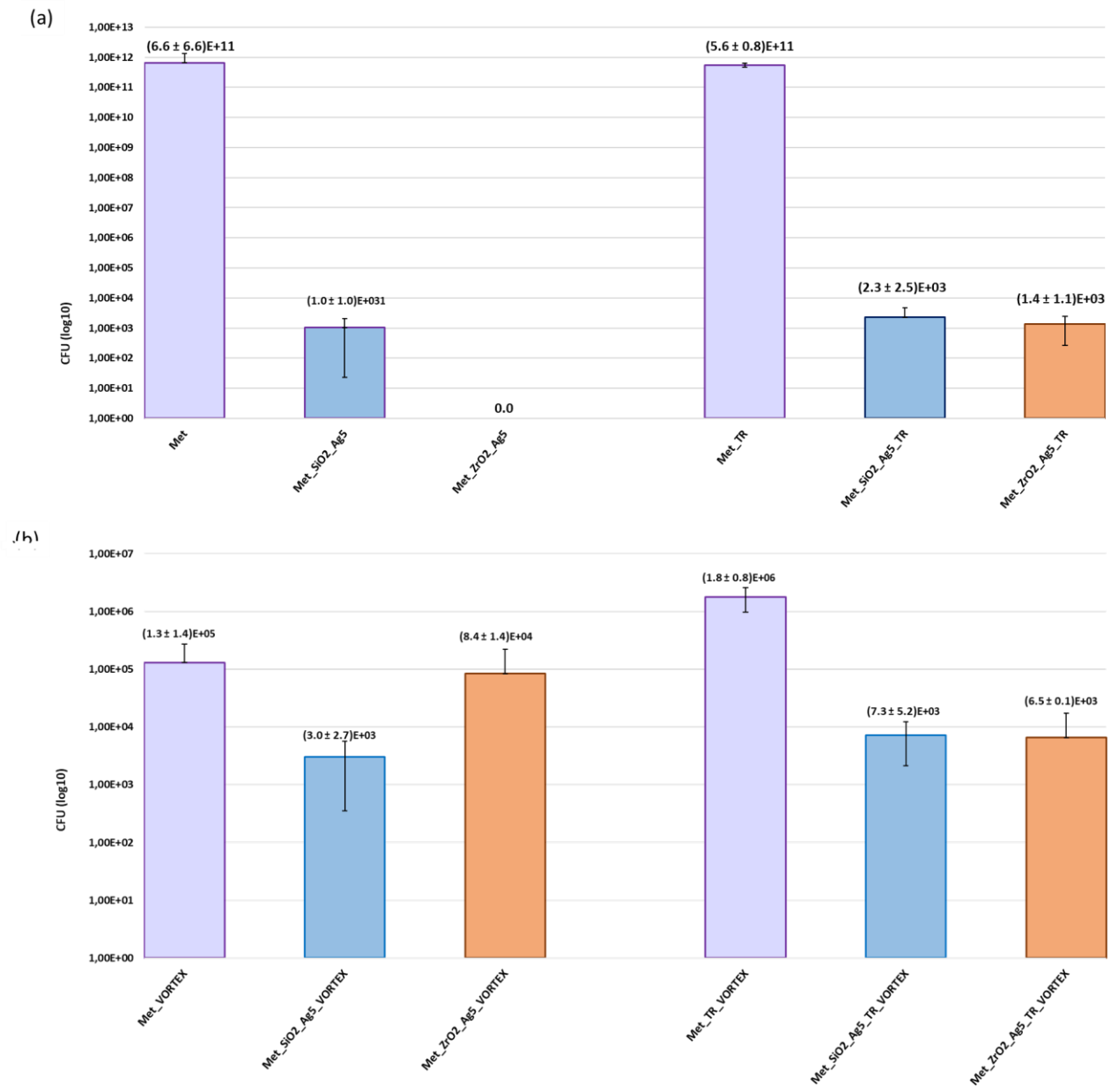

Figure 62: (a) Count of S. epidermidis colonies proliferated in broths with uncoated and SiO2_Ag5 and ZrO2_Ag5 coated Met, before and thermal regeneration process; (b) Count of S. epidermidis colonies adhered on the surface of uncoated and SiO2_Ag5 and ZrO2_Ag5 coated Met filter, before and after thermal regeneration process

In the case of vortex solution containing surface-adhered colonies, Figure 63 (b), the experimental data reported related to the filters after the first contamination are coherent with those obtained from the broth evaluation. More colonies were adhered to the zirconia/Ag-coated filter (about 10^4 CFU/ml) compared to those on the silica/Ag-coated filter (10^2 CFU/ml). Conversely, after the thermal cycles at 200°C, the colonies adhered to the silica-based coating are slightly more abundant compared to the zirconia case. However, it can be noted that, in all the analyzed cases, the antibacterial activity of the coatings is not influenced by thermal treatment, but it remains extremely strong. This suggests that

possible repeated thermal treatments can be performed on the studied coatings without losing effectiveness and potency in bactericidal action.

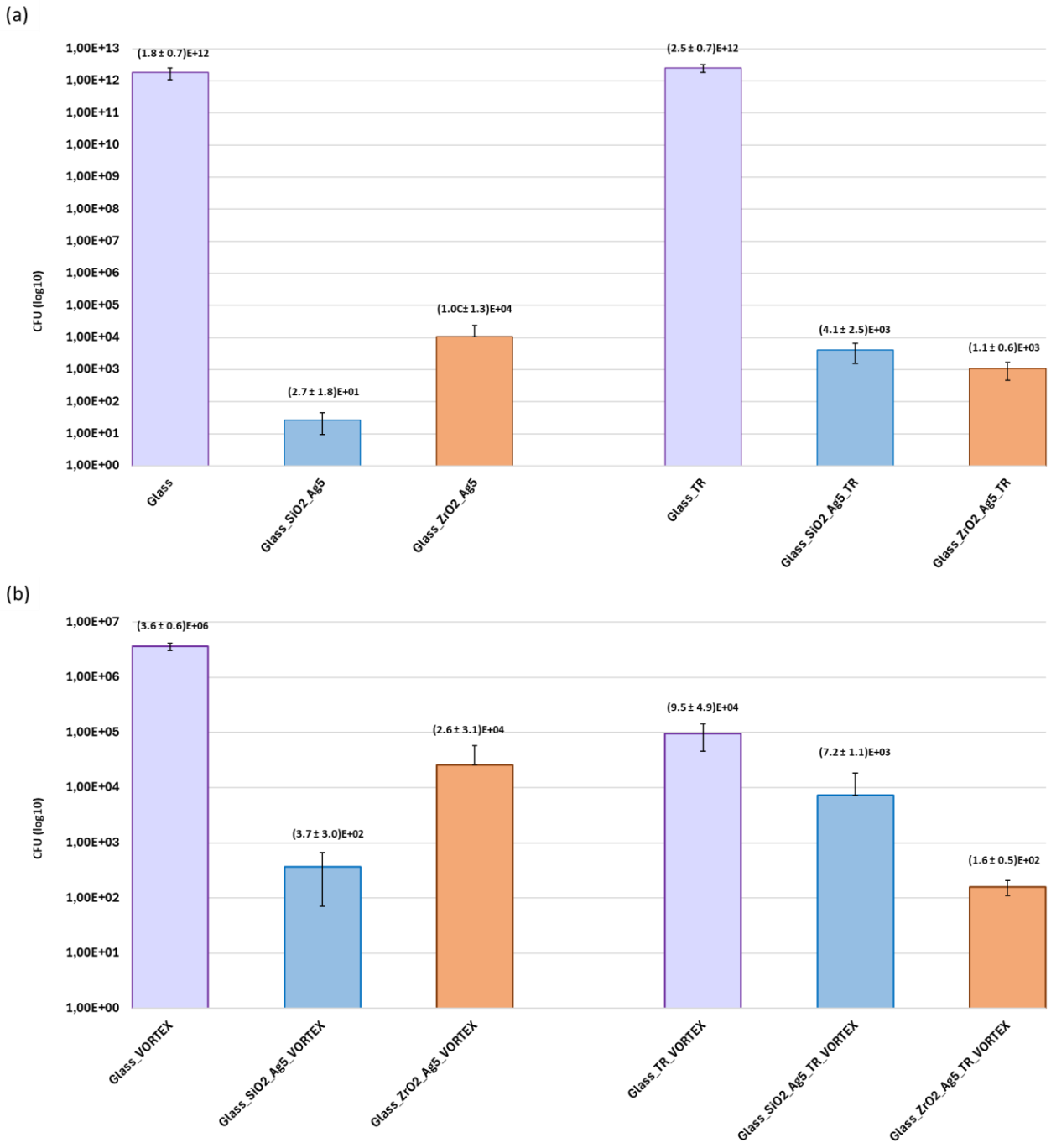

Figure 63: (a) Count of S. epidermidis colonies proliferated in broths with uncoated and SiO2_Ag5 and ZrO2_Ag5 coated Glass, before and thermal regeneration process; (b) Count of S. epidermidis colonies adhered on the surface of uncoated and SiO2_Ag5 and ZrO2_Ag5 coated Glass and after thermal regeneration process

The study was then completed with the contamination of the polymeric membrane. In this case, as previously mentioned, the thermal regeneration process was not performed. The number of proliferated colonies in the broths, reported in Figure 64, is significantly lower in the presence of the SiO2_Ag3 and ZrO2_Ag5 coatings compared to the as-received filter. In particular, the reduction was

of 7 or 8 orders of magnitude compared to the uncoated Memb. After vortexing the samples, it was found that a higher number of colonies adhered to the ZrO_2/Ag coating, in contrast in the case of Memb_SiO2_Ag3_VORTEX the number of adhered colonies was slightly minor.

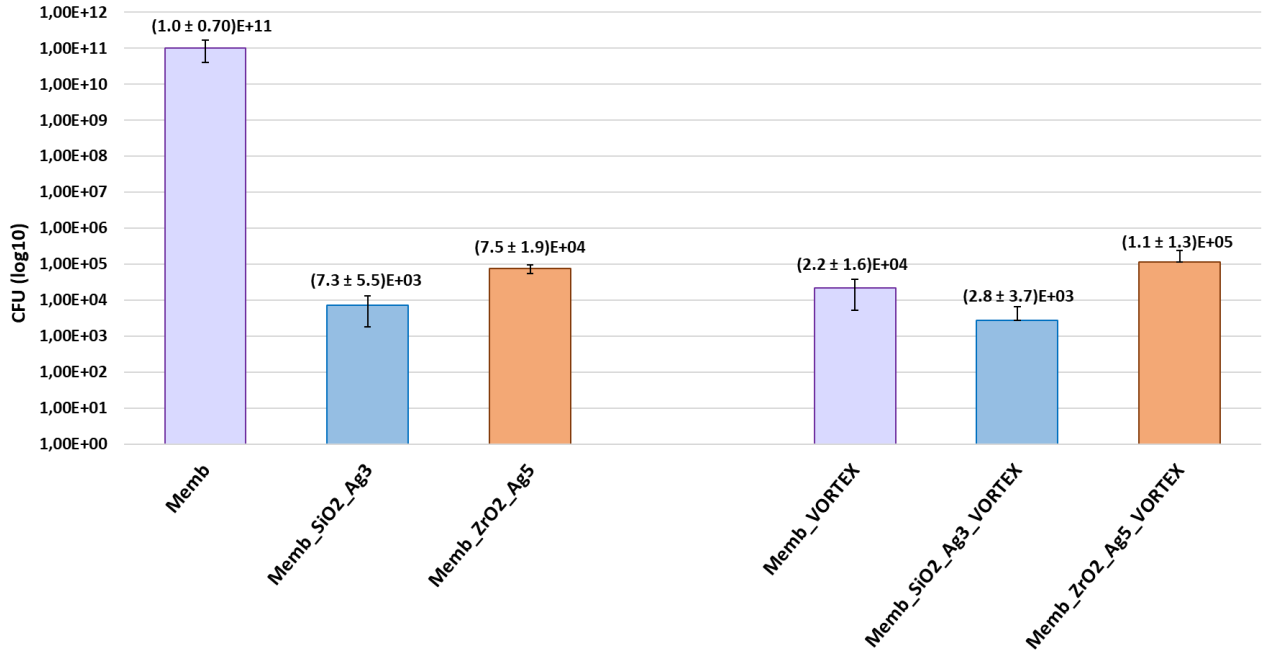

Figure 64: Count of S. epidermidis colonies proliferated in broths and adhered on the surface of uncoated and SiO2_Ag3 and ZrO2_Ag5 coated Memb filter

The choice of this thermal treatment process with a temperature set at 200°C and a number of cycles equal to three was done considering as a starting point a standard sterilization process, typically conducted at 121°C in an autoclave, where there is also an effect due to the pressure. As the coatings suffer prolonged contact with aqueous solution, the procedure reported here involved higher temperatures and more thermal cycles in order to have more severe conditions.

FESEM analysis of SiO2_Ag5 and ZrO2_Ag5 coatings after the thermal process was conducted, to evaluate if changes in morphological structures were promoted. The images reported in Figure 65, confirmed that this temperature is too low to modify or damage composite coatings, which remained globular and porous. Big aggregates of silica and matrix are visible, as already found in and described in the section dedicated to coatings morphologies. Another consideration to be done is the potential increment in the dimension of silver nanoclusters due to the coalescence effect which could compromise the antibacterial effect. However as reported in [212], the antibacterial activity of silver nanocluster/silica composite coatings deposited via RF co-sputtering was evaluated after heat treatments at different temperatures, demonstrating that the value of 450°C can be considered the

maximum temperature for a thermal treatment, as higher temperatures can induce a significant decrease in bactericidal performance due to agglomeration and growth phenomena of nanoparticles.

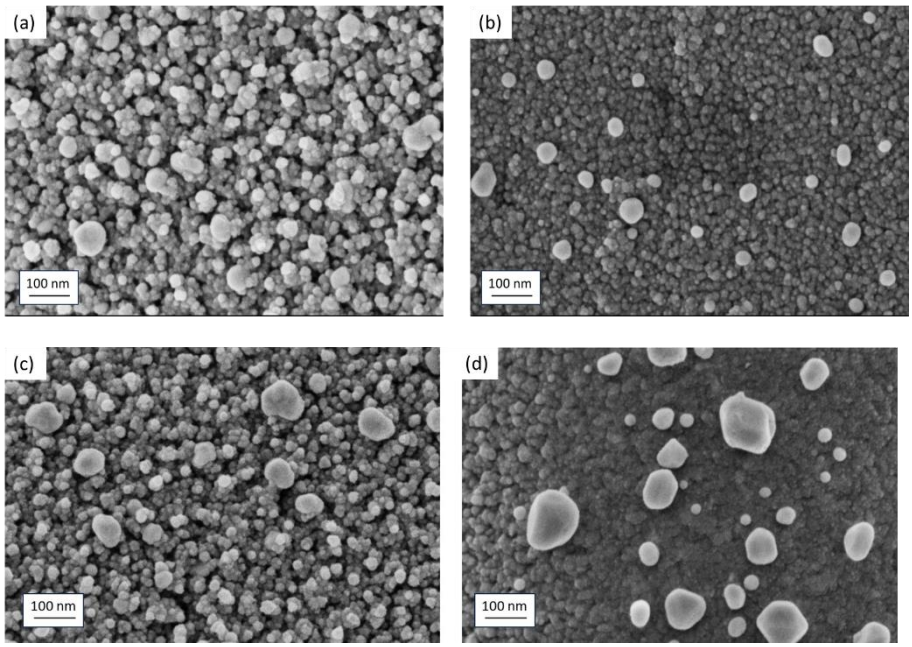

Figure 65: Morphological analysis of SiO2_Ag5 coating deposited on (a) Met and (b) Glass filters after the thermal regeneration process; and of ZrO2_Ag5 coating deposited on (c) Met and (d) Glass filters after the thermal regeneration process

In general, different methods could be employed for the sterilization of air filters. The most simple and economical involve the use of water or water and ethanol solutions [213] [214], but in this work, these methods could not be applied, due to the solubility of silica coating in water. Other methods involve thermal and UV treatments.

Yong-Il Kim et al. [215] developed an air filter with virucidal and bactericidal properties, which could be thermally sterilized. The filters studied contained a heating layer that can be heated up to 100°C through Joule heating, which has been found to effectively inhibit *E. coli.* A similar system was used for facial masks, to avoid the use of chemical products for the disinfection and inactivation of *E. coli* [216]. The germicidal action of UV rays was tested in heating, ventilation, and air conditioning (HVAC) systems, where *Aspergillus versicolor* spores and *Mycobacterium* bacterial colonies were aerosolized. The results demonstrated that UV rays inactivated 75% of fungal spores and 87% of bacterial cells, confirming the UV sterilization method as effective for air filter reuse [217].

The antibacterial effectiveness against *S. epidermidis* and *E. coli*, as well as the antifungal effectiveness against *C. albicans*, was assessed qualitatively and quantitatively, and results showed strong efficacy of the composite coatings with Ag nanoclusters in inhibiting or reducing bacterial and

fungal proliferation, even after thermal treatments, suggesting potential filter reuse after sterilization treatments at 200°C.

Given the promising results, further analyses were conducted to evaluate the virucidal effect of the silica and zirconia-based composite coatings. The antiviral assays of Glass_SiO2_Ag3, Glass_SiO2_Ag5, and Memb_SiO2_Ag3 against the Human Coronavirus OC43 strain, HCoV-OC43, were performed at the Università di Torino by Professor David Lembo and his research team. Results, published in [185], showed a reduction in the virus titer of about 0.8 log for SiO2_Ag coated glass fibers-based filters, compared to uncoated Glass, without differences between the two coatings, and a reduction of approximately 1.1 log, for coated polymeric membrane (named Pol-Ag3 in the figure) compared to the uncoated one (named Pol in the figure), as shown in Figure 66.

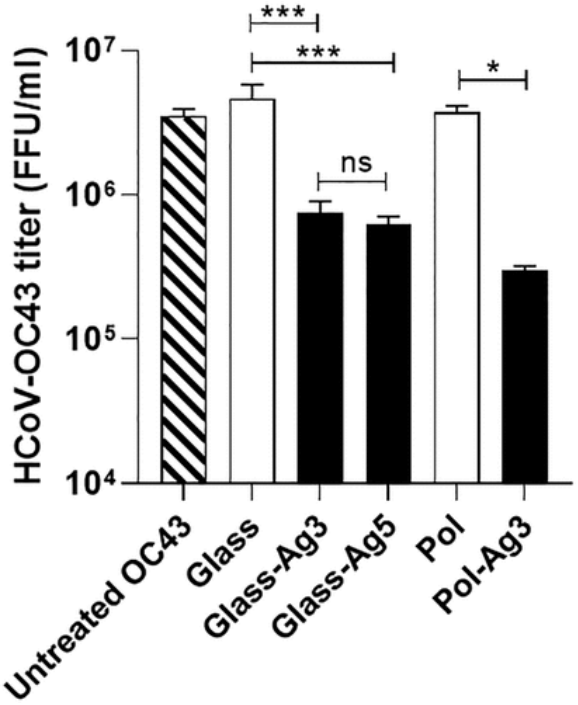

Figure 66: Antiviral test against HCoV-OC43 virus on uncoated, SiO_Ag3 and SiO2_Ag5 coated Glass and Memb [185]

Deeper investigations about the virucidal mechanism of the composite coatings through ions release antiviral test and virucidal assay through drying method, shown in Figure 67, suggested that coatings deposited on Glass filters exhibited indirect antiviral effect, due to the silver ions release (Figure 67 (b)), on the contrary, coated polymeric filters directly inactivated virus, resulting in an inactivation logarithm of approximately 1.4 in the test through drying method (Figure 67 (a)). The two different behaviors are related to the different natures and features of studied substrates.

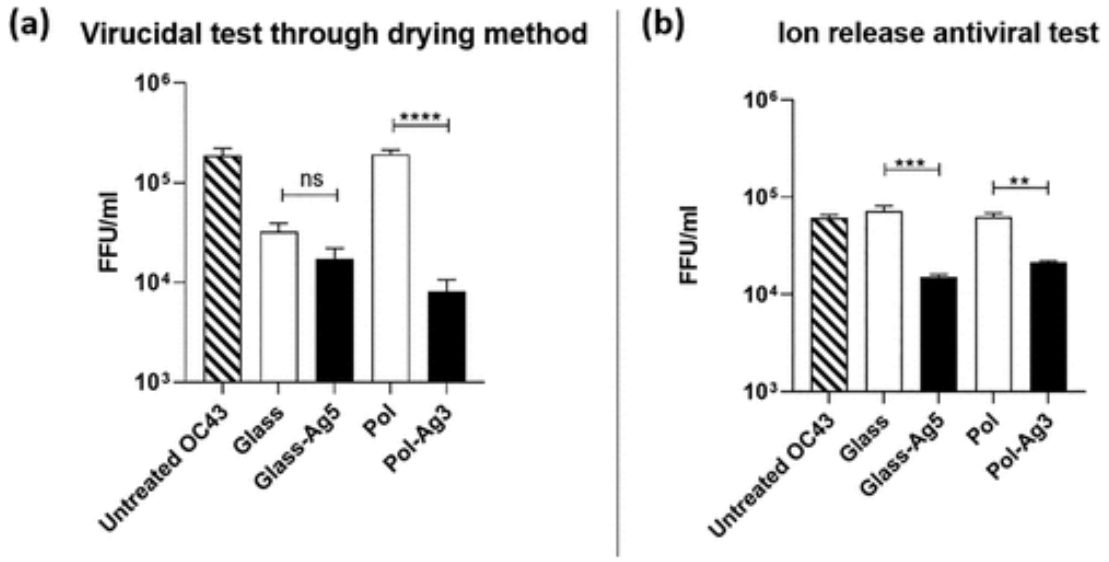

Figure 67: Antiviral test against HCoV-OC43 virus on uncoated, SiO_Ag3 and SiO2_Ag5 coated Glass and Memb, through (a) drying method, and (b) ions release test [185]

In addition, the virucidal efficacy of ZrO2_Ag4 coatings deposited on Met, Glass, and Memb filters was tested against Human Rotavirus, HRoV, Influenza A virus, Flu A H1N1, Human rhinovirus, HRhV A1, and Respiratory Syncytial virus, RSV A2. Collected data demonstrated that the coating deposited on Glass filters exhibited a virucidal efficacy, reducing the viral load from 100 times to 10000 times, compared to the uncoated substrate. In the other cases, a slight reduction, or no reduction was shown.

Due to antibacterial and virucidal properties exhibited by silica- and zirconia-based coating, further studies are currently underway in the framework of the European project "Nanobloc: Antiviral, Antibacterial & Antifungal Nanocoating Platform", as will be described in "Conclusion and future perspectives" section, which aims to develop coatings with bactericidal, virucidal and fungicidal properties to be involved in numerous applications.

Silica composite coatings containing Cu and Zn nanoparticles for air filters

In this work, a further attempt to find a good alternative to silver nanoparticles as an antibacterial agent in the coatings for air filtration systems was made. According to the well-known properties of zinc oxide [58], [88], [161], [218] and copper oxide nanoparticles [153], [156], [219], [220], it was decided to replace the silver target with zinc or copper one during the deposition process, to have new silica-based coatings with Cu or Zn nanoparticles.

As a starting point, several coatings obtained applying different powers to Cu and Zn targets were deposited on Met, Glass, and Memb filters, and EDS analysis was performed, to evaluate the

amount of silica, zinc, or copper in each coating, finding the composition with a good balance for further investigations.
Regarding silica coatings with Cu, from the results of compositional analyses, it emerged that SiO2_Cu5 and SiO2_Cu10 coatings exhibited the best balance between matrix and antibacterial agent content.

In the case of SiO_2-coatings containing Zn, since low power values result in low zinc content in the coating, it was decided to increase the deposition rate by significantly raising the set power values, in accordance with [221]. For this reason, coatings obtained by applying power of 60, 80, 120, 140, 160, and 180 W to the zinc target were studied compositionally, but EDS results revealed excessively high amounts of Zn in coatings.

From this point onward, the results obtained from compositional, structural, morphological, and antibacterial analyses of silica-based coatings containing copper, **SiO2_Cu5** and **SiO2_Cu10**, and zinc, **SiO2_Zn60** and **SiO2_Zn120**, deposited on Met, Glass, and Memb filters, will be illustrated and discussed.

Compositional, structural, and morphological analysis

The elemental composition of the selected SiO_2- based composite coating, containing Cu or Zn nanoparticles, was evaluated through EDS analysis, and results are shown in Table 11, where powers set during each deposition process were specified.

Table 11: EDS analysis on silica/copper and silica/zinc composite coatings deposited on air filters

Substrate	*SiO2_Cu coating*			*SiO_Zn coating*		
	Power to Cu target	***Si (at. %)***	***Cu (at. %)***	***Power to Zn target***	***Si (at. %)***	***Zn (at. %)***
Met	***5 W***	4.14 ± 0.24	3.93 ± 0.71	***60 W***	4.71 ± 0.11	3.43 ± 0.17
	10 W	4.91 ± 0.68	5.30 ± 0.74	***120 W***	4.98 ± 0.81	8.67 ±0.13
Glass	***5 W***	11.47 ± 0.27	0.96 ± 0.39	***60 W***	12.02 ±0.45	2.79 ± 0.24
	10 W	12.21 ± 0.39	3.31 ± 0.75	***120 W***	12.75 ± 0.35	7.73 ± 1.08
Memb	***5 W***	0.87 ± 0.05	0.91 ± 0.35	***60 W***	1.22 ± 0.11	0.95 ± 0.07
	10 W	1.64 ± 0.31	2.19 ± 0.66	***120 W***	1.99 ± 0.43	5.70 ± 1.49

As already mentioned, for the deposition of all the coatings, the power applied to the SiO_2 target was kept constant at 200 W, the same used for SiO2_Ag coatings deposition. The silicon amount in the

SiO2_Cu and SiO2_Zn coatings were approximately 4.00-5.00 at. %, in the case of the metallic filters, about 11.50-13.00 at. % in the case of Glass substrate, and around 1.00-2.00 at. % for the polymeric membrane. These values are very similar to those obtained by analyzing SiO2_Ag composite coatings, previously described. As already discussed, the higher amount of Si in coatings deposited on glass-fiber filters was due to the presence of Si in the filter composition.

In the case of Cu and Zn elements, it is important to emphasize that doubling the applied power to both targets significantly increases the amount of both elements in the deposited coatings. Specifically, increasing the power from 5 W to 10 W applied to the copper target, the Cu amount increases from approximately 4.00 at. % to about 6.00 at. % in coatings deposited on Met filter. In coatings deposited on a glass-fiber-based filter, the value is more than tripled (from 0.96 at. % to about 3.30 at. %), and in those on the polymeric membrane, it is doubled (from 0.91 at. % to about 2.00 at. %). Regarding Zn, increasing power from 60 W to 120 W resulted in a substantial increase in the Zn content in the coatings. More specifically, it was more than doubled for the metallic and glass-fiber filters, while in the case of the polymeric membrane, the copper content increased from 0.95 at. % to about 5.70 at. %.

An analysis of the surface morphology of the coatings was performed through FESEM at different magnifications. In Figure 68, the morphology of SiO2_Cu5 and SiO2_Cu10 coatings and SiO2_Zn60 and SiO2_Zn120 deposited on Met were shown, in comparison to that of the bare sample.

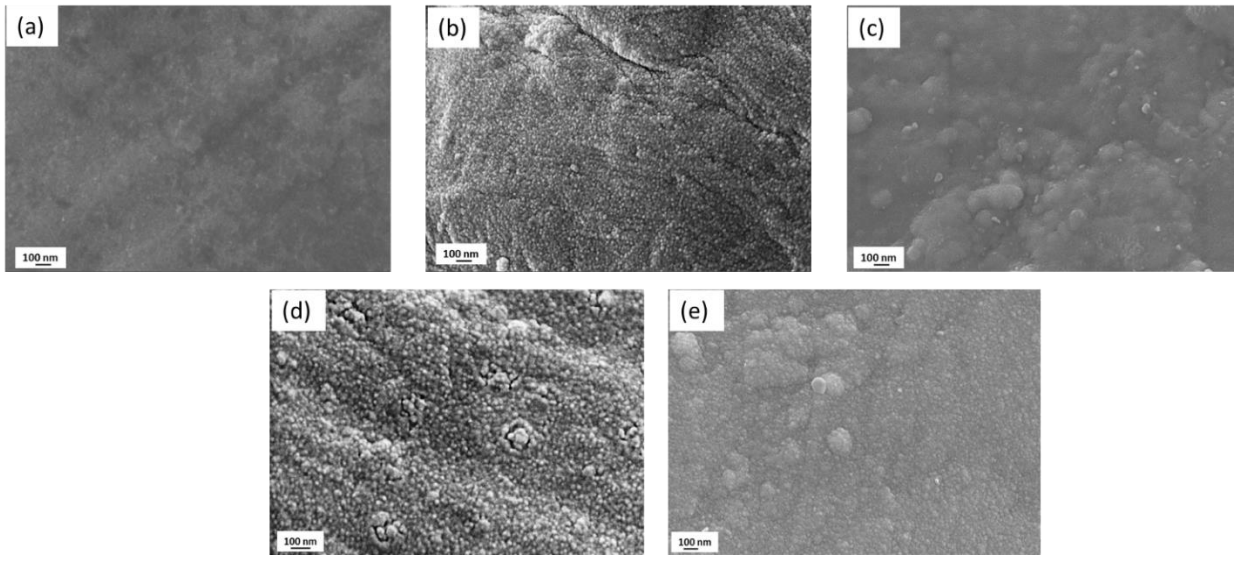

Figure 68: Morphological analysis of (a) uncoated Met, (b), Met_SiO2_Cu5, (c) Met_SiO2_Cu10, (d) Met_SiO2_Zn60 and (e) Met_SiO2_Zn120

The difference in the filter appearance before and after coating deposition is evident. The surface of uncoated Met appeared to be very smooth, but after the deposition process, the typical globular and porous structure of sputtered silica is well visible and recognizable in Met_SiO2_Cu5, which differs from that obtained with a higher power of Cu. In SiO2_Cu10 coatings, some silica aggregates were detected, but in both cases, no metallic nanoparticles were visible. Regarding SiO_2/Zn coatings, morphological investigations revealed that Met_SiO2_Zn60 shows a globular structure similar to Met_SiO2_Cu5, while Met_SiO2_Zn120 appeared finer with dispersed aggregates. No zinc nanoparticles were detected.

FESEM images of uncoated and coated Glass are shown in Figure 69. Uncoated glass is smooth, as in the previous case, but the SiO2_Cu5 coating on Glass presented a different morphology from that deposited on Met and Memb. It is smoother and finer, and unlike the other cases, no aggregates of the silica matrix are visible, while they appeared on SiO2_Cu10 coatings. In Glass_SiO2_Cu10, the homogeneity of the deposited coating is appreciable. SiO2_Zn coatings appeared similar to each other, and in the case of SiO2_Zn120 (Figure 69 (e)), an aggregate attributable to silica constituting the matrix is visible. Analyzing these images, no nanoparticles were found.

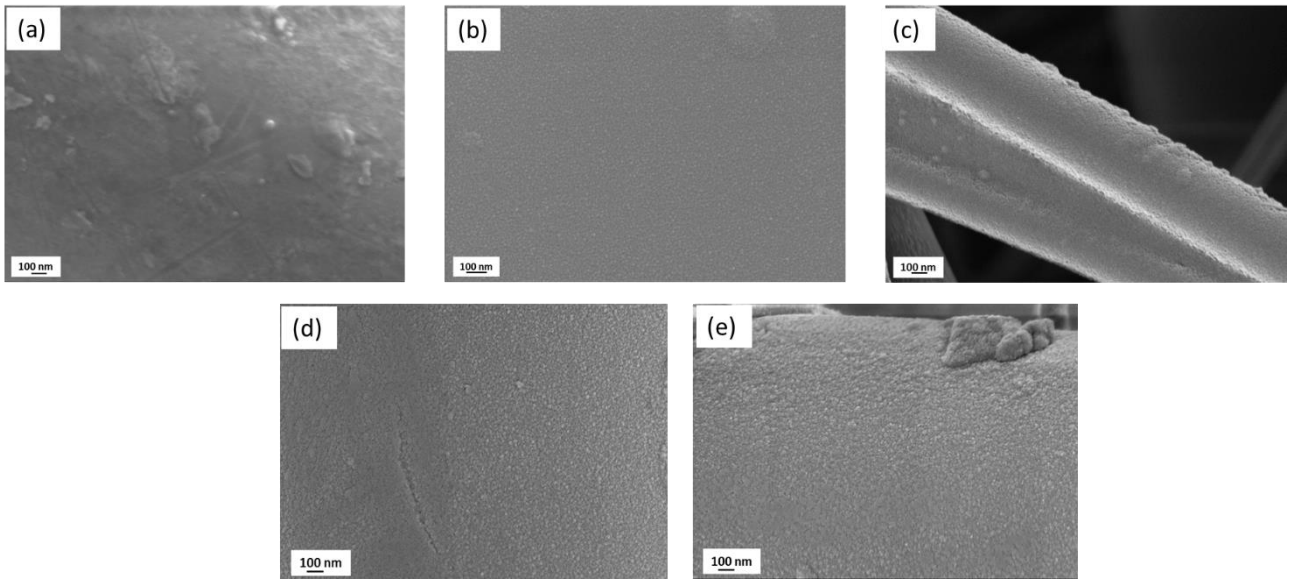

Figure 69: Morphological analysis of (a) uncoated Glass, (b), Glass_SiO2_Cu5, (c) Glass_SiO2_Cu10, (d) Glass_SiO2_Zn60 and (e) Glass_SiO2_Zn120

In Figure 70, coatings on Memb as a substrate are shown. The difference between SiO2_Cu5 and SiO2_Cu10 coatings is evident. The first one appeared globular, very similar to coatings on Met deposited under the same conditions, while Memb_SiO2_Cu10 is smoother and finer, with some

aggregates probably constituted by silica. Coatings containing Zn were compact, similar if 60 W or 120W were applied and they were homogenously distributed on the surface of the substrate.

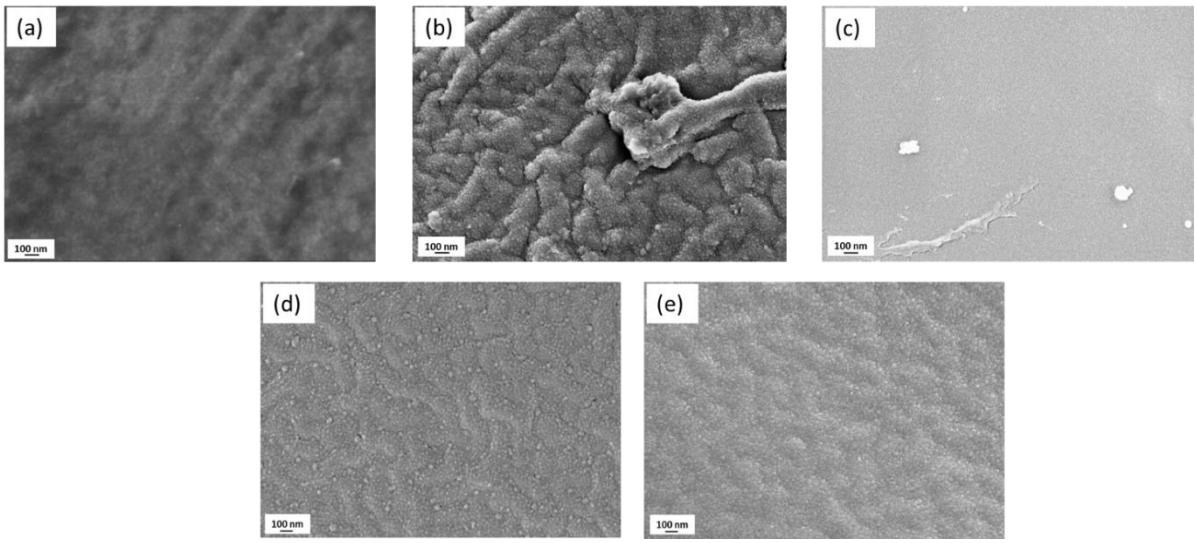

Figure 70: Morphological analysis of (a) uncoated Memb, (b), Memb_SiO2_Cu5, (c) Memb_SiO2_Cu10, (d) Memb_SiO2_Zn60 and (e) Memb_SiO2_Zn120

The composite coatings containing Cu and Zn, were then deposited on soda-lime glass samples, and underwent XRD and UV-Vis analysis, for structural investigations.

The acquired XRD spectra related to SiO2_Cu5 and SiO2_Cu10 coatings are reported in Figure 71.

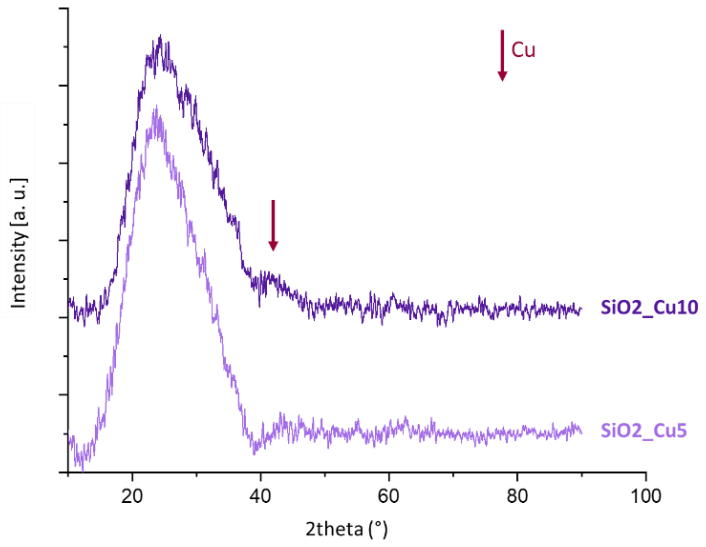

Figure 71: XRD analysis of SiO2_Cu5 and SiO2_Cu10 coatings

It shows the halo at around a value of 2θ of 15°, referring to the presence of amorphous silica, as already found in composite coatings with silver nanoclusters; in addition, a minimal peak is

discernible around a value of 2θ = 43°, which is slightly shifted in the case of SiO2_Cu5 coating. Peaks confirming the presence of copper metallic nanoparticles correspond to values of approximately 2 theta = 43°, 50°, and 75° [222], and copper oxide nanoparticles are identified for 2 theta values of approximately 3°, 39°, 49°, 54°, 58° [223], respectively. This data suggested that the coatings developed in this work contain copper in a metallic state, as also confirmed by analyzing that peak with Xpert software, using the code 00-004-0836, but in the UV-Vis spectra, shown in Figure 72, no peaks indicating the presence of copper nanoparticles were detected, generally observed at a wavelength around 570 nm for Cu Nps [224], and around 220 nm for CuO NPs [225]. The figure shows the data acquired starting from wavelengths of 300 nm. Below this value, the sample became saturated, and no curve was detected at 200 nm.

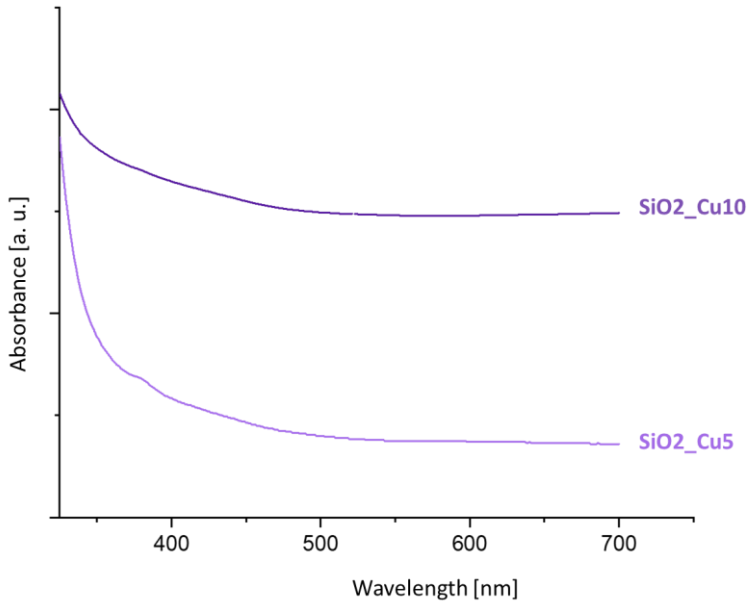

Figure 72: UV-Vis analysis of SiO2_Cu5 and SiO2_Cu10 coatings

Since EDS data on chemical composition and XRD have detected the presence of copper, it was decided to proceed with the qualitative evaluation of antibacterial activity, through the inhibition zone test against *S. epidermidis*, which will be shown below.

Regarding composite coatings made up of silica matrix with Zn nanoparticles, the results of XRD analysis are shown in Figure 73. The spectrum related to SiO2_Zn120 coating shows a peak of greater intensity, detected at an angle of approximately 2θ =42°. Analyzing this peak with the Xpert software, using the code 01-087-0713, it is possible to note that this peak corresponds to zinc nanoparticles, as also found in [226] and [227], and not to zinc oxide nanoparticles (for which

values of 2theta are about 31.50°, 34.30°, 36.30°, 47.50°, 56.50°, 62.85°, 67.80° and 76.85° [228]). The same peak, but with lower intensity is detectable for SiO2_Zn60.

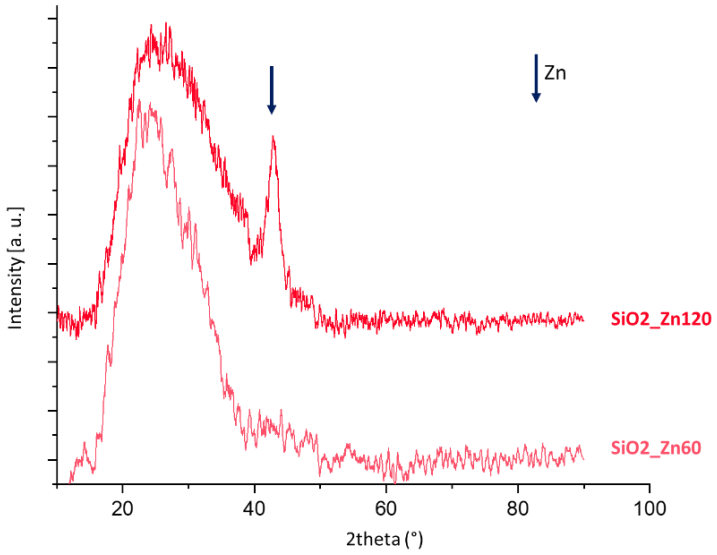

Figure 73: XRD analysis of SiO2_Zn60 and SiO2_Zn120 coatings

On the other hand, no peaks are detected in the UV-Vis spectra, Figure 74, for both SiO2_Zn60 and SiO2_Zn120, while generally, the presence of Zn nanoparticles is identifiable with a peak at about 350 nm [228].

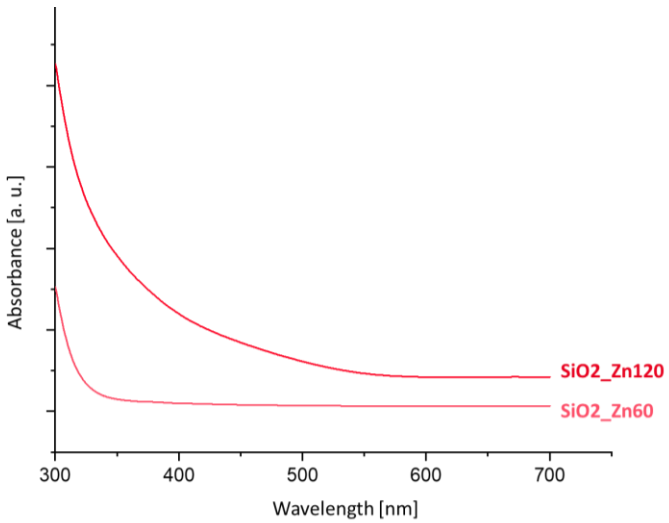

Figure 74: UV-Vis analyses of SiO2_Zn60 and SiO2_Zn120 coatings

Ions release test

For a deeper understanding of silica coatings with Cu and Zn, it was decided to evaluate whether selected coatings, SiO2_Cu5 and SiO2_Zn60, release ions and, eventually, their amount. For this reason, a leaching test was conducted in MilliQ water at room temperature for two weeks.

The results of the test performed on Met_SiO2_Cu5, Glass_SiO2_Cu5, and Memb SiO2_Cu5 are shown in Figure 75, compared to the curves related to Glass_SiO2_Cu10. For each substrate, a gradual ions release is visible, reaching a maximum amount of released ions of about 0.4 mg/L for Met_SiO2_Cu5 and Memb_SiO2_Cu5, and 0.3 mg/L for Glass_SiO2_Cu5.

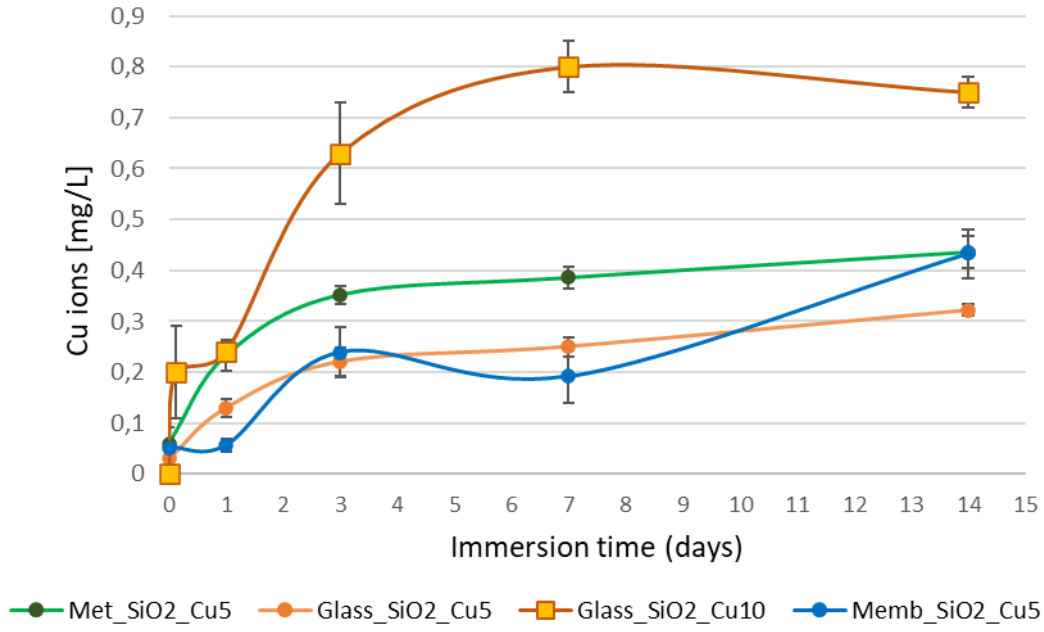

Figure 75: Amount of copper ions released from SiO2_Cu5 and SiO2_Cu10 coatings deposited on Met, Glass and Memb filter after two weeks in water at room temperature

The curve related to Glass_SiO2_Cu10 maintains a gradual trend, but the amount of released ions was higher than in the previous cases. The maximum reached value was of 0.8 mg/L after 7 days, according to the higher quantity of copper in that coating, which probably is not enough for conferring a bactericidal effect.

The kinetic release of Zn ions from each substrate coated with SiO2_Zn60 coatings is shown in Figure 76. The release was gradual, and a very high amount of ions were released after 14 days. In particular, the values were 0.8 mg/L for metallic filter, almost 1.3 mg/L for glass-fiber-based filter, and almost 0.95 mg/L for polymeric membrane.

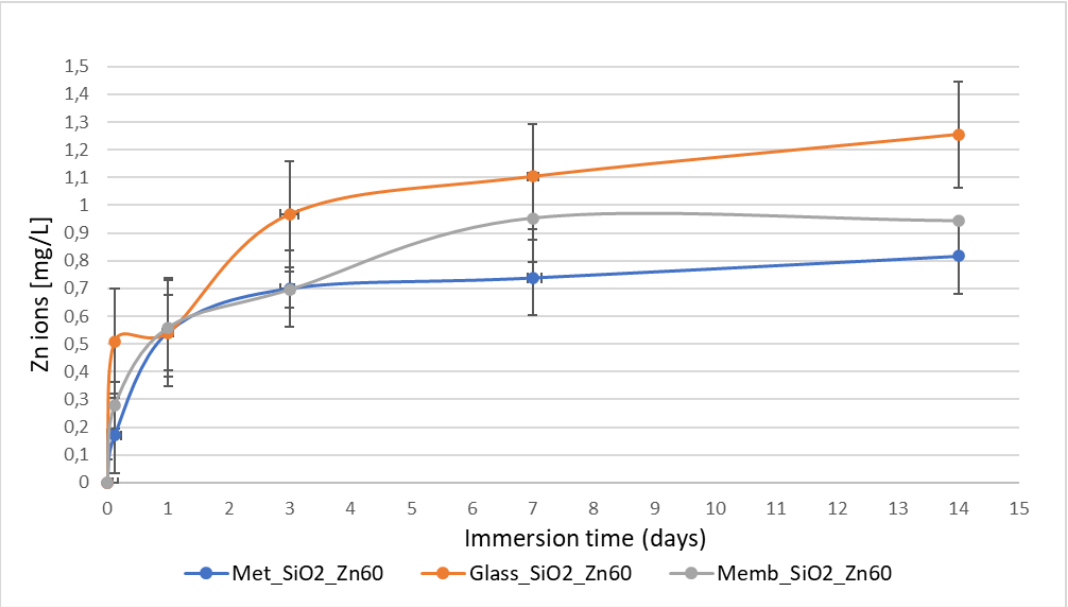

Figure 76: Amount of zinc ions released from SiO2_Zn60 coating deposited on Met, Glass and Memb filter after two weeks in water at room temperature

Antibacterial tests

Since the main goal of these coatings was to confer antibacterial and antifungal properties to air filters, the evaluation of the inhibition halo against *S. epidermidis* and *E. coli* as bacteria strains and *C. albicans*, as fungus, was conducted on all Cu or Zn/silica-based coatings and substrates selected for this application. The results are summarized in Figure 77.

The uncoated samples were not expected to show any antimicrobial activity, and they were completely colonized by both bacterial and fungal strains.

Regarding the coated metallic filter, both Met_SiO2_Cu 5 and Met_SiO2_Cu 10 did not inhibit the proliferation of bacteria and fungi, there was no halo around any of the samples, and the microorganisms also proliferated on their surfaces. This indicated a lack of antimicrobial activity from the silica-based/copper composite coatings deposited on metallic filters. The behavior of Met_SiO2_Zn60 was not so different from the previous copper/silica-coated metallic filters. On the other hand, SiO2_Zn 120 showed some resistance only against *S. epidermidis* by forming a faint halo of about 0.5 mm; but, no halos are visible testing *E. coli* and *C. albicans*. Similar considerations could be made for glass-fiber-based filters. Glass_SiO2_Cu5, Glass_SiO2_Cu1, and Glass_SiO2_Zn60 coatings didn't show an efficient effect in preventing bacteria and fungi growth, however, as for metallic filter, Glass_SiO2_Zn120 coating, exhibited a halo of 1 mm is visible towards *S. epidermidis*. No inhibition of *E. coli* and *C. albicans* was assessed.

The polymeric membrane showed the least antimicrobial activity. Colonies of the two bacteria strains and *C. albicans* grew indiscriminately around and on the surfaces of uncoated samples, on SiO2_Cu5, SiO2_Cu_10, and SiO2_Zn60 coatings. Differently from metallic and glass-fiber filters, SiO2_Zn120 coating on the polymeric membrane was not able to inhibit or reduce the growth of *S. epidermidis* colonies.

The bactericidal and fungicidal properties of zinc and copper nanoparticles and their oxide forms have been extensively investigated, and the results confirm a strong efficiency in inhibiting a wide spectrum of bacteria, both Gram-positive and Gram-negative, as well as fungal species [155] [160] [161] [162] [218] [229]. This effect is mainly attributed to the release of Zn or Cu ions, which, by interacting with microorganisms, can disrupt the membrane and induce oxidative stress, thereby inhibiting proliferation [150] [151] [152].

Based on the results obtained from the inhibition zone and ion release tests, it was decided to deeper investigate the behavior of certain coatings on selected substrates through the colony-forming unit (CFU) counting tests, against *S. epidermidis* and *E. coli*.

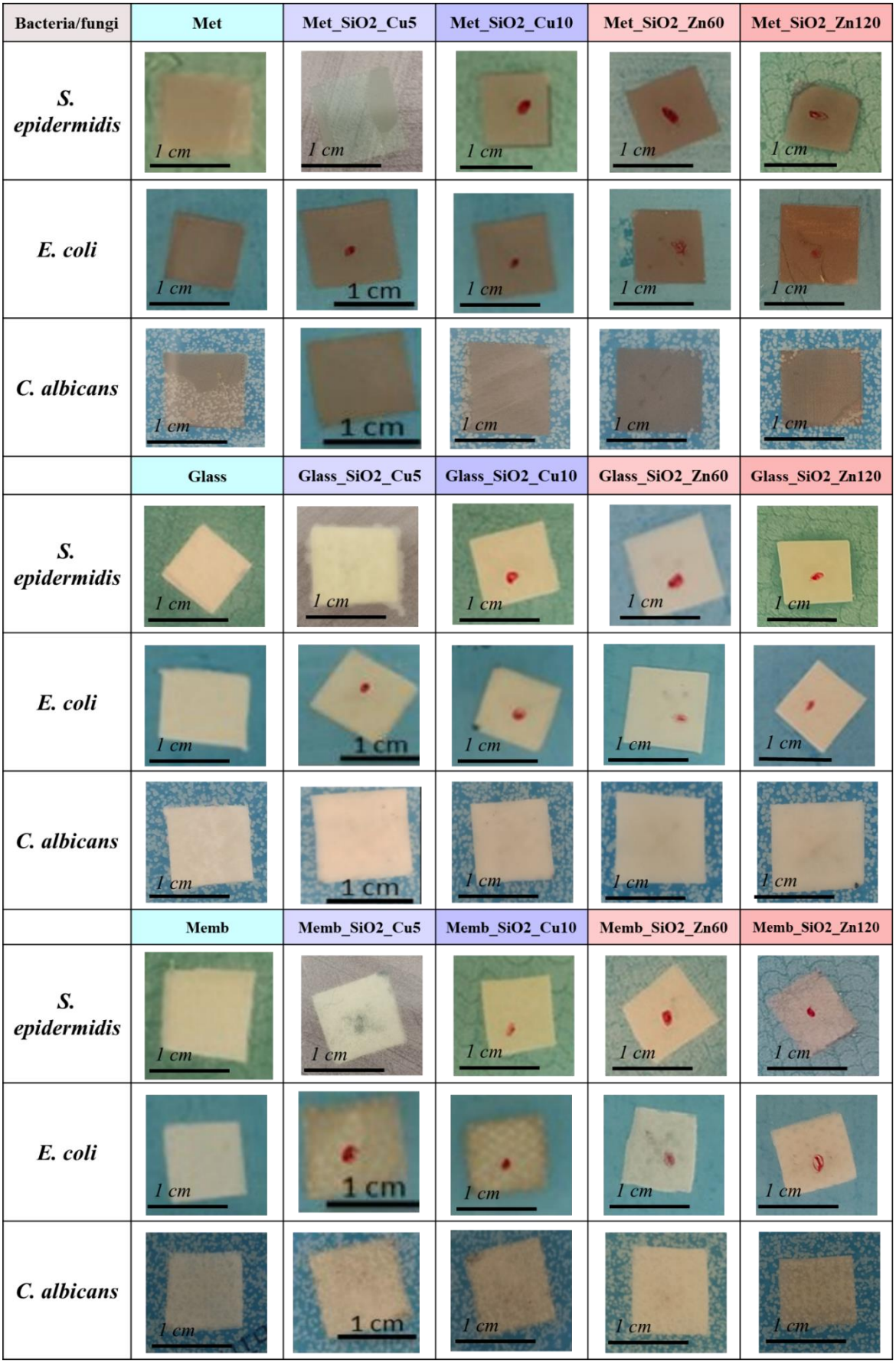

Figure 77: Inhibition halo test against S. epidermidis, E. coli, and C. albicans on uncoated and SiO2_Cu5, SiO2_Cu10, SiO2_Zn60, and SiO2_Zn120 coated Met, Glass, and Memb filters

In particular, in a first part of the study, SiO2_Cu5 coatings deposited on Met, Glass and Memb were evaluated against *S. epidermidis*, analyzing both the number of colonies that proliferated in a broth and that adhered on the surface. Analyzing the turbidity of the broths, reported in Figure 78, no differences were visible, suggesting that bacterial colonies proliferated in the presence of both uncoated and coated filters. This was confirmed by the numerical evaluation of the McFarland index.

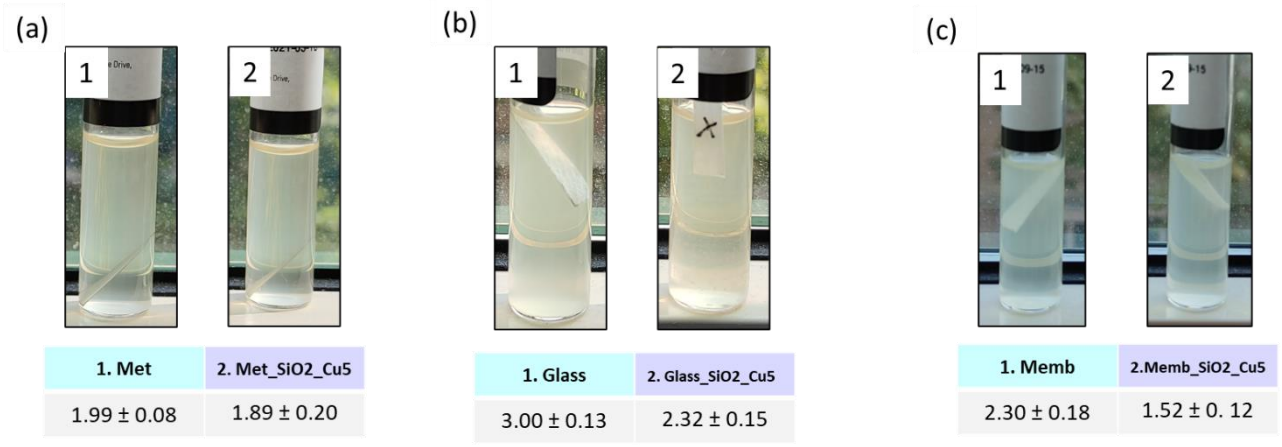

Figure 78:McFarland index of bacterial solutions with uncoated and SiO2_Cu5 coated (a) Met, (b) Glass, (c) Memb filters

More specifically, The McFarland values relative to the uncoated and coated metallic filters are around 2.00, suggesting no antibacterial effect of coatings; while in the case of glass-fiber filter and polymeric membrane, the index slightly decreases in the presence of the coatings, but it remains too high (about 2.30, and 1.50, respectively).

The count of the number of colonies proliferated in broth containing uncoated and SiO2_Cu5 coated samples, and adhered on their surfaces are depicted in Figure 79, confirming that the coating deposited on all three substrates was not efficient in inhibiting bacterial growth. Starting from an amount of colonies of about $5*10^5$ CFU/ml, indicated in the figure by the red line, they proliferated reaching a quantity of approximately 10^{12} CFU/ml for Met samples, (Figure 79(a)), and approximately 10^{13} CFU/ml, both in the case of the uncoated glass-fiber and polymeric filter, and in the presence of SiO2_Cu5 coating.

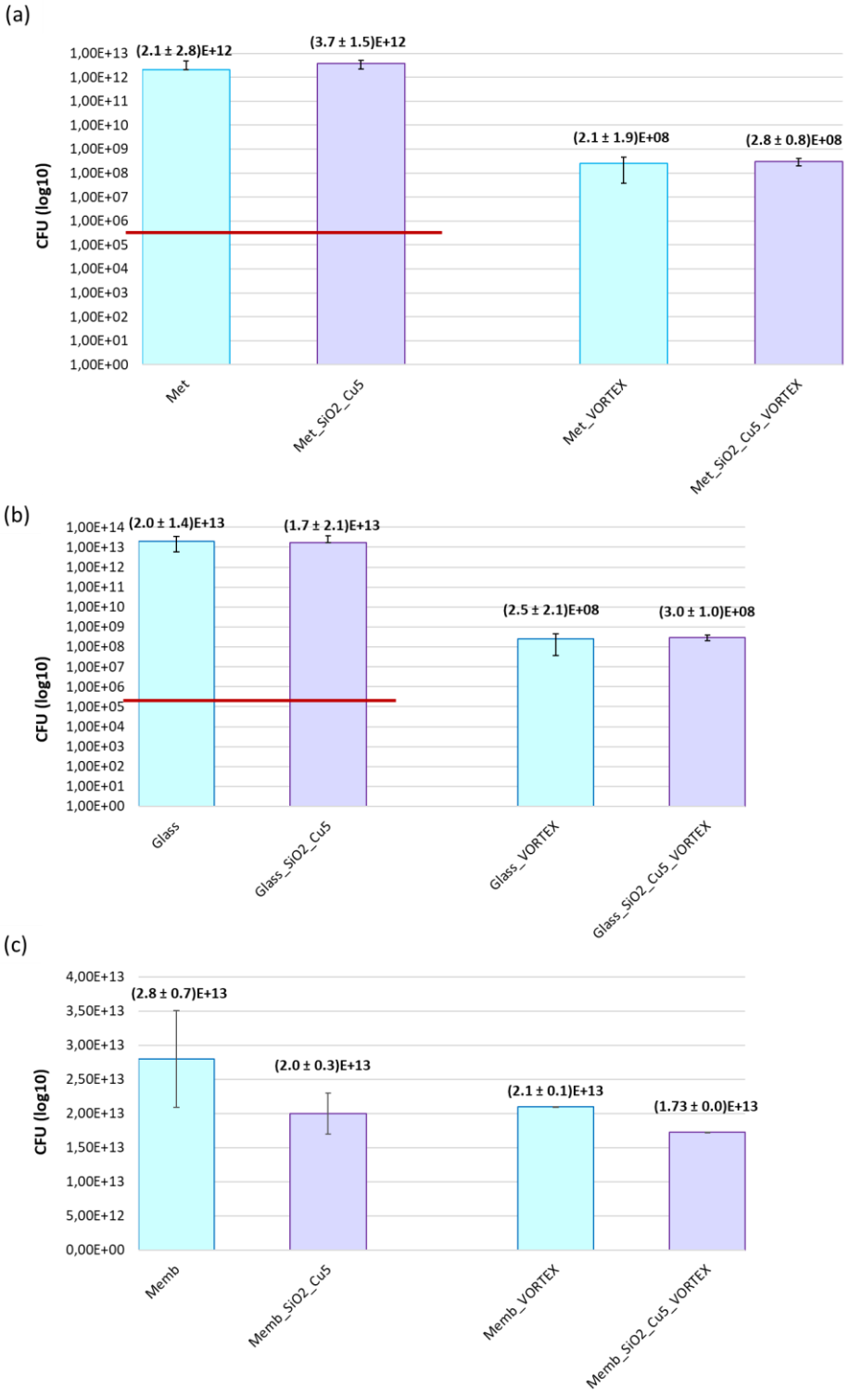

Figure 79: Count of S. epidermidis colonies proliferated in broths and count of the colonies adhered on the surface of uncoated and SiO2_Cu5 coated (a) Met; (b) Glass; (c) Memb filters

The amount of colonies detached from the substrates after the vortex process confirmed the lack of antibacterial effect of the coating. The same order of magnitude of colonies, 10^8 CFU/ml for both metallic and glass-fiber filters, and 10^{12}-10^{13} CFU/ml for polymeric membrane, was detected as adhered on the surface of both as-received and coated filters.

The same test was performed against *E. coli*, evaluating the activity of Glass_SiO2_Cu10, since the Cu amount and the concentration of released ions was high.

However, the turbidity of the solutions and the McFarland index summarized in Figure 80 suggested that bacteria proliferated in both broths, without significant differences if the uncoated or the SiO2_Cu10 coated samples were immersed.

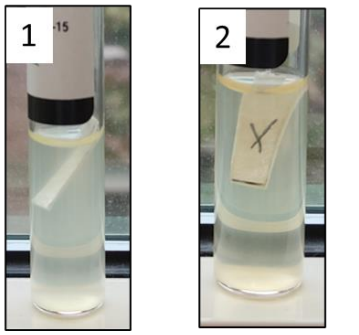

1. Glass	2. Glass_SiO2_Cu10
3.7 ± 1.2	3.8 ± 0.4

Figure 80: McFarland index of bacterial solutions with uncoated and SiO2_Cu10 coated Glass

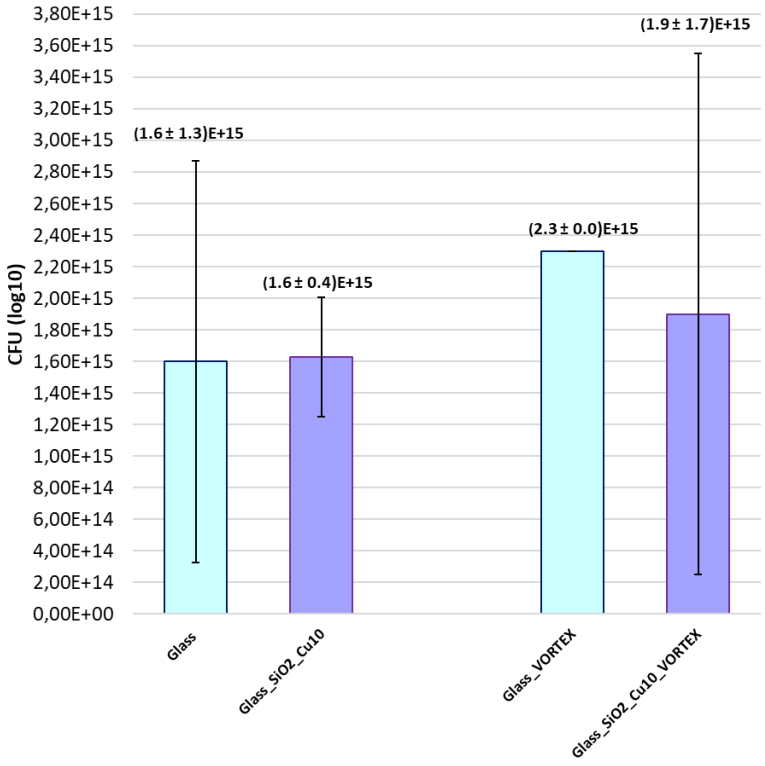

Figure 81: Count of E. coli colonies proliferated in broths and count of the colonies adhered on the surface of uncoated and SiO2_Cu10 coated Glass

As expected, the number of grown bacterial colonies is extremely high, as shown in Figure 80. It reached about 10^{15} CFU/ml in both broths and as previously, and the same number of *E. coli* colonies, nearly 10^{15} CFU/ml, was found attached to the surface of both uncoated Glass and Glass_SiO2_Cu10 filter, demonstrating no antibacterial effect of the coating.

Despite Cu ions being released from the coating, as previously discussed, none of the SiO2_Cu coatings demonstrated antibacterial activity. In the previous section, it was observed that silica- or zirconia-based coatings with silver nanoclusters exhibited strong bactericidal activities, even though the amount of released ions was lower, approximately 0.6 ppm (equivalent to about 0.6 mg/L) for silica-based coatings and about 0.2 ppm (approximately 0.2 mg/L) for zirconia matrix coatings. In a recent study, the bactericidal activity of silver nanoparticles was compared to that of copper nanoparticles against *E. coli* and *S. aureus*, and fungi species. It was observed that, despite a higher release of copper ions, the antimicrobial activity of silver was stronger, demonstrating a greater efficacy in bacterial inhibition, likely due to its stronger interaction with polysaccharides and proteins on cell walls [230].

In the case of coatings containing Zn, Met_SiO2_Zn120 and Glass_SiO2_Zn120 were able to form a very thin inhibition halo against *S. epidermidis*, as reported in Figure 77. For this reason, it was decided to deeply investigate Glass_ SiO2_Zn60 and Glass_SiO2_Zn120 behavior, compared t with that of uncoated Glass, through the CFU counting test, but against *E. coli* strain.

Evaluating the solution turbidity, Figure 82, no antibacterial effect was shown, and it was confirmed by the related McFarland indices, which are surprisingly higher for coated filters (about 3.5) than that of uncoated Glass (about 3.1).

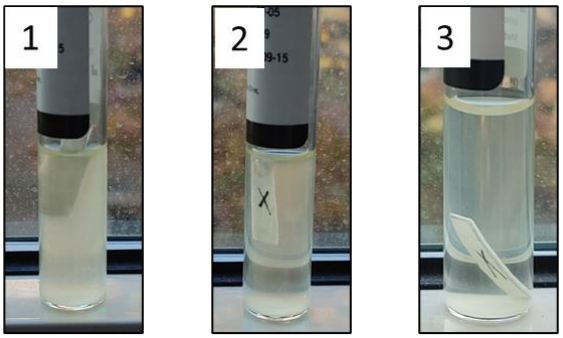

1. Glass	2. Glass_SiO2_Zn60	3. Glass_SiO2_Zn120
3.1 ± 0.4	3.5 ± 0.2	3.5 ± 0.3

Figure 82: McFarland index of bacterial solutions with uncoated and SiO2_Zn60 and SiO2_Zn120 coated Glass filter

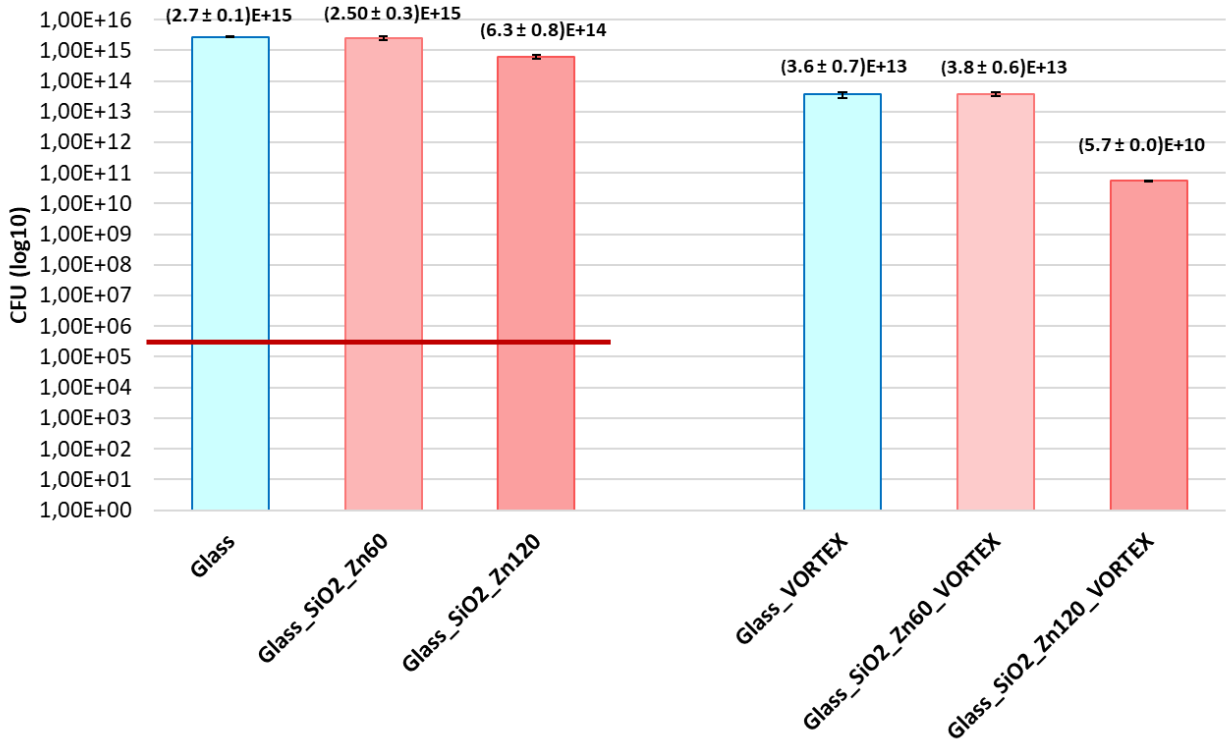

Figure 83: Count of E. coli colonies proliferated in broths and count of the colonies adhered on the surface after vortex process of uncoated and SiO2_Zn60 and SiO2_Zn120 coated Glass

Evaluating colonies proliferated, as expected, no differences were noticed compared between SiO2_Zn60 and SiO2_Zn120 coated Glass filters and uncoated ones, as shown in

Figure 83. Starting from an initial amount of 10^5 CFU/ml (red line in the graph), the number of colonies proliferated in the broths was about 10^{15} CFU/ml, both for uncoated and SiO2_Zn60 coated Glass, while a slight decrease was observed with SiO2_Zn120 coating (10^{14} CFU/ml proliferated in the broth); analyzing vortex solutions, 10^{13} CFU/ml were found adhered on uncoated and SiO2_Zn60 coated filters, and 10^{10} CFU/ml on Glass_SiO2_Zn120. However, it is worth noting a slight reduction in the number of colonies that proliferated in the broth and adhered to the surface of Glass_SiO2_Zn120, compared to the other two cases. This data, although not demonstrating efficient antibacterial activity of the coating, could be considered for potential future evaluations, which were not performed in this study.

In conclusion, the obtained co-sputtered composite coatings containing Zn or Cu as potential antimicrobial agents did not exhibit an antibacterial effect. The reasons why could be several.

From morphological analyses, it is possible to observe that the deposition process and the interaction between the matrix and the substrate do not lead to the formation of visible copper or zinc metallic nanoclusters. XRD analysis on SiO2_Cu5 and SiO2_Cu10 showed a small peak at around a value of 2theta=43°, which could be referred to metallic copper, but the absence of a peak

in the UV-Vis spectra suggested the formation of nanoparticles did not occur, which is crucial for the exhibition of the antibacterial effect. *Cattaruzza et al.* [231], showed that copper nanoparticles needed heat treatment to be formed. In his study, copper-doped silica coating was deposited on fused silica using the RF magnetron sputtering method. The process, conducted in a pure argon atmosphere, occurred by applying a power of 12W and 250W to Cu and SiO_2 targets, respectively. Heat annealing treatments in oxidizing and reducing atmospheres were performed at elevated temperatures, 700°C and 900°C, for 2 hours or 5 hours in air. XRD analyses of the as-deposited sample, before the heat treatment, did not show peaks related to the formation of copper nanoparticles, in contrast, the spectra of thermally treated coatings exhibited peaks corresponding to the formation of crystalline particles of metallic copper, Cu2O, and CuO, in nanometric dimensions. UV-Vis spectra also confirmed the absence of copper nanoparticles in the as-deposited composite coating, as well as in the one thermally treated in an oxidizing atmosphere. Heat treatment in a reducing atmosphere, typically a mixture of Ar-H_2, is indeed to obtain metallic nanoprecipitates in metal-doped glasses; in this case, the peaks are well evident. In this study, conducting severe heat treatments was deemed impractical due to the final application requirements and the substrate characteristics, which could potentially be compromised by elevated temperatures.

In a separate study, bacterial cellulose was functionalized with magnetron-sputtered Cu nanoparticles. Unlike the composite material here studied, the resulting film consisted solely of Cu without matrix support. Optimal outcomes were achieved by applying a power of 50W to the Cu target for 50 minutes [232], which is higher than that involved in this work.

However, in this scenario, an escalation in power could be correlated with a rise in the Cu content within the composite material, leading to a disproportionately high ratio between the matrix and the metallic nanoparticles. In this study, the lack of the antibacterial effect is probably related to the absence of copper or copper oxide nanoparticles, which needed particular conditions to be synthesized. In addition, as previously mentioned, the quantity of ions released by the coatings may not be sufficient to exhibit an effective inhibitory effect against the tested bacteria and fungi.

In the case of the silica/zinc coatings, XRD analyses for SiO2_Zn120 detected a peak at approximately 2theta = 43°, which as previously mentioned, could correspond to the formation of non-oxidized zinc nanoparticles. The same peak, but with lower intensity, was detected in SiO2_Zn60 coating. In this instance, the coatings did not exhibit antibacterial effects, likely due to the lack of oxidation of the particles that appear to have formed in SiO2_Zn120. *Goel et al.* [233] obtained zinc oxide nanoparticles through reactive magnetron sputtering in the presence of oxygen, in a TiO_2 nanocomposite, with excellent results in inhibiting *S. aureus* and *E. coli*. In another

interesting study, a zinc coating was obtained through DC magnetron sputtering on cotton samples. In this case, the deposition did not occur in a reactive environment, but the formation of ZnO took place due to the reaction between zinc atoms and the reactive hydroxyl groups of cellulose. Zinc, reacting with alcohols in a watery environment, oxidizes to form ZnO. These coatings were effective in antibacterial activity, demonstrated against *S. aureus* and *E. coli*, as well as showing excellent antifungal activity against *A. niger* and *C. globosum* [234].

Recently, the co-sputtering technique has also been used to deposit ZnO/CuO composite coatings with improved antibacterial activity. In this case, to obtain nanoparticles with the desired bactericidal activity, a reactive environment and heat treatment were combined. Specifically, the deposition occurred using Zn and Cu targets in a mixed atmosphere of O_2 and Ar. The resulting coatings underwent annealing at 500°C for 60 minutes, forming zinc and copper oxides, confirmed by XRD analyses. It is interesting to note that the ZnO-only coating exhibited a weak inhibitory effect against both *S. aureus* and *E. coli*, while the bactericidal activity of the CuO coating and the composite coating was very strong [235].

7.1.2. Antibacterial composite coatings for water filters

Coatings with antibacterial and antiviral properties could play an important role in water filtration systems. Using that device, it is possible to have water purified from bacteria, viruses, or other microorganisms without the use of chemicals or produced waste.

The aim of this work, conducted in collaboration with CRAB-Maedicina Ambiente, located in Biella, was to develop composite coatings deposited on thin polymeric membranes used in the filtration of bacterial solution. The obtained coated membranes, characterized in this research activity, were then used to perform filtration tests on solutions containing different types of bacterial strains, by a research group of the company, at their laboratories.

Since the sputtering technique does not require the use of heat, it is suitable for thermosensitive materials. For this reason, the co-sputtered zirconia-based composite coatings have been deposited on electrospun polymeric membranes typically used for water filtration.

As the final application involves prolonged contact with liquid or water solution, the zirconia-based coating is more durable than silica-based coating because of its lower solubility in water compared to silica and, according to [180], and, for this reason, more suitable for the final purpose.

The substrates provided were extremely thin sheets of polymeric material, PCL or PAN-PCL, with a thickness ranging from 40 to 140 μm. Considering their peculiar characteristics, the deposition time was reduced to 10 and 20 minutes to prevent the deterioration of membranes during the process.

The photographs of the membranes before and after the deposition of the zirconia/silver nanoclusters composite coatings ZrO2_Ag4_10 and ZrO2_Ag4_20 are reported in Figure 84.

From a macroscopic point of view, deposition successfully occurred without macroscopically damaging the membrane, and the color change is evident, due to the presence of silver nanoclusters and their plasmonic resonance [181]

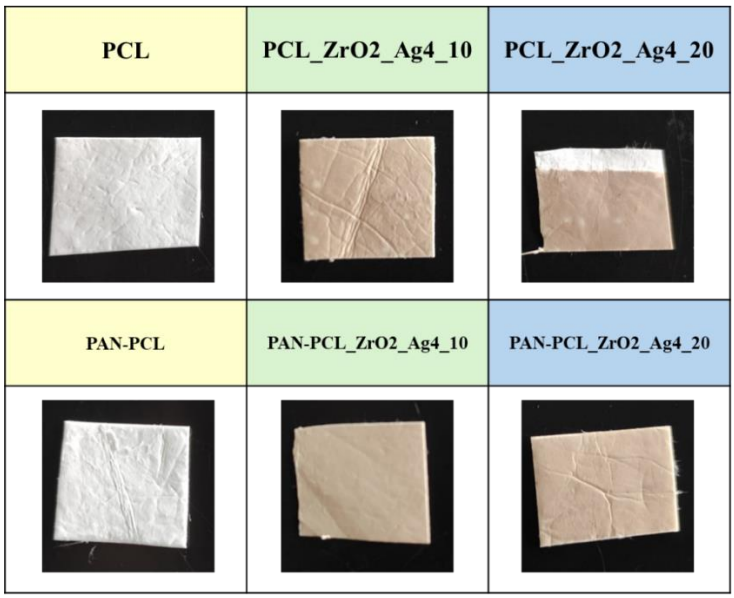

Figure 84: Macroscopic aspect of uncoated and ZrO2_Ag4_10 and ZrO2_Ag4_20 coated PCL and PAN-PCL membranes

Due to the EDS analysis performed on ZrO2_Ag10- and ZrO2_Ag20-coated samples, it is possible to evaluate the composition, and consequently, the amount of silver, in the deposited coatings, and results are shown in Table 12. Uncoated samples are mainly made of C and O, and considering that the EDS technique is not accurate in detecting carbon and oxygen elements, their compositions were not reported.

Table 12: EDS analysis of zirconia/silver composite coatings deposited on water filters for 10 and 20 minutes

Substrate	***ZrO2_Ag coatings***		
	Deposition time	***Zr (% at)***	***Ag (% at)***
PCL	**10 min**	4.51 ± 0.40	1.04 ± 0.16
	20 min	4.76 ± 0.82	1.56 ± 0.80
PAN-PCL	**10 min**	4.62 ± 0.01	1.37 ± 0.09
	20 min	4.13 ± 1.60	1.46 ± 0.90

Analyzing the results, it can be affirmed that the deposition process was successfully done in all cases. In particular, it can be observed that increasing the deposition times led to an increase in the amount of Ag and Zr. In addition, the analysis was performed on three different areas per sample, and the homogenous deposition is suggested by the low standard deviation values.

FESEM analysis showed the morphology of the surface of the electrospun fibers (Figure 85). In the case of PCL membrane, the difference in morphology is well visible before and after deposition. The fibers of the uncoated membrane, (Figure 85 (a)) appeared particularly rough and did not have a uniform surface. In contrast, coated fibers show some small particles, probably zirconia aggregates, dispersed on a smooth surface. The deposited coating appears homogeneous even after 10 and 20 minutes of process.

Similar considerations could be made for the PAN-PCL membrane. In this case, the coatings are well visible with a globular structure ((Figure 85 (e) and (f)). Comparing the coatings obtained in two different process times, no significant differences are observed from a morphological point of view.

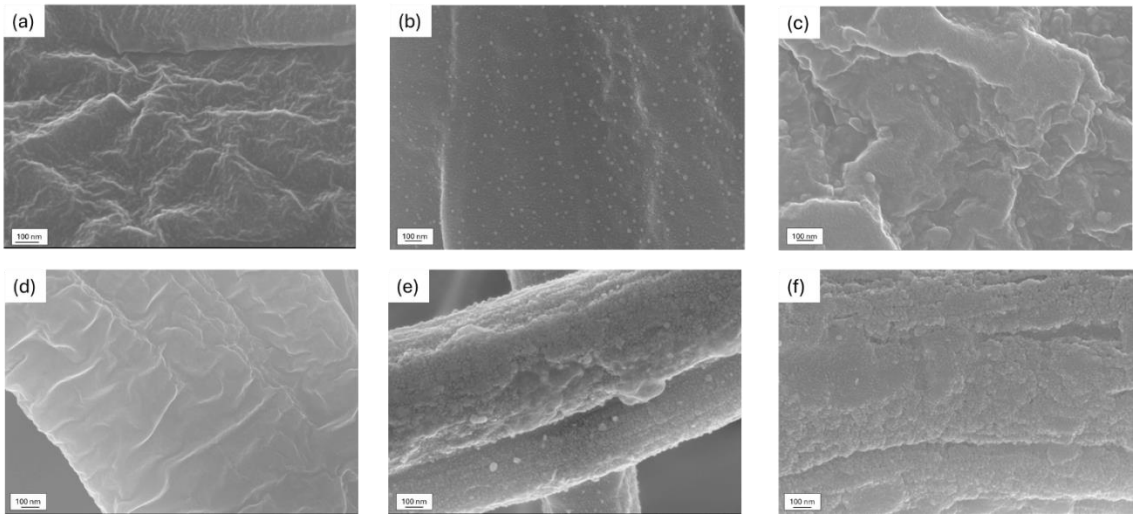

Figure 85: Morphological analysis of (a) uncoated PCL, (b), PCL_ZrO2_Ag4_10, (c) PCL_ZrO2_Ag4_20, (d) unocated PAN-PCL, (e) PAN-PCL_ZrO2_Ag4_10, (f) PAN-PCL_ZrO2_Ag4_10.

Silver nanoclusters are not visible in the FESEM images, but the data obtained from the EDS analysis reported in Table 12 confirmed the presence of silver in deposited coatings.

Structural evaluations were performed on ZrO2_Ag4_10 and ZrO2_Ag4_20 deposited on soda-lime glass substrate, through XRD and UV-Vis analysis. The XRD spectra, displayed in Figure 86 demonstrated that in all cases, the deposited matrix is amorphous. As already mentioned in the section dedicated to coatings deposited on air filters, during the deposition process of composite materials, zirconia undergoes amorphization. Peaks related to metallic silver are present in both spectra at 2theta values of 38° and 44°, with no significant differences in their intensities. Obtaining coatings with silver nanoclusters in short times, and thus also very thin, can be advantageous for coating materials particularly sensitive to the deposition process.

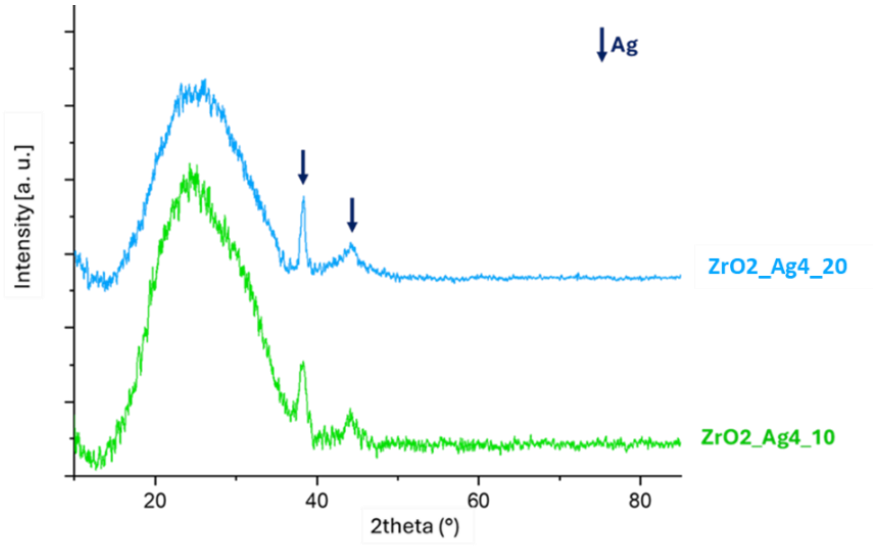

Figure 86: XRD analysis of ZrO2_Ag4_10 and ZrO2_Ag4_20 coatings

In the case of UV-Vis analyses (Figure 87), a notable peak is present around a wavelength of 414 nm, related to silver nanoclusters, in both curves, but with different intensities. This data confirmed the presence of silver nanoclusters in the coatings, deposited in a short process time, and probably embedded in the zirconia matrix.

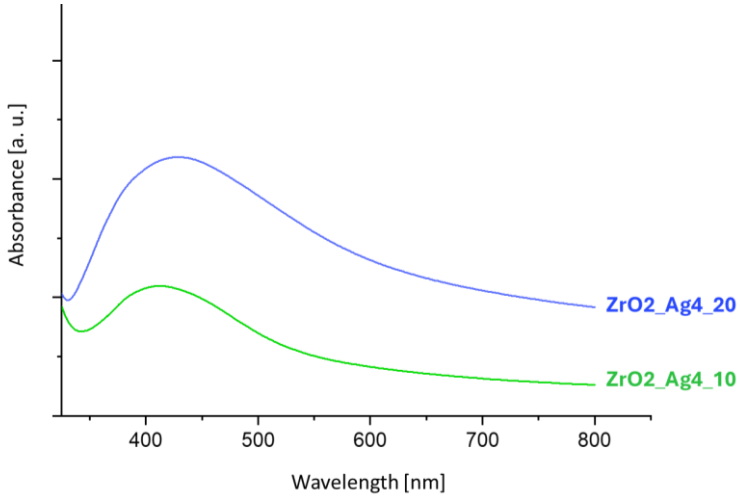

Figure 87: UV-Vis analysis of ZrO2_Ag4_10 and ZrO2_Ag4_20 coatings

Antibacterial test

The antibacterial effect of the coatings was evaluated through an inhibition halo test performed on *S. epidermis and E. coli*, and compared with uncoated PCL and PAN-PCL. The results are shown in Figure 88.

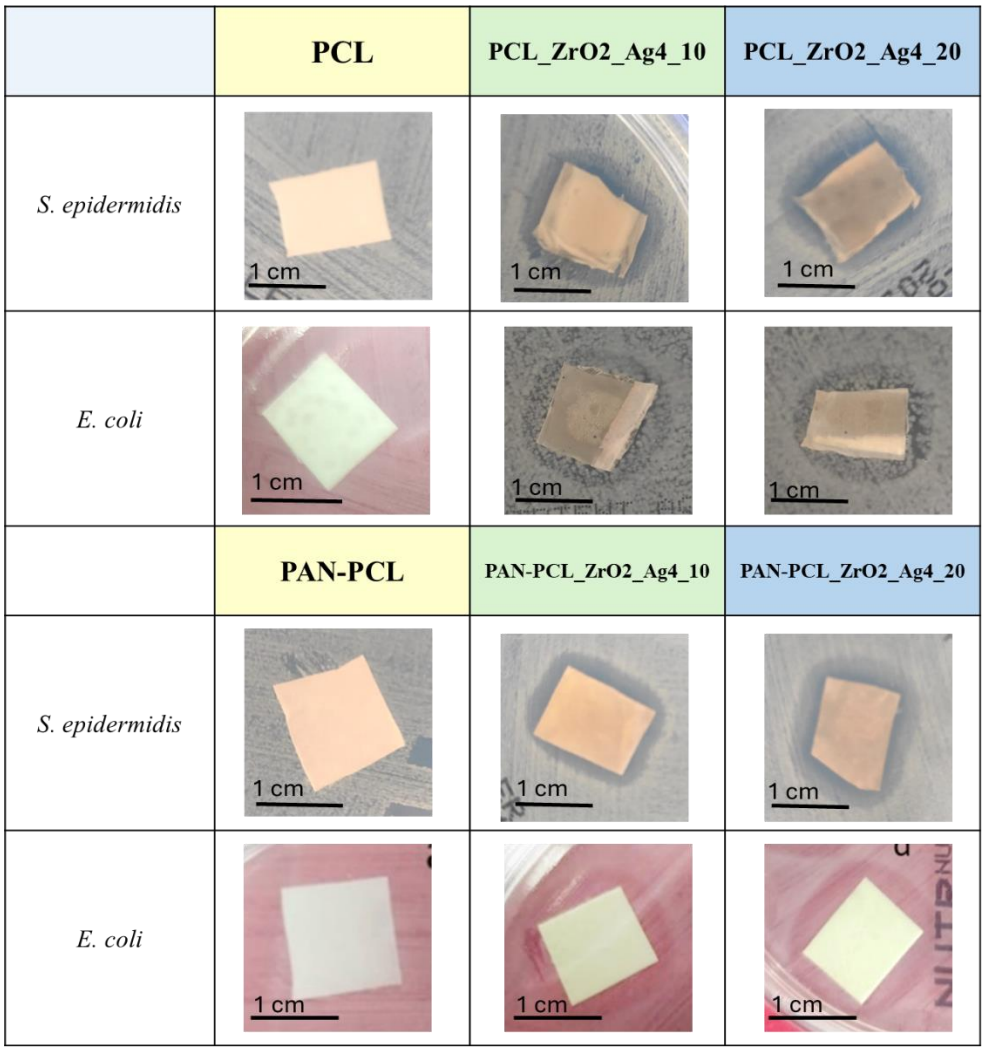

Figure 88: Inhibition halo test against S. epidermidis and E. coli on uncoated and ZrO2_Ag4_10 and ZrO2_Ag4_20 coated PCL and PAN-PCL

Considering PCL as substrate, both zirconia-based coatings exhibited a good antibacterial effect against *S. epidermidis*, demonstrated by the area free from bacteria visible around the coated samples, even if the coatings are very thin and with low silver content, due to the short deposition process. Conversely, colonies are visible in contact with untreated membranes. Increasing the deposition time from 10 to 20 minutes did not affect the bactericidal effect, and the size of the two halos was quite similar. A double halo is visible in this case, but it attested to an effective bactericidal activity as already described in the case of coatings deposited on air filters in the dedicated section.

Regarding the effect of ZrO2_Ag4 coatings against *E. coli*, an area completely devoid of bacterial colonies is not evident, but there is a zone where bacteria colonies are in smaller quantities, and therefore partially reduced, it is clearly visible. No difference could be highlighted between the two different amounts of silver content. The resistance of *E. coli* colonies to the bactericidal effect of

silver-doped zirconia systems was confirmed by *Rodriguez et al*., who demonstrated the effectiveness of ZrO_2-based porous filters doped with silver in inhibiting the S. aureus bacterial strain, but not against E. coli [236].

Similar considerations could be made by observing results about PAN-PCL membranes. The halo was well visible against *S. epidermidis,* and in the case of ZrO2_Ag4_20 coating, it seems to be larger and double, as in the external area bacterial colonies were reduced but not totally inhibited. In the case of *E. coli* bacteria, the halo is present around the coated membrane, but this area is not completely free from bacteria, suggesting a reduction, but not a complete inhibition of bacteria growth.

In addition to typical ceramic filters [127], also membranes could be employed in water disinfection process. Capillary membranes composed of AgNPs-doped zirconia were used for the filtration of solutions containing *E. coli* contaminant, showing highly efficient activity to retain bacteria colonies and to kill retained microorganisms [237]. Silver nanoparticles and zirconia incorporated in an organic framework derived from medical leaves were used as a hybrid nanocomposite, for water purification purposes, due to the strong bonding of nanoparticles and leave extract, and the good fouling resistance. The material showed a strong bactericidal effect against *S. aureus* and *E. coli* [238]. A study demonstrated that *E. coli* showed higher resistance to silver-doped zirconia bactericidal activity, compared to *S. aureus* strain [236].

Results relative to the wettability of the membrane are shown in Figure 89.

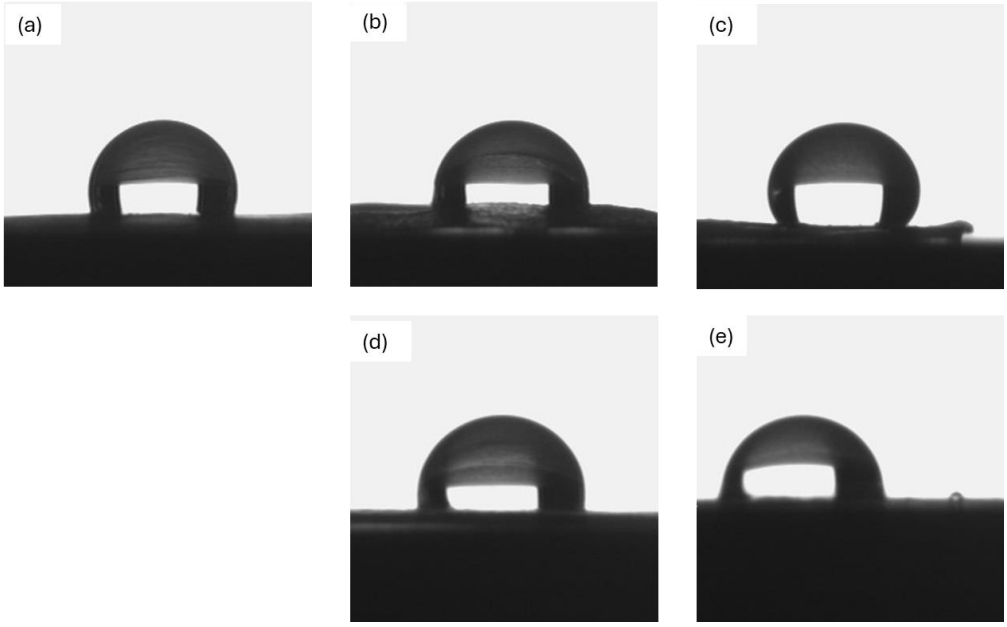

Figure 89: Contact angle with distilled water on (a) uncoated PCL, (b)PCL_ZrO2_Ag4_10 and (c) PCL_ZrO2_Ag4_20; (d) PAN-PCL_ZrO2_Ag4_10 and (e) PAN-PCL_ZrO2_Ag4_20

Bare PCL showed to be hydrophobic towards water, with a contact angle of about 107°, but for PCL-PAN membrane no evaluation was possible since the water drop was immediately filtered. Conversely, all the zirconia/silver coatings showed high contact angle values, in a range between about 98°-127°, very close to that obtained for RF sputtered zirconia coating by *Kamlesh V. Chauhan* [239].

Filtration of bacterial solutions

The so-obtained membranes with sputtered composite coating in zirconia matrix with silver nanoclusters were used to perform filtration tests on solutions containing different types of bacterial strains, at CRAB - Medicina Ambiente company, by a research group at their laboratories.

The filtration and efficiency of uncoated PCL and PAN-PCL and of ZrO2_Ag4_10 and ZrO2_Ag4_20 coated membranes were tested with aqueous solutions containing *Bacillus subtilis, Listeria Monocytogenes*, as Gram-positive bacterial strains, and *E. coli, as* Gram-negative bacterial strain.

Results showed that both uncoated PAN and PAN-PCL were able to filter bacterial aqueous solutions but allowed bacterial proliferation on the surface of the membranes. In contrast, no bacterial colonies grew on filter surfaces in contact with ZrO2_Ag4 composite coatings deposited during the 10 and 20-minute processes.

Analyzing the bacteria colonies proliferated in solution before and after the filtration test, results showed that the best performances were exhibited by PAN-PCL_ZrO2_Ag4_10 and PAN-PCL_ZrO2_Ag4_20 membranes against *L. monocytogenes* and *B. subtilis*, both Gram-positive bacteria, which caused a reduction, but not complete inhibition, of bacterial colonies. In addition, a slight reduction in *L. monocytogenes* colonies proliferated after filtration through PCL_ZrO2_Ag4_20 was observed.

Conversely, both coated PCL and PAN-PCL membranes did not exhibit efficiency in inhibiting *E. Coli* colonies, confirming its resistance to the action of zirconia/silver systems, as previously discussed.

Additionally, during the filtration process, it was observed that filtering the bacteria solutions required a lot of time. The presence of the coating, as suggested by the contact angle analysis, conferred hydrophobic behavior to the membranes, significantly slowing down the filtration rate.

For further confirmation, a drop of distilled water and olive oil was placed on the PCL_ZrO2_Ag4_10 membrane, and their behavior was observed. As seen, the contact angle of the olive oil drop was smaller than that of water, allowing a fast filtration process for the oil. This data confirmed that due to their hydrophobic behavior, zirconia-based coatings slowed down the filtration process.

In conclusion, although zirconia-based coatings sputtered on membranes for reduced times exhibited strong antibacterial efficiency, especially in inhibiting Gram-positive bacteria, their use in filtration systems for aqueous solutions is not suggested, or requires further study to overcome the issue of hydrophobic behavior.

7.1.3. Antibacterial composite coatings for automotive textiles

This activity aimed to optimize and develop the silver nanoclusters/silica, or zirconia, composite coatings in order to confer antibacterial effect to automotive textiles in the framework of the project "Antimicrobial/virucidal PVD coatings for automotive", in collaboration with FCA-CRF company.

Different textiles and fabrics, both natural and synthetic, typically used in car interiors for seats or the steering wheel, have been employed as substrates for the deposition of coatings. Two fundamental requirements needed to be fulfilled simultaneously: to have bactericidal activity and to be transparent, so as not to alter the original color of the fabric.

The substrates provided by FCA-CRF company were two black fabrics, *Fabric_1* and *Fabric_2*, composed of three layers of polyamide, polyurethane foam, and polyester fibers, of two different thicknesses, a synthetic leather, colored in black, named *Leather* in the text, and two genuine leather fabrics, a blue-colored one, *Leather_blue,* and a brown-colored one *Leather_brown*.

Since color variation is a stringent condition in the development of these coatings, it was decided to proceed by evaluating a series of coatings obtained by modifying certain process parameters during deposition.

Previous studies on coatings show a significant color variation between the uncoated material and that obtained after the deposition of silica- or zirconia-based coatings with silver nanoclusters. In particular, due to the plasmonic resonance of silver nanoclusters, the coating tends to impart a brown color to the substrates, which become darker with the increment of deposition time and, consequently, of coating thickness [240].

Therefore, to achieve the project's goal, two approaches were followed in order to reduce the color change without altering the antibacterial effect: (i) to reduce the silver content inside the matrix and, as a result, the effect of surface plasmonic resonance; (ii) to minimize the time of deposition process, and consequently silver content, for obtaining a transparent coating [241].

To optimize the coatings deposition process, parameters applied were selected after compositionally EDS analysis and rapid and qualitative antibacterial inhibition zone test, against *S. epidermidis*. Based on these data and the intensity of color variation, the parameters of the deposition process were changed, and some coatings and substrates were discarded. The coatings that exhibited better results, were then in more detail characterized, as will be illustrated later.

Compositional and antibacterial analysis

To understand how process parameters could be modified to achieve the project's goal, a first, preliminary deposition of silver nanoclusters/silica composite coating, SiO2_Ag4, with already studied process parameters (1h of deposition time) was performed, to verify the possibility of depositing the coating on leather substrates.

Bare samples and textiles obtained after coating deposition are shown in Figure 90.

It can be observed that the coating altered the original color of the fabrics, especially in the case of blue and brown leather, which became darker.

However, the results confirmed that the magnetron sputtering technique is able to successfully deposit coatings on both natural and synthetic textiles without causing damage, on both natural and synthetic textile. Even though the color variation due to the presence of the coating is less impactful for the two black fabrics and the black leather compared to the other cases, it is still unacceptable in considering the final research objective and the application requirement. The color change on leather was similar to that found in a recent work, in which a natural lining leather was modified with bio-synthesized AgNPs, showing a color change from yellow to brown [145].

Data relative to EDS were summarized in Table 13 and confirmed that coating deposition successfully occurred. The uncoated textiles were composed mainly of C and O, but since EDS analysis is not accurate in detecting oxygen and carbon, their composition was not reported, while Si and Ag were detected on the coated substrates. In particular, the amount of silicon is quite similar for both *Leather_blue* and *Leather_brown,* around 5.20 at. %, for *Fabric_1* was around 4.20 at. %, and for *Fabric_2* and *Leather* was in a range between 2.50 and 3.00 at. %, suggesting that some different interactions occurred during the coating deposition process between the silica matrix and the substrate. Regarding the Ag amount, the values detected in coating deposited on *Fabric_1* and Fabric_2 were about 3.30 at. %, and 1.80 at. % respectively, while in the case of synthetic leather, the lowest value was registered (nearly 0.80 at. %). Silver amounts in coatings deposited on natural leathers were in a range between 1.37 and 2.18 at. %.

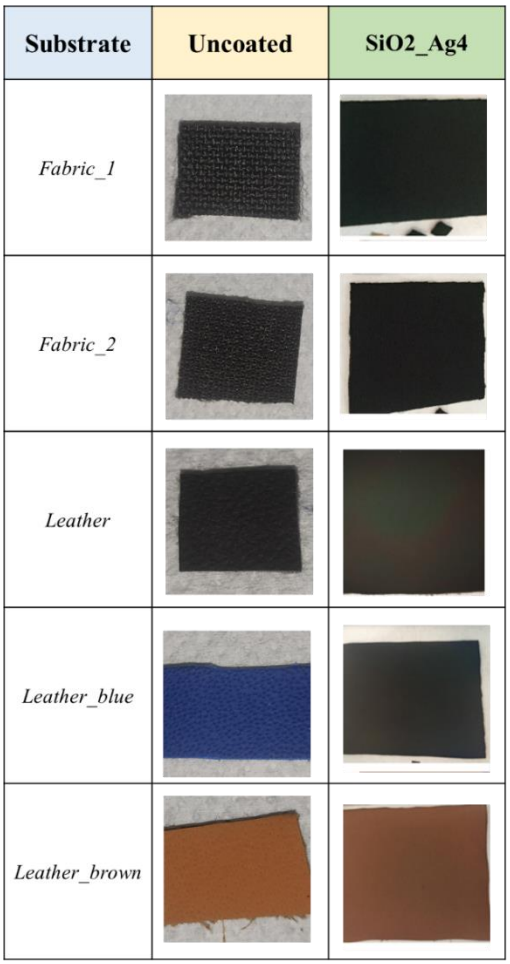

Figure 90: Macroscopic aspect of uncoated and SiO2_Ag4 coated Fabric_1, Fabric_2, (c) Leather, (d) Leather _blue and (e) Leather _brown

Table 13: EDS analysis on silica/silver composite coating deposited on fabric and leather textiles

Substrate	**SiO2_Ag4 coating**	
	Si (% at.)	**Ag (% at.)**
Fabric_1	4.19 ± 1.65	3.31 ± 1.47
Fabric_2	2.93 ± 0.28	1.71 ± 0.21
Leather	2.51 ± 0.59	0.81 ± 0.19
Lather-blue	5.35 ± 2.18	2.18 ± 0.36
Leather-brown	5.26 ± 0.08	1.37 ± 0.04

To minimize the effect of the surface plasmon resonance of the nanoclusters, the first approach involved reducing the amount of silver. For this purpose, the power applied to the silver target during the coating deposition was reduced to 1 and 2 W. Additionally, the processing time was reduced to 30 minutes, alongside the standard one-hour deposition.

As reported in "*Materials and methods*" chapter, composite silica-based coatings will be indicated as ***SiO2_Ag1_30***, ***SiO2_Ag1_60***, ***SiO2_Ag2_30*** and***, SiO2_Ag2_60***, on the other hand, those with zirconia as matrix will be named ***ZrO2_Ag1_30***, ***ZrO2_Ag1_60***, ***ZrO2_Ag2_30*** and, ***ZrO2_Ag2_60***.

The appearance of the textile after the deposition of silica and zirconia-based coatings adopting optimized new parameters are reported in Figure 91 and Figure 92, respectively.

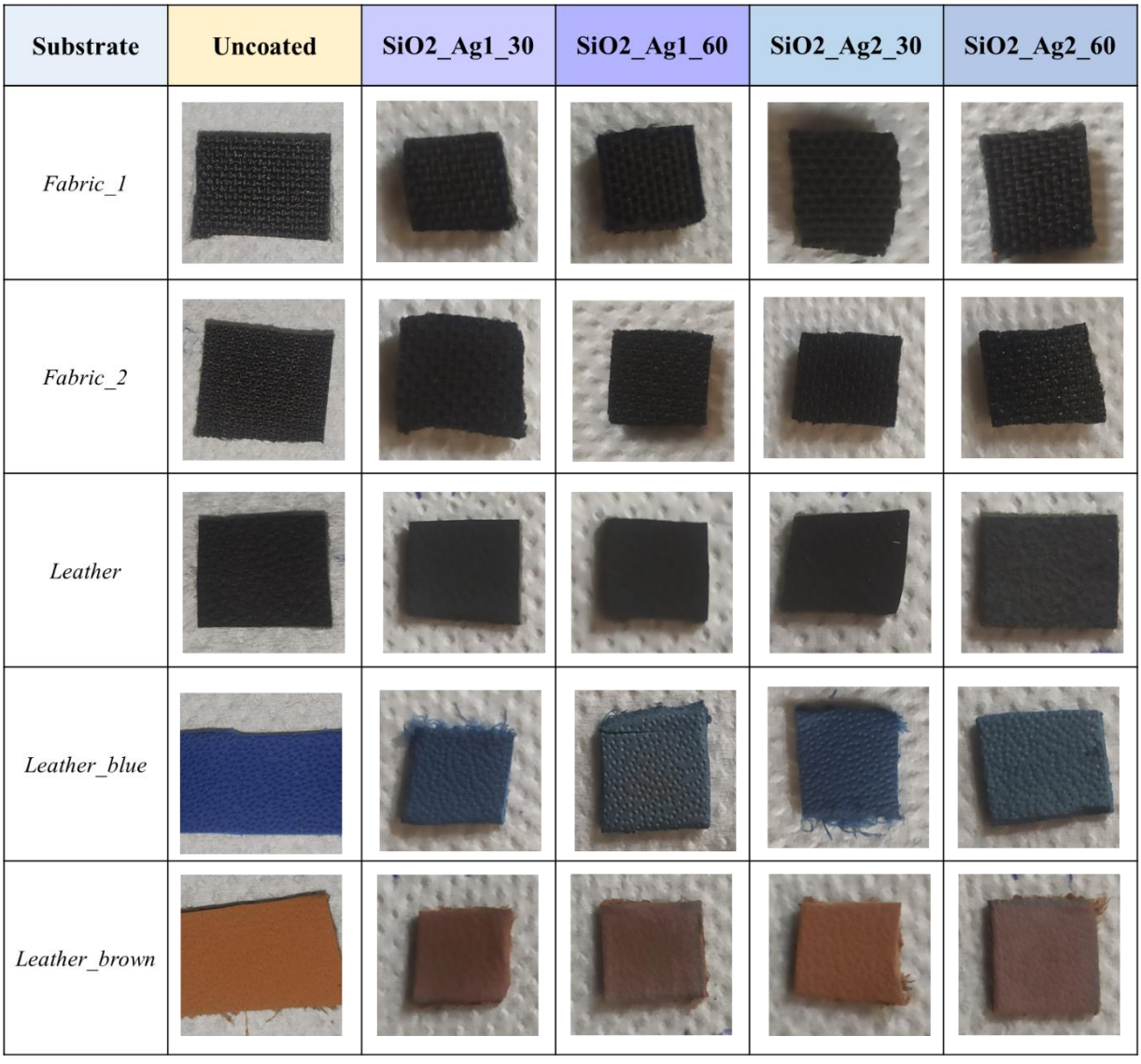

Figure 91: Macroscopic aspect of uncoated and SiO2_Ag1_30, SiO2_Ag1_60, SiO2_Ag2_30, SiO2_Ag2_60 coated Fabric_1, Fabric_2, Leather, Leather _blue and Leather _brown

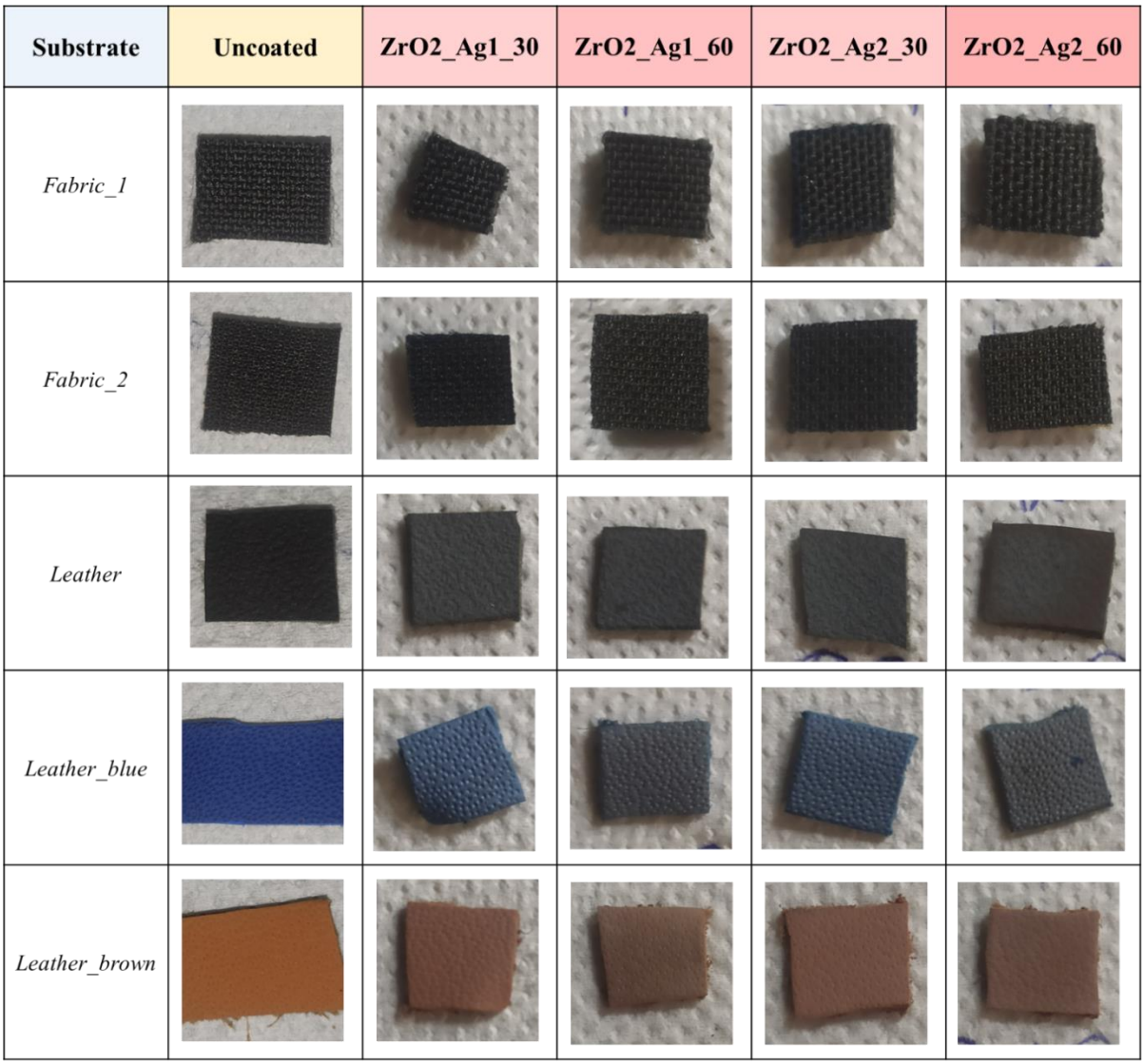

Figure 92: Macroscopic aspect of uncoated and ZrO2_Ag1_30, ZrO2_Ag1_60, ZrO2_Ag2_30, ZrO2_Ag2_60 coated Fabric_1, Fabric_2, Leather, Leather _blue and Leather _brown

Compared with the uncoated textiles, the chromatic change imparted by both SiO_2/Ag and ZrO_2/Ag optimized coatings on *Leather_blue* and *Leather_brown* is evident, even when lower power was applied to the silver target, and the process lasted half an hour. In particular, the two natural leathers appeared gray and less bright than the uncoated sample. In the case of *Leather_blue*, it is evident that increasing process time and keeping constant the Ag power results in darker coatings.

Both SiO_2- and ZrO_2-based coatings with the optimized process parameters altered the original color of the black synthetic *Leather*, making it gray and dull. In the case of the two fabrics, the color change is not so evident from the photographs, but compared to the original ones, coated samples appeared less bright, in both silica or zirconia matrix coatings.

Results from EDS analysis related to the composite coatings with silica and zirconia as matrix are shown in Table 14 and Table 15, respectively.

Table 14: EDS analysis on silica/silver composite coatings deposited on Fabric_1, Fabric_2, Leather, Leather_blue, and Leather_brown, applying optimized process parameters

Substrate	Power to Ag target	30 min		60 min	
		Si (% at.)	Ag (% at.)	Si (% at.)	Ag (% at.)
Fabric_1	***1W***	1.45 ± 0.19	0.44 ± 0.21	2.68 ± 0.14	0.70 ± 1.33
	2W	1.48 ± 0.40	0.71 ± 0.51	2.55 ± 0.42	1.03 ± 0.47
Fabric_2	***1W***	1.08 ± 0.13	0.35 ± 0.17	2.34 ± 0.29	0.88 ± 0.24
	2W	1.04 ± 0.06	0.50 ± 0.12	2.39 ± 0.23	0.97 ± 0.13
Leather	***1W***	3.29 ± 0.63	0.21 ± 0.43	3.21 ± 0.25	0.39 ± 0.05
	2W	2.09 ± 0.33	0.24 ± 0.03	3.03 ± 0.46	0.59 ± 0.14
Leather_blue	***1W***	2.84 ± 0.28	0.30 ± 0.05	3.91 ± 0.05	0.62 ± 0.04
	2W	2.38 ± 0.23	0.33 ± 0.08	4.12 ± 0.14	0.69 ± 0.16
Leather_brown	***1W***	3.87 ± 0.21	0.34 ± 0.01	4.55 ± 0.18	0.51 ± 0.04
	2W	3.05 ± 0.29	0.42 ± 0.05	6.16 ± 0.46	1.32 ± 0.24

In the case of SiO_2-based coatings, a deposition time of 30 minutes, combined with varying the power applied to the Ag target from 1 to 2 W, results in a slight increase in the silver content within the coatings. The differences in silver amount after the two depositions ranged from 0.03 at. %, for *Leather* and *Leather_blue* to about 0.27 at. %, for *Fabric_1*.

When the deposition time was extended to 60 minutes, coatings on, *Fabric_2*, and *Leather_blue* showed a slight increase in silver content when the power was increased from 1 to 2 W. However, in the case of *Leather_brown*, the increase was substantial, rising from 0.51 at. %, when 1 W was set, to 1.32 at. %, with 2 W, more than doubling the initial value and reaching the highest values observed for silica-based coatings.

On the other hand, evaluating the effect of process time in Ag content, when the power was kept constant, results revealed that, in most cases, the silver content nearly doubled when the process duration increased from 30 to 60 minutes. For example, in *Fabric_2*, the silver content increased from approximately 0.35 at. % for SiO2_Ag1_30 to about 0.88 at. % for SiO2_Ag1_60, and from around 0.50 at. % for SiO2_Ag2_30 to 0.97 at. % for SiO2_Ag2_60.

The silver concentration after coating deposition for 60 minutes was found to be doubled compared to that after 30 minutes, even in the case of blue leather and leather with SiO2_Ag2. In other cases, although the Ag amount after the two depositions was not exactly doubled, it still showed an increase. A particular case is represented by brown leather, where the SiO2_Ag2_30 coating showed a silver content of approximately 0.42 at. %, which more than tripled (approximately 1.34 at. %) after the deposition of SiO2_Ag2_60.

Table 15: EDS analysis on zirconia/silver composite coatings deposited on Fabric_1, Fabric_2, Leather, Leather_blue, and Leather_brown, applying optimized process parameters

Substrate	***Power to Ag target***	**30 min**		**60 min**	
		Zr (% at.)	**Ag (% at.)**	**Zr (% at.)**	**Ag (% at.)**
Fabric 1	***1 W***	0.55 ± 0.01	0.42 ± 0.07	1.28 ± 0.21	0.98 ± 0.38
	2 W	0.65 ± 0.04	0.49 ± 0.09	1.27 ± 0.19	1.36 ± 0.47
Fabric 2	***1 W***	0.45 ± 0.05	0.34 ± 0.06	1.10 ± 0.16	0.97 ± 0.22
	2 W	0.39 ± 0.01	0.42 ± 0.05	1.43 ± 0.28	1.74 ± 0.53
Leather	***1 W***	0.42 ± 0.07	0.33 ± 0.05	0.87 ± 0.09	0.73 ± 0.04
	2 W	0.43 ± 0.08	0.36 ± 0.08	0.93 ± 0.14	0.93 ± 0.14
Lather-blue	***1 W***	0.51 ± 0.06	0.29 ± 0.04	1.27 ± 0.04	0.83 ± 0.03
	2 W	0.55 ± 0.02	0.38 ± 0.01	1.24 ± 0.08	1.29 ± 0.05
Leather-brown	***1 W***	0.53 ± 0.06	0.35 ± 0.04	1.15 ± 0.09	0.87 ± 0.09
	2 W	0.47 ± 0.06	0.40 ± 0.06	1.34 ± 0.17	1.33 ± 0.37

Analyzing the data obtained from the EDS analysis of coatings with zirconia as the matrix, they confirm that changing the power from 1 to 2 W on the Ag target for half-hour depositions results in a silver content increase in the coatings by approximately 0.05-0.10 at. %. For all the substrates, the average Ag amount ranges between was approximately 0.3 and 0.5 at. %.

When considering one-hour depositions, the power change induces a greater increase in the Ag content in the coatings. Specifically, *Leather* showed a 0.2 at. % increase, while *Fabric_1, Leather_blue,* and *Leather_brown* exhibited an increase of approximately 0.45-0.50 at. %, reaching

a maximum of 1.36 at. % (in the case of *Fabric_1*). A notable case is represented by coatings deposited for 60 minutes on *Fabric_2*, where the silver content increases from 0.97% at. in ZrO2_Ag1_60 to approximately 1.74% at., in ZrO2_Ag2_60, nearly doubling the value. Considering the effect of time, even in the case of zirconia-based coatings, there is a significant increase in silver amount. In some cases, this increase was just over double (for example, for *Fabric_1*, it increases from 0.42% at., in ZrO2_Ag1_30, to 0.98% at. in ZrO2_Ag1_60), almost tripled for *Leather* and *Leather_blue*, increasing from 0.36 to 0.93% at. and from 0.29 to 0.83% at. with 2 W, respectively. There were cases for which the increase in silver content caused by extending the deposition times from 30 to 60 minutes, was significant. In particular, in the case of *Fabric_1*, with a rise from 0.49 to approximately 1.36% at., *Fabric_2*, with an increment from 0.42 to approximately 1.74% at., and *Leather_brown*, obtaining values of 0.40 to 1.33% at.

From this analysis, it can be concluded that deposition time is the factor that most influences the silver content in the coatings, as previously observed when analyzing the color variations of the various coated substrates.

Since the amount of silver has been reduced compared to the previously studied coatings, the antibacterial effect was tested by the rapid and qualitative inhibition halo test against *S. epidermidis*, conducted on both SiO_2/Ag and ZrO_2/Ag coatings with changed process parameters.

Results regarding SiO_2-based coatings are shown in Figure 93, and those regarding ZrO2-base coatings are shown in Figure 94.

In the case of silica-based coatings, a distinct halo is clearly visible around all coated *Fabric_1* and *Leather_brown* samples. When considering *Fabric_2* with both SiO2_Ag1 and SiO2_Ag2 coatings deposited for 30 minutes, bacterial colonies grew around and on the sample surfaces, whereas, with 60-minute depositions, areas free from bacteria became visible. The halo observed around *Leather*_SiO2_Ag2_30 is smaller compared to that on the same samples, and for *Leather_blue*, both SiO2_Ag1 coatings formed smaller halos after 30 and 60 minutes of deposition, compared to those observed with SiO2_Ag2.

Generally, larger inhibition zones were observed for coatings obtained with 60-minute depositions at a power setting of 2 W on the silver target.

Considering ZrO_2_Ag coatings, no bacteria grew around all coated *Fabric_1*, but the halos formed around ZrO2_Ag1_30 were smaller than in other cases. ZrO2_Ag2_30 and ZrO2_Ag2_60 deposited on *Fabric_2* showed good results, contrasting with those obtained with ZrO2_Ag1.

Excellent antibacterial effects were exhibited by all optimized ZrO2/Ag coatings deposited on *Leather,* which showed large halos around all samples. This demonstrates that even with a very low silver content in the coating due to low applied power, bacterial proliferation was effectively inhibited.

Areas free from bacteria were visible around *Leather_brown* with all analyzed coatings, although the dimensions were smaller than in the case of black *Leather*. The worst results were obtained for *Leather_blue*: no halo was evident around SiO2_Ag1_30-coated samples, and halos around the other coatings were smaller compared to other cases.

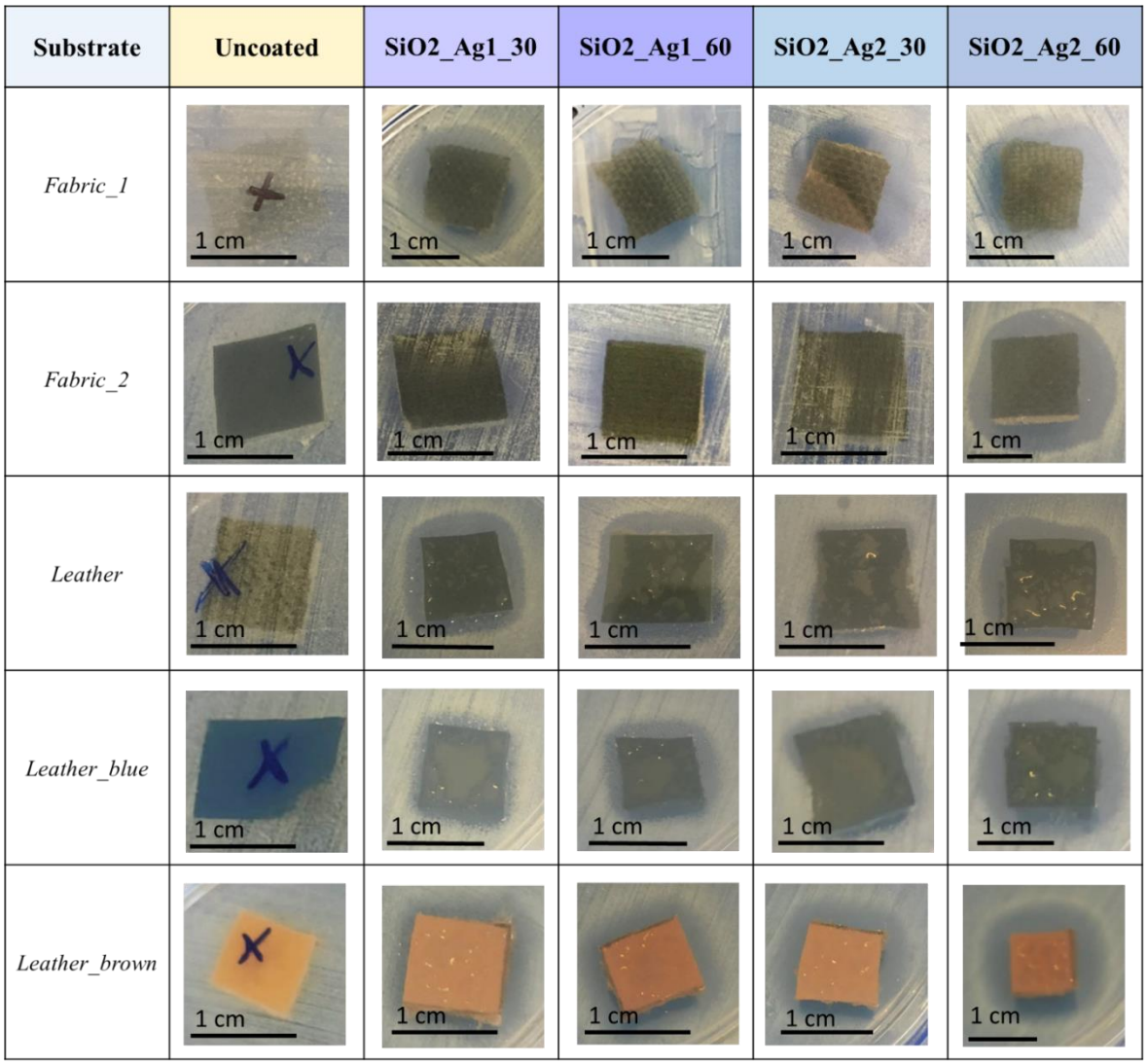

Figure 93: Inhibition halo test against S. Epidermidis on uncoated and SiO2_Ag1_30, SiO2_Ag1_60, SiO2_Ag2_30, SiO2_Ag2_60 coated Fabric_1, Fabric_2, Leather, Leather _blue and Leather _brown

Substrate	Uncoated	ZrO2_Ag1_30	ZrO2_Ag1_60	ZrO2_Ag2_30	ZrO2_Ag2_60
Fabric_1		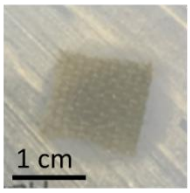	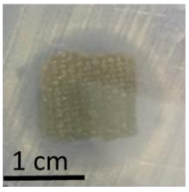	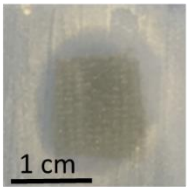	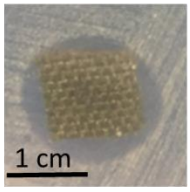
Fabric_2	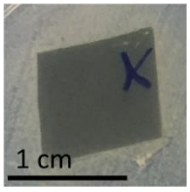	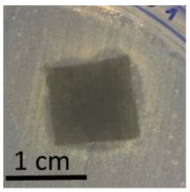	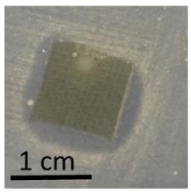	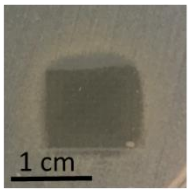	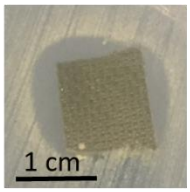
Leather	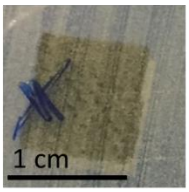	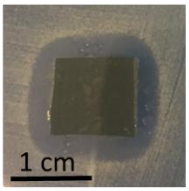	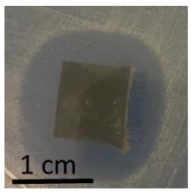	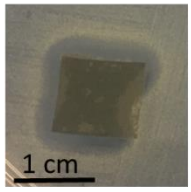	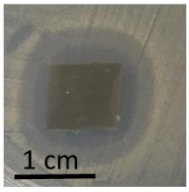
Leather_blue	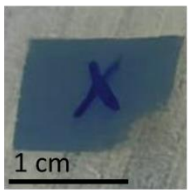	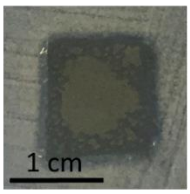	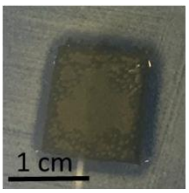	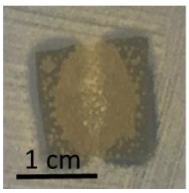	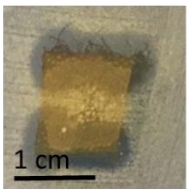
Leather_brown	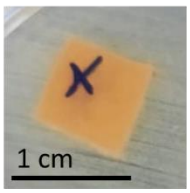	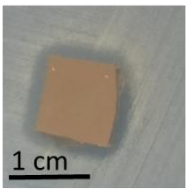	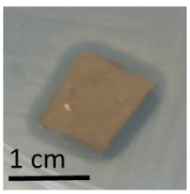	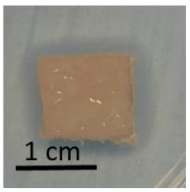	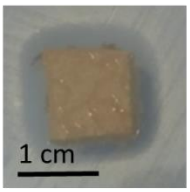

Figure 94: Inhibition halo test against S. Epidermidis on *uncoated* and *ZrO2_Ag*1_30, *ZrO2_Ag*1_60, *ZrO2_Ag*2_30, *ZrO2_Ag*2_60 *coated Fabric_1, Fabric_2, Leather, Leather _blue and Leather _brown*

In general, almost all the coated samples exhibit an inhibition halo, with a few exceptions. It is important to note that this qualitative test is intended solely to verify the potential effectiveness of the coatings. Although quantitative tests could provide a better evaluation of the effects of reducing silver concentration and deposition time in the antibacterial activity, the coatings noticeably altered the original color of the substrates, which is one of the fundamental requirements of the project.

At this point, only *Fabric_1*, *Fabric_2*, and *Leather*, which are black, were selected for deeper investigations, since their color was less altered by the coatings.

Another attempt to achieve the project goal involved a second approach aimed at obtaining a transparent and antibacterial coating through deposition times minimized to 5 and 10 minutes, while maintaining a power of 4W on the silver target, according to [241].

In fact, it has been reported that reducing the deposition time and, consequently, the thickness of the coatings makes the coatings themselves transparent, thereby reducing the effect of altering the color of the substrates, even though silver nanoclusters remain embedded in the matrix. Therefore, only coatings with a silica matrix were studied and characterized from this point onward.

The coatings obtained by depositing silver nanoclusters and silica for 5 and 10 minutes, on *Fabric_1*, *Fabric_2,* and *Leather*, are shown in Figure 95. As reported in the photographs, so thin coatings on *Fabric_1* and *Fabric_2* seem to not induce a chromatic modification of the substrates, but in the case of *Leather*, a thing grey coating is visible.

Substrate	Uncoated	SiO2_Ag4_5	SiO2_Ag4_10
Fabric_1			
Fabric_2	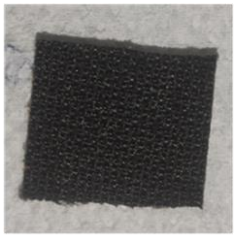		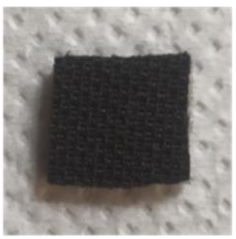
Leather	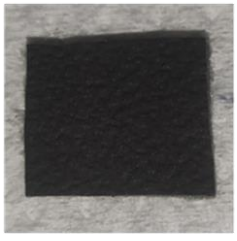	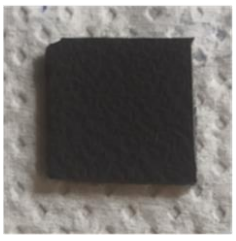	

Figure 95: Macroscopic aspect of uncoated and SiO2_Ag4_5,and SiO2_Ag4_10 coated Fabric_1, Fabric_2, Leather

To check the successful deposition of the coating, compositional evaluations were performed using the EDS analysis (Table 16) . The values reported demonstrated that the coatings have been

deposited on the substrates but the atomic percentage of the elements Si and Ag were very low compared with the first deposited coatings. In particular, Ag content in the coatings deposited for only 5 minutes on *Fabric_1* and *Leather* reached a value below 0.1 at. %, which is also the limit of the instrument.

To investigate the effect of coatings containing very low amounts of silver in inhibiting bacteria, the inhibition halo test was conducted against Gram-positive *S. epidermidis* strain, shown in Figure 96, and against Gram-negative *E. coli* strain, reported in Figure 97.

Table 16: EDS analysis on silica/silver composite coatings deposited on Fabric_1, Fabric_2 and Leather, with recuced times

Substrate	***SiO2_Ag coating***		
	Power to Ag target	***Si (at. %)***	***Ag (at. %)***
Fabric_1	***5 W***	0.31 ± 0.06	0.19 ± 0.10
	10 W	0.41 ± 0.14	0.31 ± 0.16
Fabric_2	***5 W***	0.17 ± 0.01	0.03 ± 0.03
	10 W	0.40 ± 0.01	0.16 ± 0.01
Leather	***5 W***	5.29 ± 0.25	0.06 ± 0.01
	10 W	4.29 ± 0.33	0.15 ± 0.04

For *Fabric_1* and *Fabric_2*, the area without proliferated bacteria colonies was very small and not completely around the sample. In the case of the *Leather* as substrate, the halo is more evident, especially in the case of SiO2_Ag4_10, where the area without bacteria was bigger. It was suggested that the antibacterial effect was increased by the presence of silica on leather, which increased hydrophobicity and consequently reduced bacteria growth [148].

E. coli was resistant to the antibacterial effect of both coatings deposited on *Fabric_2* and *Leather*, on the contrary, *Fabric_1* exhibited evident halos against, whose size became larger with 10 minutes of deposition time.

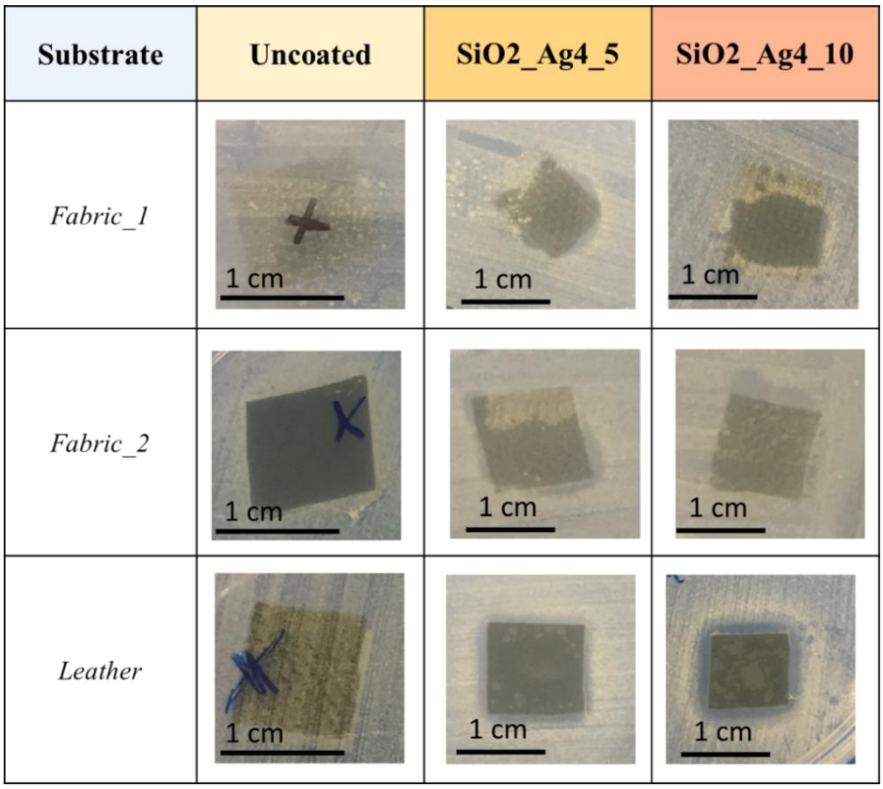

Figure 96: Inhibition halo test against S. epidermidis on uncoated and SiO2_Ag4_5 and SiO2_Ag4_10 coated Fabric_1, Fabric _2, Leather

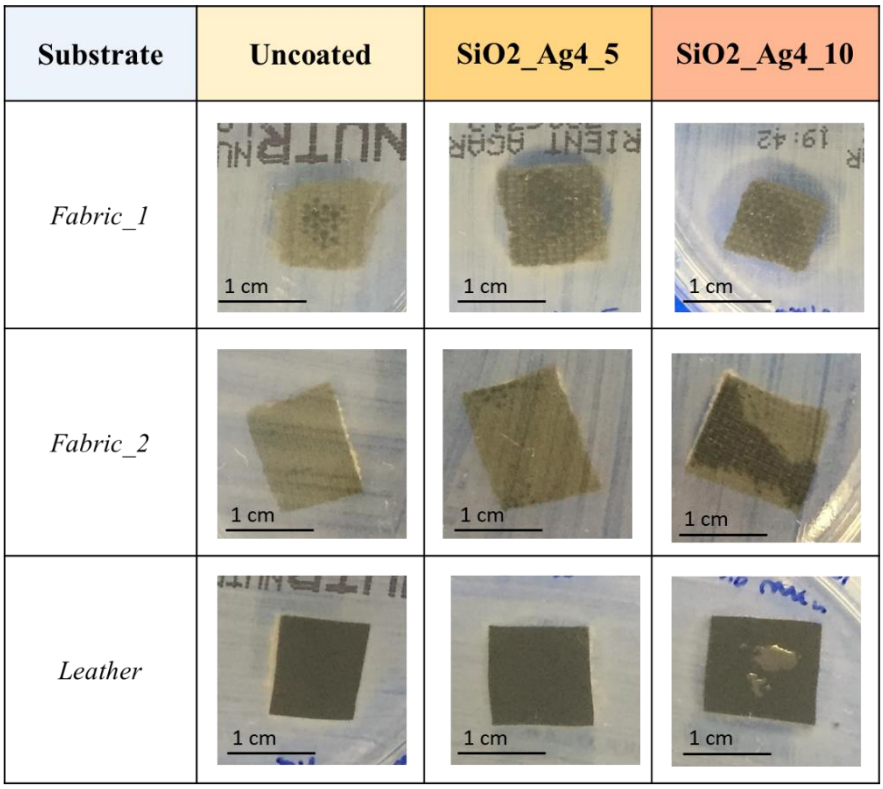

Figure 97: Inhibition halo test against E. coli on uncoated and SiO2_Ag4_5 and SiO2_Ag4_10 coated Fabric_1, Fabric_2, Leather

These results are predictable due to the low silver content, but also because the deposited layer may not be uniform and therefore not completely cover the whole surface due to the very short time of the deposition, especially 5 minutes.

Based on all these results, and considering the requirements of the project aimed to combine antibacterial effect without a chromatic modification of substrate, only the black samples *Fabric_1*, *Fabric_2* and the *Leather* coated by the coatings SiO_2_Ag1_60, SiO_2_Ag4_10 have been subjected to a complete characterization campaign.

Morphological and structural analysis

FESEM analysis (Figure 98) highlights different surface morphologies between uncoated and coated samples, confirming the deposition of sputtered coatings on synthetic and natural leather.

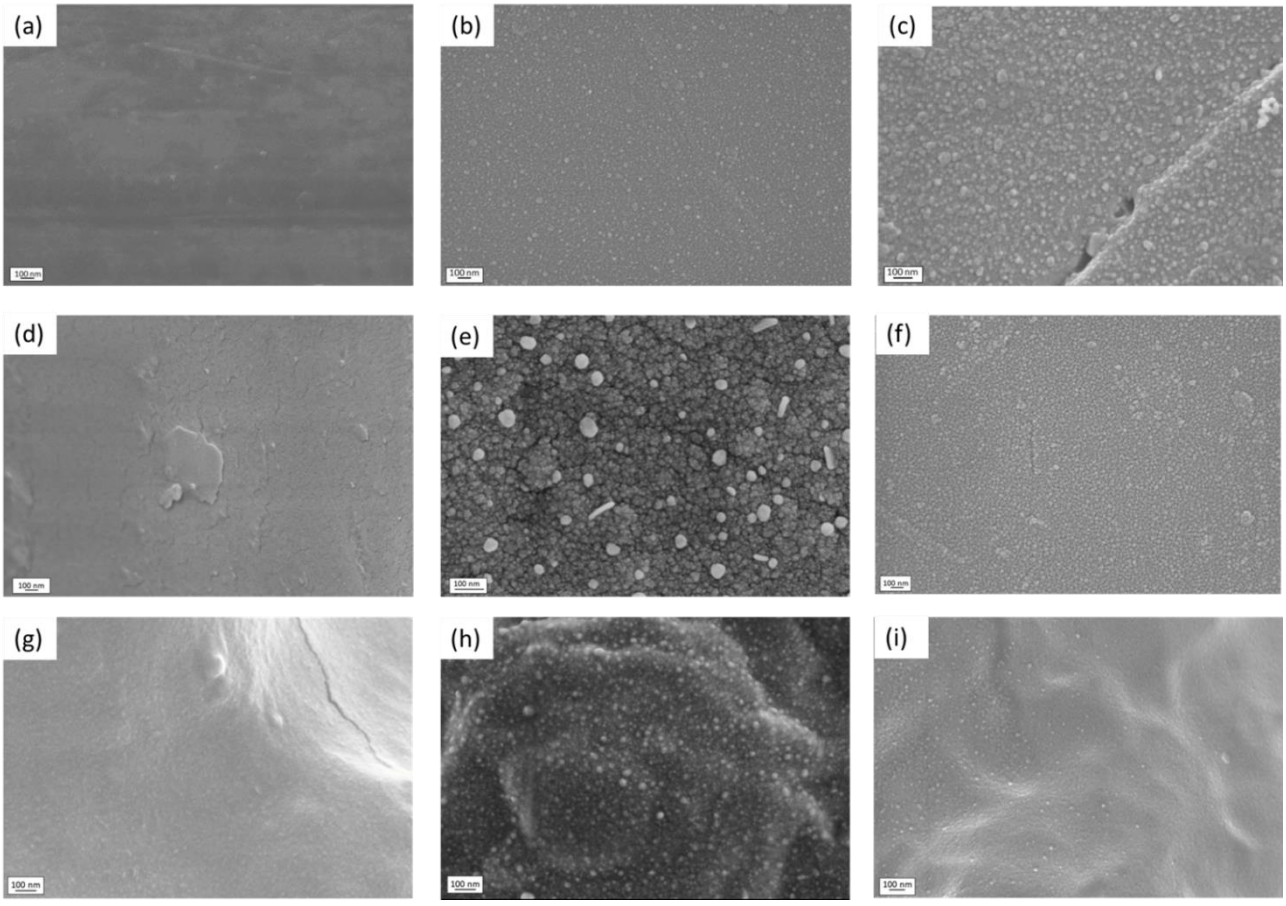

Figure 98: Morphological analysis of (a) uncoated Fabric_1, (b) Fabric_1_SiO2_Ag1_60 (c) Fabric_1_SiO2_Ag4_10; (d) uncoated Fabric_2, (e) Fabric_2_SiO2_Ag1_60, (d) Fabric_2_SiO2_Ag4_10; (g) uncoated Leather (h) Leather_SiO2_Ag1_60 (i) Leather_SiO2_Ag4_10

In all samples, both coatings are clearly visible with a typical globular and dotted structure attributable to the presence of the amorphous silica matrix. The light grey particles are more likely

ascribable to silica than to silver nanoclusters, which are smaller in dimension and embedded within the matrix. It is difficult to distinguish them precisely from those made of silica, although shining nanoparticles could be attributable to silver.

Some differences in micro/nanostructure are noticed for *Fabric_2* where the morphology relative to the coating obtained after 60-minute deposition (Figure 98 (e)) appears coarse with some globuli on the surface mainly ascribable to agglomeration of silica particles. This appearance is very similar to that obtained after the deposition of SiO2_Ag5 coatings on a metallic air filter, described in the dedicated section. SiO2_Ag4_10 coating on *Fabric_2* and *Leather* (Figure 98 (f) and (i)) and SiO2_Ag1_60 on Fabric_1 (Figure 98 (b)) appear with a more fine nanostructure.

Differences in the surface appearance of sputtered coatings were also found by *Carvalho et al.* [146], who deposited silver and silver oxide coatings through pulsed DC reactive magnetron sputtering technology. When a silver layer was deposited, a flat and homogeneous coating was obtained, while the deposition of AgOx coatings resulted in high surface roughness and uneven morphology due to the higher deposition rate and increased pressure during the process. In addition, an increase in the roughness was found after functionalization of bovine leather with SiO2-AgNPs [147]. Comparing these morphologies with those of SiO2_Ag coatings obtained through magnetron sputtering, it can be confirmed that the presence of a globular and porous structure is due to the sputtered silica. Due to the low amount of silver in the coatings, to evaluate the presence of Ag nanoclusters coatings, XRD and UV-Vis analysis were conducted on SiO_2_Ag1_60, SiO_2_Ag4_10 deposited on soda-lime substrate.

Obtained XRD spectra are shown in Figure 99. The presence of the amorphous silica matrix can be observed in both cases, even for a short deposition time of 10 minutes. In addition, peaks related to metallic silver were detected in both coatings. In particular, in SiO2_Ag1_60, the reduced power on the Ag target to 1 W, and consequently, the low content of Ag, led to the detection of peaks with low intensity only at 2theta of 38° and 44°, despite the deposition lasting 60 minutes. In the case of the coating obtained with a 10-minute deposition and a power of 4W, SiO2_Ag4_10, Ag peaks are observed at value of 2theta of 38° and 44°, as previously, but with a further reduced intensity and broadened peaks. Probably, the process time in this case is too short to allow the formation of very small silver nanoclusters.

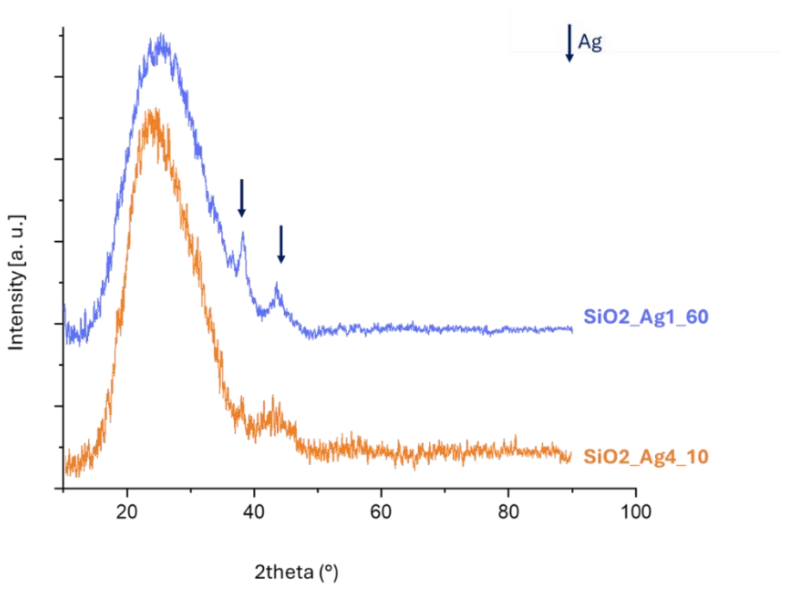

Figure 99: XRD analysis of SiO2_Ag1_60 and SiO2_Ag4_10 coatings

Experimental data obtained through UV-Vis analysis confirm what is demonstrated by XRD analysis (Figure 100). Both coatings showed a peak around a wavelength of 414 nm, related to the presence of Ag nanoclusters, but the intensity varies considerably in accordance with the set parameters. The peak intensity for SiO2_Ag1_60 coating is higher and decreases for SiO2_Ag4_10.

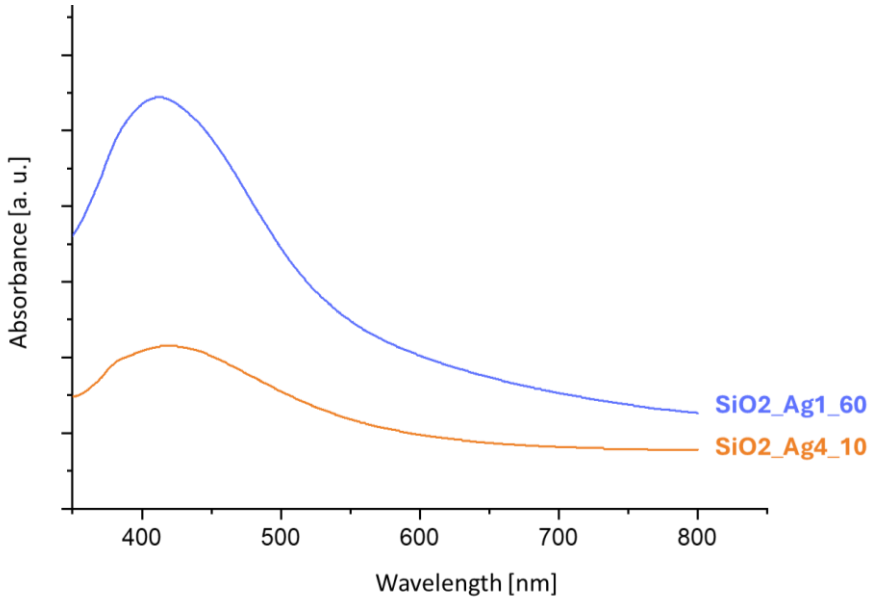

Figure 100: UV-Vis analysis of SiO2_Ag1_60 and SiO2_Ag4_10 coatings

The antibacterial activity of these two coatings was tested using *Fabric_2* and *Leather* as representative of synthetic and natural substrates, respectively, while *Fabric_1* textile was discarded because it is very similar to *Fabric_2* for its behavior and characteristics.

The CFU counting test was performed on both samples, coated with SiO2_Ag1_60 and SiO2_Ag4_10 against *S. epidermidis*. Uncoated samples were also involved in the text.

The values of the McFarland index of the bacterial solutions post-incubation, summarized in Figure 101, significantly decreased for coated samples up to 0 for *Fabric_2* and 0.5-0.8 for *Leather*, where values of related uncoated samples were about 2.00 and about 3.00, respectively

(a)

1. Fabric_2	2.Fabric_2_SiO2_Ag1_60	3.Fabric_2_SiO2_Ag4_10
1.87 ± 0.35	0.00 ± 0.00	0.00 ± 0.00

(b)

1. Leather	2. Leather_SiO2_Ag1_60	3. Leather_SiO2_Ag4_10
3.05 ± 0.08	0.72 ± 0.33	0.44 ± 0.20

Figure 101: McFarland index of bacterial solutions with uncoated and SiO_Ag1_60 and SiO2_Ag4_10 coated (a) Fabric_2 and (b) Leather

The results from the CFU counting test are presented in the histogram in *Figure 102*. It is evident that both coatings and substrates show a significant decrease in the CFU count, indicating reduced bacterial proliferation in the broth. In the graph, the red line indicates the initial bacteria concentration in the broth, which is $5*10^5$ CFU/ml.

More specifically, in the case of *Fabric_2*, the presence of the coating reduced the number of proliferated colonies by approximately 7 orders of magnitude (SiO2_Ag1_60), whereas the coating deposited for shorter times led to a lower decrease in the number of colonies, by about 4 orders of magnitude. Regarding the samples on black *Leather*, there was a reduction in bacterial proliferation by 4 and 2 orders of magnitude compared to the uncoated sample. It can be observed that both coatings had bactericidal effects, with varying intensity depending on the composition of the coatings. Since the antibacterial action depends on the amount of silver, the results obtained are congruent with the data assessed in the EDS analysis, Table 14 , where a greater amount of Ag was found in the coatings obtained after 60 minutes, about 0.88 % at. for *Fabric_2* and 0.39 % at. for

Leather, even if the power applied to the Ag target has been lower, compared to those after 10 minutes, in which the amount of silver was, for both samples, around 0.15 at. %.

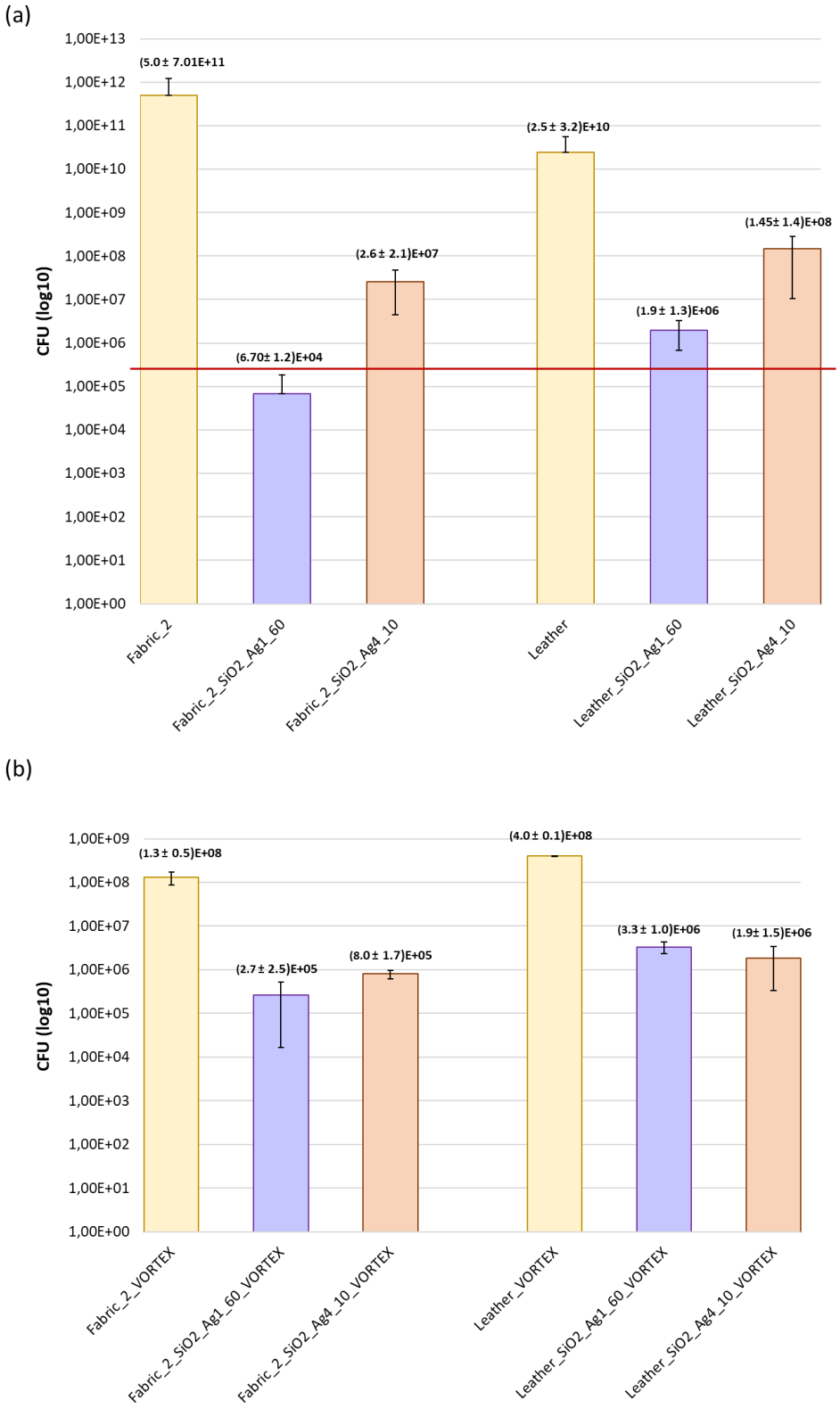

Figure 102: (a) Count of S. epidermidis colonies proliferated in broths with uncoated and SiO2_Ag1_60, and SiO2_Ag4_10 coated Fabric_1 and Leather; (b) count of S. epidermidis colonies adhered on uncoated and SiO2_Ag1_60, and SiO2_Ag4_10 coated Fabric_1 and Leather

Regarding the number of colonies adhered to the surface, reported on the right of the histograms in Figure 102, the behavior of the two coatings is very similar with the same trend just described. For both *Fabric_2* and *Leather,* bacterial colonies adherend on uncoated substrates were about 10^8 CFU/ml, while the presence of the coatings reduced them to approximately 10^5 CFU/ml and 10^6 CFU/ml, with no substantial differences between the two coatings.

In a recent study, the antibiofilm activity of composite coatings made up of silica-dendritic polymer with silver nanoparticles deposited on leather was studied against *S. Epidermidis and E. coli* colonies, starting from a solution with $1.5 * 10^5$ CFU/ml [149]. Results revealed that no bacteria colonies adhered on samples, in both *S. epidermidis* and *E. coli* strains, demonstrating antibiofilm activity of the coatings, due to the low silver content.

Strictly correlated to the antibacterial test, the ions released test was performed on *Fabric_2* and *Leather* coated by the selected coatings after immersion in MilliQ water for two weeks. The two graphs are reported in Figure 103.

As expected, the coatings deposited for 60 minutes reached a higher value in the released ions concentration, due to higher the amount of Ag than that present in the coating deposited for a lower time. The maximum value reached was 0.11 and 0.9 ppm after two weeks, for coatings SiO2_Ag1_60 deposited on the *Fabric_2* and on the *Leather,* respectively. The concentration achieved by the second coatings is very low, less than 0.02 ppm, after two weeks. These data confirmed what was found in

the CFU test, where proliferated colonies were more numerous in the case of SiO2_Ag4_10 coatings if compared with SiO2_Ag1_60 coating, and are consistent with EDS results, described previously.

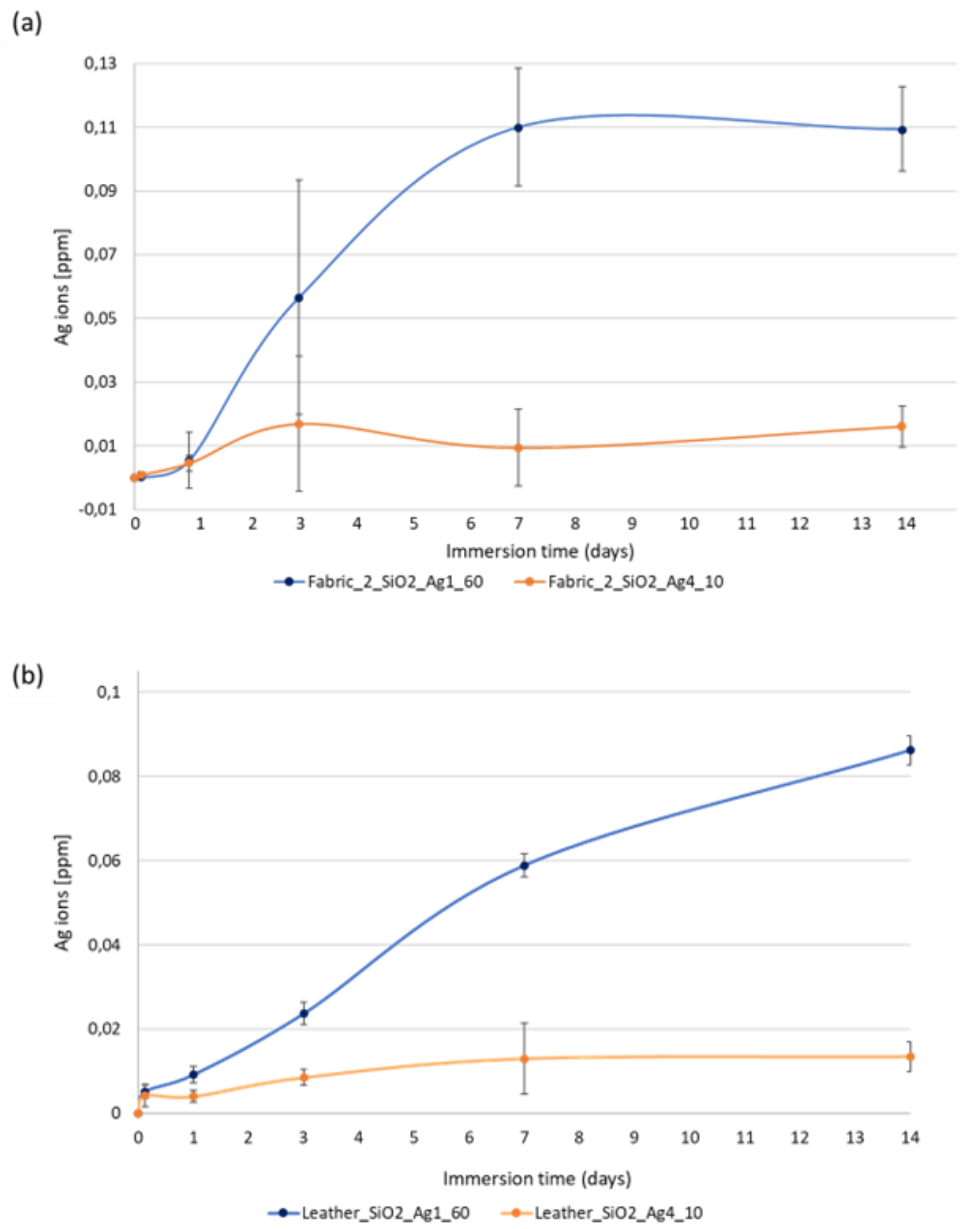

Figure 103: Amount of silver ions released from (a) SiO2_Ag1_60 and SiO2_Ag4_10 composite coatings deposited on Fabric_1 and (b) SiO2_Ag1_60 and SiO2_Ag4_10 composite coatings deposited on Leather after two weeks in water at room temperature

Previous studies investigated the antimicrobial properties of silver-coated leather. Silver and silver oxide coating oxide deposited on leather by magnetron sputtering technology revealed good antibacterial activity. The authors reported the formation of an inhibition halo free from S. *aureus* and *C. parapsilosis*, and a stronger antifungal effect, against *C. albicans* , as visible by the presence

of a larger halo [146]. Recently, bovine leather was functionalized with SiO_2-Ag composite, and bacterial and viral inactivation was investigated. The coated Fabric showed a reduction of *S. aureus* colonies growth of 99,99%, even after ten washing cycles. In addition, it was able to inactivate SARS-CoV-2 after contact of 15 and 30 min [147]. *Rosiati et al.,* compared the effect of silica coating based on volcanic ash on leather, with that functionalized with silver nanoparticles, using $AgNO_3$ solution. They found that SiO_2 coating, deposited on leather, exhibited good antibacterial properties against *S. aureus*, generating an inhibition halo of 21.25 ± 0.50 mm, but the effect was increased by the presence of silver nanoclusters in the coating, demonstrated by a bigger halo, with dimensions of 24.80 ± 1.64 mm [148]. *Alexe et al*. used different mixtures of TiO_2, including TiO_2-SiO_2-Ag-PDPA, to functionalize leather. The treated samples exhibited antibacterial activity against *E. coli* and *S. aureus,* with a reduction *of* 99.80% and 99.86%, respectively [242].

Given the promising results of the coatings in terms of antibacterial effect, it was decided to proceed with a color analysis based on the grayscale, which was conducted by the FCA-CRF company, in their laboratories. With this test, the color difference between the uncoated sample and the coated ones is evaluated. A value from 1 to 5 is assigned, depending on the chromatic difference, in particular, the value is 1 for a significant color difference, and 5 if the difference is minimal. Results are shown in Table 17.

Table 17: *Colour analysis based on grey scale on SiO2_Ag1_60 and SiO2_Ag4_10 coatings deposited on Fabric_1, Fabric_2 and Leather*

Substrate	***SiO2_Ag1_60 coating***	***SiO2_Ag4_10 coating***
Fabric_1	2/5	2/5
Fabric_2	2/5	2-3/5
Leather	1-2/5	3/5

Evaluating data obtained, SiO2_Ag1_60 coating imparted the most significant color change: it was considered between 1 and 2 in the gray scale when was deposited on the *Leather,* and 2 if deposited on two fabric textiles. In the case of SiO2_Ag_10, the color variation was more important on *Fabric_1* (2 points in the gray scale) and less significant for *Fabric_2* and *Leather.*

Considering that the stringent request of FCA-CRF company was to develop antibacterial and transparent coatings to be deposited on textiles involved in the automotive industry, even if SiO2_Ag1_60 and SiO2_Ag4_10 coatings exhibited antibacterial efficacy, especially in inhibiting *S. epidermidis* strain, the company considered the imparted color change by the deposited coatings too significant to be applied in the automotive textiles.

Further studies could be done for the optimization of coating process parameters or composition to obtain transparent coating, exhibiting bactericidal effects.

7.2. Composite silica/silver coating obtained from pre-ceramic polymer: preliminary study

Study of silica derived from PHPS

This thesis aims to propose alternative technologies to magnetron sputtering for the development of antibacterial coatings made up of a silica matrix, embedding silver nanoparticles.

In this section, the transformation of a pre-ceramic polymer, namely Peryhydropolysilazane, PHPS, into silica was exploited, and the obtained silica coating was studied. Additionally, methods for the *in situ* synthesis of silver nanoparticles were evaluated.

First of all, the transformation of PHPS into silica was investigated through FT-IR analysis. Two methods were evaluated to promote the transformation of ceramic polymer precursors into silica, which involved exposure to air at room temperature and exposure to the basic vapor of an aqueous ammonia solution. The graph in Figure 104 (a) shows the FT-IR spectra of a PHPS coating deposited on soda-lime glass at time 0 (as deposited), after 4, 8, and 24 hours in air at room temperature, and after 8 hours of exposition to ammonia vapors. The same coating was deposited on AISI steel and the FT-IR spectra at time 0, after 24h in air, and after 8 h exposed to basic vapors are shown in Figure 104 (b).

The curve which represents PHPS as-deposited showed peaks around 830 cm^{-1}, 2100 cm^{-1} and 3400 cm^{-1}, which correspond to the stretching vibration of Si-N, Si-H, and N-H bonds, as confirmed in literature [177]. During the transformation of coatings, both if exposed to air or basic vapors, peaks at around 3400 cm^{-1} and 2100 cm^{-1}, related to Si-N and Si-H bonds, decreased, indicating their rupture, and, at the same time, absorption peak around 1050 cm^{-1} appeared and increased increasing time, indicating the formation of siloxane bond, (-Si-O-Si) [243]. This is confirmed by *Bauer et al.* [170], who evidenced a progressive increase in the peaks between 1250 and 1000 cm^{-1}, which then merge into a single band at 1025 cm^{-1}.

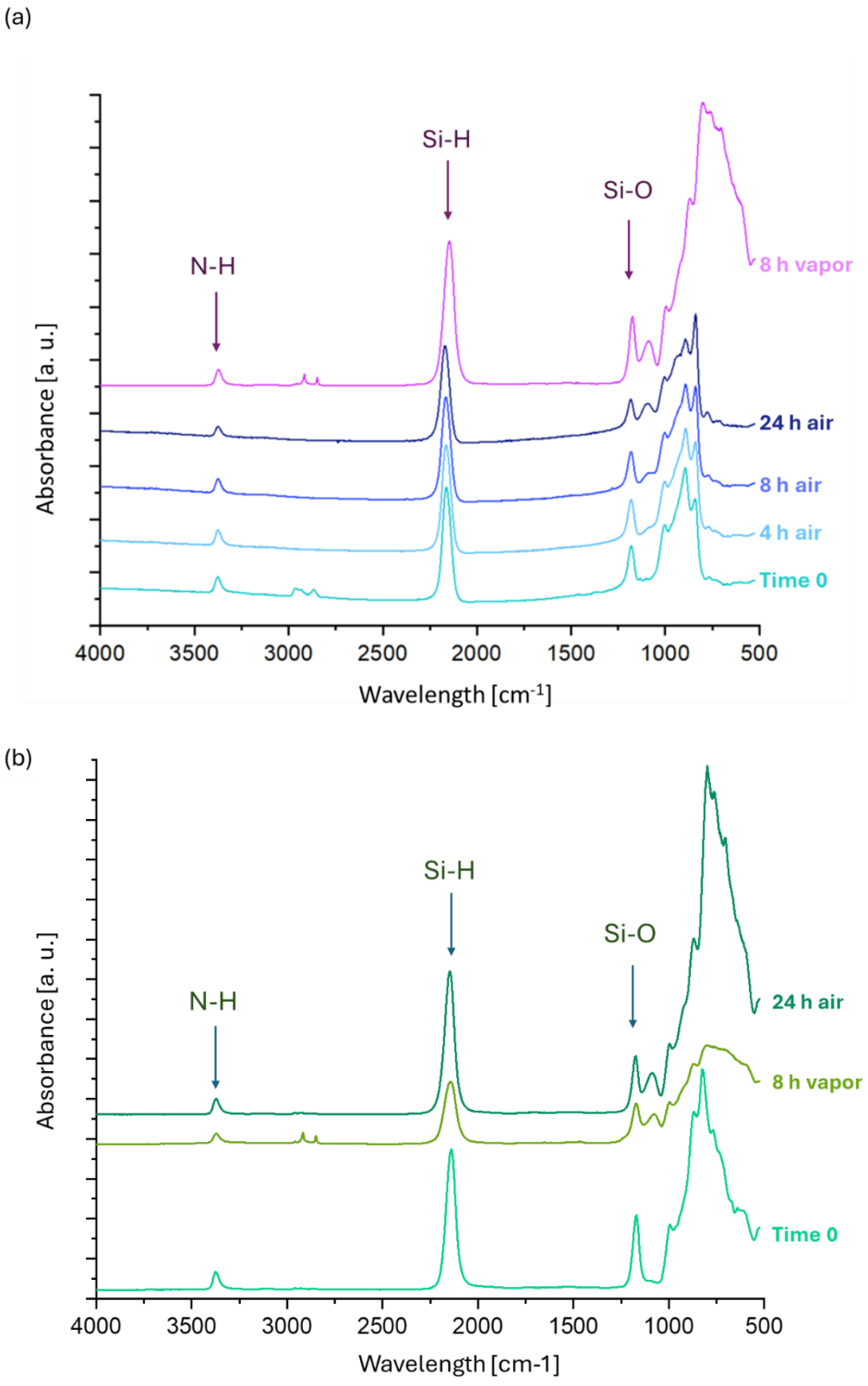

Figure 104: FT-IR analysis of PHPS deposited on (a) soda lime glass, (b) on AISI steel, at time 0 and exposed to air for 4, 8, and 24 hours, and exposed to ammonia solution vapors for 8 hours

An EDS analysis was performed on coatings deposited on soda-lime, exposed for 8 hours to the vapor of aqueous ammonia solution and results are shown in Table 18. It must be taken into account

that the EDS technique is not reliable for quantitatively assessing the carbon and oxygen content in the material.

Table 18: EDS analysis on PHPS coatings deposited on soda-lime glass, after 8h of exposure to basic vapor

Coating	***Si (at. %)***	***O (at. %)***
PHPS after 8h exposed to basic vapor	36.31 ± 7.93	63.69 ± 7.90

The morphology of the PHPS coatings deposited on soda-lime glass and on AISI steel and exposed to basic vapors of ammonia solution for 4 and 8 hours was analyzed through FESEM analysis. The obtained results are shown in Figure 105. In both cases, the produced silica did not exhibit the desired globular and porous morphology, needed for potential ions release of silver and consequential antibacterial behavior, but it appeared smooth and dense, similar to what was obtained by *Blankenburg et al.* [244].

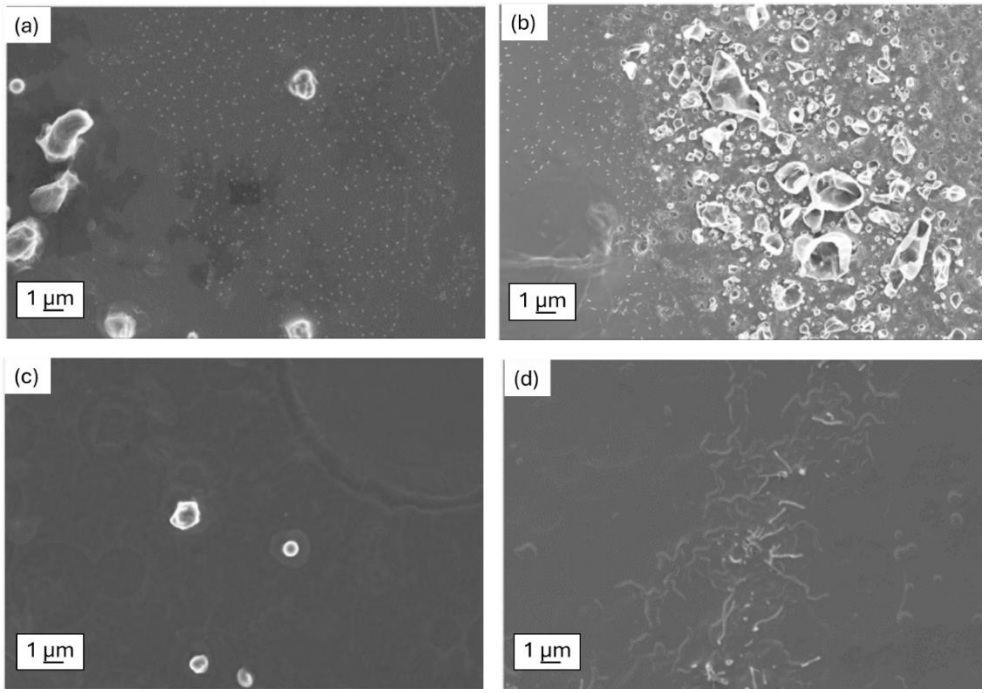

Figure 105: Morphological analysis of PHPS deposited on soda-lime glass after (a) 4h and (b) 8h exposed to basic vapors; on AISI steel after (c) 4h and (d) 8h exposed to basic vapors

Ag nanoparticles incorporated in PHPS-derived silica matrix

Silver nanoparticles were synthesized starting from silver nitrate $AgNO_3$ and reduced *in situ* through UV light irradiation. As reported in the chapter "*Materials and Methods*", an attempt to

disperse AgNPs was made starting from a solution of $AgNO_3$, acetone, and a photoinitiator, and then mixed with PHPS. This solution was deposited onto the substrates, and using a film spreader bar, a coating with a uniform thickness of 50 µm was obtained, showed in Figure 106.

In the first step, the irradiation occurred for 30 minutes at a power of 195.5 mW/cm^2.

Various ratios between PHPS and the $AgNO_3$ solution were evaluated according to those reported in the "*Composite silica/silver obtained from pre-ceramic polymer"* section in the *"Material and Method"* chapter, and summarized in Table 8. Figure 106 shows how PHPS_AgNO3_1 coating deposited on soda-lime glass and UV irradiated appeared.

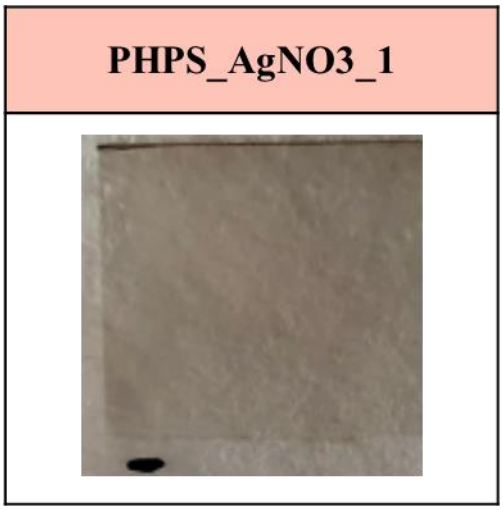

Figure 106: PHPS_AgNO3_1 coating deposited on soda-lime glass substrate after 30 min UV light irradiation

In Figure 107 the results of FT-IR analysis on PHPS, PHPS_AgNO3_0.5, and PHPS_AgNO3_1 are reported.

In the case of coating made up of only PHPS, it is possible to note that UV light had catalyzed the transformation: no peak related to the N-H bond was visible, Si-H peak decreased while the peak related to Si-O increased. Comparing different curing methods, involving exposure to air at room temperature, *Channa et al.* [243] demonstrated that UV irradiation was the best and fastest way to obtain PHPS transformation into silica. Curves referred to PHPS_AgNO3_0.5 and PHPS_AgNO3_1 confirmed the formation of Si-O bonds. This demonstrated that the presence of silver nitrate and photoinitiator did not affect the PHPS transformation.

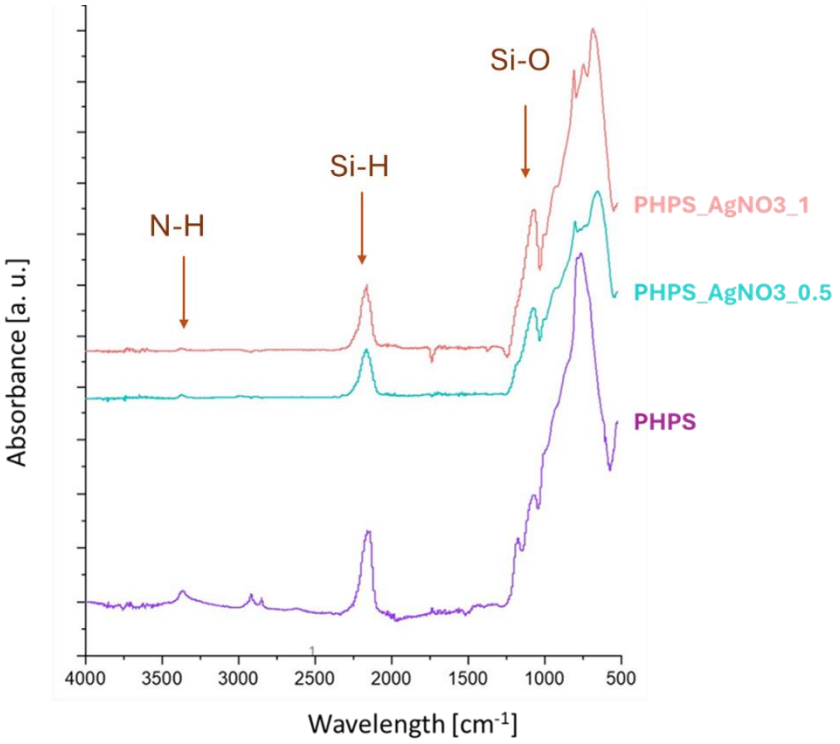

Figure 107: FT-IR analysis of PHPS, PHPS_AgNO3_0.5, and PHPS_AgNO3_1 after UV irradiation for 30 minutes

Subsequently, PHPS, PHPS_AgNO3_0.5, PHPS_AgNO3_0.75, and PHPS_AgNO3_1 coatings after UV light irradiation were analyzed using the UV-Vis technique, and the comparison of the obtained curves is shown in Figure 108. The spectra of all the coatings were very similar, showing the typical peak of polysilazane, slightly shifted at a wavelength of around 360 nm [245]. No peaks were detected around 414 nm, which is related to silver nanoparticles, suggesting a very low quantity of silver in the solution. PHPS_AgNO3_0.5 coating, which contained the lowest $AgNO_3$ concentration, was excluded, and no further analyses were conducted on it.

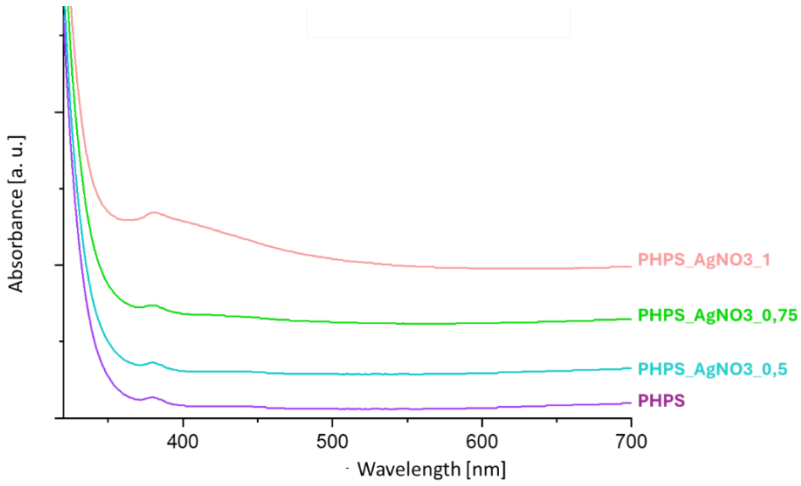

Figure 108: UV-Vis analysis on PHPS, PHPS_AgNO3_0.5, PHPS_AgNO3_0.75 and PHPS_AgNO3_1 after UV irradiation for 30 minutes

An effort was made to increase the amount of AgNPs synthesized in the solution by prolonging the irradiation time to 45 minutes. In addition, it was decided to obtain a coating with higher thickness, so the solution was not spread on the substrate using the bar, but a droplet was deposited instead, (PHPS_AgNO3_0.75_droplet, PHPS_AgNO3_1_droplet); but in this case, the thickness was not controllable.

In Figure 109, UV-Vis spectra of the solution and PHPS_AgNO3_0.75_droplet and PHPS_AgNO3_1_droplet after 45 minutes of UV light irradiation were shown. The curve related to PHPS_AgNO3_0.75_droplet did not show peaks around wavelengths of 400 nm, indicating the absence of AgNPs, on the contrary, for PHPS_AgNO3_1_droplet a peak is noticeable.

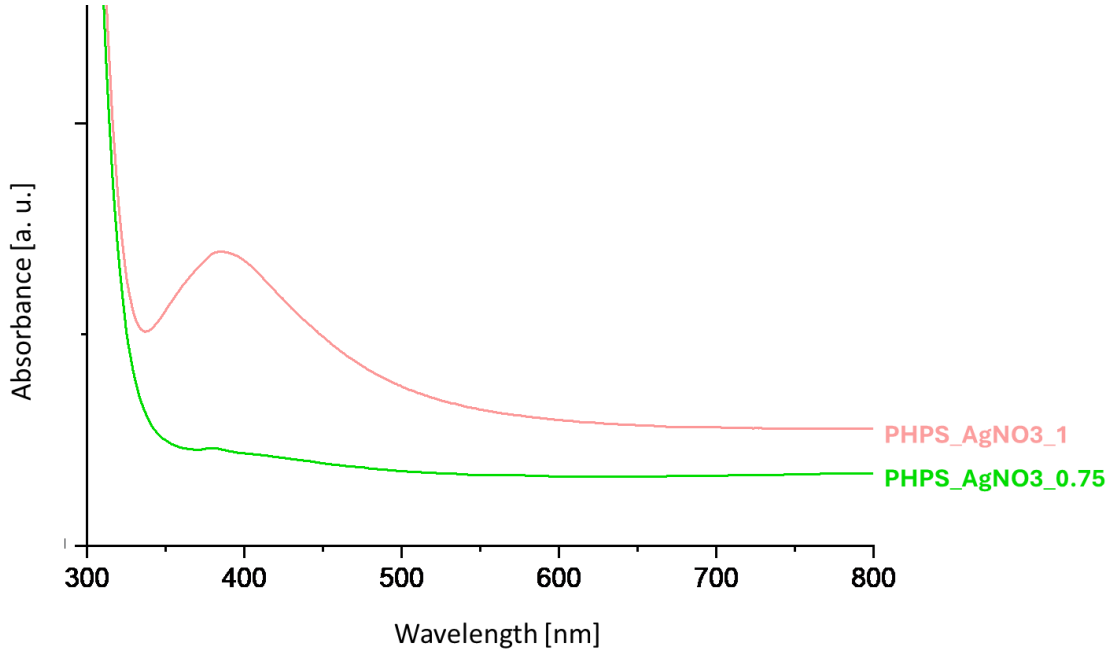

Figure 109: UV-Vis analysis of PHPS_AgNO3_0.75_droplet and PHPS_AgNO3_1_droplet after UV irradiation for 45 min

To confirm the presence of silver nanoparticles in the coating, XRD analysis was performed, and the results are shown in Figure 110. The spectrum indicates the presence of amorphous silica, indicated by the halo around 2theta values between 15 and 25°. Regarding the presence of silver in crystalline form, peaks at 2theta values of 38° and 44°C are evident, confirming data obtained by UV-Vis analysis.

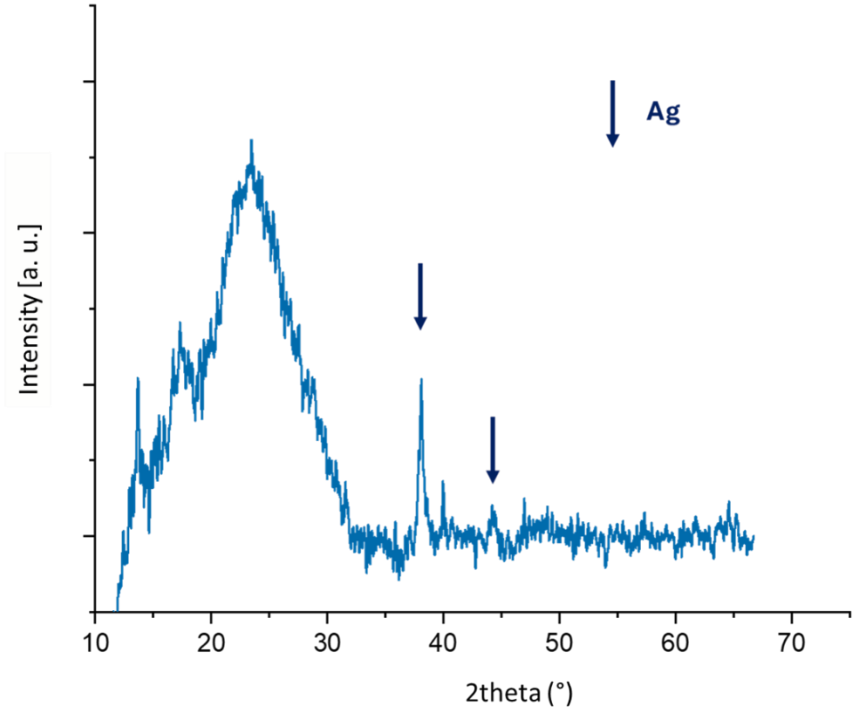

Figure 110: XRD analysis on PHPS_AgNO3_1_droplet after UV irradiation for 45 min

EDS analysis, Table 18, on the same coating, showed a low quantity of silver, even if the peaks in the XRD spectrum suggested the formation of silver nanoparticles.

Table 19: EDS analysis of PHPS_AgNO3_1_droplet

PHPS_AgNo3_1_droplet	
Si (at. %)	***Ag (at. %)***
43.22 ± 6.9	0.46 ± 0.12

To understand the morphology of the obtained coating, FESEM analyses were conducted on PHPS_droplet and PHPS_AgNO3_droplet deposited on a soda-lime glass slide and irradiated with UV light for 45 minutes. The photographs are reported in Figure 111.

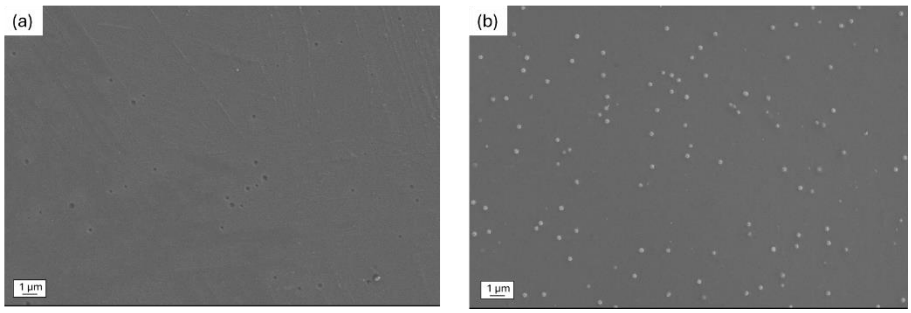

Figure 111: Morphological analysis of (a) PHPS_droplet and PHPS_AgNO3_1_droplet deposited on soda-lime glass

In the case of pure PHPS coating, the coating appears homogeneous and dense, without porosity. This morphology is similar to what is reported in [246], and it is typical of silica obtained from the transformation of Peryhydropolysilazane. In the case of coatings with PHPS and $AgNO_3$, some particles are visible. These are attributable to SiO_2 and not silver nanoparticles, which, as EDS analyses suggested, were in very low amounts.

To test the antibacterial properties of the obtained coatings, the zone of inhibition test against *S. epidermidis* was conducted on PHPS_AgNO3_1_droplet and PHPS_AgNO3_1 on soda lime glass samples. Results, displayed in Figure 112, were compared with uncoated soda lime glass and with a coating of PHPS, not mixed with $AgNO_3$.

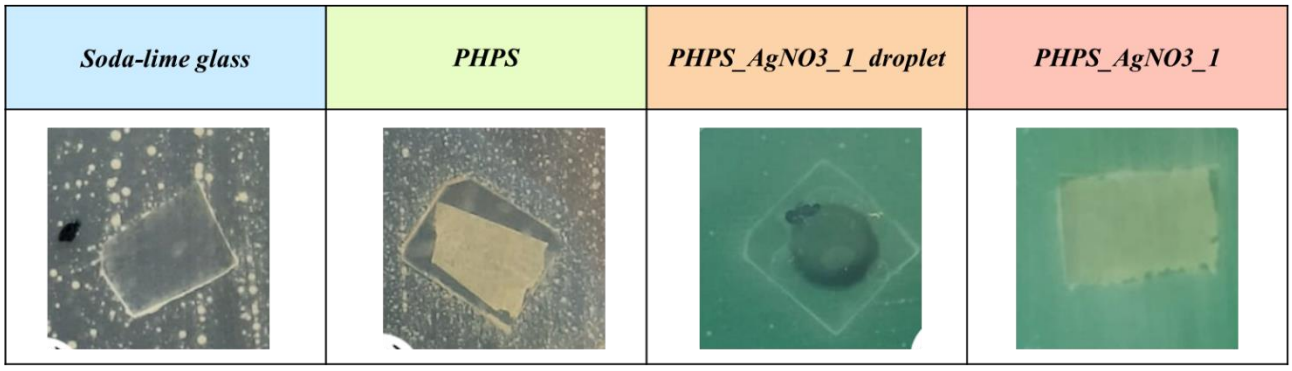

Figure 112. Inhibition halo test against S. epidermidis on (a) uncoated soda-lime glass, (b) PHPS, (c) PHPS_AgNO3_1_droplet, (d) PHPS_AgNO3_1

As shown, none of the samples inhibited bacterial growth, similar to the uncoated soda-lime glass used as a reference. The absence of antibacterial activity is likely due to the small quantity of silver present in the coating, as previously observed. Furthermore, as suggested by FESEM analyses, the coating appeared very dense and compact, which could hinder the release of silver ions, crucial in the mechanism of bacterial inhibition. For a deeper understanding, an ion release test in water for 21 days was conducted, analyzing soda lime samples coated by PHPS_AgNO3_1 spread with a bar.

The results, reported in Figure, clearly show that the coating was unable to release silver ions, justifying the inefficacy in inhibiting bacterial proliferation.

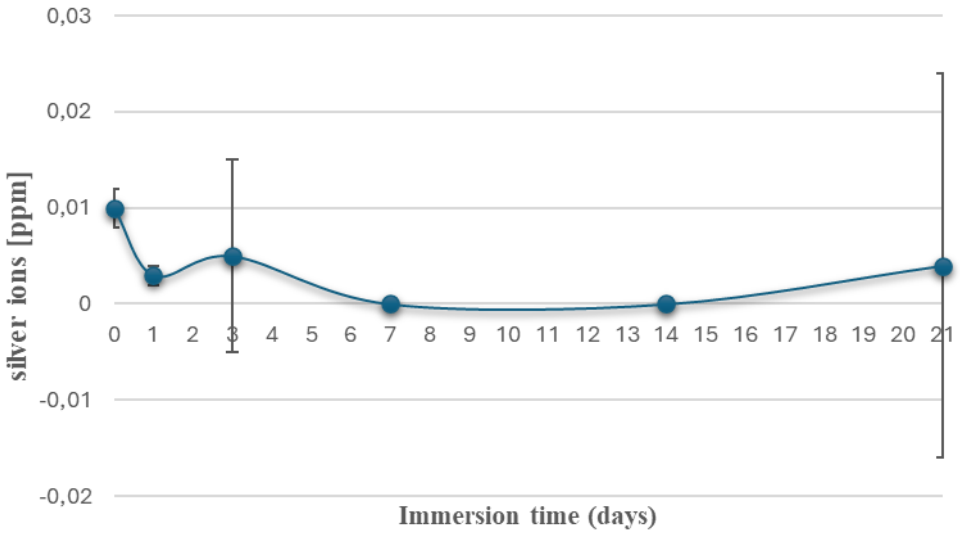

Figure 113: Amount of silver ions released from PHPS_AgNO3_1 composite coating deposited soda-lime glass after 21 days in water at room temperature

The results obtained for the development of a composite coating consisting of a silica matrix derived from the transformation of PHPS, embedding silver nanoclusters, were not satisfactory. Further investigations into methods to *in situ* synthesize silver nanoparticles or disperse them in the coatings must be conducted to achieve the desired coatings.

No previous works reported methods for the incorporation of silver metallic nanoparticles in silica coatings obtained by PHPS transformation, but, in a recent work, a silver thin film was deposited on PHPS-derived SiO_2 exploiting Si-H bonds [85]. In particular, PHPS deposited on stainless steel was annealed at 300°C and subsequently heated at 70°C and immersed in an aqueous solution containing AgNO3. During the heating stage in the coating deposition phase, hydrolysis and condensation reactions were promoted, resulting in a decrease in the peak corresponding to the Si-H bond. Additionally, exposure to water led to an increase in the peaks related to Si-OH and Si-O-Si bonds, confirming the successful transformation of PHPS into silica even in the presence of $AgNO_3$ solution. Analyzing morphology, it was discovered that silver nanoparticles were homogenously distributed on the SiO_2 surface, without agglomeration, but they were also embedded in the upper layers of silica. Differently from the coating obtained in our study, which appears dense and compact, here SiO_2 structure was characterized by micropores through which $AgNO_3$ diffused, Ag+ ions interact with Si-H bonds were reduced, resulting in AgNPs embedded in silica. In addition, silver ions release was assessed, and the Ag layer showed strong antibacterial activity against *E. coli* [247].

The outcome of this study, however, differs from the objective of this work, which aims to achieve a composite coating where nanoparticles are well dispersed and incorporated in the silica matrix. Furthermore, since this method is being evaluated as an alternative to co-sputtering technology, it is necessary for it to be applicable to all materials. The need for high-temperature heat treatment limits the use of this coating to a certain group of substrates. Subsequent methods for synthesizing silver nanoparticles dispersed in the PHPS-derived silica matrix will be evaluated to impart antibacterial activity to the obtained coating.

8. *Conclusion and Future Perspectives*

This thesis aimed to develop and study innovative antibacterial composite coatings intended for application in several fields. The developed coatings were composed of silica, or zirconia matrix, and contained silver nanoclusters, to confer antibacterial and antiviral properties. The technique used for coating deposition was magnetron sputtering, which offers the advantage of being able to deposit thin coatings on a wide range of materials without causing damage, as no heat is required during the process. The co-sputtering technology allows the simultaneous employment of two different targets, each subjected to distinct conditions, for the development of a composite coating. Consequently, a variety of substrates have been employed, including metallic filters, polymeric membranes, fabrics, and leathers, and the parameters of the deposition process were optimized to obtain several coatings according to the requirements of the final purposes.

Within the "BIOkILLER- antiBIOpollutant coatIng for reusabLe filter" project, silica- and zirconia-based coatings embedded silver nanoclusters were developed to be involved in air filtration systems. The goal of the project was to develop filter coatings capable of reducing or entirely inhibiting bacterial proliferation on the filter surface, which can otherwise be promoted by specific humidity and temperature conditions, and to ensure that the filters are reusable after the sterilization process. The coatings were deposited on three types of filters: metallic filters, glass fiber-based filters, and polymeric membranes.

Compositional and structural investigations, EDS, XRD, and UV-Vis analyses, confirmed the presence of nanoclusters distributed within the matrix in both SiO_2-based and ZrO_2-based coatings. Morphological FESEM analyses revealed a globular structure of the sputtered coating matrix, while TEM analyses verified the uniform distribution of silver nanoclusters within the coating.

Silver ions release of each coating was evaluated and attested. The antibacterial coating efficacy was tested through both qualitative and quantitative tests, towards *S. epidermidis*, *E. coli* and *C. albicans*. Obtained results demonstrated coatings' bactericidal behavior, by preventing microorganism colony growth, and creating bacteria-free zones of varying sizes around the sample, in contrast to as-received filters. The results of the CFU count test confirmed that the deposition of silica or zirconia-based coatings containing silver nanoparticles on air filters could slow down and reduce colony proliferation.

Focusing on the possibility of reusing filters, it was demonstrated that thermal regeneration treatment did not affect coatings' bactericidal activity, which could be reused post-sterilization process.

In collaboration with the Università di Torino, SiO_2-based coatings were tested against HCoV-OC43, and ZrO_2-based coatings against HRoV, FluVA H1N1, and HRhV, demonstrating strong capability to reduce the viral titer.

Further studies focused on the bactericidal and virucidal behavior of the developed coatings are ongoing within the project "*Nanobloc, Antiviral, Antibacterial & Antifungal Nanocoating Platform*", founded by the European Union's Horizon Europe program. This project aims to deeply evaluate the antibacterial effect of the silica/silver and zirconia/silver coatings and to investigate the mechanism of the virucidal effect in greater detail. These coatings are intended to be applied in several fields, including air filters, face masks, protective clothing, mattress covers, wallpaper, and various high-traffic solid surfaces such as doorknobs and handles.

Through collaboration with *AGC-Interpane* company, an upscaling process for the composite coatings is underway, intending to use industrial equipment for depositing these coatings on several substrates. Compositional and structural evaluations, as well as bactericidal and virucidal tests of the coatings, are ongoing and will enable the optimization of process parameters to achieve the best possible results.

During this research work, efforts were made to develop silica matrix composite coatings with antibacterial agents other than silver, deposited on different air filters. Zinc and copper nanoparticles as antibacterial agents were taken into account. Parameters set during the deposition process were optimized, and coatings with different compositions were obtained. Even if the presence of Zn and Cu was confirmed by EDS analysis, and the ions released were attested, antibacterial tests demonstrated the coatings' inefficacy in inhibiting bacterial proliferation. Future studies could be conducted to develop SiO_2-based or ZrO_2-based composite coatings containing Cu and Zn nanoparticles to exploit their antibacterial and antiviral effects. Potential post-deposition thermal treatments may be evaluated to obtain nanoclusters with effective antibacterial action.

An interesting application of composite coatings exhibiting antibacterial properties concerns filtration systems for aqueous solutions, in order to avoid the use of chemicals or reduce waste. In collaboration with CRAB Medicina Ambiente company, composite coatings with antibacterial

properties were studied to be deposited on thin electrospun membranes in polymeric material, PCL and PAN-PCL, used in water purification systems. Since the final use of the coatings involves prolonged contact with aqueous solutions, the study was conducted exclusively on zirconia-based coatings, as it is less soluble in water than silica. Due to the high thermal sensitivity of the substrates, the deposition process times were significantly reduced to avoid damaging the polymeric membranes. Compositional and morphological analyses confirmed the successful deposition of a homogeneous coating, and XRD and UV-Vis analyses confirmed the presence of silver nanoclusters. Coatings exhibited a bactericidal effect against *S. epidermidis*, while their action was less effective against *E. coli*.
Tests on the filtration of bacterial solutions allowed us to evaluate the bactericidal effect of the coating on the membrane surface. However, the zirconia composite coating confers hydrophobic behavior to the substrates, slowing down the filtration process.

In the framework of the project "*Antimicrobial/virucidal PVD coatings for automotive*", in collaboration with FCA-CRF, an effort to obtain antibacterial composite coatings for automotive textiles was made. The main objective of this project was to develop and study composite coatings containing silver nanoclusters, to be deposited on fabrics and leathers, intended for the automotive textile industry. The coatings were required to meet two criteria simultaneously: impart antibacterial properties to the fabric and not cause any color change to the textiles.

Due to the stringent requirement for color change, process parameters were changed and optimized, and obtained coatings were studied in terms of antibacterial efficiency and color variation. In particular, to reduce the plasmonic resonance effect of silver nanoparticles on the color of the coatings, efforts have been to reduce the silver content in the coatings while maintaining the antibacterial effect. The deposition process duration and set parameters were modified, and the effects on the characteristics of the coatings were studied. The antibacterial tests revealed that coatings obtained with low Ag content were effective in inhibiting the proliferation of *S. Epidermidis* colonies, the color evaluation tests, based on the gay scale, demonstrated that the obtained coatings were not transparent, changing the textiles' color.
Further studies could be conducted focused on the development of transparent antibacterial coatings employing other antibacterial agents and evaluating their color and bactericidal efficacy.

During this thesis work, an attempt to develop silica/silver composite coatings using alternative techniques to magnetron sputtering was made, involving pre-ceramic polymer. A preliminary study on the kinetic transformation of Perhydropolysilazane, PHPS, into SiO_2, was conducted through

FT-IR analysis considering different time intervals under several conditions. In order to obtain a composite coating, silver nanoparticles were in-situ synthetized, through the reduction of $AgNO_3$, promoted by UV irradiation. XRD and UV-Vis analyses confirmed the presence of silver nanoparticles, while morphological evaluation showed a dense structure of the coating.
The coating did not exhibit antibacterial effects against *S. epidermidis*, likely due to poor silver ions release, as shown by the leaching test.

Future studies could focus on the development of composite coatings with a ceramic matrix obtained from the transformation of pre-ceramic polymer, incorporating silver nanoparticles as antibacterial agents. Specifically, methods for achieving a porous structure that promotes the release of silver ions could be investigated, using, for example, foaming agents, or thermal treatments. Additionally, alternative methodologies to UV reduction of $AgNO_3$ for in-situ synthesis of silver nanoparticles can be considered.

References

[1] Simbine E, Rodrigues L, Lapa-Guimarães J, Kamimura E, Corassin C, Oliveira C. *Application of silver nanoparticles in food packages: a review*. Food Sci Technol. **2019**;39.

[2] Szczepańska E, Bielicka-Giełdoń A, Niska K, Strankowska J, Żebrowska J, Inkielewicz-Stępniak I, Łubkowska B, Swebocki T, Skowron P, Grobelna B. *Synthesis of silver nanoparticles in context of their cytotoxicity, antibacterial activities, skin penetration and application in skincare products*. Supramol Chem. **2020**;32(3):207–21.

[3] Kumar S, Basumatary IB, Sudhani HPK, Bajpai VK, Chen L, Shukla S, et al. *Plant extract mediated silver nanoparticles and their applications as antimicrobials and in sustainable food packaging: A state-of-the-art review.* Trends Food Sci Technol. **2021**;112:651–66.

[4] Agrawal S, Bhatt M, Rai SK, Bhatt A, Dangwal P, Agrawal PK. S*ilver nanoparticles and its potential applications: A review.* J Pharmacogn Phytochem. **2018**;7(2):930–7.

[5] Xu L, Wang YY, Huang J, Chen CY, Wang ZX, Xie H. *Silver nanoparticles: Synthesis, medical applications and biosafety*. Theranostics. **2020**;10(20):8996–9031.

[6] Shahverdi AR, Fakhimi A, Shahverdi HR, Minaian S. *Synthesis and effect of silver nanoparticles on the antibacterial activity of different antibiotics against Staphylococcus aureus and Escherichia coli.* Nanomedicine Nanotechnol Biol Med. **2007**;3(2):168–71.

[7] Lekha DC, Shanmugam R, Madhuri K, Dwarampudi LP, Bhaskaran M, Kongara D, et al. Review on *Silver Nanoparticle Synthesis Method, Antibacterial Activity, Drug Delivery Vehicles, and Toxicity Pathways: Recent Advances and Future Aspects*. J Nanomater. **2021**;2021(1):4401829.

[8] Zheludkevich M, Gusakov AG, Voropaev AG, Vecher AA, Kozyrski EN, Raspopov SA. *Oxidation of Silver by Atomic Oxygen*. Oxid Met. **2004**;61:39–48.

[9] Salleh A, Naomi R, Utami ND, Mohammad AW, Mahmoudi E, Mustafa N, et al. *The Potential of Silver Nanoparticles for Antiviral and Antibacterial Applications: A Mechanism of Action*. Nanomaterials. 9 agosto **2020**;10(8):1566.

[10] Baig N, Kammakakam I, Falath W. *Nanomaterials: a review of synthesis methods, properties, recent progress, and challenges*. Mater Adv. **2021**;2(6):1821–71.

[11] Rai M, Yadav A, Gade A. S*ilver nanoparticles as a new generation of antimicrobials*. Biotechnol Adv. **2009**;27(1):76–83.

[12] Durán N, Durán M, De Jesus MB, Seabra AB, Fávaro WJ, Nakazato G. *Silver nanoparticles: A new view on mechanistic aspects on antimicrobial activity*. Nanomedicine Nanotechnol Biol Med. **2016**;12(3):789–99.

[13] Morris D, Ansar M, Speshock J, Ivanciuc T, Qu Y, Casola A, Garofalo R. *Antiviral and Immunomodulatory Activity of Silver Nanoparticles in Experimental RSV Infection*. Viruses. **2019**;11(8):732.

[14] Barkat MA, Harshita FN, Beg S, Pottoo FH, Garg A, Singh SP, Ahmad F. *Silver Nanoparticles and their Antimicrobial Applications*. Curr Nanomedicine. **2019**;8(3):215–24.

[15] Dakal TC, Kumar A, Majumdar RS, Yadav V. *Mechanistic Basis of Antimicrobial Actions of Silver Nanoparticles*. Front Microbiol. **2016**;7:1831.

[16] Anees Ahmad S, Sachi Das S, Khatoon A, Tahir Ansari M, Afzal Mohd, Saquib Hasnain M, Kumar Nayak A. *Bactericidal activity of silver nanoparticles: A mechanistic review*. Mater Sci Energy Technol. **2020**;3:756–69.

[17] Choi O, Yu CP, Esteban Fernández G, Hu Z. I*nteractions of nanosilver with Escherichia coli cells in planktonic and biofilm cultures*. Water Res. **2010**;44(20):6095–103.

[18] Dakal TC, Kumar A, Majumdar RS, Yadav V. *Mechanistic Basis of Antimicrobial Actions of Silver Nanoparticles*. Front Microbiol. **2016**;7:1831.

[19] Duval RE, Gouyau J, Lamouroux E. *Limitations of Recent Studies Dealing with the Antibacterial Properties of Silver Nanoparticles*: Fact and Opinion. Nanomater Basel Switz. **2019**;9(12):1775.

[20] Chauhan N, Tyagi AK, Kumar P, Malik A. *Antibacterial Potential of Jatropha curcas Synthesized Silver Nanoparticles against Food Borne Pathogens*. Front Microbiol. **2016**;7:1748

[21] Durán N, Durán M, De Jesus MB, Seabra AB, Fávaro WJ, Nakazato G. *Silver nanoparticles: A new view on mechanistic aspects on antimicrobial activity*. Nanomedicine Nanotechnol Biol Med. **2016**;12(3):789–99.

[22] Li H, Gao Y, Li C, Ma G, Shang Y, Sun Y. *A comparative study of the antibacterial mechanisms of silver ion and silver nanoparticles by Fourier transform infrared spectroscopy*. Vib Spectrosc. **2016**;85:112–21.

[23] Flores-López LZ, Espinoza-Gómez H, Somanathan R. *Silver nanoparticles: Electron transfer, reactive oxygen species, oxidative stress, beneficial and toxicological effects. Mini review.* J Appl Toxicol JAT. **2019**;39(1):16–26.

[24] Lavado AS, Chauhan VM, Zen AA, Giuntini F, Jones DRE, Boyle RW, Beeby A, Chan WC, Aylott JW. *Controlled intracellular generation of reactive oxygen species in human mesenchymal stem cells using porphyrin conjugated nanoparticles*. Nanoscale. **2015**;7(34):14525–31.

[25] Jamdagni P, Sidhu PK, Khatri P, Nehra K, Rana JS. *Metallic Nanoparticles: Potential Antimicrobial and Therapeutic Agents*. Adv Anim Biotechnol Its Appl. **2018**;143.

[26] Qing Y, Cheng L, Li R, Liu G, Zhang Y, Tang X, Wang J, Liu H, Qin Y. P*otential antibacterial mechanism of silver nanoparticles and the optimization of orthopedic implants by advanced modification technologies*. Int J Nanomedicine. **2018**;13:3311–27.

[27] Wang L, Hu C, Shao L. *The antimicrobial activity of nanoparticles: present situation and prospects for the future.* Int J Nanomedicine. **2017**;12:1227–49.

[28] Adeyemi OS, Shittu EO, Akpor OB, Rotimi D, Batiha GE saber. *Silver nanoparticles restrict microbial growth by promoting oxidative stress and DNA damage.* EXCLI J. **2020**;19:492–500.

[29] Vila Domínguez A, Ayerbe Algaba R, Miró Canturri A, Rodríguez Villodres Á, Smani Y. *Antibacterial Activity of Colloidal Silver against Gram-Negative and Gram-Positive Bacteria*. Antibiot Basel Switz. **2020**;9(1):36.

[30] Raza M, Kanwal Z, Rauf A, Sabri A, Riaz S, Naseem S. S*ize- and Shape-Dependent Antibacterial Studies of Silver Nanoparticles Synthesized by Wet Chemical Routes*. Nanomaterials. **2016**;6(4):74.

[31] Helmlinger J, Sengstock C, Groß-Heitfeld C, Mayer C, A. Schildhauer T, Köller M, Epple M. *Silver nanoparticles with different size and shape: equal cytotoxicity, but different antibacterial effects*. RSC Adv. **2016**;6(22):18490–501.

[32] Menichetti A, Mavridi-Printezi A, Mordini D, Montalti M. E*ffect of Size, Shape and Surface Functionalization on the Antibacterial Activity of Silver Nanoparticles*. J Funct Biomater. **2023**;14(5):244.

[33] Li WR, Sun TL, Zhou SL, Ma YK, Shi QS, Xie XB, Huang XM. *A comparative analysis of antibacterial activity, dynamics, and effects of silver ions and silver nanoparticles against four bacterial strains*. Int Biodeterior Biodegrad. **2017**;123:304–10.

[34] Roelofs D, Makama S, De Boer TE, Vooijs R, Van Gestel CAM, Van Den Brink NW. *Surface coating and particle size are main factors explaining the transcriptome-wide responses of the earthworm Lumbricus rubellus to silver nanoparticles*. Environ Sci Nano. **2020**;7(4):1179–93.

[35] Acharya D, Singha KM, Pandey P, Mohanta B, Rajkumari J, Singha LP. *Shape dependent physical mutilation and lethal effects of silver nanoparticles on bacteria*. Sci Rep. **2018**;8(1):201.

[36] Hong X, Wen J, Xiong X, Hu Y. *Shape effect on the antibacterial activity of silver nanoparticles synthesized via a microwave-assisted method*. Environ Sci Pollut Res Int. **2016**;23(5):4489–97.

[37] Saeb ATM, Alshammari AS, Al-Brahim H, Al-Rubeaan KA. *Production of silver nanoparticles with strong and stable antimicrobial activity against highly pathogenic and multidrug resistant bacteria*. ScientificWorldJournal. **2014**;2014:704708.

[38] Rezazadeh NH, Buazar F, Matroodi S. *Synergistic effects of combinatorial chitosan and polyphenol biomolecules on enhanced antibacterial activity of biofunctionalized silver nanoparticles*. Sci Rep. **2020**;10(1):19615.

[39] Murei A, Ayinde WB, Gitari MW, Samie A. *Functionalization and antimicrobial evaluation of ampicillin, penicillin and vancomycin with Pyrenacantha grandiflora Baill and silver nanoparticles.* Sci Rep. **2020**;10(1):11596.

[40] Shang B, Xu M, Zhi Z, Xi Y, Wang Y, Peng B, Li p, Deng Z. *Synthesis of sandwich-structured silver@polydopamine@silver shells with enhanced antibacterial activities*. J Colloid Interface Sci. **2020**;558:47–54.

[41]. Khan B, Nawaz M, Hussain R, Price GJ, Warsi MF, Waseem M. *Enhanced antibacterial activity of size-controlled silver and polyethylene glycol functionalized silver nanoparticles*. Chem Pap. **2021**;75(2):743–52.

[42]. Chen Y, Wu W, Xu Z, Jiang C, Han S, Ruan J, Wang Y. *Photothermal-assisted antibacterial application of graphene oxide-Ag nanocomposites against clinically isolated multi-drug resistant Escherichia coli*. R Soc Open Sci. **2020**;7(7):192019.

[43] Cobos M, De-La-Pinta I, Quindós G, Fernández MJ, Fernández MD. *Synthesis, Physical, Mechanical and Antibacterial Properties of Nanocomposites Based on Poly(vinyl alcohol)/Graphene Oxide-Silver Nanoparticles.* Polymers. **2020**;12(3):723.

[44] Saifulazmi NF, Rohani ER, Harun S, Bunawan H, Hamezah HS, Nor Muhammad NA, Azizan KA, Ahmed QU, Fakurazi S, Mediani A, Sarian MN. *A Review with Updated Perspectives on the Antiviral Potentials of Traditional Medicinal Plants and Their Prospects in Antiviral Therapy*. Life Basel Switz. **2022**;12(8):1287.

[45] Ghosh U, Sayef Ahammed K, Mishra S, Bhaumik A. T*he Emerging Roles of Silver Nanoparticles to Target Viral Life Cycle and Detect Viral Pathogens*. Chem Asian J. **2022**;17(5):e202101149.

[46] Ratan ZA, Mashrur FR, Chhoan AP, Shahriar SMd, Haidere MF, Runa NJ, Kim S, Kweon D-H, Hosseinzadeh H, Cho JY. *Silver Nanoparticles as Potential Antiviral Agents.* Pharmaceutics. **2021**;13(12):2034.

[47] Luceri A, Francese R, Lembo D, Ferraris M, Balagna C. S*ilver Nanoparticles: Review of Antiviral Properties, Mechanism of Action and Applications*. Microorganisms. **2023**;11(3):629.

[48] Al-Radadi NS, Abu-Dief AM. *Silver nanoparticles (AgNPs) as a metal nano-therapy: possible mechanisms of antiviral action against COVID-19*. Inorg Nano-Met Chem. **2022**;0(0):1–19.

[49] Zhou J, Hu Z, Zabihi F, Chen Z, Zhu M. *Progress and Perspective of Antiviral Protective Material.* Adv Fiber Mater. **2020**;2(3):123–39.

[50] Szymańska E, Orłowski P, Winnicka K, Tomaszewska E, Bąska P, Celichowski G, Grobelny ., Basa A, Krzyżowska M. *Multifunctional Tannic Acid/Silver Nanoparticle-Based Mucoadhesive Hydrogel for Improved Local Treatment of HSV Infection: In Vitro and In Vivo Studies*. Int J Mol Sci. **2018**;19(2):387.

[51] Baram-Pinto D, Shukla S, Perkas N, Gedanken A, Sarid R. I*nhibition of Herpes Simplex Virus Type 1 Infection by Silver Nanoparticles Capped with Mercaptoethane Sulfonate*. Bioconjug Chem. **2009**;20(8):1497–502.

[52] Sinclair TR, Van Den Hengel SK, Raza BG, Rutjes SA, De Roda Husman AM, Peijnenburg WJGM, Roesink HDV, M de Vos W. *Surface chemistry-dependent antiviral activity of silver nanoparticles*. Nanotechnology. **2021**;32(36):365101.

[53] He Q, Lu J, Liu N, Lu W, Li Y, Shang C, Li X, Hu L, Jiang G. A*ntiviral Properties of Silver Nanoparticles against SARS-CoV-2: Effects of Surface Coating and Particle Size.* Nanomater Basel Switz. **2022**;12(6):990.

[54] Lam WT, Babra TS, Smith JHD, Bagley MC, Spencer J, Wright E, Greenland BW. S*ynthesis and Evaluation of a Silver Nanoparticle/Polyurethane Composite That Exhibits Antiviral Activity against SARS-CoV-2*. Polymers. **2022**;14(19):4172.

[55] Almanza-Reyes H, Moreno S, Plascencia-López I, Alvarado-Vera M, Patrón-Romero L, Borrego B, Reyes-Escamilla A, Valencia-Manzo D, Brun A, Pestryakov A, Bogdanchikova N. *Evaluation of silver nanoparticles for the prevention of SARS-CoV-2 infection in health workers: In vitro and in vivo*. PloS One. **2021**;16(8):e0256401.

[56] Naumenko K, Zahorodnia S, Pop CV, Rizun N. *Antiviral activity of silver nanoparticles against the influenza A virus.* J Virus Erad. **2023**;9(2):100330.

[57] Park S, Ko YS, Lee SJ, Lee C, Woo K, Ko G. *Inactivation of influenza A virus via exposure to silver nanoparticle-decorated silica hybrid composites*. Environ Sci Pollut Res Int. **2018**;25(27):27021–30.

[58] Zeedan GS, EL-Razik KAA, Allam AM, Abdalhamed AM, Zeina HAA. *Evaluations of Potential Antiviral Effects of Green Zinc Oxide and Silver Nanoparticles against Bovine Herpesvirus-1*. Adv Anim Vet Sci. **2020**;8(4).

[59] Zhang T, Wang L, Chen Q, Chen C. *Cytotoxic potential of silver nanoparticles.* Yonsei Med J. **2014**;55(2):283–91.

[60] Jeevanandam J, Krishnan S, Hii YS, Pan S, Chan YS, Acquah C, Danquah MK, Rodrigues J. *Synthesis approach-dependent antiviral properties of silver nanoparticles and nanocomposites.* J Nanostructure Chem. **2022**;12(5):809–31.

[61] Jain N, Jain P, Rajput D, Patil UK. *Green synthesized plant-based silver nanoparticles: therapeutic prospective for anticancer and antiviral activity*. Micro Nano Syst Lett. **2021**;9(1):5.

[62] Balagna C, Francese R, Perero S, Lembo D, Ferraris M. *Nanostructured composite coating endowed with antiviral activity against human respiratory viruses deposited on fibre-based air filters.* Surf Coat Technol. **2021**;409:126873.

[63] Chen YN, Hsueh YH, Hsieh CT, Tzou DY, Chang PL. *Antiviral Activity of Graphene–Silver Nanocomposites against Non-Enveloped and Enveloped Viruses.* Int J Environ Res Public Health. **2016**;13(4):430.

[64] Ciriminna R, Albo Y, Pagliaro M. *New Antivirals and Antibacterials Based on Silver Nanoparticles.* Chemmedchem. **2020**;15(17):1619–23.

[65] Balagna C, Perero S, Percivalle E, Nepita EV, Ferraris M. *Virucidal effect against coronavirus SARS-CoV-2 of a silver nanocluster/silica composite sputtered coating*. Open Ceram. **2020**;1:100006.

[66] Kelly PJ, Arnell RD. *Magnetron sputtering: a review of recent developments and applications.* Vacuum. **2000**;56(3):159–72.

[67] Stan GE, Montazerian M, Shearer A, Stuart BW, Baino F, Mauro JC, Ferreire JMF. *Critical advances in the field of magnetron sputtered bioactive glass thin-films: An analytical review*. Appl Surf Sci. **2024**;646:158760.

[68] Baptista A, Silva FJG, Porteiro J, Míguez JL, Pinto G, Fernandes L. *On the Physical Vapour Deposition (PVD): Evolution of Magnetron Sputtering Processes for Industrial Applications.* Procedia Manuf. **2018**;17:746–57.

[69] Rees Jr. WS. *Handbook of Deposition Technologies for Films and Coatings: Science, Technology and Applications*, 2nd Edition: Edited by Rointan F. Bunshah, Noyes, Park Ridge, NJ, **1994**, XXVI, 861 pp..

[70] Mattox DM. *Handbook of Physical Vapor Deposition (PVD) Processing*. William Andrew; **2010**. 793 p.

[71] Ghazal H, Sohail N, Ghazal H, Sohail N. *Sputtering Deposition. In: Thin Films - Deposition Methods and Applications*. IntechOpen; **2022**

[72] Daviðsdóttir S, Shabadi R, Galca AC, Andersen IH, Dirscherl K, Ambat R. *Investigation of DC magnetron-sputtered TiO2 coatings: Effect of coating thickness, structure, and morphology on photocatalytic activity*. Appl Surf Sci. **2014**;313:677–86.

[73] Ru J, Qian X, Wang Y. *Study on antibacterial finishing of cotton fabric with silver nanoparticles stabilized by nanoliposomes*. Cellulose. **2018**;25(9):5443–54.

[74] Depla D, Mahieu S, curatori. *Reactive Sputter Deposition*. Berlin, Heidelberg: Springer; **2008**. (Hull R, Osgood RM, Parisi J, Warlimont H. Springer Series in Materials Science; vol. 109).

[75] Hoche H, Groß S, Oechsner M. *Development of new PVD coatings for magnesium alloys with improved corrosion properties.* Surf Coat Technol. **2014**;259:102–8.

[76] Baptista A, Silva F, Porteiro J, Míguez J, Pinto G. *Sputtering Physical Vapour Deposition (PVD) Coatings: A Critical Review on Process Improvement and Market Trend Demands*. Coatings. **2018**;8(11):402.

[77] Wang B, Wei S, Guo L, Wang Y, Liang Y, Xu B, Pan F, Tang A, Chen X. *Effect of deposition parameters on properties of TiO2 films deposited by reactive magnetron sputtering*. Ceram Int. **2017**;43(14):10991–8.

[78] Wong LH, Lai YS. *Characterization of boron-doped ZnO thin films prepared by magnetron sputtering with (100 −x)ZnO–xB2O3 ceramic targets*. Thin Solid Films. **2015**;583:205–11.

[79] Khojier K, Moradi G. *Study of ZrO2 coatings on 316L SS as a function of sputtering gas flow rate for biomedical applications*. Surf Coat Technol. **2021**;425:127673.

[80] Xia Y, Wang P, Shi S, Zhang M, He G, Lv J, Sun Z. *Deposition and characterization of AZO thin films on flexible glass substrates using DC magnetron sputtering technique*. Ceram Int. **2017**;43(5):4536–44.

[81] Vladkova T, Angelov O, Stoyanova D, Gospodinova D, Gomes L, Soares A, Mergulhao F, Ivanova I. *Magnetron co-sputtered TiO2/SiO2/Ag nanocomposite thin coatings inhibiting bacterial adhesion and biofilm formation.* Surf Coat Technol. **2020**;384:125322.

[82] Adochițe C Ș., Vițelaru C, Parau AC, Kiss AE, Pană I, Vlădescu A, Costinaș S, Moga M, Muntean R, Badea M, Idomir M. *Synthesis and Investigation of Antibacterial Activity of Thin Films Based on TiO2-Ag and SiO2-Ag with Potential Applications in Medical Environment.* Nanomaterials. **2022**;12(6):902.

[83] Liu X, Gan K, Liu H, Song X, Chen T, Liu C. *Antibacterial properties of nano-silver coated PEEK prepared through magnetron sputtering.* Dent Mater. **2017**;33(9):e348–60.

[84] Rebelo R, Calderon SV, Fangueiro R, Henriques M, Carvalho S. *Influence of oxygen content on the antibacterial effect of Ag-O coatings deposited by magnetron sputtering*. Surf Coat Technol. **2016**;305:1–10.

[85] Ur Rehman MA, Ferraris S, Goldmann WH, Perero S, Bastan FE, Nawaz Q, Gautier di Confiengo G, Ferraris M, Boccaccini AR. *Antibacterial and Bioactive Coatings Based on Radio Frequency Co-Sputtering of Silver Nanocluster-Silica Coatings on PEEK/Bioactive Glass Layers Obtained by Electrophoretic Deposition*. ACS Appl Mater Interfaces. **2017**;9(38):32489–97.

[86] Gospodonova D, Ivanova I, Vladkova T. F*abrication and Characterization of Antimicrobial Magnetron Cosputtered TiO2/Ag/Cu Composite Coatings*. Coatings. **2021**;11(4):473.

[87] Meister TL, Fortmann J, Breisch M, Sengstock C, Steinmann E, Köller M, Pfaender S, Ludwig A. *Nanoscale copper and silver thin film systems display differences in antiviral and antibacterial properties*. Sci Rep. **2022**;12(1):7193.

[88] Lee M, Han SI, Kim C, Velumani S, Han A, Kassiba AH, Castaneda H. *ZrO_2 /ZnO/TiO_2 Nanocomposite Coatings on Stainless Steel for Improved Corrosion Resistance, Biocompatibility, and Antimicrobial Activity*. ACS Appl Mater Interfaces. **2022;**14(11):13801–11.

[89] Etiemble A, Der Loughian C, Apreutesei M, Langlois C, Cardinal S, Pelletier JM, Pierson JF, Steyer P. *Innovative Zr-Cu-Ag thin film metallic glass deposed by magnetron PVD sputtering for antibacterial applications.* J Alloys Compd. **2017**;707:155–61.

[90] Jung S, Yang JY, Byeon EY, Kim DG, Lee DG, Ryoo S, Le S, Shin CW, Jang HW, Kim HJ, Lee S. *Copper-Coated Polypropylene Filter Face Mask with SARS-CoV-2 Antiviral Ability.* Polymers. **2021**;13(9):1367.

[91] Fugiel A, Burchart-Korol D, Czaplicka-Kolarz K, Smoliński A. *Environmental impact and damage categories caused by air pollution emissions from mining and quarrying sectors of European countries*. J Clean Prod. **2017**;143:159–68.

[92] Song L, Zhou J, Wang C, Meng G, Li Y, Jarin M, Wu Z, Xie X. *Airborne pathogenic microorganisms and air cleaning technology development: A review.* J Hazard Mater. **2022**;424:127429.

[93] Guoliang L, Xiao M, Zhang X, Gal C, Chen X, Liu L, Pan S, Wu J, Tang L, Clements-Croome D. A *review of air filtration technologies for sustainable and healthy building ventilation.* Sustain Cities Soc. **2017**;32.

[94] Wu M, Liu K. *Air purification in confined spaces.* IOP Conf Ser Earth Environ Sci. **2020**;446(3):032072.

[95] Komaladewi AAIAS, Khoiruddin K, Surata IW, Subagia IDGA, Wenten IG. *Recent advances in antimicrobial air filter*. Kusrini E, Juwono FH, Yatim A, Setiawan EA, curatori. E3S Web Conf. **2018**;67:03016.

[96]. Zheng W, Hu J, Wang Z, Li J, Fu Z, Li H, Jurasz J, Chou SK, Yan J. *COVID-19 Impact on Operation and Energy Consumption of Heating, Ventilation and Air-Conditioning (HVAC) Systems.* Adv Appl Energy. **2021**;3:100040.

[97] J G, Y X, T K, Z X, C Q. *Bacterial community analysis of floor dust and HEPA filters in air purifiers used in office rooms in ILAS, Beijing*. Sci Rep. **2020**;10(1).

[98]. Song B, Zhang E, Han X, Zhu H, Shi Y, Cao Z. *Engineering and Application Perspectives on Designing an Antimicrobial Surface*. ACS Appl Mater Interfaces. **2020**;12(19):21330–41.

[99]. Ebadi M, McCague C, Vallee O, Taylor PK, Lee AHY, Bahrami M. *Salt and surfactant coated filters with antiviral properties and low pressure drop for prospective SARS-CoV2 applications*. Sci Rep. **2022**;12(1):11546.

[100]. Byun HR, Park SY, Hwang ET, Sang BI, Min J, Sung D, Choi WI, Kim S, Lee JH. *Antimicrobial Air Filter Coating with Plant Extracts Against Airborne Microbes*. Appl Sci. **2020**;10(24):9120.

[101] Druvari D, Tzoumani I, Piperigkou Z, Tzaferi K, Tselentis D, Vlamis-Gardikas A, Karamanos N, Bokia G, Kallitsis JK. *Development of Environmentally Friendly Biocidal Coatings Based on Water-soluble Copolymers for Air-cleaning Filters.* ACS Omega. **2022**;7(39):35204–16.

[102]. Cruz-Pacheco A, Muñoz-Castiblanco D, Gómez Cuaspud J, Paredes-Madrid L, Parra Vargas C, Martínez Zambrano J, Palacio Gómez CA. C*oating of Polyetheretherketone Films with Silver Nanoparticles by a Simple Chemical Reduction Method and Their Antibacterial Activity.* Coatings. **2019**;9(2):91.

[103] Ju Y, Han T, Yin J, Li Q, Chen Z, Wei Z, Zhan Y, Dong L. *Bumpy structured nanofibrous membrane as a highly efficient air filter with antibacterial and antiviral property*. Sci Total Environ. **2021**;777:145768.

[104] Hidayat MI, Adlim M, Maulana I, Suhartono S, Hayati Z, Bakar NHHA. *Green synthesis of chitosan-stabilized silver-colloidal nanoparticles immobilized on white-silica-gel beads and the antibacterial activities in a simulated-air-filter.* Arab J Chem. **2022**;15(2):103596.

[105] Mori Y, Ono T, Miyahira Y, Nguyen VQ, Matsui T, Ishihara M. *Antiviral activity of silver nanoparticle/chitosan composites against H1N1 influenza A virus.* Nanoscale Res Lett. **2013**;8(1):93.

[106] Acharya D, Mohanta B, Pandey P, Nasiri F. *Antibacterial properties of synthesized Ag and Ag@SiO2 core–shell nanoparticles: a comparative study*. Can J Phys. **2018**;96(8):955–60.

[107] Tan P, Li YH, Liu XQ, Jiang Y, Sun LB. *Core–Shell AgCl@SiO 2 Nanoparticles: Ag(I)-Based Antibacterial Materials with Enhanced Stability*. ACS Sustain Chem Eng. **2016**;4(6):3268–75.

[108] Park DH, Joe YH, Hwang J. *Dry Aerosol Coating of Anti-viral Particles on Commercial Air Filters Using a High-volume Flow Atomizer.* Aerosol Air Qual Res. **2019**;19(7):1636–44.

[109] Wu Y, Li X, Zhong Q, Wang F, Yang B. *Preparation and filtration performance of antibacterial PVDF/SiO2/Ag composite nanofiber membrane*. J Build Eng. **2023**;74:106864.

[110] Balagna C, Perero S, Percivalle E, Nepita EV, Ferraris M. *Virucidal effect against coronavirus SARS-CoV-2 of a silver nanocluster/silica composite sputtered coating.* Open Ceram. 2 **2020**;1:100006–100006.

[111] Mekonnen MM, Hoekstra AY. *Four billion people facing severe water scarcity.* Sci Adv. **2016**;2(2):e1500323.

[112] El-Aswar EI, Ramadan H, Elkik H, Taha AG. *A comprehensive review on preparation, functionalization and recent applications of nanofiber membranes in wastewater treatment.* J Environ Manage. **2022**;301:113908.

[113] Abdelfattah A, Ali SS, Ramadan H, El-Aswar EI, Eltawab R, Ho SH, Elsamahy T, Li S, El-Sheekh MM, Schagerl M, Kornaros M, Sun J. *Microalgae-based wastewater treatment: Mechanisms, challenges, recent advances, and future prospects*. Environ Sci Ecotechnology. **2022;**13:100205.

[114] Wang H, Hu C, Hu X, Yang M, Qu J. *Effects of disinfectant and biofilm on the corrosion of cast iron pipes in a reclaimed water distribution system*. Water Res. **2012**;46(4):1070–8.

[115] Maciel PMF, Fava N de MN, Lamon AW, Fernandez-Ibañez P, Byrne JA, Sabogal-Paz LP. *Household water purification system comprising cartridge filtration, UVC disinfection and chlorination to treat turbid raw water.* J Water Process Eng. **2021**;43:102203.

[116] Sharma S, Bhattacharya A. *Drinking water contamination and treatment techniques*. Appl Water Sci. **2017**;7(3):1043–67.

[117] Daschner FD, Rüden H, Simon R, Clotten J. *Microbiological contamination of drinking water in a commercial household water filter system*. Eur J Clin Microbiol Infect Dis Off Publ Eur Soc Clin Microbiol. **1996**;15(3):233–7.

[118] Zamil Al-Sudani HI. *A Review on Groundwater Pollution*. Int J Recent Eng Sci. **2019**;6(5):13–21.

[119] Khan MN, Mobin M, Abbas ZK, Alamri SA. *Fertilizers and Their Contaminants in Soils, Surface and Groundwater.* In: Encyclopedia of the Anthropocen]. Elsevier; **2018**. p. 225–40.

[120] Syafrudin M, Kristanti RA, Yuniarto A, Hadibarata T, Rhee J, Al-onazi WA, Algarni TS, Almarri AH, Al-Mohaimeed AM. *Pesticides in Drinking Water—A Review*. Int J Environ Res Public Health. **2021**;18(2):468.

[121] Xie Y. *Disinfection Byproducts in Drinking Water: Formation, Analysis, and Control*. Boca Raton: CRC Press; **2003**. 176 p.

[122] González Y, Gómez G, Moeller-Chávez GE, Vidal G. *UV Disinfection Systems for Wastewater Treatment: Emphasis on Reactivation of Microorganisms*. Sustainability. **2023**;15(14):11262.

[123] Mihut DM, Afshar A, Lackey LW, Le KN. *Antibacterial effectiveness of metallic nanoparticles deposited on water filter paper by magnetron sputtering.* Surf Coat Technol. **2019**;368:59–66.

[124] J N, Suresh A, S M A, Bavan JC, R K. *Antibacterial Coating on Filtration Membranes for Treatment of Cutting Fluid*. Int J Res Appl Sci Eng Technol. **2022**;10(12):827–30.

[125] Organization WH. *Silver in drinking water: background document for development of WHO Guidelines for drinking-water quality.* **2021**;

[126] Panico A, Paladini F, Sannino A, Pollini M. *Antibacterial silver treatments on polymeric membranes for fouling control and disinfection in water filtration*. J Appl Polym Sci. **2016**;133(34):app.43848.

[127] Wafy KR, El-Aswar EI, Mohamed WSE din, El-Sabbagh SM. *Water disinfection using durable ceramic filter coated with silver nanoparticles synthesized using actinomycetes.* Appl Water Sci. **2023**;13(6):140.

[128] Sciuto EL, Filice S, Coniglio MA, Faro G, Gradon L, Galati C, Spinella ., Libertino S, Scalese S. *Antimicrobial s-PBC Coatings for Innovative Multifunctional Water Filters*. Molecules. **2020**;25(21):5196.

[129] Izuma DS, Suzuki N, Suzuki T, Motomura H, Ando S, Fujishima A, Teshima K, Terashima CA. *A Floatable and Highly Water-Durable TiO2-Coated Net for Photocatalytic Antibacterial Water Treatment in Developing Countries.* Water. **2023**;15(2):320.

[130] Dutta D, Goswami S, Dubey R, Dwivedi SK, Puzari A. A*ntimicrobial activity of silver-coated hollow poly(methylmethacrylate) microspheres for water decontamination*. Environ Sci Eur. **2021** 33:22

[131] Hoque E, Tran P, Jacobo U, Bergfeld N, Acharya S, Shamshina JL, Reid TW, Abidi N. *Antimicrobial Coatings for Medical Textiles via Reactive Organo-Selenium Compounds*. *Molecules*. **2023**; 28(17):6381.

[132] Møllebjerg A, Palmén LG, Gori K, Meyer RL. *The Bacterial Life Cycle in Textiles is Governed by Fiber Hydrophobicity.* Microbiol Spectr. **2021**;9(2):e0118521.

[133] Singh P, Ali SW, Kale RD. *Antimicrobial Nanomaterials as Advanced Coatings for Self-Sanitizing of Textile Clothing and Personal Protective Equipment.* ACS Omega. **2023**;8(9):8159–71.

[134] Anand SC, Kennedy JF, Miraftab M, Rajendran S. *Medical and Healthcare Textiles*. **2010**;1–529.

[135] Liu M, Guinart A, Granados A, Gimbert-Suriñach C, Fernández E, Pleixats R, Vallribera A. *Coated Cotton Fabrics with Antibacterial and Anti-Inflammatory Silica Nanoparticles for Improving Wound Healing.* ACS Appl Mater Interfaces. **2024**;16(12):14595–604.

[136] Rong L, Liu H, Wang B, Mao Z, Xu H, Zhang L, Zhong Y, Feng X, Sui X. D*urable antibacterial and hydrophobic cotton fabrics utilizing enamine bonds*. Carbohydr Polym. **2019**;211:173–80.

[137] Ibrahim A, Laquerre JÉ, Forcier P, Deregnaucourt V, Decaens J, Vermeersch O. *Antimicrobial Agents for Textiles: Types, Mechanisms and Analysis Standards*. In: Kumar B, curatore. Textiles for Functional Applications, Rijeka: IntechOpen; **2021**.

[138] Dastjerdi R, Montazer M. *A review on the application of inorganic nano-structured materials in the modification of textiles: Focus on anti-microbial properties*. Colloids Surf B Biointerfaces. **2010**;79(1):5–18.

[139] Song J, Chen P, Liu W. A *Superhydrophobic and Antibacterial Surface Coated on Cotton Fabrics by Polydopamine*. Fibers Polym. **2019**;20(7):1380–6.

[140] Taheri P, Khajeh-Amiri A. *Antibacterial cotton fabrics via immobilizing silver phosphate nanoparticles onto the chitosan nanofiber coating*. Int J Biol Macromol. **2020**;158:282–9.

[141] Makhlouf G, Abdelkhalik A, Ameen H. *Preparation of highly efficient chitosan-based flame retardant coatings with good antibacterial properties for cotton fabrics.* Prog Org Coat. **2022**;163:106627.

[142] Lange A, Sawosz E, Wierzbicki M, Kutwin M, Daniluk K, Strojny B, Ostrowska A, Wójcik B, Łojkowski M, Gołębiewski M, Chwaliborg A, Jaworski S. *Nanocomposites of Graphene Oxide-Silver Nanoparticles for Enhanced Antibacterial Activity: Mechanism of Action and Medical Textiles Coating*. Mater Basel Switz. **2022**;15(9):3122.

[143] Bai Z, Wang X, Zheng M, Yue O, Xie L, Zha S, Dong S, Li T, Song Y, Huang M, Liu X. *Leather for flexible multifunctional bio-based materials: a review.* J Leather Sci Eng. **2022**;4.

[144] Wu X, Wu J, Mu C, Wang C, Lin W. *Advances in Antimicrobial Polymer Coatings in the Leather Industry: A Comprehensive Review.* Ind Eng Chem Res. **2021**;60:15004–18.

[145] Nguyen NT, Vu TH, Bui VH. A*ntibacterial and Antifungal Fabrication of Natural Lining Leather Using Bio-Synthesized Silver Nanoparticles from Piper Betle L. Leaf Extract.* Polymers. **2023**;15(12):2634.

[146] Carvalho I, Lima M, Nobre D, Marques S, Castro D, Leite T, Henriques M, Duarte F, Ramalho A, Carvalho S. *Silver oxide coatings deposited on leathers to prevent diabetic foot infections*. Surf Coat Technol. **2022;**442:128338.

[147] Marques GN, Reis RYN, Ribeiro LK, Simões LGP, Minozzi D, Andres J, Assis M, Mascaro LH, Longo E. *Antiviral leather: A functional coating based on SiO2-AgNPs to eliminate pathogens*. **2023**;11:5.

[148] Rosiati N, Silvianti F, Udkhiyati M. *Characterization of Silica/Silver-based Antibacterial Leather.* Leather Footwear J. **2020**;20:109–18.

[149] Arkas M, Kythreoti G, Favvas EP, Giannakopoulos K, Mouti N, Arvanitopoulou M, thanasiou A, Douloudi M, Nikoli E, Vardavoulias M et al. *Hydrophilic Antimicrobial Coatings for Medical Leathers from Silica-Dendritic Polymer-Silver Nanoparticle Composite Xerogels*. Textiles. **2022**;2(3):464–85.

[150] Ma X, Zhou S, Xu X, Du Q. *Copper-containing nanoparticles: Mechanism of antimicrobial effect and application in dentistry-a narrative review*. Front Surg. **2022**;9:905892.

[151] Vasiliev G, Kubo AL, Vija H, Kahru A, Bondar D, Karpichev Y, Bondarenko O. *Synergistic antibacterial effect of copper and silver nanoparticles and their mechanism of action*. Sci Rep **2023**;13(1):9202.

[152] Lallo da Silva B, Abuçafy MP, Berbel Manaia E, Oshiro Junior JA, Chiari-Andréo BG, Pietro RCR, Chiavacci LA. *Relationship Between Structure And Antimicrobial Activity Of Zinc Oxide Nanoparticles: An Overview.* Int J Nanomedicine. **2019**;14:9395–410.

[153] Zhao H, Su H, Ahmeda A, Sun Y, Li Z, Zangeneh MM, Nowroz Mi, Zangeneh A, Moradi R. *Biosynthesis of copper nanoparticles using Allium eriophyllum Boiss leaf aqueous extract; characterization and analysis of their antimicrobial and cutaneous wound-healing potentials.* Appl Organomet Chem. **2022**;36(12):e5587.

[154] Govindasamy GA, S. M. N. Mydin RB, Harun NH, Effendy WNFWE, Sreekantan S. Giant milkweed plant-based copper oxide nanoparticles for wound dressing application:

physicochemical, bactericidal and cytocompatibility profiles. Chem Pap. **2023**;77(2):1181–200.

[155] Jung S, Yang JY, Jang D, Kim T, Baek KH, Yoon H, Ryoo S, Jang HW, Lee S. *Sustainable Antibacterial and Antiviral High-Performance Copper-Coated Filter Produced via Ion Beam Treatment.* Polymers. **2022**;14(5):1007.

[156] SadrHaghighi A, Sarvari R, Fakhri E, Poortahmasebi V, Sedighnia N, Torabi M, Mohammadzadeh M, Azhiri AH, Eskandarinezhad M, Moharamzadeh K, Keyhanvar P. *Copper-Nanoparticle-Coated Melt-Blown Facemask Filter with Antibacterial and SARS-CoV-2 Antiviral Ability*. ACS Appl Nano Mater. **2023**;6(14):12849–61.

[157] Perelshtein I, Levi I, Perkas N, Pollak A, Gedanken A. *CuO-Coated Antibacterial and Antiviral Car Air-Conditioning Filters.* ACS Appl Mater Interfaces. **2022**;14(21):24850–5.

[158] He X, Zhang G, Wang X, Hang R, Huang X, Qin L, Tang B, Zhang X. *Biocompatibility, corrosion resistance and antibacterial activity of TiO2/CuO coating on titanium.* Ceram Int. **2017**;43(18):16185–95.

[159] Ohtsu N, Kakuchi Y, Ohtsuki T. *Antibacterial effect of zinc oxide/hydroxyapatite coatings prepared by chemical solution deposition*. Appl Surf Sci. **2018**;445:596–600.

[160] Khademjafari S, Rabiee SM, Nourouzi S, Shabannia Rami R. *In-vitro evaluation and antibacterial activity of ZnO nanoparticles deposited on hydroxyapatite tablets by RF magnetron sputtering.* Mater Today Commun. **2021;**28:102520.

[161] Roy TS, Shamim SUD, Rahman MK, Ahmed F, Gafur MA. *The Development of ZnO Nanoparticle Coated Cotton Fabrics for Antifungal and Antibacterial Applications*. Mater Sci Appl. **2020**;11(9):601–10.

[162] Lyu J, Xing S, Meng Y, Wu N, Yin C. *Flexible superhydrophobic ZnO coating harvesting antibacterial and washable properties*. Mater Lett. **2022**;314:131730.

[163] Wasim M, Khan MR, Mushtaq M, Naeem A, Han M, Wei Q. S*urface Modification of Bacterial Cellulose by Copper and Zinc Oxide Sputter Coating for UV-Resistance/Antistatic/Antibacterial Characteristics*. Coatings. **2020**;10(4):364.

[164] Deokar AR, Perelshtein I, Saibene M, Perkas N, Mantecca P, Nitzan Y, Gedanken A. *Antibacterial and In Vivo Studies of a Green, One-Pot Preparation of Copper/Zinc Oxide Nanoparticle-Coated Bandages.* Membranes. **2021**;11(7):462.

[165] Merkl P, Long S, McInerney GM, Sotiriou GA. *Antiviral Activity of Silver, Copper Oxide and Zinc Oxide Nanoparticle Coatings against SARS-CoV-2*. Nanomaterials. **2021**;11(5):1312.

[166] Sembiring S, Riyanto A, Firdaus I, Junaidi, Situmeang R. *Structure and properties of silver-silica composite prepared from rice husk silica and silver nitrate*. Ceram - Silik. **2022**;66:167–77.

[167] Allafchian A, Banifatemi S, Jalali SAH. S*ynthesis and Characterization of Ag/SiO2 Nanoparticles Embedded in TPS and TEOS Sol-gel Matrix with Excellent Antibacterial Activity.* Nanosci Nanotechnol-Asia. **2017**;11.

[168] Niizeki T, Nagayama S, Hasegawa Y, Miyata N, Sahara M, Akutsu K. *Structural Study of Silica Coating Thin Layers Prepared from Perhydropolysilazane: Substrate Dependence and Water Penetration Structure*. Coatings. **2016**;6(4):64.

[169] Bertoncello R, Monti M, Sada C. *Silica thin-films from perhydropolysilazane*. AJSIR.**2016**;4(7)

[170] Bauer F, Decker U, Dierdorf A, Ernst H, Heller R, Liebe H, Mehnert R. *Preparation of moisture curable polysilazane coatings: Part I. Elucidation of low temperature curing kinetics by FT-IR spectroscopy.* Prog Org Coat. 2005;53(3):183–90.

[171] Hideki M, Kazuhiro Y. Topics on coating.*Ceramic coating capable low-temperature formation using inorganic polysilazane*. **1995**;23(5):25–9.

[172] Wang WY, Zhang YL, Guo X, Wang LM, Zhang JR, Yang H, Dong GJ, Zhang ZB, Xu CH. *Rapid Conversion of Perhydropolysilazane into Thin Silica Coating at Low Temperature*. Chin J Polym Sci. **2023**;41(8):1198–205.

[173] Ohishi T, Yamazaki Y. *Formation and Gas Barrier Characteristics of Polysilazane-Derived Silica Coatings Formed by Excimer Light Irradiation on PET Films with Vacuum Evaporated Silica Coatings*. Mater Sci Appl. **2016**;8(1):1–14.

[174] Morlier A, Cros S, Garandet JP, Alberola N. *Structural properties of ultraviolet cured polysilazane gas barrier layers on polymer substrates.* Thin Solid Films. **2014**;550:85–9.

[175] Kubo T, Kozuka H. *Conversion of Perhydropolysilazane-to-Silica Thin Films by Exposure to Vapor from Aqueous Ammonia at Room Temperature.* J Ceram Soc Jpn - J Ceram SOC JPN. **2006**;114:517–23.

[176] Baek JJ, Park SM, Kim YR, Chang KC, Heo YJ, Bae GY, Choi KH, Shin G. I*ntense pulsed UV light treatment to design functional optical films from perhydropolysilazane: an alternative to conventional heat treatment processes*. J Mater Sci. **2022**;57(1):254–73.

[177] Channa IA, Distler A, Zaiser M, Brabec CJ, Egelhaaf HJ. *Thin Film Encapsulation of Organic Solar Cells by Direct Deposition of Polysilazanes from Solution*. Adv Energy Mater. **2019**;9(26):1900598.

[178]. Wang J, Gili A, Grünbacher M, Praetz S, Epping JD, Görke O, Schuck G, Penner S, Schlesiger C, Schomacker R, Gurlo A, Bekheet M. *Silicon oxycarbonitride ceramic containing nickel nanoparticles: from design to catalytic application*. Mater Adv. **2021**;2(5):1715–30.

[179] Katagiri K, Takabatake R, Inumaru K. *Robust Infrared-Shielding Coating Films Prepared Using Perhydropolysilazane and Hydrophobized Indium Tin Oxide Nanoparticles with Tuned Surface Plasmon Resonance.* ACS Appl Mater Interfaces. 2013;5(20):10240–5.

[180] Luceri A, Perero S, Cochis A, Scalia A, Rimondini L, Ferraris M, Balagna C. *Washing resistant antibacterial composite coatings on cotton textiles*. Cellulose. **2023**;1–21.

[181] Chhatre A, Solasa P, Sakle S, Thaokar R, Mehra A. *Color and surface plasmon effects in nanoparticle systems: Case of silver nanoparticles prepared by microemulsion route*. Colloids Surf Physicochem Eng Asp. **2012**;404:83–92.

[182]. NCCLS M2-A9, Performance Standards for Antimicrobial Disk Susceptibility Tests, Approved Standard, 9th ed., NCCLS, Villanova,PA, 2003.

[183] NCCLS M7-A6, MethodNCCLS M7-A6, Methods for DilutionAntimicrobial Susceptibility Tests or Bacteria that grow Aerobically, Approved standard 6th ed. NCCLS, Villanova, PA, USA 2003s for Dilution Antimicrobial Susceptibility Tests for Bacteria that grow Aerobically, Approved standard 6th ed. NCCLS, Villanova, PA, 2003.

[184] Balagna C, Perero S, Bosco F, Mollea C, Irfan M, Ferraris M. *Antipathogen nanostructured coating for air filters.* Appl Surf Sci. **2020**;508:145283.

[185] Luceri A, Francese R, Perero S, Lembo D, Ferraris M, Balagna C. *Antibacterial and Antiviral Activities of Silver Nanocluster/Silica Composite Coatings Deposited onto Air Filters*. ACS Appl Mater Interfaces. **2024**;16(3):3955–65.

[186] Egger S, Lehmann RP, Height MJ, Loessner MJ, Schuppler M. *Antimicrobial properties of a novel silver-silica nanocomposite material*. Appl Environ Microbiol. **2009;**75(9):2973–6.

[187] Pham DP, Kim Khanh H, Tran CV, Vu V, Van T. *Preparation and Structural Characterization of Sol-Gel-Derived Silver Silica Nanocomposite Powders*. Int J Mater Sci Appl. **2014**;3:147–51.

[188] Pradhaban G, Kaliaraj GS, Vishwakarma V. *Antibacterial effects of silver–zirconia composite coatings using pulsed laser deposition onto 316L SS for bio implants*. Prog Biomater. **2014**;3(2–4):123–30.

[189] Anton R, Laska N, Schulz U, Obert S, Heilmaier M. *Magnetron Sputtered Silicon Coatings as Oxidation Protection for Mo-Based Alloys*. Adv Eng Mater. **2020**;22(7):2000218.

[190] Ben Khemis S, Burov E, Montigaud H, Skrelic D, Gouillart E, Cormier L. *Structural analysis of sputtered amorphous silica thin films: A Raman spectroscopy investigation*. Thin Solid Films. **2021**;733:138811.

[191] Al-Khedhairy AA, Wahab R. *Silver Nanoparticles: An Instantaneous Solution for Anticancer Activity against Human Liver (HepG2) and Breast (MCF-7) Cancer Cells*. Metals. 2022;12(1):148.

[192] Sharma K, Guleria S, Razdan VK. *Green synthesis of silver nanoparticles using Ocimum gratissimum leaf extract: characterization, antimicrobial activity and toxicity analysis.* J Plant Biochem Biotechnol. **2020**;29(2):213–24.

[193] Krylova GV, Gnatyuk YI, Smirnova NP, Eremenko AM, Gun'ko VM. *Ag nanoparticles deposited onto silica, titania, and zirconia mesoporous films synthesized by sol–gel template method.* J Sol-Gel Sci Technol. **2009**;2(50):216–28.

[194] D. Rushton MJ, Ipatova I, J. Evitts L, E. Lee W, C. *Middleburgh S. Stoichiometry deviation in amorphous zirconium dioxide.* RSC Adv. **2019**;9(29):16320–7.

[195] Shivanna M, Nagappa N, Siddalingappa DM. *Structural, Morphological and Photoluminescence Studies of Pure ZrO2 and ZrO2: Eu+3 Nanophosphors Synthesised by Microwave-Assisted Hydrothermal Technique*. Plasmonics. **2020**;15(6):1629–37.

[196] Kuo DH, Chien CH, Huang CH. *Zirconia and zirconia–silica thin films deposited by magnetron sputtering*. Thin Solid Films. **2002**;420–421:47–53.

[197] Chen W, Liu Y, Courtney HS, Bettenga M, Agrawal CM, Bumgardner JD, Ong JL. *In vitro anti-bacterial and biological properties of magnetron co-sputtered silver-containing hydroxyapatite coating.* Biomaterials. **2006**;27(32):5512–7.

[198] Jamuna-Thevi K, Bakar SA, Ibrahim S, Shahab N, Toff MRM. *Quantification of silver ion release, in vitro cytotoxicity and antibacterial properties of nanostuctured Ag doped TiO2 coatings on stainless steel deposited by RF magnetron sputtering.* Vacuum. **2011**;86(3):235–41.

[199] Das I, De G. *Zirconia based superhydrophobic coatings on cotton fabrics exhibiting excellent durability for versatile use*. Sci Rep. **2015**;5(1):18503.

[200] Chen H, Zhang G, Zhang W, Gao W. S*ilver nanoparticles deposited on a cotton fabric surface via an in situ method using reactive hyperbranched polymers and their antibacterial properties*. RSC **2023**;Adv. 13(17):11450–6.

[201] Jain A, Kongkham B, Puttaswamy H, Butola BS, Malik HK, Malik A. *Development of Wash-Durable Antimicrobial Cotton Fabrics by In Situ Green Synthesis of Silver Nanoparticles and*

Investigation of Their Antimicrobial Efficacy against Drug-Resistant Bacteria. Antibiot Basel Switz. o **2022**;11(7):864.

[202] Scott CP, Higham PA. *Antibiotic bone cement for the treatment of Pseudomonas aeruginosa in joint arthroplasty: comparison of tobramycin and gentamicin-loaded cements.* J Biomed Mater Res B Appl Biomater. **2003**;64(2):94–8.

[203] Mollea C, Bosco F, Fissore D. *Agar Plate Methods for Assessing the Antibacterial Activity of Thyme and Oregano Essential Oils against S. epidermidis and E. coli.* Antibiotics. **2022**;11(12):1809.

[204] Ahmad A, Wei Y, Syed F, Tahir K, Rehman AU, Khan A, Ullah S, Yuan Q. *The effects of bacteria-nanoparticles interface on the antibacterial activity of green synthesized silver nanoparticles*. Microb Pathog. **2017**;102:133–42.

[205] Mikhailova EO. S*ilver Nanoparticles: Mechanism of Action and Probable Bio-Application*. J Funct Biomater. **2020**;11(4):84.

[206] Ko YS, Joe Y, Seo M, Lim K, Hwang J, Woo K. *Prompt and Synergistic Antibacterial Activity of Silver Nanoparticle-Decorated Silica Hybrid Particles on Air Filtration*. J Mater Chem B. **2014**;2.

[207] Rossi NR, de Menezes BRC, Sampaio A da G, da Silva DM, Koga-Ito CY, Thim GP, Paes-Junior TJdA. S*ilver-Coated Silica Nanoparticles Modified with MPS: Potential Antimicrobial Biomaterials Applied in Glaze and Soft Reliner*. Polymers. **2022**;14(20):4306.

[208] Gautam C, Joyner J, Gautam A, Rao J, Vajtai R. *Zirconia based dental ceramics: structure, mechanical properties, biocompatibility and applications.* Dalton Trans. **2016**;45(48):19194–215.

[209] D'Agostino A, Tana F, Ettorre A, Pavarini M, Serafini A, Cochis A, Scalia AC, Rimondini L, De Giglio E, Cometa S, Chiesa R, De Nardo L. *Mesoporous zirconia surfaces with anti-biofilm properties for dental implants*. Biomed Mater Bristol Engl. **2021**;16(4).

[210] Sredojevic D, Pirkovic A, Periša J, Murafa N, Spremo-Potparevic B, Zivkovic L, Topalović D, Zarubica A, Jovanović Krivokuća M, Nedeljković JM. *Toxicity of Silver Nanoparticles Supported by Surface-Modified Zirconium Dioxide with Dihydroquercetin*. Nanomaterials. **2022**;12:3195.

[211] Rocha AC da S, Pinheiro MVDS, Menezes LR de, Silva EO da. *Core-shell nanoparticles based on zirconia covered with silver as an advantageous perspective for obtaining antimicrobial nanocomposites with good mechanical properties and less cytotoxicity.* J Mech Behav Biomed Mater. **2021**;123:104726.

[212] Ferraris M, Ferraris S, Miola M, Perero S, Balagna C, Vernè E, Gautier G, Manfredotti Ch, Battiato A, Vittone E, Speranza G, Bogdanovic I. *Effect of thermal treatments on sputtered silver nanocluster/silica composite coatings on soda-lime glasses: ionic exchange and antibacterial activity.* J Nanoparticle Res. **2012**;14(12):1287.

[213] Song Y, Lee Y ki, Lee Y, Hwang WT, Lee J, Park S, Park N, Song H, Kim H, Lee KG, Kim ID, Kim Y, Im SG. *Anti-viral, anti-bacterial, but non-cytotoxic nanocoating for reusable face mask with efficient filtration, breathability, and robustness in humid environmen*t. Chem Eng J. **2023**;470:144224.

[214] Choi YH, Kim MJ, Lee J, Pyun JC, Khang DY. Recyclable, *Antibacterial, Isoporous Through-Hole Membrane Air Filters with Hydrothermally Grown ZnO Nanorods.* Nanomaterials. 2021;11(12):3381.

[215] Kim YI, Kim MW, An S, Yarin AL, Yoon SS. *Reusable Filters Augmented with Heating Microfibers for Antibacterial and Antiviral Sterilization*. ACS Appl Mater Interfaces. **2021**;13(1):857–67.

[216] Han S, Kim J, Lee Y, Bang J, Kim CG, Choi J, Min J, Ha I, Yoon Y, Yun CH, Cruz M, Wiley BJ, Ko SH. T*ransparent Air Filters with Active Thermal Sterilization.* Nano Lett. **2022**;22(1):524–32.

[217] Kujundzic E, Hernandez M, Miller SL. *Ultraviolet germicidal irradiation inactivation of airborne fungal spores and bacteria in upper-room air and HVAC in-duct configurations*. J Environ Eng Sci. **2007**;6(1):1–9.

[218] Raja FNS, Worthington T, Martin RA. *The antimicrobial efficacy of copper, cobalt, zinc and silver nanoparticles: alone and in combination.* Biomed Mater. **2023**;18(4):045003.

[219] Xu Q, Ke X, Ge N, Shen L, Zhang Y, Fu F, Liu X. *Preparation of Copper Nanoparticles Coated Cotton Fabrics with Durable Antibacterial Properties.* Fibers Polym. **2018;**19(5):1004–13.

[220] Wang S, Zhu W, Yu P, Wang X, He T, Tan G, Ning C. *Antibacterial nanostructured copper coatings deposited on tantalum by magnetron sputtering.* Mater Technol. **2015**;30(sup6):B120–5.

[221] Miandal K, Lam ML, Shain FL, Manie A, Mohamad KA, Alias A. *RF Power Dependence of ZnO Thin Film Deposited by RF Powered Magnetron Sputtering System*. Journal of Advanced Research in Materials Science. **2016**;20(1).

[222] Phul R, Kaur C, Farooq U, Ahmad T. *Ascorbic acid assisted synthesis, characterization and catalytic application of copper nanoparticles*. Mater Sci Eng Int J. **2018** ;2(4).

[223] Rather MY, Sundarapandian S. *Facile Green Synthesis of Copper Oxide Nanoparticles and Their Rhodamine-b Dye Adsorption Property*. J Clust Sci. **2022**;33(3):925–33.

[224] Aguilar MS, Esparza R, Rosas G. *Synthesis of Cu nanoparticles by chemical reduction method.* Trans Nonferrous Met Soc China. **2019**;29(7):1510–5.

[225] Khalaji AD, Pazhand Z, Kiani K, Machek P, Jarosova M, Mazandarani R. *CuO nanoparticles: preparation, characterization, optical properties, and antibacterial activities*. J Mater Sci Mater Electron. **2020**;31(14):11949–54.

[226] Ullah S, Badshah A, Ahmed F, Raza R, Altaf AA, Hussain R. *Electrodeposited Zinc Electrodes for High Current Zn/AgO Bipolar Batteries*. Int J Electrochem Sci. **2011**;6(9):3801–11.

[227] Qasim I, Mumtaz M, Nadeem K, Abbas SQ. *Zinc Nanoparticles at Intercrystallite Sites of* $(Cu_{0.5}Tl_{0.5})Ba_2Ca_3Cu_4O_{12-\delta}$ *Superconductor*. J Nanomater. **2016**;2016:e9781790.

[228] Fakhari S, Jamzad M, Kabiri Fard H. *Green synthesis of zinc oxide nanoparticles: a comparison.* Green Chem Lett Rev. **2019**;12(1):19–24.

[229] Vibornijs V, Zubkins M, Strods E, Rudevica Z, Korotkaja K, Ogurcovs A, Kundzins K, Purans J, Zajakina A. *Analysis of Antibacterial and Antiviral Properties of ZnO and Cu Coatings Deposited by Magnetron Sputtering: Evaluation of Cell Viability and ROS Production.* Coatings. **2023**;14(1):14.

[230] Fan X, Yahia L, Sacher E. *Antimicrobial Properties of the Ag, Cu Nanoparticle System*. Biology. **2021**;10(2):137.

[231] Cattaruzza E, Battaglin G, Canton P, Finotto T, Sada C. *Copper-based nanocluster composite silica films by rf-sputtering deposition*. Mater Sci Eng C. **2006**;26(5):1092–6.

[232] Lv P, Wei A, Wang Y, Li D, Zhang J, Lucia LA, Wei Q. C*opper nanoparticles-sputtered bacterial cellulose nanocomposites displaying enhanced electromagnetic shielding, thermal, conduction, and mechanical properties*. Cellulose. **2016**;23(5):3117–27.

[233] Goel S, Dubey P, Ray S, Jayaganthan R, Pant AB, Chandra R. *Co-sputtered Antibacterial and Biocompatible Nanocomposite Titania-Zinc Oxide thin films on Si substrates for Dental Implant applications.* Mater Technol. **2019**;34(1):32–42.

[234] Kudzin MH, Giełdowska M, Król P, Sobańska Z. *Preparation of Cotton–Zinc Composites by Magnetron Sputtering Metallization and Evaluation of their Antimicrobial Properties and Cytotoxicity.* Materials. **2022**;15(8):2746.

[235] Zhang G, Liu J, Zhu Y, Shen T, Yang D quan. *Enhanced antibacterial efficacies, corrosion resistance, and cytocompatibility of ZnO/CuO composite coatings through designed sputtering orders.* Appl Surf Sci. **2023**;635:157724.

[236] Rodrigues E, Miranda Jr EJP, Oliveira M. *Silver-Doped Zirconia Nanoparticles as Possible Bactericide in Water Filters*. Mater Sci Forum. **2014**;798–799:69–74.

[237] Wehling J, Köser J, Lindner P, Lüder C, Beutel S, Kroll S, et Rezwan K. *Silver nanoparticle-doped zirconia capillaries for enhanced bacterial filtration*. Mater Sci Eng C. **2015**;48:179–87.

[238] Abdulla NK, Siddiqui SI, Fatima B, Sultana R, Tara N, Hashmi AA, Ahmad R, Mohsin M, Nirala RK, Linh NT, Bach QV, Chaudhry SA. *Silver based hybrid nanocomposite: A novel antibacterial material for water cleansing*. J Clean Prod. febbraio **2021**;284:124746.

[239] Chauhan KV, Subhedar DG, Prajapati R, Dave D. *Experimental investigation of wettability properties for zirconia based coatings by RF magnetron sputtering*. Mater Today Proc. **2020**;26:2447–51.

[240] Gonzalez A, Noguez C, Beránek J, Barnard A. *Size, Shape, Stability, and Color of Plasmonic Silver Nanoparticles.* J Phys Chem C. **2014**;118:9128–36.

[241] Noikaew B, Wangmooklang L, Niyomsoan S, Larpkiattaworn S. P*reparation of transparent alumina thin films deposited by RF magnetron sputtering*. J Met Mater Miner. **2021**;31(2):96–103.

[242] Alexe CA, Gaidau C, Stanca M, Radu A, Stroe M, Baibarac M, Mateescu G, Mateescu A, Stanculescu I. *Multifunctional leather surfaces coated with nanocomposites through conventional and unconventional methods*. Mater Today Proc. 2021;54.

[243] Channa IA, Shah AA, Rizwan M, Makhdoom MA, Chandio AD, Shar MA, Mahmood A. *Process Parameter Optimization of a Polymer Derived Ceramic Coatings for Producing Ultra-High Gas Barrier.* Materials. **2021**;14(22):7000.

[244] Blankenburg L, Schrödner M. *Perhydropolysilazane derived silica for flexible transparent barrier foils using a reel-to-reel wet coating technique: Single- and multilayer structures*. Surf Coat Technol. **2015**;275.

[245] Ohishi T, Yamazaki Y, Nabatame T. P*reparation, structure and gas barrier characteristics of poly silazane-derived silica thin film formed on PET by simultaneously applying ultraviolet-irradiation and heat-treatment*. Front Nanosci Nanotechnol. **2016**;2(4).

[246] Kozuka H, Fujita M, Tamoto S. *Polysilazane as the source of silica: the formation of dense silica coatings at room temperature and the new route to organic–inorganic hybrids*. J Sol-Gel Sci Technol. **2008**;48(1):148–55.

[247] Burak D, Rahman MA, Seo DC, Byun JY, Han J, Lee SE, Cho SH. I*n Situ Metal Deposition on Perhydropolysilazane-Derived Silica for Structural Color Surfaces with Antiviral Activity.* ACS Appl Mater Interfaces. **2023;**15(46):54143–56.